

Efficiency, Feasibility, and Application of The Discrete Element Method for Ballasted Railway Track Design

Jia, W.

DOI

[10.4233/uuid:c08689f3-f27f-4ada-81b0-b60fd9b73d57](https://doi.org/10.4233/uuid:c08689f3-f27f-4ada-81b0-b60fd9b73d57)

Publication date

2023

Document Version

Final published version

Citation (APA)

Jia, W. (2023). *Efficiency, Feasibility, and Application of The Discrete Element Method for Ballasted Railway Track Design*. [Dissertation (TU Delft), Delft University of Technology].
<https://doi.org/10.4233/uuid:c08689f3-f27f-4ada-81b0-b60fd9b73d57>

Important note

To cite this publication, please use the final published version (if applicable).
Please check the document version above.

Copyright

Other than for strictly personal use, it is not permitted to download, forward or distribute the text or part of it, without the consent of the author(s) and/or copyright holder(s), unless the work is under an open content license such as Creative Commons.

Takedown policy

Please contact us and provide details if you believe this document breaches copyrights.
We will remove access to the work immediately and investigate your claim.

Efficiency, Feasibility, and Application of The Discrete Element Method for Ballasted Railway Track Design

Wenli JIA

Efficiency, Feasibility, and Application of The Discrete Element Method for Ballasted Railway Track Design

Dissertation

for the purpose of obtaining the degree of doctor
at Delft University of Technology
by the authority of the Rector Magnificus, Prof.dr.ir. T.H.J.J. van der Hagen,
chair of the Board for Doctorates
to be defended publicly on
Tuesday 12, December 2023 at 10:00 o'clock
By

Wenli JIA

Master of Science in Road and Railway Engineering, Beijing Jiaotong University, China
born in Chengde, China

This dissertation has been approved by the promotor.

Rector Magnificus,	Chairperson
Prof.dr.ir. R.P.J.B. Dollevoet,	Delft University of Technology, promotor
Dr. V.L. Markine,	Delft University of Technology, promotor

Independent members:

Prof.dr. D.P. Connolly,	University of Leeds, UK
Prof.dr.ir. C. Jommi,	Delft University of Technology
Prof.dr.ir. D.L. Schott,	Delft University of Technology
Prof.dr. Z. Li,	Delft University of Technology
Dr. X. Liu	Delft University of Technology, reserve member

Other member:

Prof.dr. G. Jing,	Beijing Jiaotong University, China
-------------------	------------------------------------

This research was funded by European Commission (Horizon 2020, In2zone Project), Delft University of Technology, and Beijing Jiaotong University.



Printed by: Glideprint

Cover by: Wenli Jia based on The Persistence of Memory by Salvador Dalí

Copyright © 2023 by Wenli Jia (jiawenli5067@126.com)

ISBN

All rights reserved. No part of the material by this copyright notice may be reproduced or utilized in any form or by any means, electronic or mechanical, including photocopying, recording or by any information storage and retrieval system, without written permission of the author.

An electronic version of this dissertation is available at

<http://repository.tudelft.nl/>.

To my Family

Summary

The ballast bed of a railway track consists of two granular layers, the ballast layer and the sub-ballast layer, and it is typically constructed of crushed, angular hard rocks. Studies on ballast degradation and structural performance improvement is needed to optimise reliability, availability, maintainability and safety of the railway track. Typically, the studies are conducted by laboratory/in situ tests and numerical simulations.

Within different research methods, the Discrete Element Method (**DEM**) is utilized to analyse behaviour of granular materials on particle level, making it suitable for railway ballast-related research. A DEM model allows for the description of interaction between particle on a mesoscopic level, while presenting the overall performance of the assembly on a macroscopic level. However, the large number of elements in a model along with the complex algorithm lead to high computational efforts, resulting in **low efficiency** of the DEM models. This problem limits the number of elements acceptable in a model, which means that only a limited amount of materials in a limited scale is possible to be generated and analysed. Considering the calculation time, the accepted number of elements in a mode depends on various simulated particle sizes (e.g., soil, sub-ballast, ballast) and simulated model sizes (e.g., box model, full-scale model). Additionally, it also affects the simulated loading condition, e.g. static loading or cyclic loading.

For railway ballast-related DEM simulations, the efficiency problems primarily arise from the large number of elements due to the complex generation of irregular particle shapes, because ballast particle size must satisfy a certain requirement of Particle Size Distribution (PSD) to maintain the ballast bed functions. Due to this required property the simulation of ballast cannot use the most of simplification methods to improve the calculation efficiency. For example, in soil-related simulations, particle upscaling method is employed to reduce the number of elements and decrease the calculation efforts. Since the size of the soil particle (0.002mm to 2.000mm) is much smaller than the interacted components (e.g., piles, plough, 70m³ bulk handling equipment), a proper upscaling factor does not influence the macroscopic behaviour, which is the main focus in such simulation. Unlike soil-related simulations, size of railway ballast is relatively big. the size of ballast particles ranges from 20-65mm, and the bottom area of the sleeper is only around 0.7m². The particle size effect is mentioned in several ballast-related tests, particle upscaling decrease the accuracy in both mesoscopic and macroscopic results. Based on that, railway ballast-related simulations typically use **shape simplification** method. However, the shape of the particles also contributes to the force and displacement behaviour of the railway ballast layer. The influence of the simplifications on accuracy of the results depends on the type of the results required, namely, macro or meso. Therefore, a proper choice of the particle shape is crucial to obtain meaningful results on the railway ballast layer behaviour.

With those ideas, the DEM-based simulations need to be specially optimised for ballast-related research. The optimisation is done here focussing on the following 3 aspects:

- **Efficiency:** reducing computational efforts (calculation time) while keeping required accuracy by applying proper particle shape simplifications.
- **Feasibility:** increasing possibility of using DEM in railway applications focusing on different research objects and expected results. Developing cooperative simulation schemes for analysis of the long-term dynamic structural behaviour.
- **Application:** demonstration of the developed methods to assess the performance of new designs and materials in railway track.

To improve the efficiency, different shapes are generated with complexity varying from the sphere (ball, simplest) to high-fidelity clumps (cluster of spheres, closest to a real ballast particle). In case of

the simplest shape (ball and 2-sphere shapes) it is proposed to use additional **rolling resistance** (friction coefficient) to account for the loss of interlocking between the particles. The macroscopic and mesoscopic results are both obtained, compared, and analysed using a series of numerical simulations with box loading tests. The results include the coordination number (the average number of contact points of one particle), contact forces (average contact force, maximum contact force, force distribution), and the sleeper displacement.

As a demonstration, a box (600mm*600mm*500mm) cyclic loading 5Hz, 1second simulation time is reduced from 5 hours to less than 1 hour as compared to the high-fidelity reference shape. In the same simulation, the ball shape only takes 5 minutes to compute, but when simplified, the mesoscopic results become unreliable.

Results show that the level of complexity of the particle has different influence on the macro- and mesoscopic results. Therefore, the simplification of the particles should be applied depending on which effects (e.g. ballast bed settlement or ballast particle breakage) are important and which results (on macro- or meso- level) are needed.

In case of the macroscopic results are of interest: the complexity of the particle can be reduced even without compensation in contact law (rolling resistance). When drastically reducing the complexity of the particle, the loss of accuracy of the results can be compensated by adjusting the contact law and using the rolling resistance to compensate for the loss of interlocking between the particles.

In case of mesoscopic results are of interest, the simplification of the particle complexity is not recommended since the loss of accuracy of the results cannot be compensated by adjusting the contact law (adding rolling resistance).

In case of the simulations, which considering the fresh and degraded ballast, the different particles can be used by controlling shape complexity and surface friction coefficient.

In addition, optimised model building methods were developed including the Particle **Replacement and Radius Adjustment (PRRA)** and the **Adaptive Particle Shape Simplification (APSS)** The efficiency of the DEM simulations in the model preparation stage is improved significantly. For instance, the optimized model building method is 10-20 times faster than the typically used method when building a box (600mm*600mm*500mm) model, and the optimized box model for cyclic loading simulations is 30 times faster while maintaining similar accuracy when compared to a high-fidelity reference model.

The aforementioned DEM simulations were carried out in 3D. However, these efficiency optimised models are still unable to be used in the analysis on long-term or dynamic-related behaviour, which raises DEM feasibility questions.

To address the feasibility questions, **Co-simulations** (cooperative simulations) were developed, which use a two-dimensional DEM model as a supplement for the efficiency loss of the 3D DEM model. The results of the 3D DEM model are used as a resource for calibration to improve the accuracy of the 2D DEM model, thereby largely improving the feasibility of the DEM modelling method.

Similarly, DEM and FEM (Finite Element Method) co-simulations were introduced to simulate the interaction between the train and track in the transition zone. The contact force between the sleepers and ballast bed under train passing, referred to as sleeper force, is calculated using FEM model and used as the input for the sleeper-ballast DEM model. In this way, the severe moment of a dynamic process (for example, the moment when peak contact force is observed) can be accurately simulated to present the movement of ballast particles and forces between ballast particles.

Further, the developed modelling methods are used in **applications** to assess several designs, aiming to improve the performance of ballasted track. In this study, four applications were carried out that comprehensively cover different components of the ballasted track.

1. Design of a wedge sleeper to eliminate hanging sleepers and reduce track degradation. In this application, 3D DEM simulations are conducted to analyse the contact forces in the ballast resulting from various single wedge designs. Additionally, 2D DEM simulations are employed to investigate the long-term settlement behaviour. The cooperative modelling method circumvents the efficiency issues associated with 3D DEM and enhances the accuracy of 2D DEM simulations. This approach resolves the feasibility challenge of utilizing DEM simulations for analysing long-term behaviour.
2. Analysis of behaviour of recycled ballast. In this application, particle shape is evaluated to simulate material differences. The main challenge of this research lies in simulating varying surfaces while utilizing shape simplification. The simplified shapes do not capture surface intricacies as precisely as high-fidelity particles. Conversely, using high-fidelity particles would lead to significantly lower calculation efficiency. This application effectively addresses this challenge, enhancing efficiency while preserving the accuracy of DEM simulations.
3. Analysis of using furnace slag as subballast. In this application, small-sized particles, specifically sub-ballast, are simulated. This demonstration showcases the utilization of shape simplification and rolling resistance. The application provides a method to address the efficiency and feasibility challenges in DEM caused by particles that are relatively small yet irregular in shape.
4. Analysis of the force behaviour of ballast in transition zones to provide a mesoscopic understanding of differential settlement. In this application, the movement of the hanging sleepers during train passage is simulated in the FEM model and used as input for the DEM method to calculate the detailed behaviour of ballast particles. This application demonstrates a DEM&FEM cooperative method, successfully addressing the feasibility challenge of accurately studying ballast behaviour under dynamic conditions.

Overall, the optimisation of DEM-based numerical simulations provides an improvement in ballast-related research. The related applications provide new materials for railway construction and maintenance.

Samenvatting

Het ballastbed van een spoorweg bestaat uit twee korrelige lagen: de ballast laag en de subballast laag. Het wordt doorgaans opgebouwd uit gebroken, hoekige harde rotsen. Onderzoek naar de degradatie van ballast en verbetering van de structurele prestaties is nodig om de betrouwbaarheid, beschikbaarheid, onderhoud baarheid en veiligheid van het spoorwegtraject te optimaliseren. Dit onderzoek wordt typisch uitgevoerd met laboratorium/in situ tests en numerieke simulaties.

Binnen verschillende onderzoeksmethoden wordt de Discrete Elementen Methode (DEM) gebruikt om het gedrag van korrelige materialen op deeltjesniveau te analyseren, wat geschikt is voor ballast gerelateerd onderzoek. Een DEM-model maakt de beschrijving van de interactie tussen deeltjes op een mesoscopisch niveau mogelijk, terwijl het de algehele prestaties van de assemblage op macroniveau presenteert. Echter, het grote aantal elementen in een model samen met het complexe algoritme leidt tot hoge rekeninspanningen, resulterend in lage efficiëntie van de DEM-modellen. Dit probleem beperkt het aantal acceptabele elementen in een model, wat betekent dat slechts een beperkte hoeveelheid materiaal op beperkte schaal kan worden gegenereerd en geanalyseerd. Gezien de berekeningstijd hangt het geaccepteerde aantal elementen in een model af van verschillende gesimuleerde deeltjesgroottes (bijv. bodem, subballast, ballast) en gesimuleerde modelgroottes (bijv. box model, grootschalig model). Daarnaast heeft het ook invloed op de gesimuleerde belasting conditie, bijvoorbeeld statische belasting of cyclische belasting.

Voor DEM-simulaties met betrekking tot spoorwegballast komen de efficiëntieproblemen voornamelijk voort uit het grote aantal elementen door de complexe generatie van onregelmatige deeltjesvormen, omdat de grootte van ballastdeeltjes moet voldoen aan bepaalde eisen van de Deeltjesgrootteverdeling (PSD) om de functies van het ballastbed te behouden. Vanwege deze vereiste eigenschap kan de simulatie van ballast niet de meeste vereenvoudigingsmethoden gebruiken om de rekenefficiëntie te verbeteren. Bijvoorbeeld, in bodem gerelateerde simulaties wordt de methode van deeltjesopschaling toegepast om het aantal elementen te verminderen en de rekeninspanningen te verminderen. Aangezien de grootte van het bodemdeeltje (0,002 mm tot 2,000 mm) veel kleiner is dan de samenwerkende onderdelen (bijv. palen, ploeg, bulkverwerkingsapparatuur van 70 m³), heeft een geschikte opschalingsfactor geen invloed op het macroscopische gedrag, wat het belangrijkste focuspunt is in dergelijke simulatie. In tegenstelling tot bodem gerelateerde simulaties is de grootte van spoorwegballast relatief groot. De grootte van ballastdeeltjes varieert van 20-65 mm, en het bodemgebied van de dwarsligger is slechts ongeveer 0,7 m². Het effect van de deeltjesgrootte wordt genoemd in verschillende ballast gerelateerde tests; de deeltjesopschaling vermindert de nauwkeurigheid in zowel mesoscopische als macroniveau resultaten. Op basis daarvan gebruiken spoorweg ballast gerelateerde simulaties meestal een methode van vormvereenvoudiging. Echter, de vorm van de deeltjes draagt ook bij aan het kracht- en verplaatsingsgedrag van de ballast laag. De invloed van de vereenvoudigingen op de nauwkeurigheid van de resultaten hangt af van het type resultaten dat vereist is, namelijk macro- of meso. Daarom is een juiste keuze van de deeltjesvorm cruciaal om zinvolle resultaten te verkrijgen over het gedrag van de spoorweg ballast laag.

Met deze ideeën moeten de DEM-gebaseerde simulaties speciaal worden geoptimaliseerd voor ballast gerelateerd onderzoek. De optimalisatie richt zich hier op de volgende 3 aspecten:

- Efficiëntie: het verminderen van rekeninspanningen (berekeningstijd) terwijl de vereiste nauwkeurigheid behouden blijft door het toepassen van geschikte vereenvoudigingen van de deeltjesvorm.
- Haalbaarheid: het vergroten van de mogelijkheid om DEM in spoorwegtoepassingen te gebruiken, gericht op verschillende onderzoeksobjecten en verwachte resultaten. Het ontwikkelen van samenwerkende simulatieschema's voor de analyse van het lange termijn dynamisch structureel gedrag.
- Toepassing: demonstratie van de ontwikkelde methoden om de prestaties van nieuwe ontwerpen en materialen in het spoorwegtraject te beoordelen.

Om de efficiëntie te verbeteren, worden verschillende vormen gegenereerd met complexiteit variërend van de bol (bal, eenvoudigst) tot hoogwaardige brokken (cluster van bollen, dichtst bij een echt ballastdeeltje). In geval van de eenvoudigste vorm (bol en 2-bolvormen) wordt voorgesteld om extra rolweerstand (wrijvingscoëfficiënt) te gebruiken om het verlies van in elkaar grijpen tussen de deeltjes in rekening te brengen. De macroscopische en mesoscopische resultaten worden beide verkregen, vergeleken en geanalyseerd met behulp van een reeks numerieke simulaties met belasting tests in een doos. De resultaten omvatten het coördinatiegetal (het gemiddelde aantal contactpunten van één deeltje), contactkrachten (gemiddelde contactkracht, maximale contactkracht, krachtsverdeling) en de verplaatsing van de dwarsligger.

Als demonstratie wordt een doos (600 mm * 600 mm * 500 mm) cyclische belasting 5 Hz, 1 seconde simulatietijd verminderd van 5 uur tot minder dan 1 uur in vergelijking met de hoogwaardige referentievorm. In dezelfde simulatie duurt het berekenen van de bolvorm slechts 5 minuten, maar wanneer vereenvoudigd, worden de mesoscopische resultaten onbetrouwbaar.

De resultaten tonen aan dat het niveau van complexiteit van het deeltje verschillende invloed heeft op de macro- en mesoscopische resultaten. Daarom moet de vereenvoudiging van de deeltjes worden toegepast, afhankelijk van welke effecten (bijv. verzakking van het ballastbed of breuk van ballastdeeltjes) belangrijk zijn en welke resultaten (op macro- of mesoniveau) nodig zijn.

In het geval dat macroscopische resultaten van belang zijn: de complexiteit van het deeltje kan worden verminderd zonder compensatie in de contactwet - Rolweerstand. Bij het drastisch verminderen van de complexiteit van het deeltje kan het verlies aan nauwkeurigheid van de resultaten worden gecompenseerd door de contactwet aan te passen en rolweerstand te gebruiken om het verlies van in elkaar grijpen tussen de deeltjes te compenseren.

In het geval dat mesoscopische resultaten van belang zijn, wordt de vereenvoudiging van de deeltjescomplexiteit niet aanbevolen, aangezien het verlies van nauwkeurigheid van de resultaten niet kan worden gecompenseerd door aanpassing van de contactwet (toevoegen van rolweerstand).

In het geval van de simulaties, die rekening houden met de verse en gedegradeerde ballast, kunnen verschillende deeltjes worden gebruikt door de vormcomplexiteit en oppervlaktewrijvingscoëfficiënt te controleren.

Bovendien zijn geoptimaliseerde modelbouwmethoden ontwikkeld, waaronder de Methode van Deeltjesvervanging en Straal Aanpassing (PRRA) en de Adaptieve Vereenvoudiging van Deeltjesvorm (APSS). De efficiëntie van de DEM-simulaties in de modelvoorbereidingsfase is aanzienlijk verbeterd. Bijvoorbeeld, de geoptimaliseerde modelbouwmethode is 10-20 keer sneller dan de typisch gebruikte methode bij het bouwen van een model in een doos (600 mm * 600 mm * 500 mm), en het geoptimaliseerde doosmodel voor cyclische belastingsimulaties is 30 keer sneller

met behoud van een vergelijkbare nauwkeurigheid in vergelijking met een hoogwaardig referentiemodel.

De eerder genoemde DEM-simulaties werden in 3D uitgevoerd. Echter, deze efficiënte geoptimaliseerde modellen kunnen nog steeds niet worden gebruikt voor de analyse van gedrag op lange termijn of dynamisch gerelateerd gedrag, wat vragen oproept over de haalbaarheid van DEM.

Om de haalbaarheidsvragen aan te pakken, werden co-simulaties (samenwerkende simulaties) ontwikkeld, die een tweedimensionaal DEM-model gebruiken als aanvulling op het verlies aan efficiëntie van het 3D DEM-model. De resultaten van het 3D DEM-model worden gebruikt als een bron voor kalibratie om de nauwkeurigheid van het 2D DEM-model te verbeteren, waardoor de haalbaarheid van de DEM-modelleringsmethode grotendeels wordt verbeterd.

Op dezelfde manier werden DEM- en FEM (Eindige Elementen Methode) co-simulaties geïntroduceerd om de interactie tussen de trein en het spoor in de overgangszone te simuleren. De contactkracht tussen de dwarsliggers en het ballastbed onder de passerende trein, ook wel dwarsliggers kracht genoemd, wordt berekend met behulp van een FEM-model en gebruikt als invoer voor het DEM-model van dwarsligger-ballast. Op deze manier kan het hevige moment van een dynamisch proces (bijvoorbeeld het moment waarop de piekcontactkracht wordt waargenomen) nauwkeurig worden gesimuleerd om de beweging van ballastdeeltjes en krachten tussen ballastdeeltjes weer te geven.

Verder worden de ontwikkelde modelleringsmethoden gebruikt in toepassingen om verschillende ontwerpen te beoordelen, met als doel de prestaties van het ballastspoor te verbeteren. In deze studie zijn vier toepassingen uitgevoerd die verschillende componenten van het ballastspoor uitgebreid behandelen.

1. Ontwerp van een wigvormige dwarsligger om hangende dwarsliggers te elimineren en de spoordegradatie te verminderen. In deze toepassing worden 3D DEM-simulaties uitgevoerd om de contactkrachten in de ballast te analyseren als gevolg van verschillende enkele wigontwerpen. Bovendien worden 2D DEM-simulaties gebruikt om het lange termijn zetting te onderzoeken. De samenwerkende modelleringsmethode omzeilt de efficiëntieproblemen die gepaard gaan met 3D DEM en verbetert de nauwkeurigheid van 2D DEM-simulaties. Deze aanpak lost het haalbaarheidsprobleem op bij het gebruik van DEM-simulaties voor het analyseren van langdurig gedrag.
2. Analyse van het gedrag van gerecyclede ballast. In deze toepassing wordt de deeltjesvorm geëvalueerd om materiaalverschillen te simuleren. De belangrijkste uitdaging van dit onderzoek ligt in het simuleren van variërende oppervlakken terwijl vormvereenvoudiging wordt gebruikt. De vereenvoudigde vormen vangen oppervlaktedetails niet zo nauwkeurig op als hoogwaardige deeltjes. Aan de andere kant zou het gebruik van hoogwaardige deeltjes leiden tot aanzienlijk lagere berekeningsefficiëntie. Deze toepassing lost dit probleem effectief op, verbetert de efficiëntie en behoudt tegelijkertijd de nauwkeurigheid van DEM-simulaties.
3. Analyse van het gebruik van hoogoven-slag als subballast. In deze toepassing worden kleine deeltjes, specifiek subballast, gesimuleerd. Deze demonstratie laat het gebruik van vormvereenvoudiging en rolweerstand zien. De toepassing biedt een methode om de efficiëntie- en haalbaarheidsproblemen in DEM aan te pakken die worden veroorzaakt door deeltjes die relatief klein maar onregelmatig van vorm zijn.

4. Analyse van het krachtgedrag van ballast in overgangszones om een mesoscopisch begrip van differentiële verzakking te bieden. In deze toepassing wordt de beweging van de hangende dwarsliggers tijdens het passeren van de trein gesimuleerd in het FEM-model en gebruikt als invoer voor de DEM-methode om het gedetailleerde gedrag van ballastdeeltjes te berekenen. Deze toepassing toont een DEM&FEM-samenwerkingsmethode, die met succes het haalbaarheidsprobleem aanpakt van het nauwkeurig bestuderen van ballastgedrag onder dynamische omstandigheden.

Al met al zorgt de optimalisatie van DEM-gebaseerde numerieke simulaties voor een verbetering in ballast gerelateerd onderzoek. De gerelateerde toepassingen leveren nieuwe materialen op voor de bouw en het onderhoud van spoorwegen.

Contents

Summary	vii
Samenvatting.....	xi
Contents.....	xv
Thesis Contents.....	xvii
Part I Extended Summary	
Chapter 1 Railway ballast and Discrete Element Method simulation-general introduction.....	1
1.1 Railway ballast and ballast bed.....	1
1.2 DEM simulations	2
1.3 Research questions and outline	5
Chapter 2. Optimised DEM particles	7
2.1 DEM particles and contact specification	7
2.2 Particle simplification and assessment.....	10
2.2.1 Simplified particles.....	11
2.2.2 Shape assessment	11
2.3 Additional explanation	16
2.4 Conclusions	18
Chapter 3 Optimised DEM model building method	21
3.1 Optimised model building method.....	21
3.2 Adaptive particle shape simplification.....	23
3.3 Validation of APSS optimised model	26
3.4 Conclusions	29
Chapter 4 Co-simulation method.....	31
4.1 2D & 3D model.....	32
4.2 DEM & FEM model	34
4.3 Conclusions	36
Chapter 5. Applications	39
5.1 Sleeper-----Wedge sleeper in transition zones.....	39

5.2 Ballast-----Recycled ballast	46
5.3 Sub-ballast-----Furnace slag	49
5.4 Transition zones-----Ballast behaviour	52
Chapter 6. Conclusion	57
6.1 Conclusion	57
6.2 Recommendation	61
Reference	63
Part II Appendix Paper I-VI	
Paper I.....	71
Paper II.....	87
Paper III.....	107
Paper IV.....	131
Paper V.....	149
Paper VI.....	163

Thesis Contents

The material presented in this dissertation is based on the following papers and report.

Paper A

Wenli Jia, Valeri Markine. Parameter and efficiency analysis on particle shape of railway ballast in DEM simulations. Proceedings of the Institution of Mechanical Engineers, Part F: Journal of Rail and Rapid Transit. 2023

Paper B

Wenli Jia, Valeri Markine, Yunlong Guo. Efficiency analysis and optimisation of DEM for railway ballasted track simulations—the multi-layer model. Transportation Geotechnics.2023 (40):100977

Paper C

Wenli Jia, Valeri Markine, Mario Carvalho, David P. Connolly, Yunlong Guo. Design of a concept wedge-shaped self-levelling sleeper. Construction and building materials.2023 (386):131524.

Paper D

Wenli Jia, Valeri Markine, Yunlong Guo, Guoqing Jing. Experimental and numerical investigations on the shear behaviour of recycled railway ballast. Construction and building materials. 2019(217):310-320

Paper E

Wenli Jia, Valeri Markine, Yunlong Guo, Guoqing Jing. Analysis of furnace slag in railway sub-ballast based on experimental tests and DEM simulations. Construction and building materials. 2021 288(1):123114

Paper F

Wenli Jia, Haoyu Wang, Valeri Markine. Dynamic behaviour of ballast under hanging sleepers in railways track transition zones using FEM-DEM method. 2023

Report A

Wenli Jia, Yunlong Guo, Valeri Markine. Deliverable 4.1 Report on development of numerical models. Project Acronym: IN2ZONE. Project title: The Next Generation of Railway Transition Zones. Grant Agreement Number: 101014571 – IP/ITD/CCA – IP3

Report B

Wenli Jia, Yunlong Guo, Valeri Markine. Deliverable 4.2 Report on use of the numerical model in the development and improvement of the design solution for transition zones. Project Acronym: IN2ZONE. Project title: The Next Generation of Railway Transition Zones. Grant Agreement Number: 101014571 – IP/ITD/CCA – IP3

Part I

Extended Summary

Chapter 1 Railway ballast and Discrete Element Method simulation-general introduction

In this chapter, the ballast material used in railway track is introduced, including its functions, degradation, and problems. Focusing on ballast, the Discrete Element Method (DEM) simulation, which is a proper tool for ballast related research, is introduced with its efficiency and feasibility problems. The background, research questions, and outline of the thesis are presented.

1.1 Railway ballast and ballast bed

The ballast bed of a railway track consists of two granular layers, namely the ballast layer and the sub-ballast layer, and it is typically constructed of crushed, angular hard rock with particle size ranged from 20mm to 65mm [1, 2]. The sleepers are embedded in the ballast layer, and rails are installed on the sleeper using fastening systems. The main functions of the ballast bed are [3]:

- Provide bearing to forces generated from the train passage and transmitted from rail-wheel to sleeper;
- Contribute to elasticity of the tracks;
- Provide lateral and longitudinal resistance, keep the geometry of the track;
- Be responsible for draining water away from the track.

A typical ballasted track is shown in Figure 1.

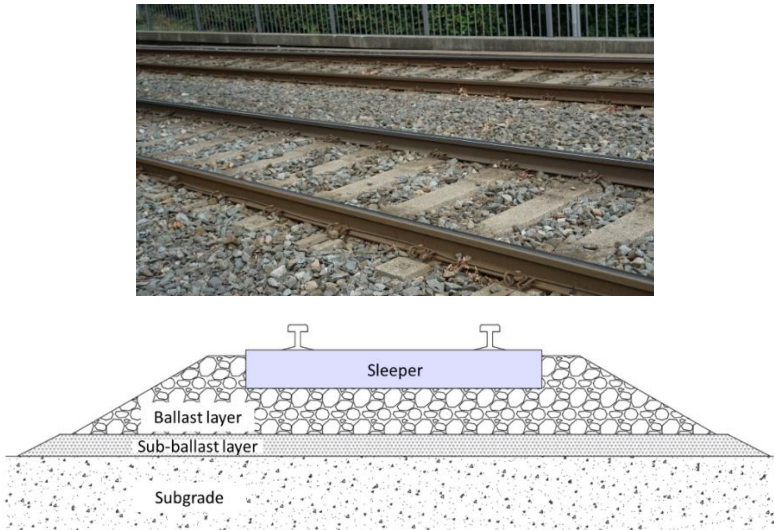


Figure 1. Ballasted track

The quality of the ballast bed is determined by several factors, such as strength, elasticity, lateral resistance. These factors are mainly influenced by the ballast material. Therefore, it is important to check the quality of the ballast material before track construction and various indicators are used for this purpose. The Los Angeles Abrasion (LAA) index together with Flaky Index (FI) and Elongated Index (EI) are used to qualify the abrasion and breakage resistance of ballast [4, 5]. The Particle Size Distribution (PSD) obtained by sieving is to fulfil the characteristics of drainage and elasticity [6, 7]. The type of mother rock, irregular shape, and coarse surface are ensuring the strength to bearing [8, 9].

However, the ballast bed will deteriorate due to ballast degradation, which includes particle breakage, abrasion, translation, and rotation. During the degradation process, ballast particles become less angular, and the surface texture wears down from coarse to smooth. The particle size also decreases, which affects the PSD and produces fine particles (fouling composition [10]), finally leading to differential settlement, reduction in drainage ability and capacity [11, 12]. With the emergence of heavier axle and higher speed loading in recent years, these problems have become more severe [13].

Degradation in transition zones tends to occur more rapidly. These zones are typically located near engineering structures (e.g., embankment-bridge, as shown in Figure 2). The supporting stiffness of the track changes dramatically, leading to a rapid change in the elevation of wheels and causing an increase in dynamic wheel loads [14-16]. And, the deformation difference leads to differential settlement, which results in hanging sleepers that are unsupported by the ballast layer [17]. Consequently, degradation in transition zones has been observed much more often than in free tracks [18-23].

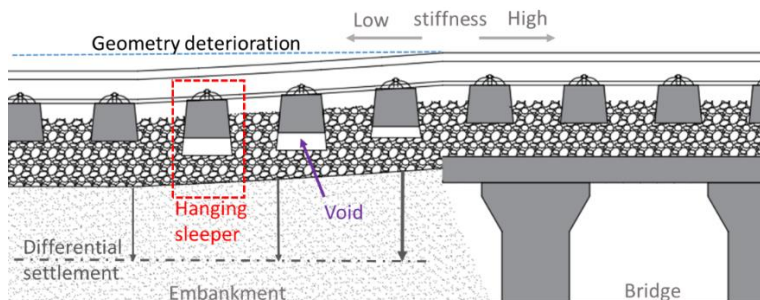


Figure 2. Differential settlement and hanging sleepers at a transition zone. Modified from [17]

The focus on degradation is due to the significant effort and costs involved in performing maintenance work. Therefore, improving the performance and extending the service life of the ballasted track is considered a major challenge in railway ballast. Research on ballast performance and the development of research tools are being progressively improved.

1.2 DEM simulations

In the existing research methods, laboratory and in-situ tests are typically used, which provide the most direct and reliable results, although they are costly. Therefore, numerical tools are often used as an economical alternative.

In the field of railway engineering, the Finite Element Method (FEM) is typically used to accurately analyse the interaction between trains, rails, sleepers, and ballast, as seen in previous studies [24-31]. However, FEM models treat the ballast layer as a whole component and are often modelled using beam or solid elements, which may not accurately capture the movement of ballast particles and stress within the ballast layer.

On the other hand, the Discrete Element Method (DEM) is a numerical solution that is commonly used to analyse the behaviour of granular material [32-34]. In DEM-based models, the particle (sphere, or clump which is a cluster of spheres) is the basic element, along with the wall element used to represent boundary. The interactions between particles are calculated according to the contact law, thus presenting the behaviour of a sample or a structure [35-37]. In this research, the software Particle Flow Code (PFC) is used.

As an example, a DEM model of a single sleeper section of a ballasted track is built and shown in Figure 3. The model has 3 boundaries: 2 side walls and 1 bottom wall. Ballast layer is built with compacted particles, and a sleeper is embedded in the ballast layer. The interaction between contacted elements is calculated based on the contact law.

However, the efficiency of DEM is low due to its calculation algorithm. Every element in a model works as a unit, which contains its property information, such as volume, density and stiffness, and behaviour information, such as force and displacement. Every contact between elements needs to be detected and updated separately based on position and applied contact parameters (or inherited attributes from particles)[38, 39]. In addition, a particle can be generated by a cluster of several spheres to achieve irregularity[40-42]. All those spheres contain their information, and a wall contains several triangle facets.

For example, in the Figure 3, the model contains 647,323 elements of 24,311 particles (each particle is generated with several spheres), 86 elements of the sleeper and 3 boundaries, and 91,925 contacts. When using this model to simulate a lateral resistance test, the calculation time for the 15-second process is more than 40 hours.(hardware: Intel Xeon CPU E5, RAM 64G, software PFC3D 5.0)

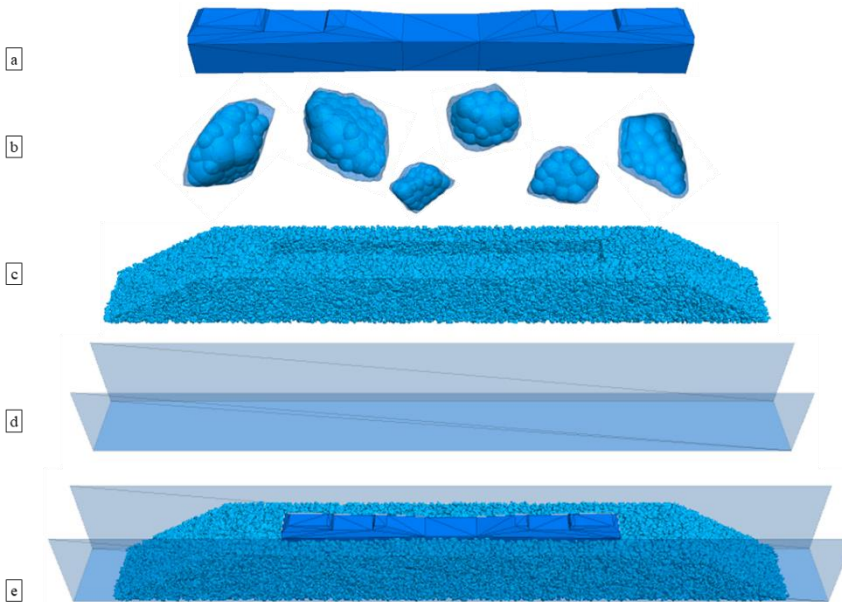


Figure 3. Ballasted track model of a single sleeper section: a) Sleeper, b) Ballast particles, c) Ballast layer, d) Boundary walls, e) Balanced model

A conflict exists that limits the usage of DEM. The DEM model should present the irregular shape of the ballast in order to capture accurate results, and a proper contact model should be applied to simulate the physical reality, that is the high-fidelity model. However, due to the complexity of the particle shape in the high-fidelity model and the algorithm of DEM, the efficiency of DEM simulations is low. It becomes a major problem, presenting as that the convincing DEM simulations need an unacceptable time consumption (maybe years of a large-scale model or the long-term behaviour). Under this limitation, the DEM model for ballast research is normally built on a small scale, such as the direct shear test, tri-axial compression test, ballast box test, etc.

This huge time consumption compared with real-time restricts the feasibility of DEM simulations. Thus, several simplified methods have been considered by researchers to enhance efficiency. The model simplification methods focus on how to use a low-fidelity model to obtain the required results [43-45]. The low-fidelity model can increase efficiency by omitting some physical performance. For example, increasing the particle size can decrease the number of the particle in the model, thus decreasing the calculation time. However, the low-fidelity model may not present the physical reality for example, the elasticity of ballast layer mainly comes from the friction between angular and coarse surface, using simplified ball particles in a simulations cannot present the elasticity, especially at particle level. Modelling approaches can be corrected and biased towards the desired macroscopic outcome, for example, simulating the elasticity by applying contact parameters on the calculated contact points. The possible methods to correct the results contain 2 main types.

First, the model fitting method uses mathematical equations to calculate the relationship between the results obtained from a simplified model and those from the accurate model or experimental tests. To achieve this, proper parameters are required, and the results typically serve as key performance indicators.

The second method is the reduce-order-modelling. This approach is based on the simplified model (such as, in state space dimension, degrees of freedom), while it still includes the needed spatial and transient information

For example, in reference[46], researchers analysed the influence of soil particle size on the accuracy of results, as simulating soil particles with their actual size and distribution is impossible. Natural soil particles are ranged from 0.002mm to 2.000mm[47]. Using the particle sizes that are closer to the actual size leads to higher accuracy. The results show that reducing particle radius from 5mm to 3mm lead to approximately sevenfold increase of computational time (500 hours). Therefore, the particle upscaling method is used to improve the efficiency. Similarly, in reference [48] upscaling method was used to study the interaction of bulk handling equipment and a large volume (77m^3) of iron ore pellets.

Efficiency problems in ballast-related research are different from those encountered in other areas. Particle upscaling is not suitable for reducing the calculation efforts in this case, as ballast particles typically range in size from 20-65mm [1, 3]. Due to the relatively large size of ballast particles, up-scaling methods are not as efficient as they are for smaller particles. Moreover, particle size distribution is a critical parameter that influences the behaviour of the ballast layer in terms of drainage ability, elasticity, and bearing [49, 50]. When ballast interacts with the sleeper, the contact area is less than 1% of the sleeper's surface area [51]. Particle upscaling can further decrease the contact area, leading to highly inaccurate results of ballast-sleeper contact forces and displacement. This makes the results sensitive to the size of the ballast particle..

The results to be obtained in the numerical simulations of ballast can be divided into 2 groups:

- **Macroscopic results:** the behaviour of an assembly of granular materials or objects in contact with them. For example, the settlement of a ballast layer can be assessed by the displacement of a sleeper.
- **Mesoscopic results:** the behaviour of particles, such as the displacement of a particle in the assembly, and contact forces on the ballast particle.

Accuracy of the results depends on the demanded scope of the results. For example, reference[52] reports that their simplified model presents the macroscopic results well, but the mesoscopic results were inaccurate. Therefore, a proper simplification method should be used depending on the desired scope. It is essential to develop simplification methods specifically for railway ballast-related research.

1.3 Research questions and outline

In the dissertation, the research was focused on the following 3 aspect:

- **Efficiency:** reducing computational efforts (calculation time) while keeping required accuracy by applying proper particle shape simplifications.
- **Feasibility:** increasing possibility of using DEM in railway applications focusing on different research objects and expected results. Developing cooperative simulation schemes for analysis of the long-term dynamic structural behaviour.
- **Application:** demonstration of the developed methods to assess the performance of new designs and materials in railway track.

In the context of railway ballast, efficiency problems arise mainly from the complexity of irregular shape generation, rather than particle size. Therefore, the railway ballast-related simulations typically use shape simplification methods. For example, in reference [53] the particles were generated using a single ball, while in reference [54] the ballast particles were 3-ball clusters. However, shape also contributes to the behaviour of the ballast layer as reported in reference [10, 40], because the shape provides interlock and force re-distribution. A proper choice of the simplified particle shape and contact parameters also presents meaningful results [55]. As a supplement to the interlock loss of shape simplification, reference [39] simulated the angle of repose tests using different shapes and contact parameters (rolling resistance). In reference [56], researchers used simplified shapes with rolling resistance to correct the results of the direct shear tests.

Despite the progress made in DEM-based simulations for railway ballast, the number of studies that uses DEM models is still limited (feasibility). Further analysis and optimization of the DEM simulations are necessary to improve their efficiency and thus feasibility for railway applications. Specifically, the influence of particle simplifications on the accuracy of the results must be studied carefully, depending on the scope of the research. Two main questions remain unanswered and require further investigation:

- What is the influence of shape simplifications on calculation efficiency?
- What is the relation between complexity (simplification) of particle shape and accuracy of results in macroscopic and mesoscopic?

These 2 questions are answered in Chapter 2 and Chapter 3. Next to particle simplifications, a novel model-building procedure for DEM developed in this study to improve the efficiency of DEM simulations is presented in these chapters. Once this knowledge is applied, the efficiency of DEM is improved. For instance, in the presented demonstration (a box model), the optimised model building method is 10-20 times quicker than the typical method used, and the cyclic loading simulation can be 30 times quicker while maintaining similar accuracy to a reference high-fidelity model.

Even though the efficiency-optimised 3D models can be successfully used in static loading simulations, they are still unsuitable in long-term or dynamic simulations, raising DEM feasibility concerns. Therefore, reduction of the problem dimensionality as one of the model simplifications was considered as well.

In comparison, the 2D DEM models are less time consuming due to the loss of one dimension. Using a low-fidelity model, such as in reference [57-59], 2D models can be used to simulate the long-term behaviour. However, they are less accurate and their accuracy is questionable. The Finite Element Method model is suitable for dynamic analysis, yet the mesoscopic results is unavailable, because FEM does not considering the performance of individual particles. The collaboration of different types of models is attractive if their advantages can be. Thus, the following questions arise:

- How to validate the 2D models based on the mesoscopic results of 3D DEM models to obtain the long-term behaviour on macroscopic level?
- How to use the macroscopic results of FEM model in 3D DEM models to obtain the dynamic-related behaviour on mesoscopic level?

These two questions are answered in Chapter 4. Co-simulation procedure to use the 2D DEM model as a supplement for the efficiency loss of the 3D DEM model were developed. The results of the 3D model are used as a resource of calibration to improve the accuracy of the 2D DEM model. This combination largely improves the feasibility of the DEM modelling method. Similarly, DEM-FEM co-simulations are introduced. The interaction between the train and track in the transition zone is simulated using the FEM model. The contact force between the sleepers and ballast bed under train passing (referred to as sleeper force) can be obtained. Then, those data are used as input conditions in the sleeper-ballast DEM simulations. In this way, the severe moment of a dynamic process, for example the moment when peak contact force appears, can be accurately simulated to obtain the movement of ballast particles and forces between ballast particles.

With the modelling developed, the efficiency and feasibility of DEM simulations are improved, those simulation methods are then used in the application to analyse the performance new designs and materials in railway construction:

- Application: demonstration of the developed methods, and use developed modelling methods to assess the function of new designs and materials in railway track.

Chapter 5 presents four applications, they are done with the optimised DEM simulations. First, it analyses the force behaviour of ballast in transition zones to provide a mesoscopic understanding of differential settlement. Second, it presents the design of wedge sleepers aimed at preventing hanging sleepers and reducing track degradation. Third, it assesses the performance of recycled ballast to ensure the function and maintenance of railway track. Lastly, it analyses the stability of furnace slag, offering sustainable solutions for ballast and sub-ballast layer construction.

The outline of the dissertation is shown in Figure 4

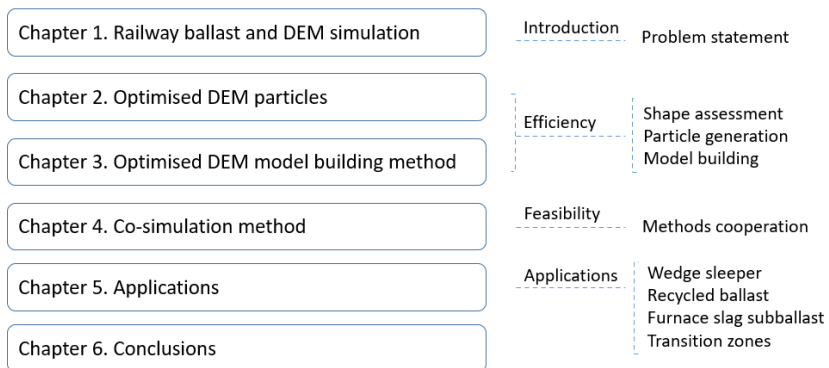


Figure 4. Outline of the dissertation

Chapter 2. Optimised DEM particles

The efficiency problem is mainly caused by large number of elements in a model, especially for the ballast particle with irregular shape, a particle consists of several elements. However, the actual shape of particle model contributes to more reliable results, simplification methods are needed to improve efficiency. In this chapter, the complexity of particle shape and complementary contact parameters are analysed to optimise the efficiency, and verification of accuracy is presented.

2.1 DEM particles and contact specification

Particle shape is a key factor that affects the accuracy of results because the irregular shape of ballast particles contributes to uneven force transmission and force redistribution paths. Furthermore, the angular interlock of the particles limits their displacement and rotation, providing strength and elasticity to the ballast layer.

The basic DEM particle is a sphere also called a ball element. More complex particles can be created using a clump element generated by fitting balls in a shape template (a cluster of balls). The distance parameter controls the overlap of the spheres, and the ratio parameter controls their radius, as illustrated in Figure 5. Using this method, a clump particle can be generated that closely resembles the shape of real ballast particles. As shown in Figure 6(a), the shape template is obtained through 3D scanning of a real ballast particle. Using this template the clump particle is generated as it is shown in Figure 6(b). Typically, multiple templates are used to generate ballast layer in a model, Figure 6(c) shows 10 of them.

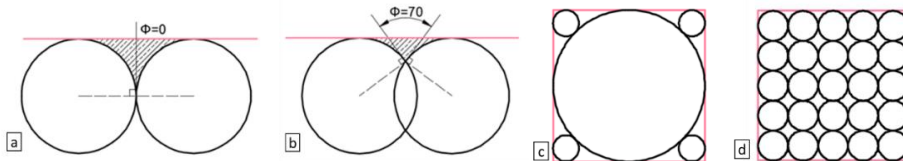


Figure 5. Definition of the Distance and Ratio: (a) Distance=0, (b) Distance=70, (c) Ratio=0.2, (d) Ratio=1

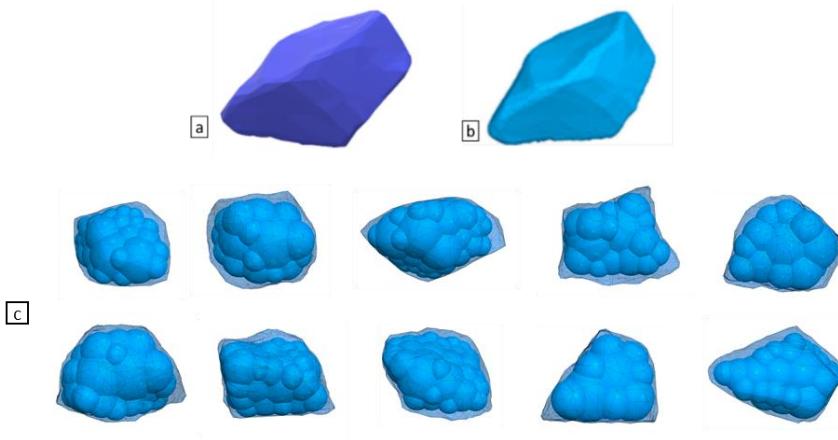


Figure 6. A real shape clump generated in PFC3D software: (a) Geometry from 3D scanning, (b) Clump with 13148 balls, (c) 10 templates & particles.

The high-fidelity particle contributes to high accuracy of the DEM models. Firstly, the irregular shape affects force transmission. The comparison between a ball shape and an irregular shape illustrates it as shown in Figure 7(a-b). When the relative position between two components and the centre of mass is the same, the motion and force transmission will be relatively similar. While this relative position is highly likely to be the same in a ball, it is less likely to be the same in an irregular shape. For example, forces F_1 and F_2 are applied to the ball. Their normal components are located at the same position in the local spherical coordinate system (with the centre of mass as the origin), and their tangent components are also the same due to D_1 and D_2 . In contrast, the forces on the clump have varying effects on force states, thus contributing to different motion.

Secondly, the angular shape is related to the contact force distribution between particles because a curved surface will lead to additional contact points. As shown in Figure 7(c), if the particle surface consists of several spherical surfaces, the contact points will change from a 1-point surface contact to 2-point insertion (also illustrated in the following Table 1: total contact number), leading to different behaviour of compressional and frictional force.

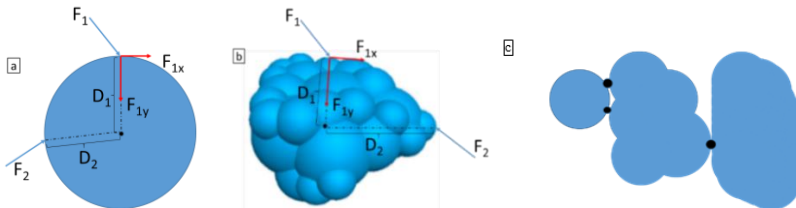


Figure 7. Applied force on sphere and irregular shape: (a) ball shape, (b) clump shape, (c) Different contact caused by spherical surface (black dot: contact point)

The contact parameters work in combination with the physical parameters of the elements, which include density and particle size distribution (PSD). Under external conditions, such as applied force, the assembly of particles (ballast layer) exhibits its performance. Since the ballast layer is a non-cohesive granular assembly, the linear contact model can be used to simulate the contact behaviour between ballast particles or ballast and sleepers. These contact parameters include the shear stiffness, normal stiffness, friction coefficient, and reference gap.

In addition, to compensate for the interlock loss (angular loss) caused by shape simplification, the rolling resistance can be used. The rolling resistance-related parameter is the friction coefficient (or stiffness). This setting restricts the rolling of a ball, thereby compensating for the interlock loss [38, 39, 56]. In PFC3D software, the rolling resistance is defined by rolling friction. The contact model is shown in Figure 8. Where, F_n^l is the normal component, F_s^l is the shear component, k_n is the normal stiffness, k_s is the shear stiffness, s is the state of slip determination, μ is the friction coefficient, g_s is the surface gap (defining whether a contact is valid), M^r is the rolling resistance moment to restrict the rotation, k_r is the rolling resistance, $\Delta\theta_b$ is the relative bend-rotation increment of a contact, details can be seen in Appendix Paper II.

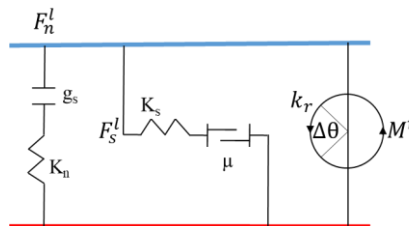


Figure 8. linear contact model with rolling resistance

The force-displacement information is updated discretely in a calculation cycle, according to a time step. A proper time step is necessary to keep the model balanced as a large time step may cause sudden and significant changes in displacement. This sudden change in displacement can lead to a sudden increase in contact force, causing the elements to fly away. The final critical time step is determined as the minimum of all critical time steps computed for all degrees of freedom of all bodies. The selection of minimum timesteps can reduce the time consumption of each cycle thus reaching the highest calculation efficiency of the certain model.

To define a time step, the stiffness is the key factor to consider because the contact force is directly calculated based on the stiffness and deformation. Typically, the stiffness used for ballast particles is set to a certain value. For example, in reference [60], the normal stiffness and shear stiffness for ballast-ballast contact are set to $2e6$ N/m and $1e6$ N/m, respectively. Additionally, reference [61] (review paper) summarises commonly used contact stiffness ranges from $1e6$ N/m to $5e9$ N/m. Within this range, the force behaviour is proved suitable for ballast simulation.

Comparison between different simplifications is used to illustrate the contacts (the model is related to the application of wedge sleeper design, Section 5.1). In the series of simulations, 3 models were the same, except for the complexity of particle shapes. The different complexity of particle shapes include the simplest ball, the highly simplified clumps (spherical surfaces) and the slightly simplified clumps ((non-spherical surfaces). The models analyse the contact behaviour between a (wedge-shape) sleeper and the ballast layer. This box model is shown in Figure 9, and the Particle Size Distribution (PSD) of the ballast layer used in these models is shown in Figure 10. The contact parameters are listed in Table 1.

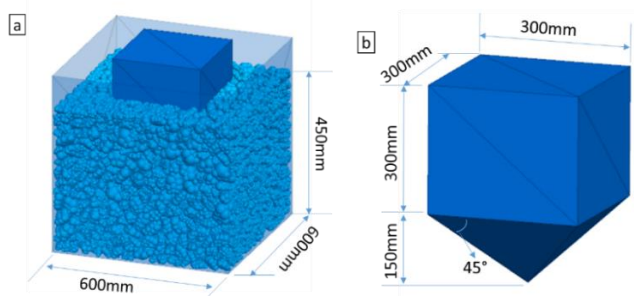


Figure 9. Ballast box model: (a) Ballast box with sleeper, (b) sleeper

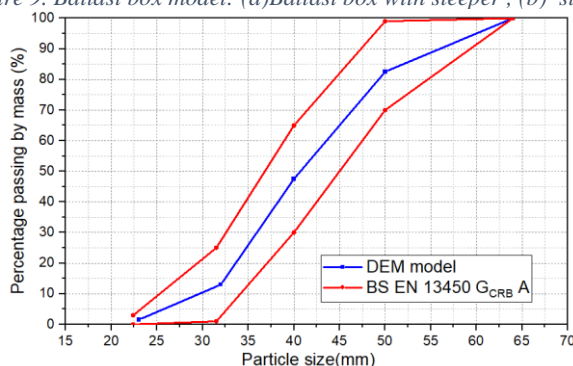

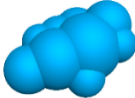
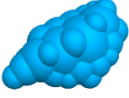
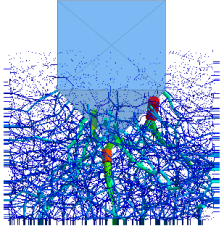
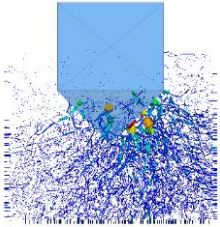
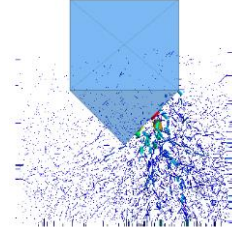


Figure 10. Particle Size Distribution (square mesh sieve size: 22.4mm, 31.5mm, 40mm, 50mm, 63mm)

After the model reaches an initial balanced state, a vertical load is applied to the sleeper, which is then transmitted to the ballast. The results are collected in Table 1, which also includes the Distance/Ratio (D/R) values and representative particles from each model. By using different simplifications of particle shapes, the results show differences in several aspects, such as force distribution, maximum contact force, and displacement. This highlights the importance of using irregular ballast particle shapes. Under the same loading conditions, different levels of shape complexity result in varying behaviours of contact forces. This includes the total contact number (number of activated contact points), force distribution (force chain), and the maximum contact forces on particles and the sleeper. For example, the Maximum contact force of particle-sleeper is 13.5 kN when using ball, and the value of slightly simplified clumps is 80.1kN, the difference is significantly influenced by particles. details can be seen in Appendix Paper II.

Table 1. Influence of different particle shapes on contact behaviour

Shape description	Ball	Clump (spherical surfaces)	Clump (non-spherical surfaces)
Representative particle shape			
D/R value	NA	D120/R0.5	D130/R0.4
Contact force distribution (red for the highest value, blue for the smallest)			
Total contact number	5991	11573	10536
Maximum contact force particle-particle (kN)	1.3	13.0	21.9
Maximum contact force particle-sleeper (kN)	13.5	101.6	80.1

2.2 Particle simplification and assessment

As presented in section 2.1, the particle shape simplification significantly affects the results. A comprehensive analysis of the influence of particle simplification on the results is presented in this section (also in Appendix Paper I). Results show the influence of shape simplification on the accuracy of both macroscopic and mesoscopic behaviour.

2.2.1 Simplified particles

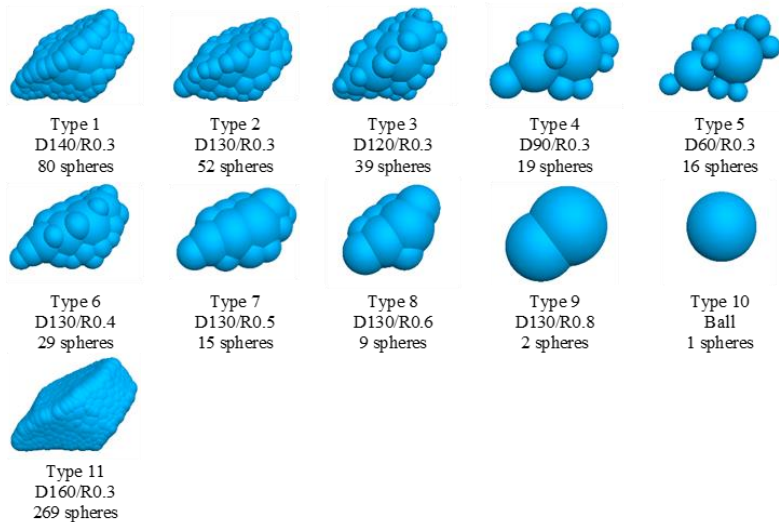
To analyse the effect of the particle shape simplifications 11 ballast particle models of various complexity were generated using the same template of a real ballast particle. As shown in Table 2, those ballast shapes are generated by controlling the arrangement of spheres using 2 parameters, namely Distance (D) and Ratio (R). 11 ballast particle models have been generated, taking into account their complexity.

Type 11 and Type 1 to Type 5 by decreasing the Distance (Group 1). Type 2 and Type 6 to Type 10 are related to an increase in Ratio (Group 2). Type 11 is the reference type; it has the most complex arrangement of spheres and can be regarded as real ballast particle.

To correct the loss of contact behaviour due to shape simplification, the rolling resistance is added to Type 9 (Group 3) and Type 10 (Group 4) by adding the friction coefficient, with values of 0.1, 0.3, 0.5, and 0.7. Because rolling resistance is only a computational parameter used to compensate for the loss of interlocking between the particles, the relatively high rolling resistance of 5, 10, and 100 was used for the particles of Type 10 (ball).

Overall, the particle shapes listed here cover the simplest ball shape to a complex shape close to real ballast. These conditions are expected to show the significance of the parameters for particle generation. The assessment can comprehensively present the behaviour difference caused by shape simplification.

Table 2. Different ballast models



2.2.2 Shape assessment

The analysis of the model accuracy using various particle shapes is performed using the box model described earlier that is shown in Figure 11. A 5Hz cyclic loading is applied to the sleeper to show the behaviour of different shapes. The contact parameters are listed in Table 3. Since the scale of the model is relatively small, the simulations were computationally not expensive. Therefore, every simulation was repeated 10 times (the corresponding model was generated again in each simulation). The presented results are therefore the average values. Finally, all the data are compared to analyse the influence of particle shapes on the behaviour of the assembly.

The DEM simulations provide results in three parts. Firstly, the coordination number that indicates the difference in the number of the contact points due to particle shape. Secondly, the sleeper displacement that is the macroscopic result presenting the influence of particle shape and correction parameters on the behaviour of non-particle elements. Thirdly, the average and maximum contact forces between the particles that characterise the mesoscopic contact behaviour. These three types of results cover all the typically used results of numerical simulations based on DEM. Additionally, the time consumption of the simulations with the different shapes is recorded to highlight the efficiency of the models.

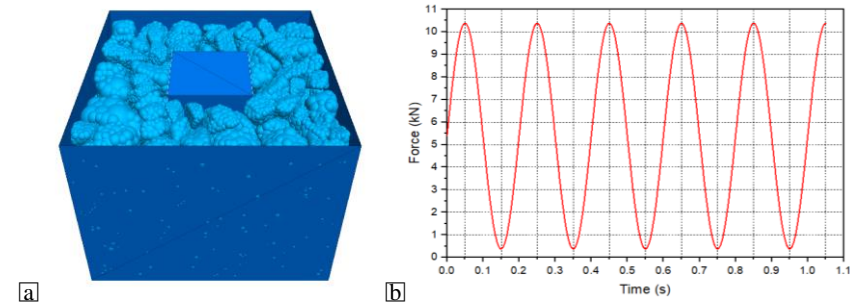


Figure 11. Box model with sleeper embedded (a), and applied vertical load (b)

Table 3. Contact parameters of DEM model

Parameter	Ballast particle	Sleeper/Box
Tangential stiffness (N/m)	1.0e7	6.0e8
Normal stiffness (N/m)	1.0e7	6.0e8
Friction coefficient	0.1/0.3/0.5/0.7/5/10/100	0.5
Mass density (kg/m ³)	2630	-
Damping coefficient	0.7	0.7

Coordination number

The Coordination Number (CN) is the average number of the activated contacts per particle, and is directly related to particle shape. The higher CN indicates more contact points are worked in force bearing and transmitting, resulting in a more uniform force distribution when a load is applied. The CN has a significant impact on the conclusions regarding ballast degradation, as observed in the analyse on contacts forces.

Figure 12 displays the CN of the balanced model before loading. The irregularity of the particles affects the contact points, but the influence is not always significant depending on the parameters used to generate the particle shapes. For Group 1, the particle simplification did not decrease angularity, which still provided interlock. In contrast, Group 2 had decreased angularity due to the increase in Ratio, resulting in fewer contact points. The CN slightly changed for the same shape with different rolling resistance but remained at a similar level. Notably, the CN decreased from 2.7 to 1.7 when comparing Type 10 (reference shape) with Type 11 (ball shape).

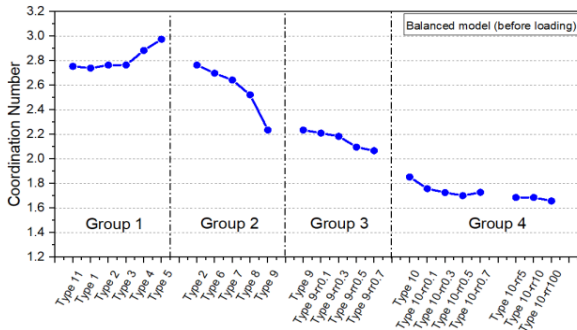


Figure 12. The influence of shape simplification on coordination number (before loading)

Figure 13 shows the coordination number at the final state (after loading). It is increased compared to the same shape before loading because the sleeper works as a compactor under cyclic loading. Note that for Type 10 (ball shape) without rolling resistance, the coordination number is decreased. This is because the ball shape is more likely to rotate, rearrange, and squeeze, thus particles are moving above the sleeper and no longer bearing the applied force. Further explanations can be found in the following section on sleeper displacement.

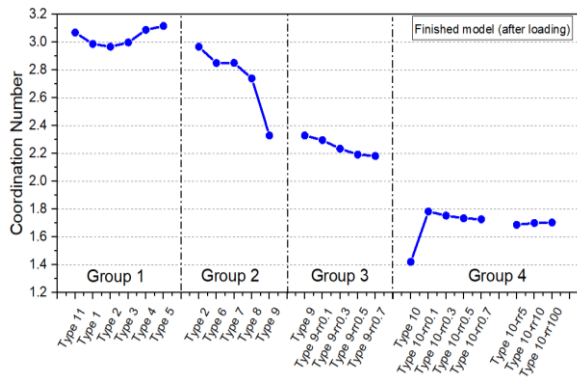


Figure 13. The influence of shape simplification on coordination number (after loading)

Sleeper displacement

The macroscopic results are typically used to present or validate the behaviour of a design that interacts with particles (for example, the performance of a sleeper). In this research, the sleeper displacement is the macroscopic result, and it shows how the sleeper interacts with different shapes of ballast particles.

Figure 14 shows the sleeper displacement of different shapes after loading. In the simulations of the Distance decrease (Group 1), the sleeper displacement only fluctuates slightly. This indicates that the macroscopic results are not influenced by the Distance parameter. This is because although the shape is simplified, the interlock is at a similar level, as seen in the coordination number analysis. On the contrary, with the ratio increase (Group 2), the shape becomes rounder, and the sleeper displacement decreases. Due to the loading method and the scale of the model, the ball shape is more prone to rotation. However, within the confined space of the small fixed box, these rotations do not result in additional voids that could increase settlement.

For the ball shape (Type 10), the sleeper displacement is significantly higher than that of other shapes. When the rolling resistance of 0.1 is added, the value returns to the reasonable range (0.9 mm). The results also show that when the applied rolling resistance is 0.3 and higher, the displacement is even closer to the reference shape than Type 7 (15 spheres). This proves that the rolling resistance can compensate for the interlock loss and contribute to the accuracy of the macroscopic results. Additionally, for Type 9 (2 balls made particle), the influence of adding rolling resistance is not as significant as it is on Type 10 (ball) because this shape still provides resistance to rotation by itself.

PI

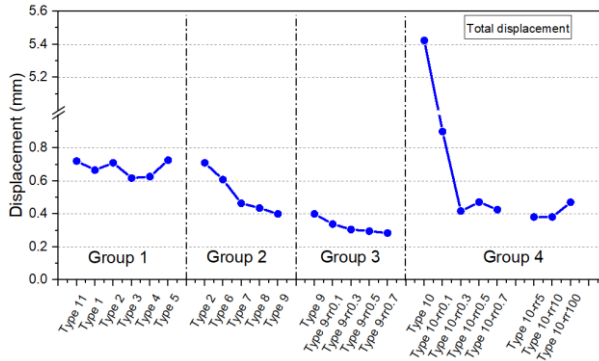


Figure 14. The influence of shape simplification on sleeper displacement (in total)

As described above, in macroscopic results, where the behaviour of particles is not the primary consideration, the accuracy of the results is predictable. Therefore, structure-focused simulations can opt for ball-shaped particles and apply rolling resistance to reduce calculation effort. Additionally, the rolling resistance of 0.3 already indicates compensation for the interlock loss due to shape simplification.

Contact force

The contact force between particle is a mesoscopic result. However, the macroscopic results of different particle shapes can be similar. The contact force shows differences, which are crucial to the accuracy of the results. Significant changes can be found here compared with the sleeper displacement. The average contact force is shown in Figure 15. The average contact force is increased mainly because a fewer number of contact points are participating in loading bearing.

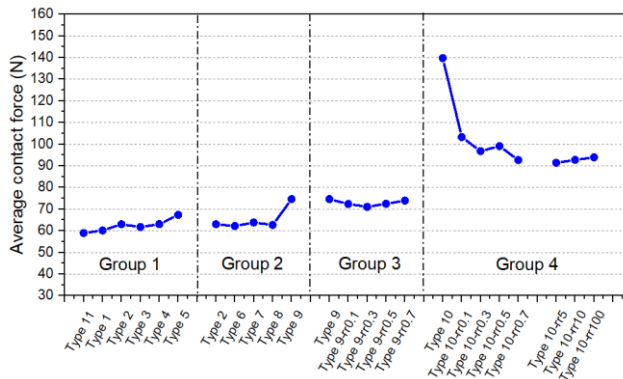


Figure 15. The influence of shape simplification on average contact force

It should be noted that Type 4 and Type 5 in Group 1, despite the increase in the coordination number, show an increase in the average contact force. This phenomenon contradicts the theory that a larger coordination number leads to a smaller average contact force because the particle shapes of Type 4 and Type 5 are no longer a "natural coarse" surface due to the knobs present on them.

The maximum contact force is shown in Figure 16. Some fluctuations are observed, which result in slight differences in shape simplification. Type 10 (ball) still shows the highest maximum contact force, as it is related to force concentration.

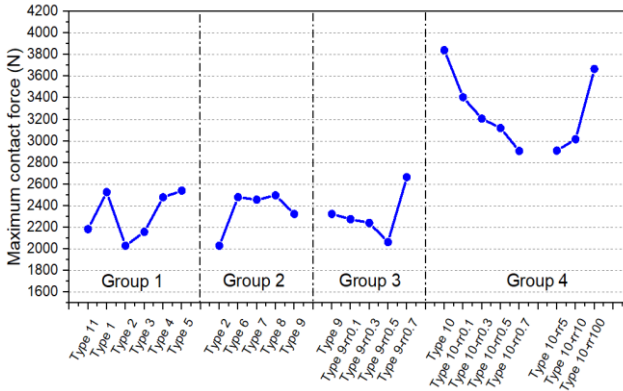


Figure 16. The influence of shape simplification on maximum contact force

Table 4. Activated contact number of different shape (counted by force)

Force range (N)	Type 11 Reference	Type 1	Type 2	Type 6	Type 9	Type 10
>3000	0.2	0.4	0.1	0.1	0.1	1.7
2000-3000	1	0.8	0.4	1.1	0.7	3.2
1000-2000	7.7	5.9	6	6.4	8.7	15.2
500-1000	26.8	23.3	23.3	24.1	27.2	35.7
100-500	231	244.1	230.8	201.3	222.3	178.1
<100	1292.4	1332.6	1322.2	1273.6	1057.8	600
Total	1540.6	1607.1	1582.8	1506.6	1316.8	833.9

Force range (N)	Type 9/rr0.3	Type 9/rr0.7	Type 10/rr0.3	Type 10/rr5	Type 10/rr100
>3000	0.1	0.3	0.6	0.5	1.1
2000-3000	0.3	1	2.2	2.7	3.4
1000-2000	6.8	8.8	11.4	9.2	11.2
500-1000	28.6	25.8	29.6	27.2	23.9
100-500	191.3	183.4	173.3	160.4	147.2
<100	1040.1	1006.9	770.4	753.4	778.1
Total	1267.2	1226.2	987.5	953.4	964.9

As a further explanation, the number of contacts counted by force range is partly listed in the Table 4 (full table is shown in Appendix Paper I). Those numbers are also the average values of 10 random repeated simulations. Most forces are smaller than 1kN. The results show that the shape simplification by Distance decrease leads to a relatively smaller number in the high force range due to the “unnatural

coarser surface”. Moreover, for most of the contacts (more than 99%) in the lower range (<500) the contact number fluctuates insignificantly. Those results explain why the macroscopic results are not significantly influenced by Distance.

On the contrary, the simplification by Ratio increase leads to a decreasing trend of the contact number in the lower force range and a sharp decrease in the total contact number. Under the same loading condition, the contact number of a higher range is increased. When applying the rolling resistance on Type 10 (ball) to correct the force behaviour, the total activated contact number increased, and the number distribution in each range was more uniform than Type 10 without rolling resistance.

All the above results show that the shape simplifications can distort the mesoscopic results, decreasing the accuracy from high to low. However, the macroscopic results are not sensitive to shape simplification and can be corrected. Therefore, shape simplification can be used depending on the demanded balance of time consumption and accuracy.

Computational time

For a given scale, such as the box model, the accuracy of a DEM simulation is inversely proportional to the complexity of the particle shapes used. Higher-fidelity particles require greater computational effort, and the time required for calculations is a limiting factor. Therefore, model simplification is a direct motivation for reducing the computational time consumption. Therefore, the time required for models with different shapes was recorded. As shown in Figure 17, the model's time consumption is directly related to the complexity and the number of elements. The reference Type 11 calculation took approximately 5 hours. When the shape was simplified to Type 2, the time was reduced to less than 0.5 hours, and when the shape was simplified to a sphere, the simulation for 1.05s took around 3 minutes.

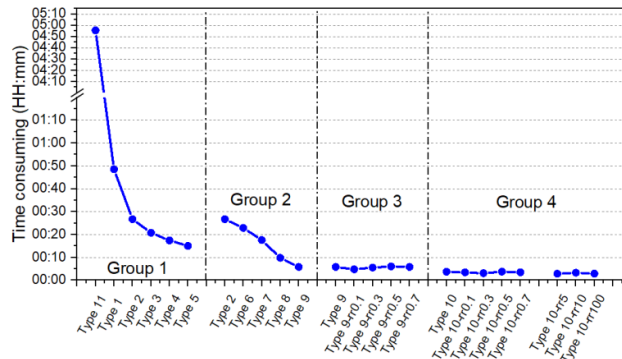


Figure 17. The influence of shape simplification on calculation effort

2.3 Additional explanation

The shapes presented in the former sections are related to simplifications, and they can also be related to the condition of the ballast. For instance, in the appendix paper IV, the study on recycled ballast highlights the difference between fresh and degraded ballast by controlling the shape. The shapes obtained through 3D scanning are shown in Figure 18.

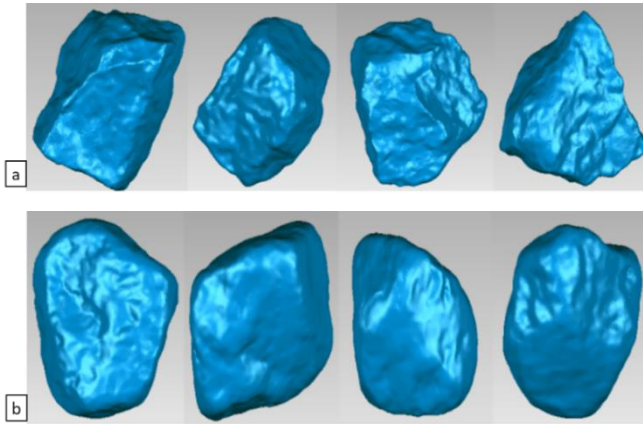


Figure 18. Shapes obtained by 3D scanning: (a) Fresh ballast, (b) Recycled ballast

In the model, Figure 19(a) was set with more angularity using Distance 120 and Ratio 0.3 to present fresh ballast, and the clump in Figure 19(b) was smoother with Distance 150 and Ratio 0.3 to present recycled ballast. The border of those 2 ballast models were exported in 2D image as Figure 19(c) and (d) for roundness calculation.

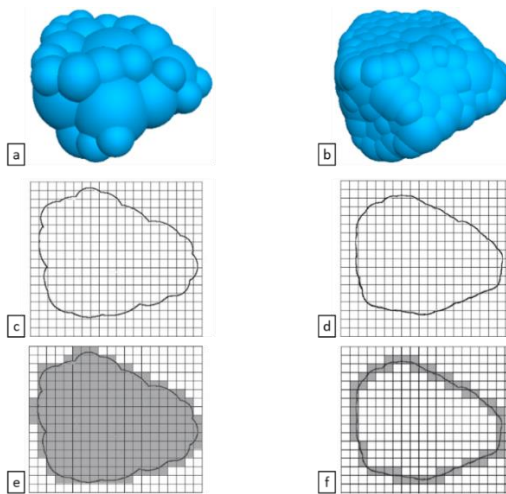


Figure 19. Ballast particle models in DEM simulations: (a) Fresh ballast, (b) Recycled ballast, (c) The border of fresh ballast, (d) The border of recycled ballast, (e) The sketch map of A , (f) The sketch map of p

By the method in reference[62], the roundness can be calculated using the following expression

$$R_n = \frac{4\pi A}{p^2} \quad , \quad (1)$$

where R_n is the Roundness Index (RI); the value of 1 indicates a perfect rounded shape, which means the most rounded shape. The closer the value is to 1, the rounder and less angular the shape is. A denotes the area of the particle projection, which corresponds to the number of pixels

(0.2639mm/pixel) within the border as shown in Figure 19(e). The perimeter of the particle, which corresponds to the number of pixels surrounding the ballast, is denoted as p , as shown in Figure 19(f). Based on (1) the RI for fresh ballast is 0.6737, and the value for recycled ballast is 0.7729. This difference in RI provides a means of distinguishing between the two types of ballast.

Different friction coefficient is used to present the wear of the surface texture. The linear contact model is selected for ballast particles due to its cohesion-less physics [63]. The mechanical parameters of the ballast particles and the shear box in PFC3D are summarised in Table 5, which are referred from former studies [64, 65] and verified corresponding to laboratory tests. The simulation does not include ballast breakage or abrasion as their influence on the direct shear test is considered negligible. By omitting these factors, the calculation efficiency can be improved.

Table 5. Parameters of linear contact model in simulations

Parameters	Fresh Ballast	Recycled ballast	Shear box
Distance	120	150	-
Ratio	0.3	0.3	-
Tangential stiffness(N/m)	$1e^8$	$1e^8$	$6e^8$
Normal stiffness(N/m)	$1e^8$	$1e^8$	$6e^8$
Friction coefficient	0.5	0.47	0.2
Mass density(kg/m ³)		2630	
Damping coefficient		0.7	

The model was verified through a series of direct shear tests and simulations, The strain-stress curve of simulations and laboratory test for fresh ballast and recycle ballast are shown in Figure 20(a) and (b), respectively. The peak data and changing trend of the curves highly match, indicating the validity and accuracy of the particle shapes used in the simulations. the validation proved that the shape simplification also can be used to simulate different materials according to their properties.

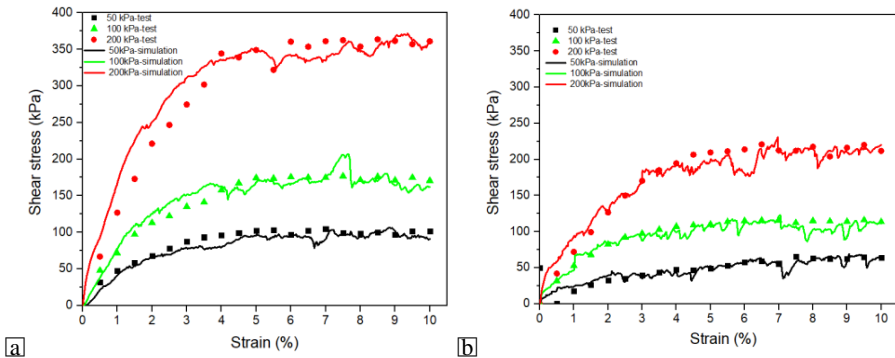


Figure 20. Comparison of the simulation and the laboratory test results: (a) fresh ballast, (b) recycled ballast

2.4 Conclusions

In this chapter, the ballast particle shape generation is introduced, and the influence of the particle shape on the accuracy of the results is analysed. The focus is mainly on shape simplification, which is analysed using different shapes generated by controlling two parameters: Distance and Ratio. The rolling resistance (friction coefficient) is applied to the simplest ball and 2-sphere shape to

compensate for the loss of interlocking between the particles due to shape simplification. The macroscopic and mesoscopic results are obtained, compared, and analysed by a series of box loading tests, including the coordination number, contact force, and sleeper displacement. Based on the above-mentioned results and analysis, the main conclusions on shape optimizations are listed below:

1. The computational time can be drastically decreased by simplification of the particle shape and texture (Figure 17 Group 1-4).
2. The level of complexity of the particle has different influence on the macro- and mesoscopic results. Therefore, the simplification of the particles should be applied depending on which effects (e.g. ballast bed settlement or ballast particle breakage) are important and which results (on macro- or meso- level) are needed.
3. In case of the macroscopic results are of interest:
 - a. the complexity of the particle can be reduced even without compensation in contact law (Figure 14 Group 1).
 - b. when drastically reducing the complexity of the particle, the loss of accuracy of the results can be compensated by adjusting the contact law and using the rolling resistance to compensate for the loss of interlocking between the particles (Figure 15 Group 4).
4. In case of mesoscopic results are of interest, the simplification of the particle complexity is not recommended since the loss of accuracy of the results cannot be compensated by adjusting the contact law.
5. In case of the simulations, which considering the fresh and degraded ballast, the different particles can be used by controlling shape complexity and surface friction coefficient (Figure 19 and Figure 20).

Chapter 3 Optimised DEM model building method

The DEM model building method is the foundation of the simulations. The status of a generated ballast layer, such as porosity and force balance, is vital to accurate and reliable results. However, the efficiency of the typically used model building method is low, and it may take days to generate a desired model.

This chapter introduces an improved model building method and describes its efficiency verification by comparing it with the currently most popular model building method. Then, the Adaptive shape simplification refinement model building method developed based on the optimized model building method is described. It is specially developed for mesoscopic results that the particle shape simplified model cannot accurately represent (analysed in Chapter 2).

3.1 Optimised model building method

During the model building, i.e. preparing a model for simulation, a proper code flow to control the process is needed. Normally, methods that generate a dense granular assembly in a loose state are followed by compacting the layer to a required porosity. One such method is the dropping method, which is briefly introduced in this chapter and consists of four steps, as shown in Figure 21 (Also in Appendix Paper II).

This method maintains model balance throughout the model building process, making it safe but not very efficient, because the method uses only natural (gravity) solutions to eliminate the unbalanced forces, and the balanced force state only can be reached using automatic timestep (which means longer calculation time). The 4 steps of the dropping method are as follows:

1. Fill a tall box with clump elements with high porosity;
2. Drop these particles and compact them by applying extremely high gravity (100g). Such high gravity is used to increase the dropping efficiency;
3. Re-set the gravity to natural value and continuously repeat the calculation to cease the bouncing of the particles after gravity reset;
4. Generate a sleeper, delete clumps inside the sleeper, and iterate to the balanced force state.

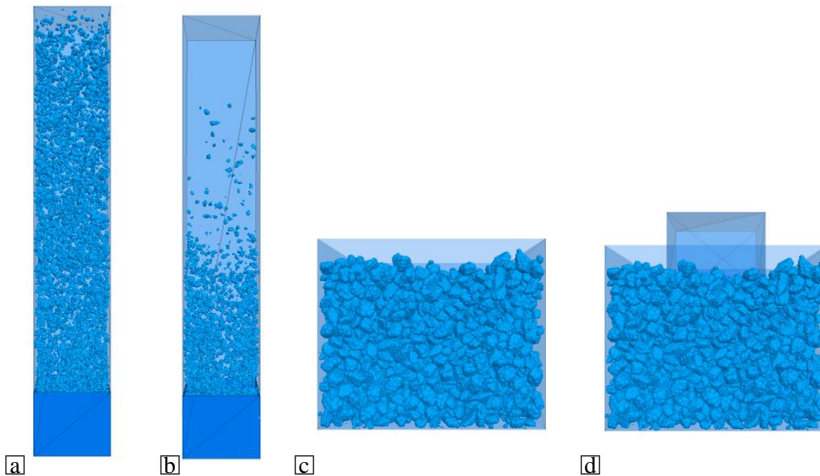


Figure 21. Dropping method: (a) Filling tall box with clump particles, (b) Dropping particles, (c) resetting gravity, (d) Generating sleeper and deleting particles inside the sleeper.

An improved model building method is proposed to optimize the efficiency and feasibility of the DEM in railway applications. The method is based on the particle replacement and radius adjustment (PRRA). This method is a user-controlled process used instead of the natural (gravity) solution. It only considers and eliminates the unbalanced force state in the last stage by adjusting the radius of the clump elements to reduce the particle overlapping. Thus, the enlarged timestep can be used in other steps. The method involves 7 steps as described below and illustrated in Figure 22.

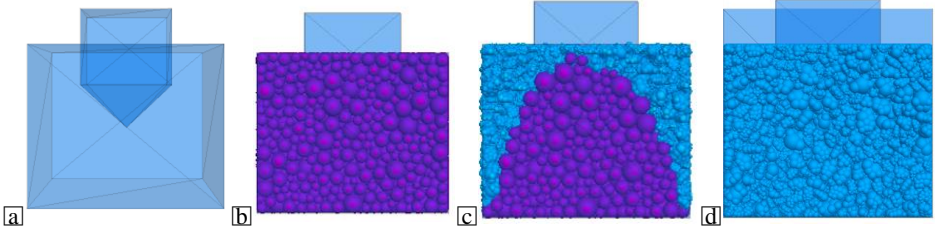


Figure 22. Particle replacement and radius adjustment method: (a) Box and sleeper definition, (b) Filling the box with ball elements, (c) Replacement & expansion, (d) Balanced model

1. Import all the shape files, including the template for clump, the sleeper and the box;
2. Fill the box with ball elements according to the PSD and porosity. At this stage, the enlarged timestep will be used to enhance calculation efficiency;
3. Set the gravity and parameters for the balls and the box;
4. Iterate (calculate) using gravity until the unbalanced force is almost zero;
5. **Replace** the balls by clumps. The clumps have the same volume and position. At this stage the material and contact parameters are applied to the clumps;
6. Perform the clumps **radius adjustment**. A spherical ball and an irregular clump have different geometries. Therefore, after replacement, the force state of the model is changed caused by overlap of clumps. Radius adjustment is used to eliminate the high contact forces caused by clump overlaps, thus reaching the final balanced force state. The following empirical adjustment coefficient β was proposed:

$$\beta = -\lambda V_b \Delta \sigma k_{sum}^n \quad (2)$$

Where: β is the expansion/reduction coefficient

λ is the dimension of the model (in a 3D model, the value is 3)

V_b is the volume of the whole ballast bed model (or the box model)

$\Delta \sigma$ is defined by: $\Delta \sigma = \sigma_{in} - \sigma_m$

σ_{in} is the input target stress

σ_m is the average stress of the model

k_{sum}^n is defined by: $k_{sum}^n = \sum_i (k_i^n * (R_i^a + R_i^b) * R_i)$

R_i^a is the radius of the pebble (which is included in a clump and direct contact another element) at the contact end, (if the end is a wall then the value is 0)

R_i is the distance, tangential component of vector from the contact point to the centroid of the element

k_i^n is the stiffness of the i th contact

n is the total number of the particles in the model.

7. Set the enlarged timestep back to automatic timestep, ensuring the stability of the model for further calculations.

Note that the adjustment coefficient is very small and therefore during this process the changes in the PSD are negligible.

In comparison, the dropping method (the clump shape, particle size distribution, contact parameters, and the method to detect the balance state were the same) took 39.5 hours to complete the model, while the particle replacement and radius adjustment method took only 1.2 hours, resulting in an efficiency improvement of approximately 40 times. Based on the experience, when the scale of the model is larger, the efficiency improvement may be lower, but it can still be at least 10-20 times faster because of the limitation of CPU.

3.2 Adaptive particle shape simplification

With the aforementioned knowledge, the particle replacement and radius adjustment method also provides a possibility to generate an assigned ballast shape in a specific area of the model, which is impossible to do using the traditionally used dropping method. Based on that, a Adaptive Particle Shape Simplification (APSS) building method has been developed. As a case to demonstrate the efficiency improvement by the multi-layer model and APSS optimised model, the single sleeper section of a ballasted track has been built in this section.

The reference model, using clumps for all particles, is shown in Figure 23. It is the commonly used full-scale model before optimization. The model contains 647,323 ballast particles elements, and 86 elements representing the sleeper and the boundary wall. The boundary wall is shown with the transparency setting and is not displayed in the consecutive figures. Related research using this model can be found in references [36, 66-68] wherein accuracy of the model were validated.

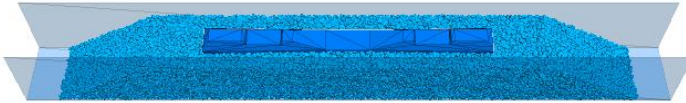


Figure 23. Clump-built model of a single sleeper section

Also, an additional reference model is built with ball particles to show the loss of behaviour due to shape simplification, as shown in Figure 24. This model is calculated with and without Rolling resistance separately. The model contains 24,394 ballast particle elements, with 86 elements for the sleeper and boundary wall.

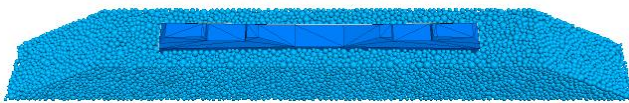


Figure 24. Ball-built model of a single sleeper section

The multi-layer model, which aims to reduce the number of elements while maintaining relatively high-fidelity results, is shown in Figure 25. This method uses the ball-shaped particles as ballast in the bottom layer and the irregular-shaped particles (clumps) in the area where the sleeper contacts the ballast. It ensures that the sleeper is in good contact with the clump particles.

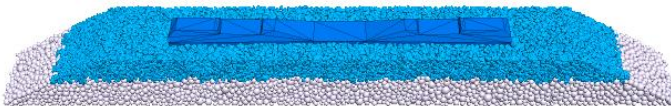


Figure 25. Multi-layer model with clumps and balls of a single sleeper section model

This method significantly reduces the number of elements in the model, with 14,887 ball-shaped elements and 229,222 irregular-shaped elements (clumps), making a total of 264,109 particles. The bottom layer is simplified to ball shape, and rolling resistance is added to simulate interlocking between the irregular particles. The number of elements for the sleeper and boundary wall is 86, which is the same as the reference model. Compared with the model built with only clumps, this multi-layer model reduces the number of elements by 59%.

Furthermore, the simplification can be optimized based on different test types, i.e. APSS optimisation such as loading-controlled tests or displacement-controlled tests, depending on the loading conditions. For instance, in a settlement test where the loading condition is vertically applied to the sleeper, the most significant ballast is situated at the bottom of the sleeper. Therefore, the bottom ballast particles should be represented as irregular clumps, while other particles such as crib and shoulder ballast can be simplified to the ball. This indicates that the multi-layer model is optimized based on force distribution. The APSS method is illustrated in Figure 26.

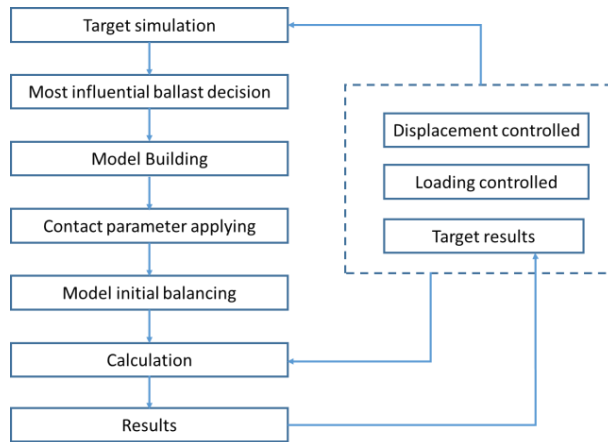


Figure 26. Process of Adaptive Shape Simplification method

As a case to show the APSS in model building process, the optimised single sleeper section DEM model specially for lateral resistance simulations is shown in Figure 27,

The ballast in the most influential area is generated by the clump elements with a linear contact model, and other particles are the ball elements with rolling resistance linear contact model. This model-building method ensures that the number of elements is decreased to the largest extent possible. It contains 19358 ball elements and 131388 clump elements, which amount to 150746 total particles generated. The number of elements for the sleeper and boundary wall is 86. Compared with the reference model (fully clump-built model in Figure 23), the total number of elements decreases by 77%.

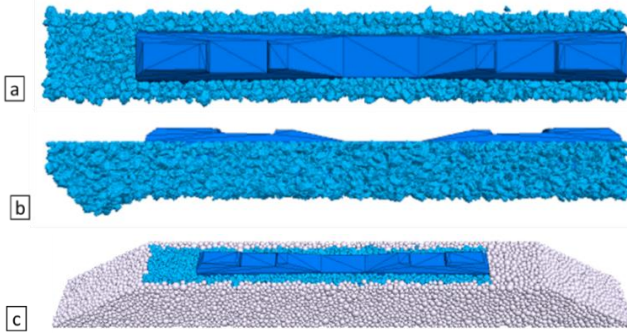


Figure 27. APSS Optimized model of a single sleeper section: (a) Top-view of the clump-build layer, (b) Side-view of the clump-build layer, (c) Over-view of the model

The most influential area in the above model is defined by a previous work of the author, where Particle Image Velocimetry (PIV) was used to analyse the displacement distribution [67]. The ballast displacement can be obtained through video analysis, as demonstrated in Figure 28 and the ballast displacement map shown in Figure 29. These results provide information on the most influenced (displacement) ballast area.

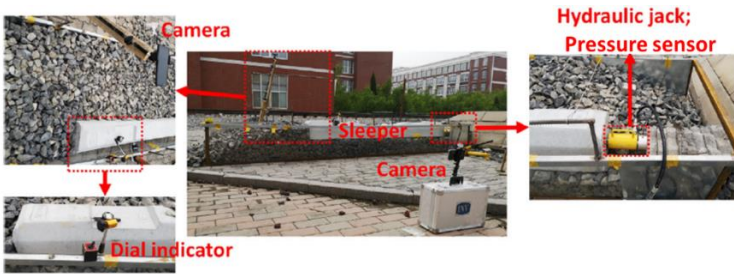


Figure 28. PIV setting on lateral resistance test [67]

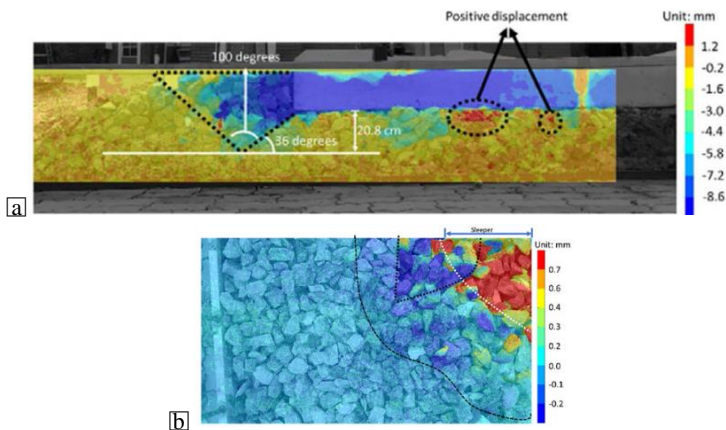


Figure 29. PIV data of the lateral resistance test (under 7mm sleeper displacement): a) Side-view of ballast displacement, b) Top-view of the ballast displacement [67]

3.3 Validation of APSS optimised model

In order to validate the optimised model using APSS method, a single sleeper pushing test is conducted on the 3 different models. A lateral velocity is applied to the sleeper, and it is stopped when the sleeper displacement reaches 5mm. During this process, the contact force-displacement data of the sleeper is recorded. In addition, the force distribution at the end state is saved to show the difference between each model, thus providing validation. The assessed models include the reference model (using Hi-Fidelity particles), multi-layer model, APSS optimised model, and ball-build models (with or without rolling resistance). The time consumption shows efficiency. All results are listed in following Table 6.

In Table 6, the clump-built model took 43.38 hours, whereas the ball model only costs 2.5 and 3 hours. This result highlights the significant impact of the number of elements on efficiency. With optimisation, the efficiency has been greatly improved. The multi-layer model (half clump and half ball) took 15.75 hours. For the further APSS optimised model, the time consumption was 10.41 hours, and the force behaviour was also the closest to the results of the clump-built model. The force-displacement curves of the sleeper are shown in Figure 30 below. The increasing trend and peak force between the reference model and the optimised multi-layer model are in a similar state. In contrast, the results of other models are less reliable.

Table 6. Key performance of lateral resistance simulations

Particle type	Time consuming	Peak lateral force (sleeper)	Maximum contact force (particle)
Clump (Reference model)	43h 23 min	12.03kN	2.18kN
Multi-layer Half clump/ half ball by height	15h 45 min	9.92kN	1.56kN
APSS optimised model	10h 25min	11.20kN	2.93kN
Ball With rolling resistance	2h 32 min	16.02kN	4.65kN
Ball Without rolling resistance	3h 05 min	3.76kN	0.37kN

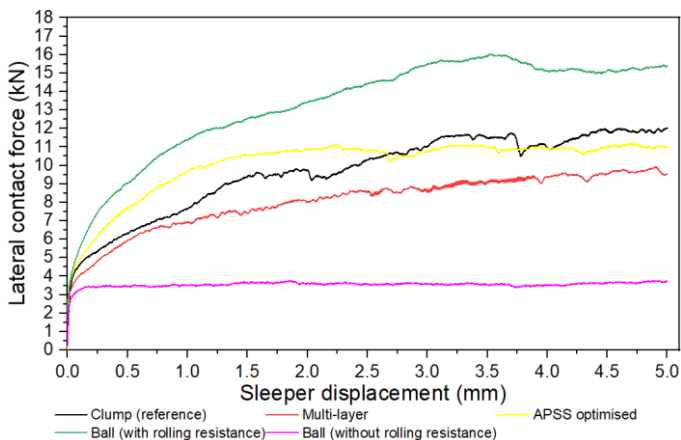


Figure 30. Sleeper displacement-lateral contact force curve

Furthermore, it is noteworthy that the inclusion of rolling resistance significantly increases the peak lateral force from 3.76kN to 16.02kN as it restricts particle movement and compensates for shape loss due to interlocking. Interestingly, the peak lateral force of the ball-built model with rolling resistance is even higher than that of the clump-built model. However, it is important to note that using a lower value of rolling resistance may not necessarily result in better accuracy, as illustrated in section 2.2.

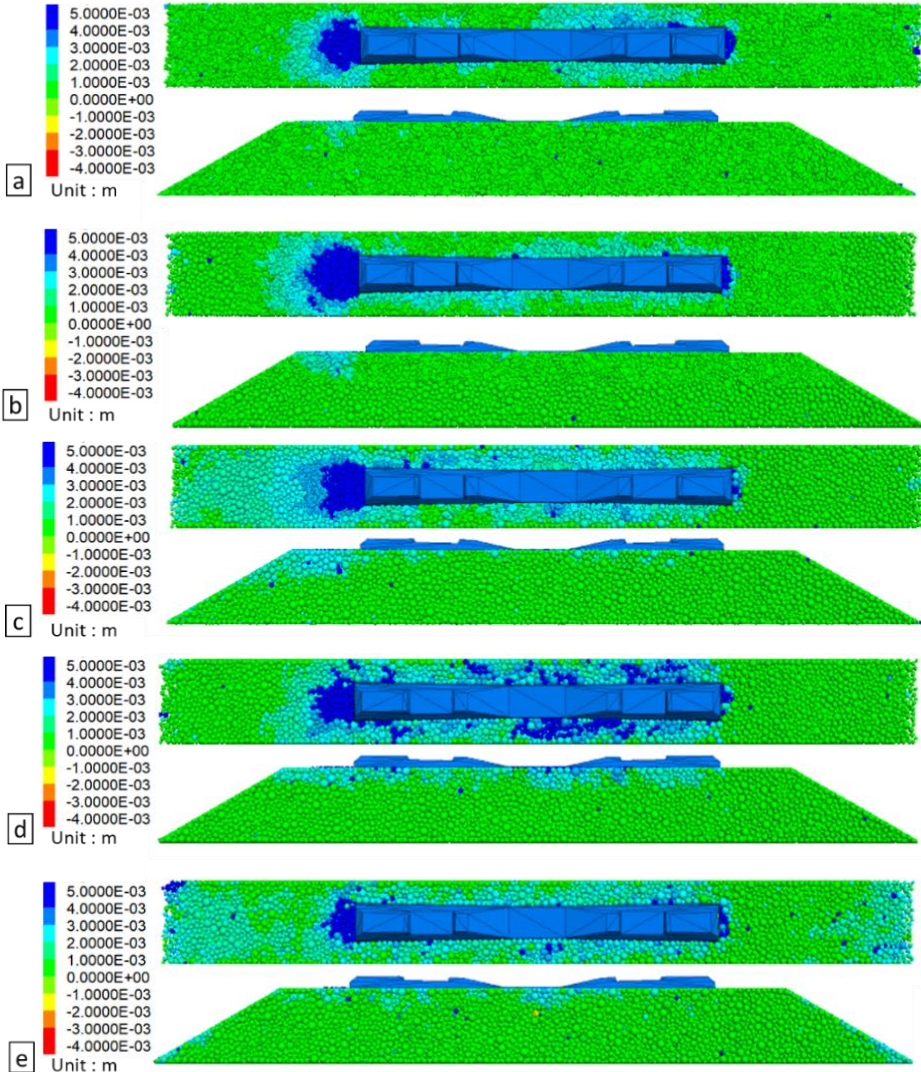


Figure 31. Ballast displacement under 5mm sleeper displacement: (a) Reference model (all particles are clump), (b) Multi-layer model (Half clump and half ball, by height), (c) APSS optimised model (based on most influential ballast area), (d) Ball-built model (with rolling resistance), (e) Ball-built model (without rolling resistance)

The accuracy of the APSS optimised model is further demonstrated through particle displacement (Figure 31) and the force distribution (Figure 32) analysis, which highlight its high accuracy compared to the reference model. Therefore, the APSS optimised model not only exhibits higher efficiency but also higher accuracy.

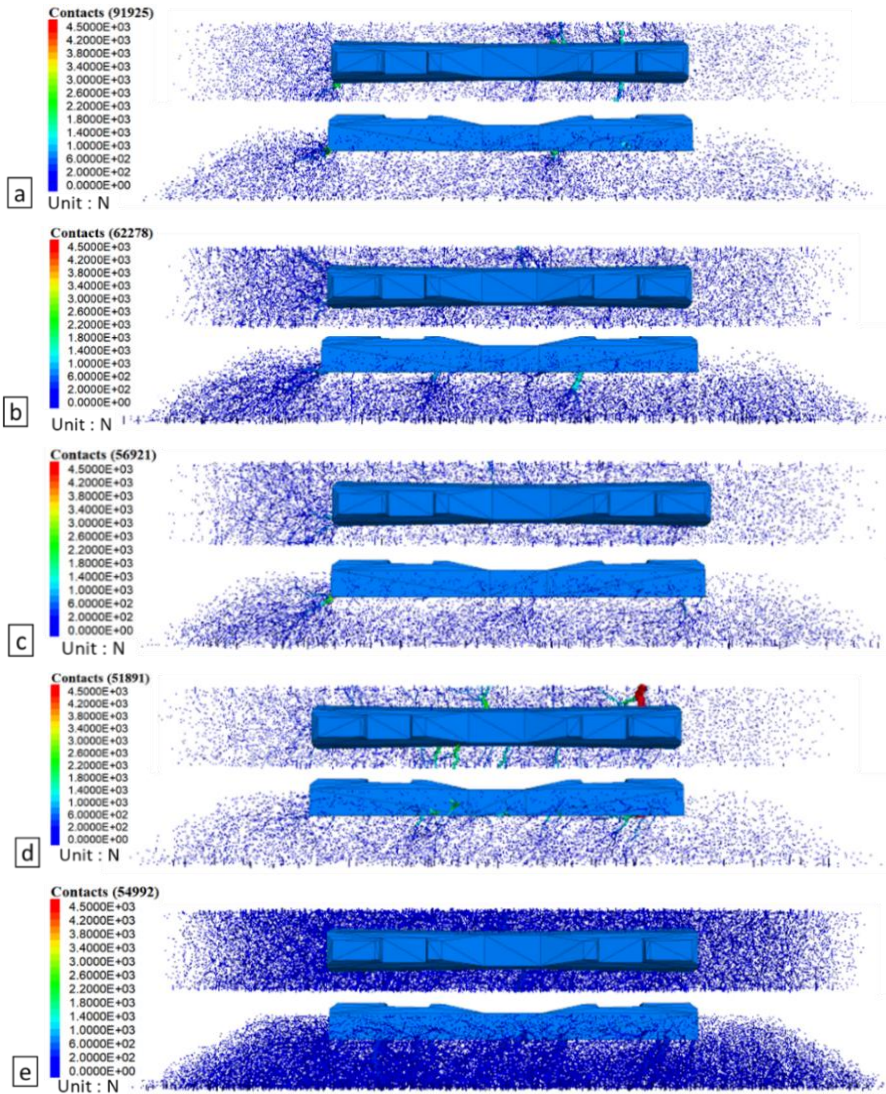


Figure 32. Contact force chain under 5mm sleeper displacement: (a) Reference model (all particles are clump), (b) Multi-layer model (Half clump and half ball, by height), (c) APSS optimised model (based on most influential ballast area), (d) Ball-built model (with rolling resistance), (e) Ball-built model (without rolling resistance)

3.4 Conclusions

For ballast research, the DEM simulations can provide mesoscopic results. However, the efficiency problem restricts the usage of this method. Except for the particle shape, the model building process is also a source of low efficiency. It may take days to prepare a balanced model for simulation. The model building method can be optimised, and thus developed. In this chapter, the Particle Replacement and Radius Adjustment method (PRRA) is introduced, this method is quicker and more controllable compared with typically used method.

In addition Adaptive Particle Shape Simplification method (APSS) is introduced. It is based on the PRRA, using complex shape in the most influential area, and simplifying the ballast shape to sphere in other areas. It focuses on the mesoscopic results, increases efficiency, and maintains accuracy.

The main conclusions are listed below:

1. PRRA method:
 - a. The method can increase the efficiency in model building stage, with a 10-20 times faster speed than the typically used dropping method. The increase comes from that the PRRA allows to use enlarged timestep.
 - b. The method also allows for precise definition of particle shape in specific areas. It is a universal method for all kinds of simulations to generate a granular layer.
2. APSS optimisation:
 - a. This method increases efficiency and maintains accuracy, by simplifying the particle shape according to the particle position, i.e. the most influential areas.
 - b. In general, when using the most influential areas (layers), a narrower area contributes to high efficiency but less accurate results. A proper definition can reach the optimum equilibrium point between efficiency and accuracy.
 - c. In defining the most influential area for different simulations. The area selection should be based on the type of simulations and the target results. For example, Particle Image Velocimetry (PIV) tests can be used in area definition for a lateral resistance simulation.

Chapter 4 Co-simulation method

As mentioned in the previous chapters, the 3D DEM model has been optimized and its efficiency has been improved for the macroscopic results by shape simplification, and mesoscopic results by shape assessment and multi-layer model. However, those optimisations on shape simplification and model building still require months or years to answer a long-term- (under cyclic loading) or dynamic-related questions. Additional simulation methods are needed to be developed to increase the feasibility of DEM models.

In this chapter, two co-simulation methods are introduced, combining the advantages of different modelling method. The first method combines 2D and 3D DEM modelling to analyse long-term behaviour of ballast-sleeper interaction, which provides solutions for macroscopic (sleeper-related) results. The second method combines FEM and DEM modelling to analyse the mesoscopic behaviour (particle-particle contacts) of ballast layer under dynamic loading.

Models and simulations in this section is related to the design of wedge sleeper, as shown in the following Figure 33. The working principle of the wedge sleeper is that the crib and shoulder ballast can, via gravitational forces and dynamic vibration during train passage, migrate into the gap between sleeper and ballast. This behaviour works as (automatic) settlement correction in transition zones, aiming to diminish the degradation caused by hanging sleeper. Details can be found in Appendix paper III.

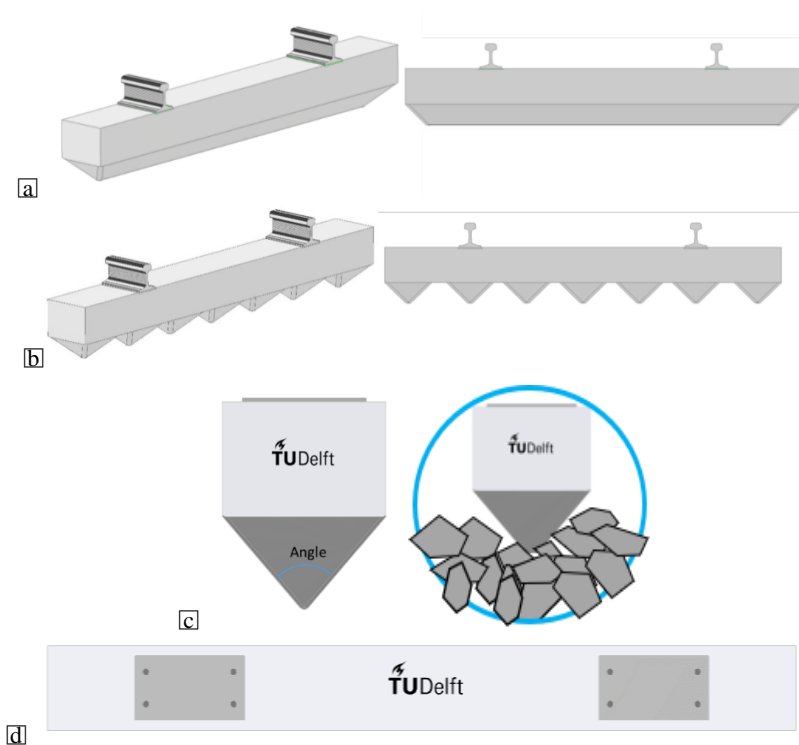


Figure 33. Wedge-sleeper designs. (a) Single wedge design, (b) Multi-wedge design, (c) Side-view of both designs, (d) Top-view of both designs

4.1 2D & 3D model

In the 2D and 3D co-simulation method, 2D DEM simulations were used to study longer-term settlement behaviour instead of 3D simulations due to their higher efficiency. The 2D DEM models are timesaving, making long-term behaviour analysis possible, but the accuracy is low. The calculations show that even if the same parameters are used to build models, the results still qualitatively vary, because the 2D DEM model only contains a limited number of elements (as explained in Appendix Paper III). The 3D models in cooperation are used to simulate a short time period within the 2D DEM simulations. Then, the contact results, especially the force, are used to calibrate the 2D model. Details can be found in Appendix Paper III.

An example of 2D and 3D co-simulations, the models (in Chapter 5), which involve the application of the wedge sleeper design, are briefly introduced here. The example shows how the calibration is used to distinguish and discard the incorrect model.

The contact force distribution and displacement results in Figure 34 show typical example of incorrect calculation (the design of the wedge sleeper, which provides the self-levelling function to correct settlement). The incorrectness was detected when the force and compaction status of ballast was compared against the results of the more accurate 3D simulations, as shown in Figure 35.

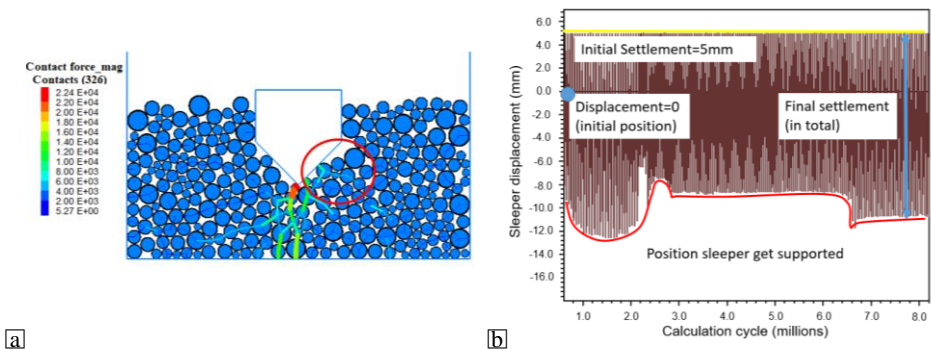


Figure 34. A case of wedge sleeper with bad correction: (a) Contact force distribution(units: N), (b) Sleeper displacement (units: mm)

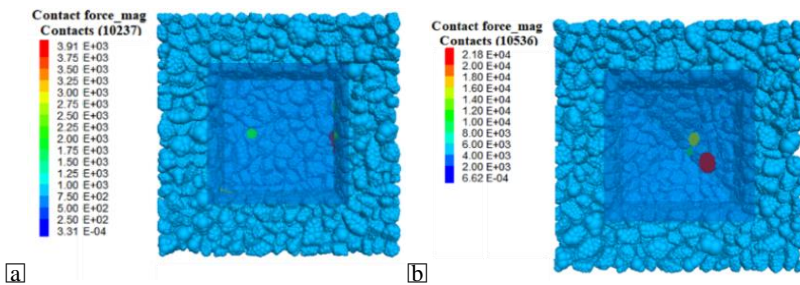


Figure 35. Contact force on sleeper (unit: N): (a) Mono-block sleeper, (b) 45-degree wedge sleeper

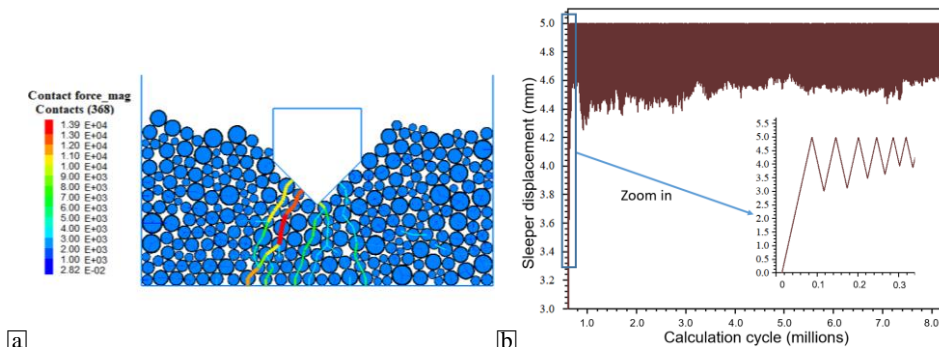
Note that the curve shape in Figure 34 contains around 500 loading cycles (8.2million calculation cycles) in a limited axle length, thus leading to a dense and black layout. As an explanation, the curve contains 4 parts:

- a. The zero point is the sleeper location before settlement;

- b. The top yellow line is the location of the sleeper after the initial settlement. The location is fixed because of the restriction of the fastening system and rail;
- c. The red bottom line is the location of the sleeper when the loading (of the wheel) is fully applied on the sleeper;
- d. The distance between the yellow line and the red line is the settlement under cyclic loading.

In detail, the settlement of the failure model is 16mm in total, and no settlement correction through all the loading cycles. This behaviour is attributed to the un-compacted contact between the sleeper bottom and the ballast (shown in the red circle in Figure 34). In addition, the maximum contact force is 2.25kN, which is observed at the tip of wedged sleeper, but this peak force did not appear in the 3D model (Figure 35). All of the force and compaction status of ballast are against the results of 3D simulations. For this reason, this simulation is considered to be incorrect then discarded.

On the other hand, a correct 2D DEM model, which produced results consistent with the 3D DEM simulations, is illustrated in Figure 36. In this case, the settlement correction occurred at the beginning of the cyclic loading, and the final correction was over 4mm. The sleeper remained stable throughout the cyclic loading process. In the 2D DEM simulations, the maximum contact force observed was 13.9kN. The distribution of contact force was similar to that of the 3D ballast box model, as shown in Figure 35. Both the force distribution and the maximum contact force agreed with the 3D simulations (as shown in Figure 35(b)). Hence, this model was deemed suitable for further analysis.



a

b

Figure 36. A case of wedge sleeper with good correction, (a) Contact force distribution (unit: N), (b) Sleeper displacement (unit: m)

In the case of mono-block sleepers, the 2D results were generally consistent with the 3D results, although calibration was still conducted to ensure accuracy. Figure 37 shows a representative result, where no correction effect was observed and the maximum force appeared near the edge of the sleeper bottom. The force distribution and maximum contact force were in agreement with the 3D simulations.

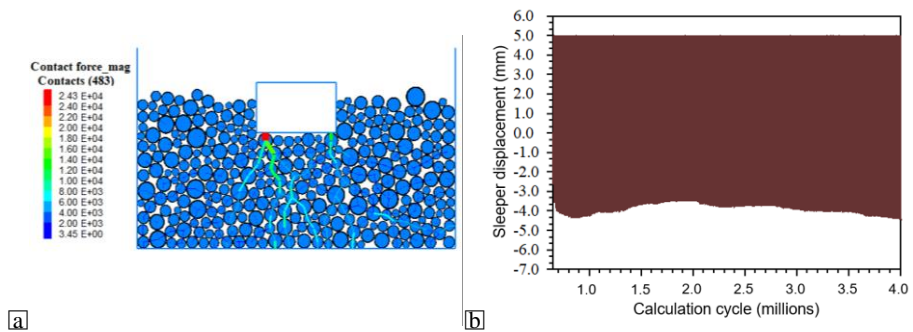


Figure 37. A case of mono-block sleeper, (a) Contact force distribution (unit: N), (b) Sleeper displacement (unit: m)

The DEM simulations provided both mesoscopic and macroscopic results. The particle shape and contact behaviour were verified in the author's previous research using 3D models. The force distribution of the 2D models were qualified through calibration and the incorrect calculation was discarded. The remaining 2D models exhibited similar mesoscopic results. Since the macroscopic results are the external manifestation of mesoscopic behaviour, the 2D models were also verified through the 2D/3D calibration. Detailed results can be seen in Appendix Paper III.

4.2 DEM & FEM model

The proposed DEM and FEM cooperative method involves combining a FEM model to analyse the interaction between the train and the track and a DEM model to analyse the interaction between the sleeper and the ballast, as illustrated in Figure 38. The FEM model calculates the maximum loads on the sleepers as the train passes through various locations, and these values are used as input for the DEM model to calculate the detailed stress status of the ballast bed. Details of the models used in this section can be found in Appendix Paper VI.

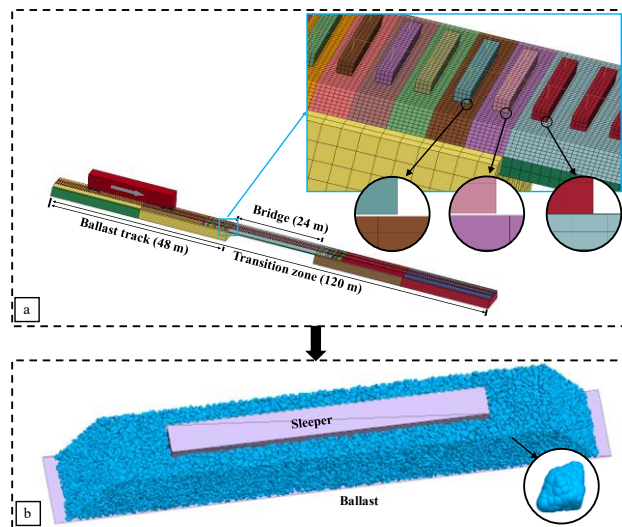


Figure 38. FEM-DEM method: (a) FEM model; (b) DEM model

The FEM model is developed according to typical transition zones, which consist of two ballasted tracks on embankments and a slab track on a bridge. The model has a total length of 120m, with two ballasted tracks of 48 m and a bridge of 24 m. The components of ballasted tracks are rails, fasteners, sleepers, ballast and subgrade. The rails are modelled by Hughes-Liu beam elements with 2*2 Gauss quadrature integration. The cross-sectional and mass properties of the UIC54 rails are used. Fasteners are modelled by spring-damper elements with nonlinear properties in the vertical direction. In compression, the stiffness of rail pads is used, while in tension, a much higher stiffness is used to simulate the clamping effect. The sleepers, ballast, and bridge are modelled by three-dimensional elastic bodies which are composed of the selective reduced integrated hexahedral solid elements, with element sizes of 75mm.

In the FEM model, different levels of settlement in the transition zones are considered. The maximum contact forces between the sleeper and ballast are collected for the good (0mm differential settlement), moderate (4mm differential settlement), and degraded (8mm differential settlement) cases, as shown in Figure 39. The sleeper forces increase as the transition zone degrades. The minimum sleeper contact force occurs at the free track, which is approximately 76.6kN. In the degraded case, the sleeper forces reach a maximum of 119.6kN in the bridge-embankment transition.

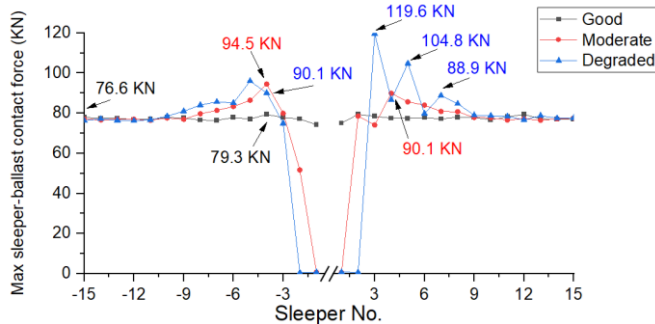


Figure 39. Maximum sleeper forces in good, moderate, and degraded cases

The DEM model is developed in accordance with the FEM model, wherein a sleeper of 2400 mm (length) \times 240 mm (width) \times 200 mm (height) and the corresponding dimension of the ballast bed are modelled. In the DEM simulation, the sleeper is lowered at a rate of 1 mm/s onto the ballast until the sleeper force reaches the expected values got from FEM results. The results contains 7 cases, the good condition is named Case 1, it shows the smallest contact forces (76.6 kN), the degraded condition, named Case 7, shows the highest contact forces (119.6kN), and other 5 cases can be found in Section 5.4 and Appendix Paper IV.

Afterwards, the contact forces between ballast particles are collected to study the behaviour of the ballast bed under hanging sleepers. The simulation results of the sleeper in the free track (Case 1: 76.6kN) and the sleeper with the largest contact force (Case 7: 119.6kN) are compared, as shown in Figure 40, which includes both side and bottom views of the ballast layers. The contact forces at the particle level (particle-particle and particle-sleeper) are colour-coded based on their values. Note that an upper limit of 2kN and a lower limit of 0.3kN are selected for better presentation. Contact forces larger than the upper limit are all shown in red, while forces below the lower limit (0.3kN) are discarded.

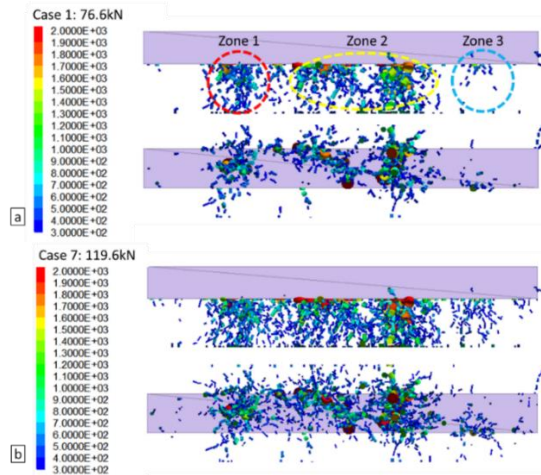


Figure 40. Contact force between ballast particles (a) Case 1: 76.6 kN; (b) Case 7: 119.6 kN

As shown in Figure 40, Comparing Case 1 with Case 7, it can be seen that when the sleeper force grows from 76.6kN to 119.6kN, increased by 56%, the average contact force between the sleeper and ballast particles grows from 0.218kN to 0.300kN, increased by 38%, while the maximum of that grows from 3.326kN to 4.307kN, increased by 29%. The percentage of increase in sleeper force is larger than that of the average (or maximum) of the contact forces between the sleeper and ballast particles. It is because the ballast transmits and re-distributes the load from the sleeper. This shows that the sleeper-ballast contact can be more accurately simulated using the DEM model and also proves the advantage of the FEM-DEM method.

4.3 Conclusions

Simulation methods for dynamic analysis of ballast long-term behaviour are necessary, because the simplifications on 3D models cannot provide an access to those analysis (in Chapter 2). Aiming to increase the feasibility of DEM simulations for railway ballast applications, this chapter introduces cooperative simulation method. The 2D&3D DEM co-simulations for long-term behaviour analysis, and the FEM-DEM co-simulations for force analysis under dynamic loading. The main conclusions are as follows:

- 2D&3D DEM cooperation:
 - a. 2D models ensure accepted calculation time for long-term behaviour analysis under cyclic loading. However, the results of 2D simulations qualitatively vary even same parameters are use. Thus, the simulations should be repeated several times, and each simulation should be calibrated.
 - b. In the cooperative process, 3D simulations can provide the reference for 2D calibration, because of its high accuracy. Particularly, the force distribution should be used to detect whether the results of 2D simulations to be accepted or discarded for further analysis.
- DEM&FEM cooperation:
 - a. The DEM 3D models can present the ballast behaviour in a certain moment, for example, the moment when the peak force appears. When using a realistic input

condition, the moment can be simulated, thus presenting the force behaviour of particles under dynamic conditions.

- b. The FEM method, in the cooperative process, is proposed to analyse the dynamic response between the train and track. the contact force between the sleepers and ballast bed under train passing, referred to as sleeper force, can be obtained, thus providing the realistic input condition for DEM simulations.

Chapter 5. Applications

Applications using DEM simulations are presented in this chapter to demonstrate the feasibility of optimised DEM simulations. it includes :

Using 2D & 3D DEM co-simulations in the design of wedge sleepers for transition zones, this application demonstrates the developed method's aim to analyse the long-term behaviour of ballast.

Utilizing shape simplification to assess the performance of recycled ballast, this application demonstrates the feasibility of employing the simplified shape to represent material surface differences.

Applying the simplest ball shape with complementary rolling resistance to simulate small-sized particles and assess the behaviour of furnace slag as sub-ballast, this application demonstrates a method to tackle the efficiency and feasibility challenges in DEM caused by relatively small yet irregularly shaped particles.

Employing FEM & DEM co-simulations to analyse ballast behaviour in transition zones, this application demonstrate a solution to the feasibility challenge, enabling accurate study of ballast behaviour under dynamic conditions.

5.1 Sleeper-----Wedge sleeper in transition zones

Differential railway track settlement can result in ballast voids under sleepers, leading to sleepers that no longer supported by the ballast bed. These hanging sleepers are particularly common at track transition zones due to the rapid change in track stiffness over a short length. When a train passes unsupported sleepers, their impact on the ballast surface when excited generates a dynamic force, thus further enlarging the differential settlement and voids. This results in a progressive degradation loop. Track irregularities are an important contributor to the increase in dynamic loads, and compared with plain line, the degradation of ballast and other track components at transition zones is much faster. Thus higher maintenance costs are needed to ensure the safety and stability of the railway. As analysed in the appendix paper III.

As a solution, this research (as part of the IN2ZONE project) proposes and investigates a new concept sleeper with a wedge-shaped geometry, intended to stimulate the migration of ballast into any voids, thus reducing the occurrence of hanging sleepers. The 2D&3D DEM co-simulations are used in this research, more information on the application can be found in Appendix Paper III.

Discrete element modelling

DEM simulations are used to develop detailed understanding of the contact behaviour between the sleeper and the ballast particles [39, 53, 69]. The cooperation between the 2D and 3D methods (co-simulations, Section 4.1) is employed in this research.

3D model

The 3D model includes 3 parts: a box, ballast particles, and a sleeper, as shown in Figure 41.

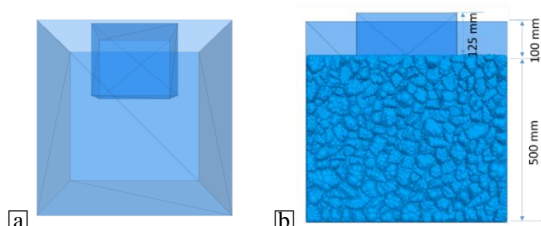


Figure 41. Sleeper & Ballast box model. (a) Box and sleeper, (b) Box filled with ballast

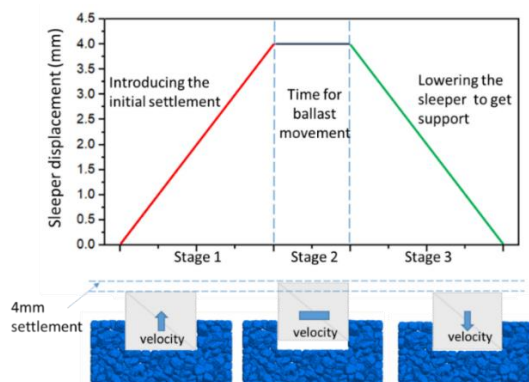


Figure 42. Loading process in 3D DEM simulations

The support correction effect was validated using a loading simulation with a pre-set settlement condition. Considering the high computational costs of 3D DEM simulation, only 1 cycle loading process is used, as shown in Figure 42, the loading process was divided into 3 stages:

Stage 1: Lift the sleeper 4 mm, for the purpose of introducing initial ballast settlement.

Stage 2: Stopping the sleeper movement at a fixed position, followed by time window to allow the ballast to move (under gravity) and fill the ballast-sleeper void. The time window was controlled with 50k calculation cycles to ensure the ballast movement was sufficient. Note that the calculation cycle is a timestep for the software to determine and update information used to keep the kinetic balance of the model through all calculation processes. It is different from the loading cycle and presents no physical significance.

Stage 3: Lower the sleeper 4mm back to its initial location. This process is used to calculate the force behaviour after settlement.

The Sleepers were simulated according to the different wedge geometries under test. The mono-block reference sleeper has dimensions 300*300*250mm and acted as the basis for the different wedge geometries (Figure 43). The contact parameters used in the model were verified in the earlier studies [36, 66-68]. Additional details regarding the contact models and parameters can be found in [61].

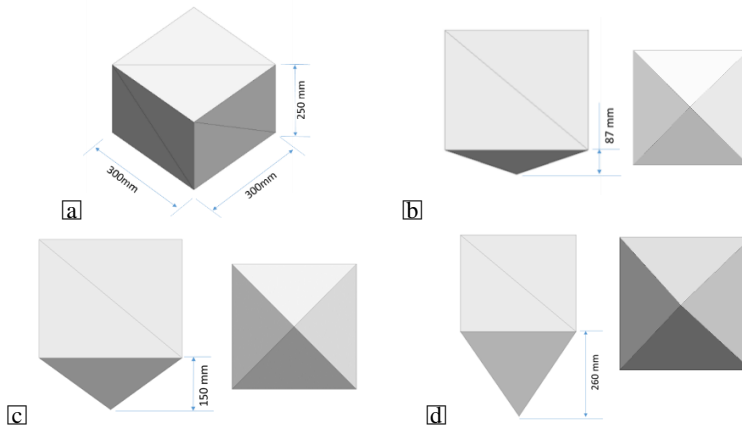


Figure 43. Wedge sleeper designs used in DEM model, (a) Mono-block sleeper, (b) 30-degree wedge sleeper, (c) 45-degree wedge sleeper, (d) 60-degree wedged sleeper

2D model

It is challenging to use 3D FEM simulations to study the long-term ballast settlement. Thus, as an alternative, a series of 2D DEM simulations were used. The 2D model contained particles simplified to ball shape to maximise computational efficiency. 3D simulations were used to calibrate the 2D model and thus ensure accuracy. The method is described in Section 4.1 and the 2D model is shown in Figure 44.

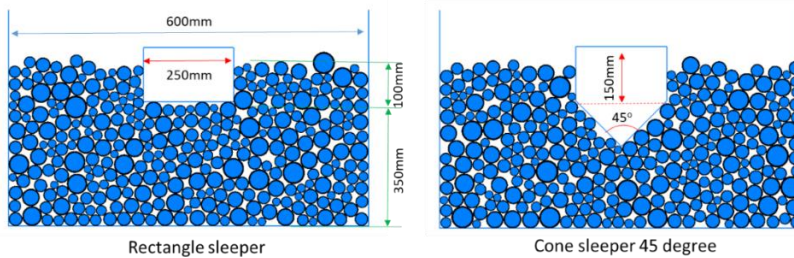


Figure 44. 2D ballast box model

Due to the characteristics of the DEM wall elements, the sleepers could not obtain an acceleration for an unbalanced force (the wall element doesn't obey Newton's second law in the PFC3D software)[70]. Therefore, a suitable loading method was important to simulate the long-term behaviour under repeated loading from the train and positional restriction from the rail/fasteners. The loading approach was the displacement and force double-controlled method, which is described in the following 4 stages in Figure 45: The total loading was around 500 cycles, and the calculation cycles were around 600,000.

Step1: Lift the sleeper 5mm to produce an initial settlement.

Step2: Set a downward velocity (4mm/s) on the sleeper. Stop the sleeper when the ballast-sleeper contact force reaches 40kN (corresponding to the contact force in [6]). This step is force controlled, aiming to simulate the process when a wheel passes and produces loading on the sleeper.

Step 3: Reverse the velocity direction (so now upward 4mm/s). Stop the sleeper when it reaches the location from step 1. In this step, the sleeper movement is displacement controlled, aiming to simulate the process when wheels have passed the sleeper. Then, reverse the velocity downwards and repeat step 2 and step 3. Step 2 and step 3 combine together, making up the whole process of the train passage.

Step 4: After several cycles, the correction effect of the sleeper leads to a steady state. The total loading was around 500 cycles, and the calculation cycles were around 600k.

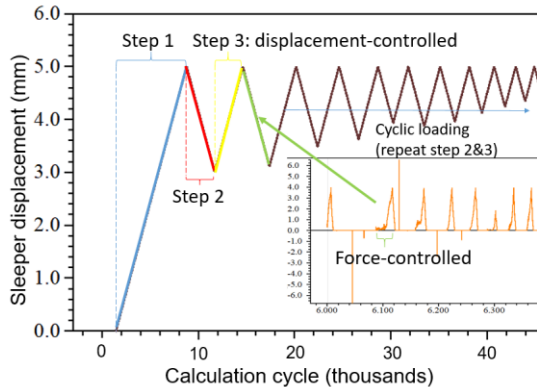


Figure 45. Loading process of the 2D model

Wedge sleeper angle

To analyse the influence of wedge angle on the support correction effect, the contact behaviour between the sleeper and the ballast particles was analysed using the 3D DEM model described in the previous section. During the loading process, the displacement of the sleeper and the contact force between the sleeper and ballast were recorded. Figure 46 shows the results corresponding to the 45-degree sleeper. Two points (Point a and Point b) and 1 range (Range c) were used to analyse the performance of the wedge sleeper.

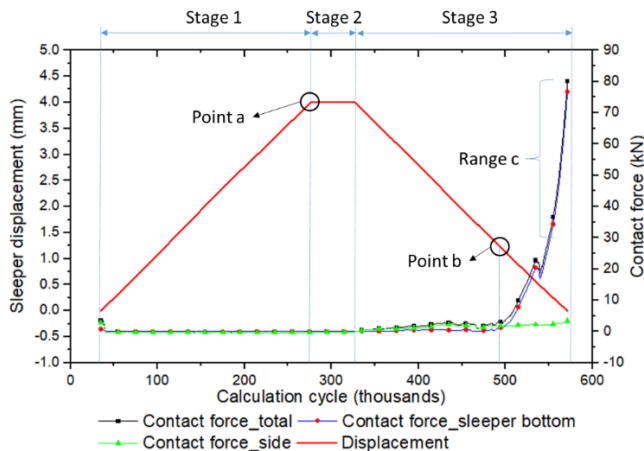


Figure 46. Sleeper displacement and contact force for the 45-degree wedge sleeper

Point a: When the sleeper lifting process is finished and stops at the position represented for settlement. The biggest frictional force (z-direction) can be seen near this point. It presents the frictional interaction between the hanging sleeper and ballast.

Point b: The point where the contact force between the sleeper and particles begins to increase rapidly. Thus the displacement at this point can be regarded as ballast beginning to provide effective support. The global displacement at this point is an indicator. A higher value presents a better support correction.

Range c: The increase in contact force during the last 1 mm displacement in Stage 3. A higher value indicates a better support correction.

The contact forces of 30 and 60 degree wedge sleepers are collected in Table 7 (Figures are shown in Appendix paper III), which reflects the support correction effect due to the different angles. When the wedge angle increased from 30 degrees to 45 degrees, the sleeper displacement at point b increased from 0.86mm to 1.51mm. When the wedge angle was 60 degrees, the sleeper displacement was 2.36mm. These results demonstrate that a bigger wedge angle led to a better settlement correction. The correction is related to the angle of repose for ballast, which is normally observed to range from 30 to 45 degrees [39, 71, 72]. When the slope of the ballast-sleeper interface is higher than that range, ballast particles have the freedom to migrate into the ballast-sleeper void. This statement also explains why an increased correction effect occurred with the angle increase. As for the ballast-sleeper contact force distribution, the maximum contact forces (red dot in Figure 47) are observed on the slope of the wedge. In contrast, the maximum contact forces of the mono-block sleeper are observed at the edge of the bottom.

Table 7. Key results of wedge sleeper

Wedge angle (degree)	Biggest frictional force (Z-direction) (kN)	Displacement when sleeper begins to get support (mm) (point b)	Force increase in last 1 mm (kN) (range c)	Peak sleeper contact force (Z-direction) (kN)
30	-0.14	0.86	1.56	39.31
45	-0.32	1.51	74.95	80.12
60	-0.34	2.36	21.88	284.33
Mono-block	-0.29	0.98	11.71	13.49

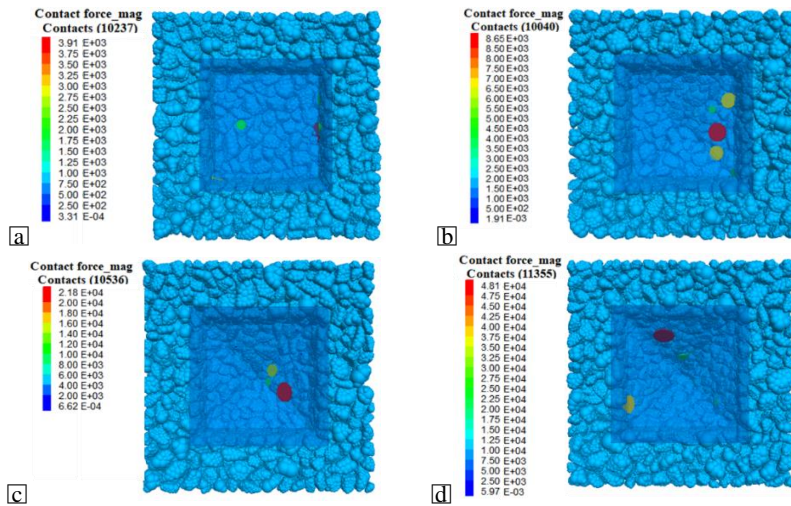


Figure 47. Contact force on sleeper (unit: N). (a) Mono-block sleeper (b) 30-degree wedge sleeper, (c) 45-degree wedge sleeper, (d) 60-degree wedge sleeper

The bigger angle leads to improved support correction behaviour, force distribution, and maximum contact force. Details can be seen in Appendix Paper III. However, the effective ballast thickness for the 60-degree wedge sleeper is less than 100mm, which is not enough to provide resilience [73]. Thus, 45 degrees was selected as the solution to take forward for the long-term settlement analysis.

Settlement behaviour

As mentioned in Chapter 4.1, the 2D models are calibrated according to the results of 3D models. The results of the correct models are listed in Table 8. The 3 representative results are selected to show the deviation according to the value of maximum contact forces. 3 results are the biggest value, the middle value, and the smallest value. as shown in the right column. Note that the negative value means no correction, but a further settlement beyond the initial settlement is observed after the loading process.

The final settlement of the mono-block sleeper after the cyclic loading is 8mm to 9.3mm, whereas the final settlement of the wedge sleeper is only 0mm or 1mm. The maximum contact force for the mono-block sleeper ranges from 17.57kN to 37.96kN, whereas the maximum contact force of wedge sleeper range from 13.94kN to 23.40kN; the decrease ratio is around 20% to 38%. In addition, the force distribution area of a mono-block sleeper is much smaller than the wedge sleeper. That is to say, the wedge sleeper not only provides a support correction effect but also decreases the maximum force on ballast.

Table 8. Results of the 2D model under 5mm initial settlement

Sleeper type	Correction (mm)	Final settlement (mm)	Maximum contact force (kN)
Mono-block sleeper	-3.8	8.8	37.96 (biggest)
	-4.3	9.3	24.31 (middle)
	-4	8	17.57 (smallest)
Wedge sleeper (45-degree)	4	1	23.40 (biggest)
	5	0	18.49 (middle)
	5	0	13.94 (smallest)

Further, the calibrated 2D DEM model of wedge sleeper in ballast box (described in section 4.1) is employed to analyse the correction effect under a bigger settlement. The initial settlement is enlarged to 10mm, 15mm and 20mm, and the loading was applied. The loading method is designed to simulate the cyclic loading of train passing, details can be found in Appendix Paper III. The results are shown in Figure 48, Figure 49, and Figure 50 and Table 9. These results show that the wedge sleeper can correct all the settlements under 5mm and 10mm conditions. For example, in Figure 48(b), the initial sleeper displacement was 10mm, and its movement spanned from 0mm to 10mm, visually depicted by the black area covering the range of 0 to 10mm. As the loading process proceeded, the black area shrank, signifying a reduction in sleeper displacement. By the end of the simulation, the black area was narrower, indicating that the movement of the sleeper was approaching a relatively stable state. Considering the elasticity of the ballast layer, this stable state can be interpreted as a reduction in settlement. When the settlement increases to 15mm and 20mm, the correction is still effective, and the contact forces shown similar behaviour to that of cases under 5mm settlements, considering the value of force and the force chain.

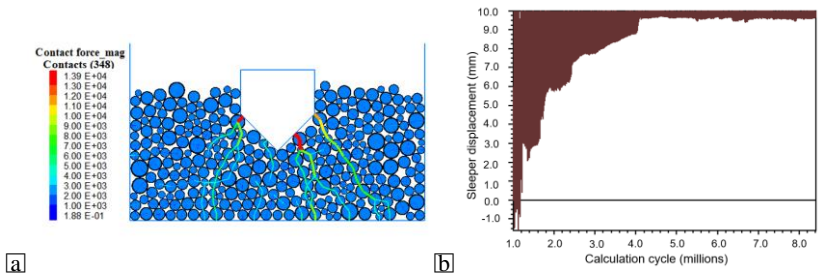


Figure 48. 45-degree wedge sleeper under 10mm settlement. (a) Contact force distribution (units: N), (b) Sleeper displacement (units: mm)

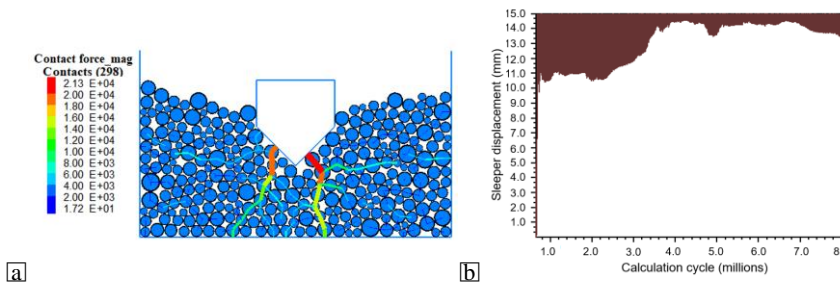


Figure 49. 45-degree wedge sleeper under 15mm settlement. (a) Contact force distribution (unit: N), (b) Sleeper displacement (units: mm)

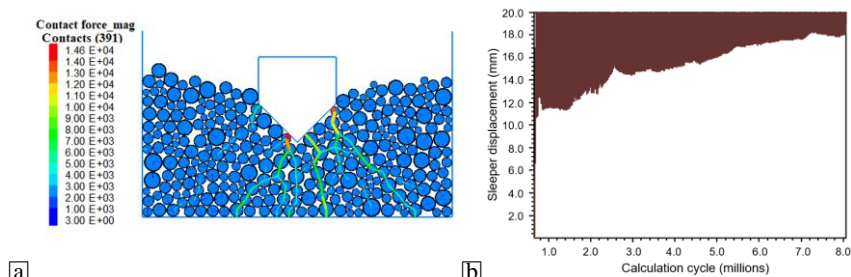


Figure 50. 45-degree wedge sleeper with good correction under 20mm settlement. (a) Contact force distribution (unit: N), (b) Sleeper displacement (units: mm)

Table 9. Correction for higher settlement

Settlement (mm)	Correction (mm)	Maximum contact force (kN)
10	10	14.0
15	14	21.31
20	18	14.60

The main conclusions are:

1. When the bottom angle of wedge sleeper is larger than the repose angle of ballast material, particles have the freedom to migrate into the settlement induced voids
2. An increased wedge sleeper angle stimulates greater particle migration and thus improved, the support correction. However, the longer wedge also leads to a decrease in effective ballast height under sleeper.
3. The ability of wedge-shaped sleepers to reduce the presence of sleeper voids is promising, however further study is needed.
4. Compared with the mono-block sleeper, the wedge sleeper reduces the contact force between the sleeper and the ballast due to a wider contact area.

In this application, 3D DEM simulations are conducted to analyse the contact forces in the ballast resulting from various single wedge designs. Additionally, 2D DEM simulations are employed to investigate the long-term settlement behaviour. The cooperative modelling method circumvents the efficiency issues associated with 3D DEM and enhances the accuracy of 2D DEM simulations. This approach resolves the feasibility challenge of utilizing DEM simulations for analysing long-term behaviour.

5.2 Ballast-----Recycled ballast

Degradation of ballast under cyclic loading can lead to problems with bearing capacity and drainage in railway tracks. Regular maintenance, such as cleaning and replacement, is necessary to maintain stability and safety, which results in a large amount of waste ballast. Therefore, reusing deteriorated ballast can be an effective method for sustainable railway development and environmental protection. One application is adding cleaned deteriorated ballast (i.e., recycled ballast) to fresh ballast. Additionally, it is common for the ballast bed to consist of a mixture of fresh and deteriorated ballast. This research lays the foundation for the application of recycled ballast and includes a series of tests, with only numerical simulations presented here. More information on the application can be found in Appendix Paper IV. This research employs varying shape simplifications to simulate fresh ballast and recycled ballast. By assessing the shape complexity, different materials can be accurately simulated using this approach. ...

Material preparation

The deteriorated ballast was mixed with fresh ballast in different ratios of 10%, 20%, 30%, 40% and 50% by weight. Moreover, fresh ballast only (0%) and recycle ballast only (100%) are concluded as reference groups. In total, 7 different specimens were used, as shown in Figure 51.



Figure 51. Recycled ballast

DEM simulation

In the series of simulations, the shapes of fresh and recycled ballast are presented in section 2.3. The mechanical behaviour of degraded-fresh ballast is evaluated through the direct shear test, and the large-scale strain-controlled direct shear apparatus is depicted in Figure 52. The recycled-fresh ballast mixture was filled in the shear box and compacted by layers using a vibrating compactor. Normal stress of 50kPa, 100kPa, or 200kPa was applied to the mixed sample. The corresponding DEM model is shown in Figure 53, in accordance with the tests.

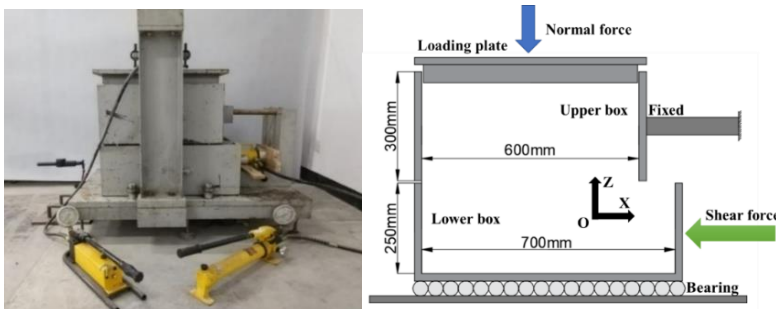


Figure 52. Large-scale direct shear apparatus

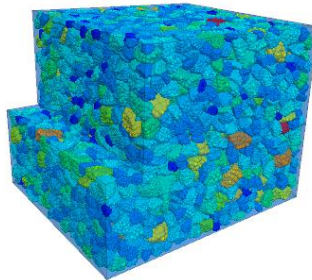


Figure 53. The DEM numerical model of ballast direct shear test

Shear strength

For laboratory tests, the shear stresses of different proportions of recycled ballast under different normal stresses are shown in Figure 54. Based on this data, the cohesion and friction angle were calculated and are listed in Table 10.

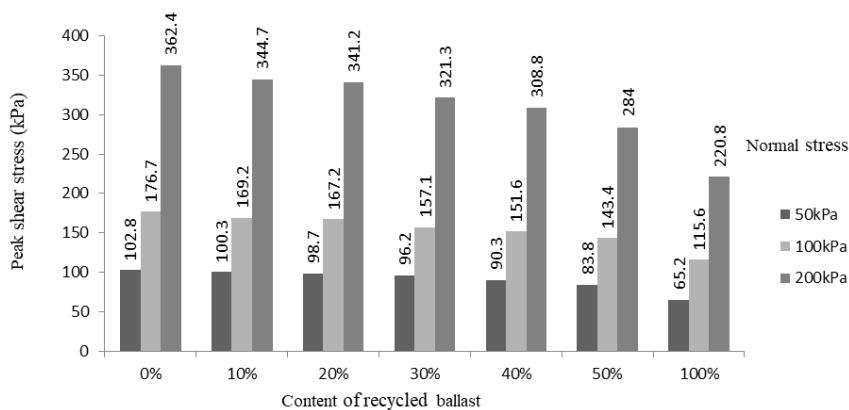


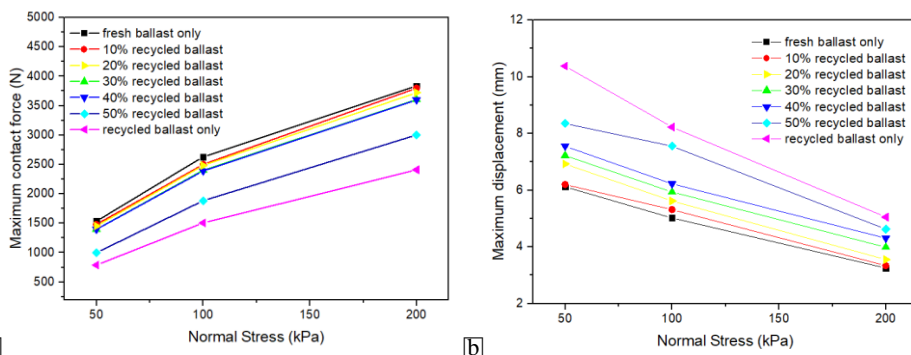
Figure 54. Shear strength under different normal stresses

Table 10. Cohesion and friction angel by linear fitting

Content of recycled ballast	Cohesion (kPa)	Friction angle (degree)
fresh ballast only (0%)	9.95	60.27
10% recycled ballast	12.55	58.77
20% recycled ballast	11.7	58.56
30% recycled ballast	14.1	56.71
40% recycled ballast	11.7	55.85
50% recycled ballast	13.5	53.39
recycled ballast only (100%)	12.6	46.13

Mesoscopic behaviour

It can be seen from Figure 55 (a) and (b) that the maximum contact force and maximum displacement decrease as the percentage of recycled ballast increases. This indicates that the mechanical behaviour of the ballast mixture is affected by the presence of recycled ballast. However, the reduction in these values is insignificant when the percentage of recycled ballast is between 10% and 30%. Therefore, it can be concluded that the addition of up to 30% recycled ballast can still maintain the mechanical stability of the ballast mixture.



(a)

(b)

Figure 55. Mesoscopic results: (a) Maximum contact force on particles, (b) Maximum displacement of particles

The main conclusions are:

1. Due to the loss of angularity and reduction in surface texture, the interlock between recycled ballast is weaker compared to fresh ballast. As the proportion of recycled ballast in the mixture increases, the shear strength and friction angle of the mixture decrease while shear dilatancy increases. These changes are particularly significant for mixtures with more than 50% recycled ballast, but for mixtures with less than 30% recycled ballast, the reduction in shear stress is negligible.
2. The numerical simulations used clumps to represent ballast particles based on the 3D scanning. Different settings for the Ratio/Distance and friction coefficient in ballast generation can distinguish fresh and recycled ballast, resulting in more reliable results. As the volume ratio of recycled ballast increases, both the coordination number and maximum contact force decrease, leading to an increase in the maximum displacement of ballast particles.
3. Recycled ballast exhibits lower capacity and stability compared to fresh ballast. However, it should be noted that adding recycled ballast in a proportion of less than 30% does not significantly affect the overall performance. Therefore, adding recycled ballast to fresh ballast can be a method of reusing the deteriorated ballast bed, provided it is within the recommended ratio. This result can also serve as a guide for maintenance, where fresh ballast can be used to reinforce recycled ballast.

In this application, particle shape is evaluated to simulate material differences. The main challenge of this research lies in simulating varying surfaces while utilizing shape simplification. The simplified shapes do not capture surface intricacies as precisely as high-fidelity particles. Conversely, using high-fidelity particles would lead to significantly lower calculation efficiency. This application effectively addresses this challenge, enhancing efficiency while preserving the accuracy of DEM simulations.

5.3 Sub-ballast-----Furnace slag

Under the high requirements for ballast materials and the frequent maintenance needed for high-speed and heavy-haul railways, maintenance costs and material consumption have become important issues. Several methods have been used to increase the stability and service life of railway structures. Additionally, using recycled materials in ballast bed construction can be a way to promote sustainable railway development. Hence, the idea of using furnace slag as sub-ballast was proposed in this research. To assess the performance of furnace slag, a series of tests were conducted, including the single particle crushing test, direct shear test, and box stiffness test. Crushed stone, the traditional sub-ballast material, was used as a comparison. This research involves a series of tests, and only numerical simulations are presented here. In the simulation, the sub-ballast is represented using the simplest spherical shape. This choice is driven by the challenge that generating a box model filled with irregularly shaped small sub-ballast particles is nearly impossible. Complementary contact parameter, i.e. the Rolling Resistance, is introduced to simulate particle interlocking. Details of the application are shown in Appendix Paper V.

Material preparation

The furnace slag used in this research is shown in Figure 56(a). Its density is 2250kg/m^3 . In comparison, the traditional sub-ballast material is crushed granite, and it is shown in Figure 56(b), with the density of 2800kg/m^3 , and it is saved and mixed by the same PSD with furnace slag.

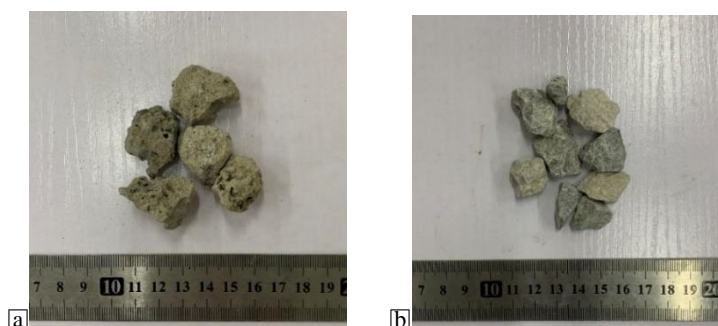


Figure 56. Material for tests: (a) Furnace slag, (b) Crushed stone

DEM simulations

The stiffness tests were carried by the device in Figure 57(a). The device is designed for direct shear tests, but also used for stiffness tests because it has the servo system.

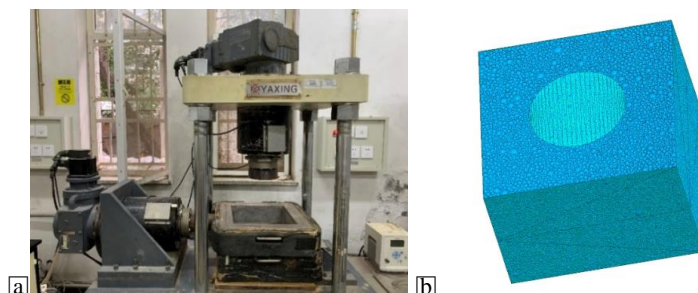


Figure 57. Direct shear test apparatus: (a) Test apparatus, (b) Schematic diagram

The model is in accordance with the laboratory test. Due to the particle size and porosity, the model contains more than 500,000 particles. Considering the model scale, particle size and time-consuming problem, the model uses a ball element to present the aggregate material. The model is shown in Figure 57(b). According to the tests (in Appendix Paper IV), the friction coefficient of furnace slag is higher than that of crushed stone. Thus, a higher friction coefficient is set for the furnace slag model. Together with the reference from previous researches [60, 74, 75], the parameter is shown in Table 11, where the curve of the simulation fits the test results.

Table 11. Parameters of linear contact model in simulations

Parameters	Furnace slag	Crushed stone	Box
Tangential stiffness(N/m)	2.7e6	2.2e6	1e8
Normal stiffness(N/m)	2.6e6	2.3e6	1e8
Friction coefficient	0.5	0.4	0.2
Mass density (kg/m ³)	2250	2800	-
Damping coefficient	0.7	0.7	-

Stiffness

In Figure 58, the peak force of furnace slag is 14.03kN (14.41kN in laboratory test), and the displacement at peak force is 3.11mm (3.15mm in the laboratory test). For crushed stone, the peak

compressive force is 11.44kN (11.89kN in laboratory test), and the displacement at peak force is 2.16mm (2.06mm in laboratory test).

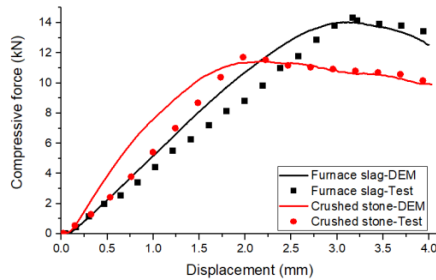


Figure 58. Stiffness response of tests and simulations

Force distribution

In Figure 59, the force chain at the peak state and finish state of the simulation is shown, where the line represents the contact, and the colour represents the value of the force. In Figure 59 (a) and (c), the peak state shows a denser force distribution than the finish state in Figure 59 (b) and (d). Especially in the top corner, along with the loading process after the peak state, the ballast in this area gradually loses its function. This is because under the unconfined top layer (except the loading plate), the interlock between the ballast is broken. When comparing the two materials, it is obvious that the furnace slag shows a denser force chain and wider distribution, as the dash-line provides an explanation for the macroscopic result.

From the peak state to the finish state, the maximum contact force increases. This behaviour is related to the force chain changes. During this process, the force in some contacts exceeds the maximum capacity, thus leading to failure. With those contacts no longer contributing and the loading continuing, the force in left effective contacts increases. However, because the increase only happens in some contacts between the particle and the loading plate, as shown in Figure 59 (b) and (d), it cannot offset the overall decreasing trend of compressive force.

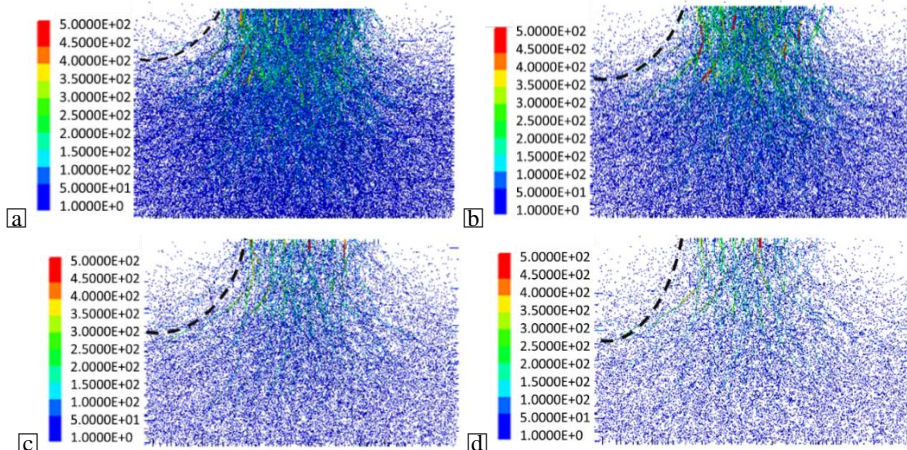


Figure 59. Force chain (unit: N): (a) Furnace slag at peak state, (b) Furnace slag at finish state, (c) Crushed stone at peak state, (d) Crushed stone at finish state

The main conclusions are:

1. In SPCT, furnace slag shows a 20% to 39% increase in peak compressive force compared to crushed stone. The result indicates that furnace slag is better in resisting particle breakage.
2. However, furnace slag shows more angular breakage, the LAA value is still lower than crushed stone. This indicates better resistance to abrasion, with the value for furnace slag being 26.04%, compared to 31.28% for crushed stone.
3. In direct shear tests, furnace slag shows 16.46%, 18.91%, and 19.48% increase compared to crushed stone, corresponding to normal stress of 50kPa, 100kPa, and 200kPa, respectively. Additionally, the performance of furnace slag is better in friction angle, cohesion, and shear dilatancy.
4. In the box stiffness test, the peak compressive force of furnace slag is 14.41kN (815.57kPa), while for crushed stone it is 11.89kN (673.02MPa). Under these test conditions, the stiffness of furnace slag is 4.57e6N/m, and for crushed stone, it is 5.77e6N/m.
5. In the DEM model for box stiffness, furnace slag shows better performance than crushed stone in terms of contact and force distribution.

In this application, small-sized particles, specifically sub-ballast, are simulated. This demonstration showcases the utilization of shape simplification and Rolling Resistance. The application provides a method to address the efficiency and feasibility challenges in DEM caused by particles that are relatively small yet irregular in shape.

5.4 Transition zones-----Ballast behaviour

Transition zones in railways are a weak of all the structures, which requires higher maintenance costs. As described in Section 5.1, the force state in transition zones is complex, and it is not possible to simulate the behaviour of the ballast layer under dynamic forces using DEM. To accurately study the dynamic behaviour of ballast particles under hanging sleepers in transition zones, a DEM-FEM cooperative method is developed. The Co-simulation method is introduced in Chapter 4.2. Details of the application is shown in Appendix Paper VI.

FEM model

The FEM model, as shown in Figure 60, is developed according to typical transition zones, In the research, three conditions of transition zones are considered, including good, moderate, and degraded, which are modelled by the differential settlements of 0 mm, 4 mm, and 8 mm, respectively, according to the measurements in [76, 77]. Also shown in Section 4.2 and Appendix Paper VI.

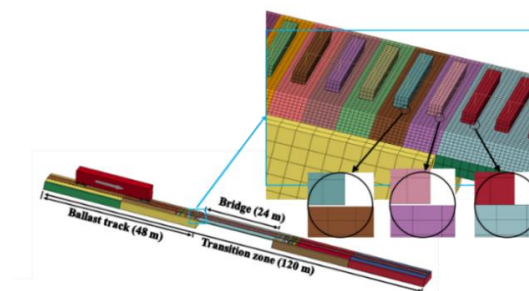


Figure 60. FEM model of a typically transition zone

DEM model

The DEM model is developed in accordance with the FEM model, the ballast particles are modelled by slightly simplified clump elements, as shown in Figure 61. The sleeper is modelled as the wall element, as well as the boundary. The Particle Size Distribution (PSD) shown in Figure 10 (Section 2.1) is used.

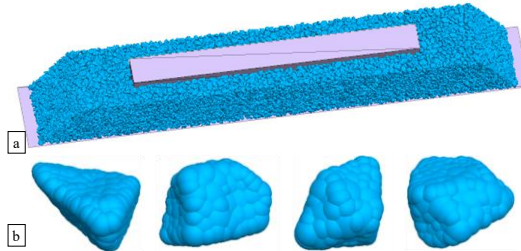


Figure 61. DEM model for sleeper and ballast: (a) Overview; (b) Representative ballast particles.

Sleeper force in transition zone

The FEM model is used to calculate the contact forces between the sleepers and ballast during the train's passage. The sleepers are numbered starting from the one closest to the bridge, with the ones in the embankment-ballast transition (left of the bridge) having a negative sign, and those in the ballast-embankment transition (right of the bridge) being positive. As shown in the following Figure 62. As the train passes, the sleepers are pushed downwards to the ballast, resulting in an increase in the contact forces between the sleepers and ballast. The sleepers with large sleeper forces in the transition zone are then collected in Table 12, which is used as input for the DEM model to further analyse the behaviour of the ballast.

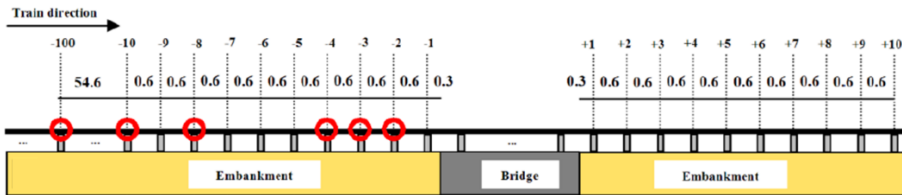


Figure 62 Schematic diagram of sleeper numbering

Table 12. Typical sleeper forces in transition zones under various conditions.

Case No.	Sleeper force (kN)	Increase to open track	Collected from
1	76.6	-	Open track
2	79.3	4%	Sleeper-4 in good
3	88.9	16%	Sleeper+7 in degraded
4	90.1	18%	Sleeper-4 in degraded; Sleeper+4 in moderate
5	94.5	23%	Sleeper-4 in moderate
6	104.8	37%	Sleeper+5 in degraded
7	119.6	56%	Sleeper+3 in degraded

Contact behaviour between ballast particles

The contact forces between ballast particles are then collected using the above mentioned methods to study the behaviour of the ballast beds under hanging sleepers.

To compare the results, the simulation is conducted for both the free track case (Case 1) and the case with the largest contact force (Case 7). Figure 63 presents the results in both a side view and bottom view of the ballast layers, with the contact forces at the particle level (particle-particle and particle-sleeper) color-coded according to their values. For clarity, an upper limit of 2kN and a lower limit of 0.3kN are selected, and contact forces exceeding the upper limit are shown in red while those below the lower limit (0.3kN) are not shown.

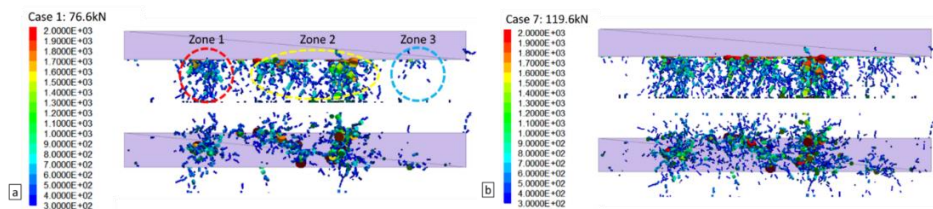


Figure 63. Contact force between ballast particles (a) Case 1: 76.6 kN; (b) Case 7: 119.6 kN

Comparing Case 1 with Case 7, it can be seen that when the sleeper force grows from 76.6kN to 119.6kN, which is an increase of 56%, the average contact force between the sleeper and ballast particles also grows from 0.218kN to 0.300kN, which is an increase of 38%. Additionally, the maximum contact force increases from 3.326kN to 4.307kN, which is a 29% increase. The contact forces in the ballast of the other cases (Case 2 to Case 6) are shown in Appendix Paper VI. It is important to note that the results of Case 1 and Case 7 are also included to show the evolution of the contact forces. The statistical analysis of the contact forces in all cases is presented in Table 13.

Table 13. Contact number counting by force range

Case No.	Sleeper force(kN)	Number of activated contact points (According to the range of contact forces)					Sum
		0.1-0.5 kN	0.5-1kN	1-2 kN	2-3 kN	>3kN	
1	76.6	4080	240	47	3	1	4371
2	79.3	4254	256	47	4	1	4562
3	88.9	4733	300	59	6	2	5100
4	90.1	4830	303	61	9	2	5205
5	94.5	5042	327	65	9	2	5445
6	104.8	5550	385	73	11	2	6021
7	119.6	6153	468	92	14	3	6730

Table 13 shows the contact forces in each case. Most contact forces are small in all cases, which are between 0.1kN and 0.5kN. Also, as the sleeper force increases, the contacts in the range of 0.5kN and 2kN become more and scattered distributed, the growth in the number of which is much larger than that higher than 2kN. It indicates that during the track degradation process, a high sleeper force tends to cause a wide range of small damage to the ballast rather than a small range of larger damage to the ballast.

To further study the relationship between sleeper force and ballast behaviour, the sleeper forces ranging from 70kN to 120kN with an interval of 2.5kN are calculated using the DEM model. The average and maximum contact forces between the ballast particle and sleeper, are collected and shown

in Figure 64(a), where the x-axis also represents the total contact forces on sleeper. And, the total and maximum contact force between the ballast particle and bottom wall (sub-ballast) are collected and shown in Figure 64(b). Note that the average forces on the bottom of all cases are smaller than 0.1kN, they are discarded.

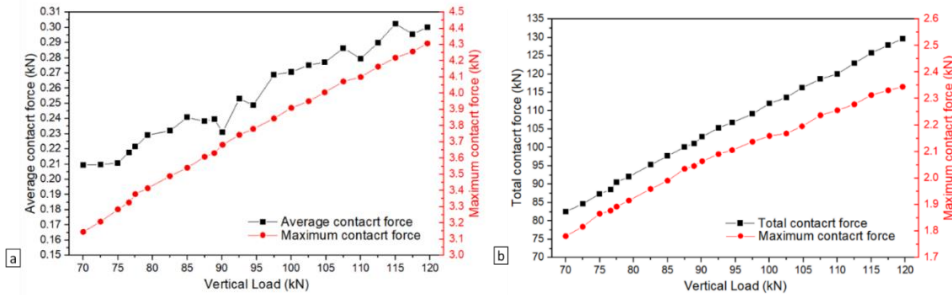


Figure 64. Relationship between sleeper contact force and ballast behaviour: (a) Contact forces between ballast particle and sleeper; (b) Contact forces between ballast particle and bottom.

As shown in Figure 64(a), both the average and maximum contact forces between the sleeper and ballast particles increase linearly as the sleeper force increases. It is important to note that there are local drops in the curve of the average contact force at 90.1kN, 94.5kN, 110kN, and 117.5kN, which can be explained by the sudden change in ballast displacement caused by interlock failure (or ballast breakage in reality). In comparison, the results in Figure 64(b) show that the pattern of contact forces between the ballast particles and bottom is much smoother, without fluctuations. Additionally, the maximum contact force is much smaller. This is because the contact forces are redistributed in the ballast layer.

The main conclusions are:

1. Impact forces on hanging sleepers increase as the transition zone degrades, with the range of increase being from the 3rd sleeper to the 9th sleeper on both sides of the bridge. Under good conditions, the maximum sleeper ballast contact force only slightly increases in the transition zones. However, in moderate and degraded cases, the sleeper forces increase significantly, up to 94.5kN (23%) and 119.6kN (56%), respectively.
2. The percentage increase in sleeper force is greater than that of the average contact forces between the sleeper and ballast particles, which are 56% and 38%, respectively. This is because the ballast redistributes and transmits the load from the sleeper. The DEM model provides more accurate simulation of sleeper-ballast contact and demonstrates the advantage of the FEM-DEM method.
3. When the hanging sleeper contacts the ballast, the largest contact forces between ballast particles occur at the top layer of the ballast in all zones in both Case 1 (76.6kN) and Case 7 (119.6kN). Contact forces gradually decrease as the ballast particles become deeper in both cases.
4. Statistical analysis of contact forces under various sleeper forces reveals that most contact forces are small, ranging between 0.1kN and 0.5kN in all cases. As the sleeper force increases, the contacts in the range of 0.5kN and 2kN become more widely and randomly distributed. This suggests that during the track degradation process, high sleeper force tends to cause a broader range of small damage to the ballast rather than a smaller range of larger damage.

5. Both the average and maximum contact forces between the sleeper and ballast particles under the hanging sleeper increase linearly as the sleeper force grows. Similarly, contact forces between the ballast particle and bottom under the hanging sleeper increase linearly but more smoothly. This is because the contact forces are redistributed within the ballast layer.

In this application, the movement of the hanging sleepers during train passage is simulated in the FEM model and used as input for the DEM method to calculate the detailed behaviour of ballast particles. This application demonstrates a DEM&FEM cooperative method, successfully addressing the feasibility challenge of accurately studying ballast behaviour under dynamic conditions

Chapter 6. Conclusion

6.1 Conclusion

The research of DEM-based and ballast-related development is described in 3 aspects, which are

- **Efficiency:** reducing computational efforts (calculation time) while keeping required accuracy by applying proper particle shape simplifications.
- **Feasibility:** increasing possibility of using DEM in railway applications focusing on different research objects and expected results. Developing cooperative simulation schemes for analysis of the long-term dynamic structural behaviour.
- **Application:** demonstration of the developed methods to assess the performance of new designs and materials in railway track.

Chapter 2 and Chapter 3 answer the efficiency questions:

- What is the influence of the simplification on the accuracy in different scopes.
- How to improve the efficiency of DEM-based numerical simulation, which is mainly related to shape simplification.

In Chapter 2, particle shape is introduced, and the influence of particle shape on the accuracy of the results is presented. The focus is mainly on shape simplification, which is analysed using 11 different shapes generated by controlling two parameters: Distance and Ratio. The rolling resistance (friction coefficient) is applied to the simplest ball and 2-sphere shape. The macroscopic and mesoscopic results are obtained, compared, and analysed by a series of box loading tests, including the coordination number, contact force, and sleeper displacement. Based on the above-mentioned results and analysis. The main conclusions on shape optimizations are listed below:

- The computational time can be drastically decreased by simplification of the particle shape and texture.
- The level of complexity of the particle has different influence on the macro- and mesoscopic results. Therefore, the simplification of the particles should be applied depending on which effects (e.g. ballast bed settlement or ballast particle breakage) are important and which results (on macro- or meso- level) are needed.
- In case of the macroscopic results are of interest:
 - a. the complexity of the particle can be reduced even without compensation in contact law (by adding Rolling Resistance).
 - b. When drastically reducing the complexity of the particle, the loss of accuracy of the results can be compensated by adjusting the contact law
- In case of mesoscopic results are of interest, the simplification of the particle complexity is not recommended since the loss of accuracy of the results cannot be compensated by adjusting the contact law (by adding Rolling Resistance).
- In case of the simulations, which considering the fresh and degraded ballast, the different particles can be used by controlling shape complexity and surface friction coefficient.

In Chapter 3, the replacement and expansion method is introduced, this method is quicker and more controllable compared with typically used method. In addition, an particle shape simplification refinement method (APSS optimised model-building method) is introduced. This method, based on the aiming simulations, simplifies the irregular ballast shape to ball shape and uses irregular shape (clump) in the most influential area. The main conclusions are listed below:

- Optimising efficiency of modelling building:

- a. The replacement and expansion method can increase the efficiency, with a 10-20 times faster speed than the typically used dropping method.
- b. This method also allows for precise definition of particle shape in specific areas. It is a universal method for all kinds of simulations to generate a granular layer.
- Optimising accuracy and efficiency by using Adaptive Particle Shape Simplification (APSS):
 - a. The APSS optimized model decreases the number of elements by using complex shapes in the most influential areas and simplified shapes in other areas. The case study demonstrates that this method increases efficiency and maintains accuracy for mesoscopic analysis.
 - b. In defining the most influential area for different simulations. The area selection should be based on the type of simulations and the target results. As an example in this research, the lateral resistance is simulated, and the most influential area is defined by particle displacement, which is obtained by previous tests using the PIV method.

Chapter 4 answers the feasibility questions:

- How to validate the 2D models based on the mesoscopic results of 3D DEM models to obtain the long-term behaviour in macroscopic level?
- How to use the macroscopic results of FEM model in 3D DEM models to obtain the dynamic-related behaviour in mesoscopic level?

In this chapter, the advantages of different numerical modelling methods are combined. The 2D&3D DEM co-simulations are introduced to analyse the long-term behaviour, and the FEM-DEM co-simulations are introduced to analyse the dynamic behaviour. This combination largely improves the feasibility of the DEM modelling method. The main conclusions are listed below:

- Analyse on the long-term behaviour can be done by using 2D&3D DEM cooperation:
 - a. The 3D models are used to simulate a short period. The contact force results, particularly the force distribution, are used to calibrate the 2D model.
 - b. 2D models are used to simulate long-term period and simulations should be repeated for several times. The qualitatively varied results of each simulation can be detected. Then, the results are discarded or accepted for further analysis.
- Analyse on the dynamic behaviour can be done by using DEM&FEM cooperation:
 - a. The FEM method is proposed to analyse the dynamic response between the train and track, including the interaction between sleepers and the ballast layer. After calculation, the contact force between the sleepers and ballast bed under train passing, referred to as sleeper force, can be obtained.
 - b. The DEM 3D models use the FEM results as input condition for the sleeper-ballast interaction. In this way, the movement of ballast particles and forces between ballast particles under dynamic conditions can be accurately simulated.

Chapter 5 presents the applications to answer the question:

- Application: demonstration of the developed methods, and using developed modelling methods to assess the function of new designs and materials in railway track.

This chapter presents 4 applications. The force behaviour of ballast in transition zones are analysed to present the mesoscopic understanding of the differential settlement. A design of wedge sleeper is to delaminate the hanging sleepers thus reduce the track degradation. The qualification of recycle

ballast, also the qualification of furnace slag provides a sustainable solution of ballast and sub-ballast layer construction.

Wedge sleeper

Railway track transition zones are areas with rapidly changing track stiffness. It is common for hanging sleepers to develop on the softer side due to differential settlement. To address this problem, this research proposed and investigated a new concept sleeper with a wedge-shaped geometry. When the bottom angle of wedge sleeper is larger than the repose angle of ballast material, particles have the freedom to migrate into the settlement induced voids. Tests and simulations proved the working principles of the wedge sleeper:

- When the bottom angle of wedge sleeper is larger than the repose angle of ballast material, particles have the freedom to migrate into the settlement induced voids
- An increased wedge sleeper angle stimulates greater particle migration and thus improved, the support correction. However the longer wedge also leads to a decrease in effective ballast height under sleeper.
- The ability of wedge-shaped sleepers to reduce the presence of sleeper voids is promising, however further study is needed.
- Compared with the mono-block sleeper, the wedge sleeper reduces the contact force between the sleeper and the ballast due to a wider contact area.

In this application, 3D DEM simulations are conducted to analyse the contact forces in the ballast resulting from various single wedge designs. Additionally, 2D DEM simulations are employed to investigate the long-term settlement behaviour. The cooperative modelling method circumvents the efficiency issues associated with 3D DEM and enhances the accuracy of 2D DEM simulations. This approach resolves the feasibility challenge of utilizing DEM simulations for analysing long-term behaviour.

Recycled ballast

In this research, the fresh-recycled ballast mixture was analysed by a series of experimental direct shear tests and numerical simulations based on the DEM, with the aim of investigating the mechanical characteristics of recycled ballast. With particle shapes and contact parameter setting, the DEM simulations were in good agreement with laboratory results, and the conclusions were given as follows:

- Due to the loss of angularity and reduction in surface texture, the interlock between recycled ballast is weaker compared to fresh ballast. As the proportion of recycled ballast in the mixture increases, the shear strength and friction angle of the mixture decrease while shear dilatancy increases. These changes are particularly significant for mixtures with more than 50% recycled ballast, but for mixtures with less than 30% recycled ballast, the reduction in shear stress is negligible.
- The numerical simulations used clumps to represent ballast particles based on the 3D scanning. Different settings for the Ratio/Distance and friction coefficient in ballast generation can distinguish fresh and recycled ballast, resulting in more reliable results. As the volume ratio of recycled ballast increases, both the coordination number and maximum contact force decrease, leading to an increase in the maximum displacement of ballast particles.
- Recycled ballast exhibits lower capacity and stability compared to fresh ballast. However, it should be noted that adding recycled ballast in a proportion of less than 30% does not significantly affect the overall performance. Therefore, adding recycled ballast to fresh ballast can be a method of reusing the deteriorated ballast bed, provided it is within the

recommended ratio. This result can also serve as a guide for maintenance, where fresh ballast can be used to reinforce recycled ballast.

In this application, particle shape is evaluated to simulate material differences. The main challenge of this research lies in simulating varying surfaces while utilizing shape simplification. The simplified shapes do not capture surface intricacies as precisely as high-fidelity particles. Conversely, using high-fidelity particles would lead to significantly lower calculation efficiency. This application effectively addresses this challenge, enhancing efficiency while preserving the accuracy of DEM simulations.

Furnace slag as sub-ballast

This research introduces the use of furnace slag as the sub-ballast in railway construction. Furnace slag is a byproduct of using iron ore to produce pig iron. Because of its characteristic, the reuse of furnace slag is not as wide as steel slag. However, compared with the requirement of the railway sub-ballast, furnace slag can be a good material and also works for environmental-friendly development. Several experimental tests were employed, including the Single Particle Crushing Test (SPCT), the Los Angeles Abrasion (LAA) tests, the direct shear test, the box stiffness tests. In comparison, the crushed stone (i.e. the traditional material for sub-ballast) was tested as the reference. A DEM simulation in accordance with the box stiffness test was carried out. The main conclusions are listed below:

- In SPCT, furnace slag shows a 20% to 39% increase in peak compressive force compared to crushed stone. The result indicates that furnace slag is better in resisting particle breakage.
- However, furnace slag shows more angular breakage, the LAA value is still lower than crushed stone. This indicates better resistance to abrasion, with the value for furnace slag being 26.04%, compared to 31.28% for crushed stone.
- In direct shear tests, furnace slag shows 16.46%, 18.91%, and 19.48% increase compared to crushed stone, corresponding to normal stress of 50kPa, 100kPa, and 200kPa, respectively. Additionally, the performance of furnace slag is better in friction angle, cohesion, and shear dilatancy.
- In the box stiffness test, the peak compressive force of furnace slag is 14.41kN (815.57kPa), while for crushed stone it is 11.89kN (673.02MPa). Under these test conditions, the stiffness of furnace slag is 4.57e6N/m, and for crushed stone, it is 5.77e6N/m.
- In the DEM model for box stiffness, furnace slag shows better performance than crushed stone in terms of contact and force distribution.

In this application, small-sized particles, specifically sub-ballast, are simulated. This demonstration showcases the utilization of shape simplification and Rolling Resistance. The application provides a method to address the efficiency and feasibility challenges in DEM caused by particles that are relatively small yet irregular in shape.

Ballast behaviour in transition zones

Transition zones in railways are the locations with considerable changes in the vertical support due to the sudden stiffness change and differential settlement, which requires higher maintenance costs. Hanging sleepers are one of the most common defects in transition zones, which can cause a significant increase in sleeper velocity and ballast stress, leading to poor elasticity and drainage of tracks and spreading the issue to adjacent sleepers. To accurately study the dynamic behaviour of ballast particles under hanging sleepers in transition zones, a FEM-DEM co-simulation method is developed. Using the method, the dynamic behaviour of ballast under multiple hanging conditions in transition zones are presented. The following conclusions can be drawn, which can be used to guide maintenance in railway transition zones. The main conclusions are listed below:

- Impact forces on hanging sleepers increase as the transition zone degrades, with the range of increase being from the 3rd sleeper to the 9th sleeper on both sides of the bridge. Under good conditions, the maximum sleeper ballast contact force only slightly increases in the transition zones. However, in moderate and degraded cases, the sleeper forces increase significantly, up to 94.5kN (23%) and 119.6kN (56%), respectively.
- The percentage increase in sleeper force is greater than that of the average contact forces between the sleeper and ballast particles, which are 56% and 38%, respectively. This is because the ballast redistributes and transmits the load from the sleeper. The DEM model provides more accurate simulation of sleeper-ballast contact and demonstrates the advantage of the FEM-DEM method.
- When the hanging sleeper contacts the ballast, the largest contact forces between ballast particles occur at the top layer of the ballast in all zones in both Case 1 (76.6kN) and Case 7 (119.6kN). Contact forces gradually decrease as the ballast particles become deeper in both cases.
- Statistical analysis of contact forces under various sleeper forces reveals that most contact forces are small, ranging between 0.1kN and 0.5kN in all cases. As the sleeper force increases, the contacts in the range of 0.5kN and 2kN become more widely and randomly distributed. This suggests that during the track degradation process, high sleeper force tends to cause a broader range of small damage to the ballast rather than a smaller range of larger damage.
- Both the average and maximum contact forces between the sleeper and ballast particles under the hanging sleeper increase linearly as the sleeper force grows. Similarly, contact forces between the ballast particle and bottom under the hanging sleeper increase linearly but more smoothly. This is because the contact forces are redistributed within the ballast layer.

In this application, the movement of the hanging sleepers during train passage is simulated in the FEM model and used as input for the DEM method to calculate the detailed behaviour of ballast particles. This application demonstrates a DEM & FEM cooperative method, successfully addressing the feasibility challenge of accurately studying ballast behaviour under dynamic conditions.

6.2 Recommendation

Based on the conclusions of the dissertation, the following recommendations are suggested for further research.

For numerical simulations:

The results of simulations are typically used for comparison with a reference case, which is usually a structure that has been previously studied. However, when new designs are more complex and contain new elements that have not been used before, there is a gap in knowledge that needs to be addressed. This issue is mainly related to the meaning of contacts in the simulation models. Therefore, there is a need to strengthen the linkage between contact parameters and physical properties to improve the practical significance of simulations.

For new designs in railway track:

Research on new materials, elements, and components for railway tracks has shown improvement in long-term performance, maintenance, sustainability, and availability. However, these new designs also have disadvantages that need to be explored further. Understanding the unstated disadvantages is part of the reason why many designs may not be feasible in practice. Moreover, new technologies such as big data, intelligent monitoring, and digital management have been developed, and further research can explore the linkage between these technologies and new materials for a more

comprehensive system. The goal is to increase strength, decrease deterioration, save costs, and accommodate higher traffic volume.

Reference

- [1] B. Indraratna, *Advanced Rail Geotechnology-Ballasted Track*, CRC Press 2011.
- [2] Standard, EN 13450:2013, *Aggregates for railway ballast*. .
- [3] C. Esveld, *Modern railway track*, MRT-Productions, The Netherlands, 2001.
- [4] Y. Guo, V. Markine, J. Song, G. Jing, *Ballast degradation: Effect of particle size and shape using Los Angeles Abrasion test and image analysis*, *Construction and Building Materials* 169 (2018) 414-424.
- [5] Y. Qian, H. Boler, M. Moaveni, E. Tutumluer, Y.M.A. Hashash, J. Ghaboussi, *Characterizing Ballast Degradation through Los Angeles Abrasion Test and Image Analysis*, *Transportation Research Record: Journal of the Transportation Research Board* 2448(1) (2014) 142-151.
- [6] Selig E T, Waters J M. *Track geotechnology and substructure management*. Thomas Telford, 1994.
- [7] H. Huang, E. Tutumluer, W. Dombrow, *Laboratory Characterization of Fouled Railroad Ballast Behavior*, *Transportation Research Record: Journal of the Transportation Research Board* 2117(1) (2009) 93-101.
- [8] L.M. Le Pen, W. Powrie, A. Zervos, S. Ahmed, S. Aingaran, *Dependence of shape on particle size for a crushed rock railway ballast*, *Granular Matter* 15(6) (2013) 849-861.
- [9] M. Koohmishi, M. Palassi, *Evaluation of morphological properties of railway ballast particles by image processing method*, *Transportation Geotechnics* 12 (2017) 15-25.
- [10] Y. Guo, V. Markine, X. Zhang, W. Qiang, G. Jing, *Image analysis for morphology, rheology and degradation study of railway ballast: A review*, *Transportation Geotechnics* 18 (2019) 173-211.
- [11] X. Zhang, C. Zhao, W. Zhai, C. Shi, Y. Feng, *Investigation of track settlement and ballast degradation in the high-speed railway using a full-scale laboratory test*, *Proceedings of the Institution of Mechanical Engineers, Part F: Journal of Rail and Rapid Transit* 233(8) (2018) 869-881.
- [12] Q.D. Sun, B. Indraratna, S. Nimbalkar, *Deformation and Degradation Mechanisms of Railway Ballast under High Frequency Cyclic Loading*, *Journal of Geotechnical and Geoenvironmental Engineering* 142(1) (2016).
- [13] C. Charoenwong, D.P. Connolly, P.K. Woodward, P. Galvín, P. Alves Costa, *Analytical forecasting of long-term railway track settlement*, *Computers and Geotechnics* 143 (2022) 104601.
- [14] A. Lundqvist, R. Larsson, T. Dahlberg, *Influence of railway track stiffness variations on wheel/rail contact force*, in: *Workshop Track for High-Speed Railways Porto, Portugal*, 2006.

- [15] A.D. Kerr, B.E. Moroney, Track transition problems and remedies, *Bulletin*, 742 (1993), pp. 267-298.
- [16] Z.G. Li, T.X. Wu, Vehicle/track impact due to passing the transition between a floating slab and ballasted track. *Noise and Vibration Mitigation for Rail Transportation Systems*, Springer, 2008: 94–100.
- [17] A. Paixão, E. Fortunato, R. Calçada, Design and construction of backfills for railway track transition zones, *Proceedings of the Institution of Mechanical Engineers, Part F: Journal of Rail and Rapid Transit* 229(1) (2013) 58-70.
- [18] D. Li, D. Otter, G. Carr, Railway Bridge Approaches under Heavy Axle Load Traffic: Problems, Causes, and Remedies, *Proceedings of the Institution of Mechanical Engineers, Part F: Journal of Rail and Rapid Transit* 224(5) (2010) 383-390.
- [19] T.D. Stark, S.T. Wilk, Root cause of differential movement at bridge transition zones, *Proceedings of the Institution of Mechanical Engineers, Part F: Journal of Rail and Rapid Transit* 230(4) (2015) 1257-1269.
- [20] C. Alves Ribeiro, A. Paixão, E. Fortunato, R. Calçada, Under sleeper pads in transition zones at railway underpasses: numerical modelling and experimental validation, *Structure and Infrastructure Engineering* 11(11) (2014) 1432-1449.
- [21] B. Coelho, P. Hölscher, J. Priest, W. Powrie, F. Barends, An Assessment of Transition Zone Performance, *Proceedings of the Institution of Mechanical Engineers, Part F: Journal of Rail and Rapid Transit* 225(2) (2011) 129-139.
- [22] B.Z. Coelho, J. Priest, P. Hölscher, Dynamic behaviour of transition zones in soft soils during regular train traffic, *Proceedings of the Institution of Mechanical Engineers, Part F: Journal of Rail and Rapid Transit* 232(3) (2017) 645-662.
- [23] D. Li, M. ASCE, D. Davis, M. ASCE, Transition of Railroad Bridge Approaches, *Journal of Geotechnical and Geoenvironmental Engineering* 131(11) (2005) 1392-1398.
- [24] H. Wang, V. Markine, Dynamic behaviour of the track in transitions zones considering the differential settlement, *Journal of Sound and Vibration* 459 (2019) 114863.
- [25] J.N. Varandas, P. Hölscher, M.A.G. Silva, Dynamic behaviour of railway tracks on transitions zones, *Computers & Structures* 89(13-14) (2011) 1468-1479.
- [26] Y. Shan, B. Albers, S.A. Savidis, Influence of different transition zones on the dynamic response of track–subgrade systems, *Computers and Geotechnics* 48 (2013) 21-28.
- [27] X. Lei, L. Mao, Dynamic response analyses of vehicle and track coupled system on track transition of conventional high speed railway, *Journal of Sound and Vibration* 271(3-5) (2004) 1133-1146.

- [28] M. Shahraki, C. Warnakulasooriya, K.J. Witt, Numerical study of transition zone between ballasted and ballastless railway track, *Transportation Geotechnics* 3 (2015) 58-67.
- [29] J. Shi, M.P.N. Burrow, A.H. Chan, Y.J. Wang, Measurements and simulation of the dynamic responses of a bridge–embankment transition zone below a heavy haul railway line, *Proceedings of the Institution of Mechanical Engineers, Part F: Journal of Rail and Rapid Transit* 227(3) (2012) 254-268.
- [30] A. Namura, T. Suzuki, Evaluatin of countermeasures against differential settlemenr at track transitions, *Quarterly Report of RTRI* 48(3) (2007) 176-182.
- [31] A. Paixão, E. Fortunato, R. Calçada, Transition zones to railway bridges: Track measurements and numerical modelling, *Engineering Structures* 80 (2014) 435-443.
- [32] J. Mak, Y. Chen, M.A. Sadek, Determining parameters of a discrete element model for soil–tool interaction, *Soil and Tillage Research* 118 (2012) 117-122.
- [33] P.A.Cundall, O.D.L. Srrack, A discrete numerical model for franular assembles, *geotechnique* 29(1) (1979) 47-65.
- [34] M.P. Fransen, M. Langelaar, D.L. Schott, Application of DEM-based metamodels in bulk handling equipment design: Methodology and DEM case study, *Powder Technology* 393 (2021) 205-218.
- [35] Z. Wei, Y. Lifu, M. Gang, C. Xiaolin, Z. Lai, K. Xu, DEM analysis of the size effects on the behavior of crushable granular materials, *Granular Matter* 18(3) (2016).
- [36] G. Jing, X. Zhang, W. Jia, Lateral resistance of polyurethane-reinforced ballast with the application of new bonding schemes: Laboratory tests and discrete element simulations, *Construction and Building Materials* 221 (2019) 627-636.
- [37] F.A. Tavaréz, M.E. Plesha, Discrete element method for modelling solid and particulate materials, *International Journal for Numerical Methods in Engineering* 70(4) (2007) 379-404.
- [38] J. Ai, J.-F. Chen, J.M. Rotter, J.Y. Ooi, Assessment of rolling resistance models in discrete element simulations, *Powder Technology* 206(3) (2011) 269-282.
- [39] P. Aela, L. Zong, M. Esmaeili, M. Siahkouhi, G. Jing, Angle of repose in the numerical modeling of ballast particles focusing on particle-dependent specifications: Parametric study, *Particuology* 65 (2022) 39-50.
- [40] M. Lu, G.R. McDowell, The importance of modelling ballast particle shape in the discrete element method, *Granular Matter* 9(1-2) (2006) 69-80.
- [41] Y. Guo, Y. Ji, Q. Zhou, V. Markine, G. Jing, Discrete Element Modelling of Rubber-Protected Ballast Performance Subjected to Direct Shear Test and Cyclic Loading, *Sustainability* 12(7) (2020) 2836.

- [42] N.T. Ngo, B. Indraratna, C. Rujikiatkamjorn, Simulation Ballasted Track Behavior: Numerical Treatment and Field Application, *International Journal of Geomechanics* 17(6) (2017) 04016130.
- [43] V. Toropov, V. Markine, The use of simplified numerical models as mid-range approximations, 6th Symposium on Multidisciplinary Analysis and Optimization, 1996.
- [44] D.J. Lucia, P.S. Beran, W.A. Silva, Reduced-order modeling: new approaches for computational physics, *Progress in Aerospace Sciences* 40(1-2) (2004) 51-117.
- [45] R. Jin, X. Du, W. Chen, The use of metamodeling techniques for optimization under uncertainty, *Structural and Multidisciplinary Optimization* 25(2) (2003) 99-116.
- [46] X. Wang, S. Zhang, H. Pan, Z. Zheng, Y. Huang, R. Zhu, Effect of soil particle size on soil-subsoiler interactions using the discrete element method simulations, *Biosystems Engineering* 182 (2019) 138-150.
- [47] T.A. Kettler, J.W. Doran, T.L. Gilbert, Simplified Method for Soil Particle-Size Determination to Accompany Soil-Quality Analyses, *Soil Science Society of America Journal* 65(3) (2001) 849-852.
- [48] S. Lommen, M. Mohajeri, G. Lodewijks, D. Schott, DEM particle upscaling for large-scale bulk handling equipment and material interaction, *Powder Technology* 352 (2019) 273-282.
- [49] M. Koozmishi, M. Palassi, Degradation of railway ballast under compressive loads considering particles rearrangement, *International Journal of Pavement Engineering* (2018) 1-13.
- [50] H. Boler, Y. Qian, E. Tutumluer, Influence of Size and Shape Properties of Railroad Ballast on Aggregate Packing, *Transportation Research Record: Journal of the Transportation Research Board* 2448(1) (2014) 94-104.
- [51] T. Abadi, L. Le Pen, A. Zervos, W. Powrie, Measuring the Area and Number of Ballast Particle Contacts at Sleeper-Ballast and Ballast-Subgrade Interfaces, *International Journal of Railway Technology* 4(2) (2015) 45-72.
- [52] M. Obermayr, C. Vrettos, P. Eberhard, T. Däuwel, A discrete element model and its experimental validation for the prediction of draft forces in cohesive soil, *Journal of Terramechanics* 53 (2014) 93-104.
- [53] C. Chen, B. Indraratna, G. McDowell, C. Rujikiatkamjorn, Discrete element modelling of lateral displacement of a granular assembly under cyclic loading, *Computers and Geotechnics* 69 (2015) 474-484.
- [54] B. Suhr, S. Marschnig, K. Six, Comparison of two different types of railway ballast in compression and direct shear tests: experimental results and DEM model validation, *Granul Matter* 20(4) (2018) 70.

- [55] B. Suhr, K. Six, Simple particle shapes for DEM simulations of railway ballast: influence of shape descriptors on packing behaviour, *Granul Matter* 22(2) (2020) 43.
- [56] Y. Guo, C. Zhao, V. Markine, C. Shi, G. Jing, W. Zhai, Discrete element modelling of railway ballast performance considering particle shape and rolling resistance, *Railway Engineering Science* 28(4) (2020) 382-407.
- [57] Z. Hossain, B. Indraratna, F. Darve, P.K. Thakur, DEM analysis of angular ballast breakage under cyclic loading, *Geomechanics and Geoengineering* 2(3) (2007) 175-181.
- [58] E. Mahmoud, A.T. Papagiannakis, D. Renteria, Discrete Element Analysis of Railway Ballast under Cycling Loading, *Procedia Engineering* 143 (2016) 1068-1076.
- [59] S. Lobo-Guerrero, L.E. Vallejo, Discrete Element Method Analysis of Railtrack Ballast Degradation during Cyclic Loading, *Granular Matter* 8(3-4) (2006) 195-204.
- [60] X. Bian, W. Li, Y. Qian, E. Tutumluer, Micromechanical Particle Interactions in Railway Ballast through DEM Simulations of Direct Shear Tests, *International Journal of Geomechanics* 19(5) (2019) 04019031.
- [61] Y. Guo, C. Zhao, V. Markine, G. Jing, W. Zhai, Calibration for discrete element modelling of railway ballast: A review, *Transportation Geotechnics* 23 (2020) 100341.
- [62] V.C. Janoo, Quantification of Shape, Angularity, and Surface Texture of Base Course Materials, 1998.
- [63] J. Liu, P. Wang, J. Liu, Macro- and micro-mechanical characteristics of crushed rock aggregate subjected to direct shearing, *Transportation Geotechnics* 2 (2015) 10-19.
- [64] W.L. Lim, G.R. McDowell, Discrete element modelling of railway ballast, *Granular Matter* 7(1) (2005) 19-29.
- [65] J. Ferrellec, G. McDowell, Modelling realistic shape and particle inertia in DEM, *Géotechnique* 60(3) (2010) 227-232.
- [66] W. Jia, V. Markine, Y. Guo, G. Jing, Experimental and numerical investigations on the shear behaviour of recycled railway ballast, *Construction and Building Materials* 217 (2019) 310-320.
- [67] Y. Guo, W. Jia, V. Markine, G. Jing, Rheology study of ballast-sleeper interaction with particle image Velocimetry (PIV) and discrete element modelling (DEM), *Construction and Building Materials* 282 (2021) 122710.
- [68] G. Jing, W. Jia, X. Wang, V. Markine, R. Nålsund, Y. Guo, Experimental and numerical study on lateral resistance of frictional sleeper with arrowhead groove, *Transportation Geotechnics* 30 (2021) 100638.

- [69] X. Zhang, C. Zhao, W. Zhai, DEM Analysis of Ballast Breakage Under Train Loads and Its Effect on Mechanical Behaviour of Railway Track, Proceedings of the 7th International Conference on Discrete Element Methods (2017) 1323-1333.
- [70] I.C.G. Inc., PFC 5.0 document, (2018).
- [71] J. Chen, R. Gao, Y. Liu, Numerical Study of Particle Morphology Effect on the Angle of Repose for Coarse Assemblies Using DEM, Advances in Materials Science and Engineering 2019 (2019) 1-15.
- [72] M.A. Wnek, E. Tutumluer, M. Moaveni, E. Gehringer, Investigation of Aggregate Properties Influencing Railroad Ballast Performance, Transportation Research Record: Journal of the Transportation Research Board 2374(1) (2013) 180-189.
- [73] B. Indraratna, T. Ngo, Ballast railroad design: smart-uow approach, CRC Press 2018.
- [74] F. Khatibi, M. Esmaeili, S. Mohammadzadeh, DEM analysis of railway track lateral resistance, Soils and Foundations 57(4) (2017) 587-602.
- [75] E. Tutumluer, Y. Qian, Y.M.A. Hashash, J. Ghaboussi, D.D. Davis, Discrete element modelling of ballasted track deformation behaviour, International Journal of Rail Transportation 1(1-2) (2013) 57-73.
- [76] H. Wang, V. Markine, Corrective countermeasure for track transition zones in railways: Adjustable fastener, Engineering Structures 169 (2018) 1-14.
- [77] H. Wang, V. Markine, X. Liu, Experimental analysis of railway track settlement in transition zones, Proc Inst Mech Eng F J Rail Rapid Transit 232(6) (2018) 1774-1789.

Part II

Appendix Paper I-VI

Paper I

Parameter and efficiency analysis on particle shape of railway ballast in DEM simulations

Wenli Jia, Valeri Markine

Submitted to Proceedings of the Institution of Mechanical Engineers, Part F.

Under review

PII-I

Abstract

The Discrete Element Method (DEM) is a commonly used numerical tool for granular materials-related research. Due to this characteristic, numerical simulations based on DEM can provide mesoscopic results, such as the contact force and displacement at the particle level. DEM simulations are appropriately considered for railway ballast-related simulations because the irregular shape and Particle Size Distribution (PSD) are crucial to the ballast assembly behaviour. However, the efficiency of DEM simulations is low, and the algorithm of information calculations and updates limits the number of elements in a model. Thus, the scale and complexity of models are simplified in research to reach an acceptable calculation time. This paper analysed the efficiency-related questions, how the results are influenced by different complexity of particle shapes and how the results are corrected by adding compensational contact parameters. In this paper, a series of simulations are performed, both the macroscopic results (sleeper displacement) and mesoscopic results (contact forces and coordination number) are obtained and analysed, and the calculation time for every simulation is concluded and compared. The research provides a comprehensive understanding and guidance of ballast-related DEM simulations.

Keyword: Railway ballast, DEM, Simulation efficiency, Shape simplification, Shape optimisation

1. Introduction

Discrete Element Method (DEM) is a numerical solution normally used to analyse the behaviour of granular materials [1-3]. In DEM-based models, the particles are the basic elements, together with the wall element as a boundary. The interaction between particles is calculated according to the contact law and presents the behaviour of a sample or a structure [4-6].

However, the efficiency of DEM is low due to its calculation algorithm. Every element in a model works as a unit, which contains its property information, such as volume, density and stiffness, and behaviour information, such as force and displacement. Every contact between elements needs to be detected and updated separately based on position and applied contact parameters (or inherited attributes from particles) [7, 8]. The position is utilized to detect the status of adjacent particles, enabling the activation of contact interactions. Parameters such as stiffness and friction coefficient are employed to calculate the force-displacement behaviour between particles. These parameters are essential for accurately simulating the interactions and behaviour of the particles within the system. In addition, the particle shape of ballast contributes to the performance of ballast layer, i.e. the accuracy of a simulation [9-11]. Thus in several researches, the irregular particles are generated, such as using polyhedrons[12-14] and cluster of spheres. Specially for a particle can be generated by a cluster of several spheres (named as “Clump” in the software PFC3D) to achieve irregularity [15-17]. All those spheres in a clump contain its information, and a wall contains several triangle facets. The number of elements increases the calculation effort, thus lowering calculation efficiency [18, 19].

For example, in the following Figure 1-1, a single sleeper section of the ballasted track is built by the authors. This model contains 647323 (sphere) elements of 24311 particles, 86 elements as the 1 sleeper and 3 boundary wall, and 91925 contacts. When using this model to simulate a lateral resistance test, the calculation time for the 15 seconds process is more than 40 hours, as done in author’s previous work[5, 20, 21](hardware: Intel Xeon CPU E5, RAM 64G, software PFC3D 5.0).

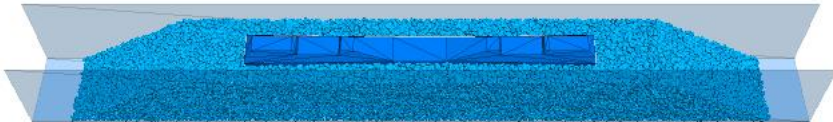


Figure 1-1. Ballasted track model of a single sleeper section

This considerable time consumption compared with real-time restricts the feasibility of DEM simulations, especially when a long-term simulation based on cyclic (or specially designed) loading are needed [22, 23]. Thus, several simplified methods are taken into consideration by researchers to enhance efficiency. For example, in reference[24], the researchers analysed the influence of soil particle size on the reliability of results because simulating soil particles with the actual size and size distribution is unachievable. The natural soil particles are around 0.002mm to 2mm[25]. However, being closer to the exact size leads to higher reliability. The results indicate that decreasing the particle radius from 5 mm to 3 mm resulted in a significant increase in calculation time, approximately seven times longer, during the simulation involving a subsoiler. This increase in time consumption amounted to approximately 500 hours, which is deemed to be unacceptable in terms of computational efficiency.

Similarly, in reference[19], the research on the interaction of bulk handling equipment and materials, it contains 77m³ iron ore pellets. Thus particle size up-scaling method is used to improve the efficiency. In addition, using a low-fidelity model, such as in reference[26-28], 2D models are used

to perform the long-term behaviour. All those methods aim to reduce the number of elements, thus reducing the calculation time.

For ballast-related research, size up-scaling is unsuitable for reducing the calculation efforts. The ballast particle size typically ranges from 20-65mm[29, 30], Ballast size is relatively big compared with soil, up-scaling method is not as efficient as for small-particles. And, the particle size distribution is one of the critical parameters to maintain the behaviour of the ballast layer, performing drainage ability, elasticity, and bearing load[31, 32]. In addition, when ballast interacts with the sleeper, the contact area is less than 1% of the sleeper[33]. Particle size up-scaling can further decrease the contact area and lead to high distortion. Therefore, the results are sensitive to the size of the ballast particle.

The efficiency problems mainly come from the complexity of irregular shape generation instead of particle size. Consequently, railway ballast-related simulations typically use shape simplification, such as the particles are generated by a ball shape in reference[34], and the ballast particles are 3-ball clusters in reference[35]. However, shape also contributes to the behaviour of the ballast layer (as reported in reference[15, 36]). A proper choice of particle shape also presents meaningful results [37]. As a supplement to the interlock loss of shape simplification, In reference[8], the research simulated the angle of repose tests using different shapes and contact parameters(rolling resistance). In reference[38], the researchers used different simplified shapes with rolling resistance to correct the results of direct shear tests.

With those ideas, the DEM-based simulations are simplified to improve efficiency. One thing that should be noticed is that those simplifications can lower the reliability of the results depending on which scope is demanded. For example, reference[39] reported that the macroscopic results are well presented by their simplified model. The mesoscopic results are unreliable, but simulations are valid depending on their target. Based on the above information, 2 questions still need answers by further research: how to improve the efficiency of DEM-based numerical simulation is mainly related to shape simplification, and what is the influence of the simplification on the accuracy and reliability in different scopes.

In this paper, the different shapes of particles are taken into consideration. The high-fidelity particles are close to a real ballast; the simplest particle shape is a ball shape. The simplified particle shapes are generated between the high-fidelity shape and the simplest ball by arranging the sphere in a cluster as a particle. The simplifications are realised using the Distance and Ratio as the controlling parameter. In addition, rolling resistance is applied in some conditions to correct the results.

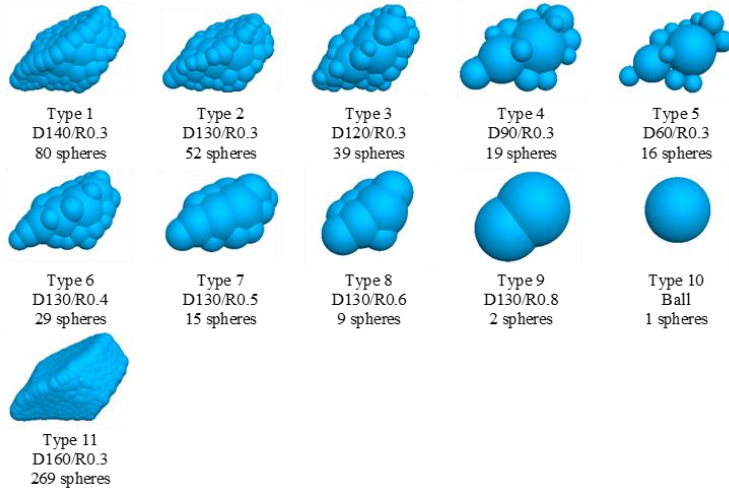
There are 22 types of shapes in total. A series of short-term cyclic loading simulations are conducted to get the results of the influence of particle shape on the results. Those models are a ballast box and a sleeper embedded in the ballast layer. Results are divided into macroscopic and mesoscopic results to validate the accuracy and determine when those simplifications are applicable. Each type is calculated 10 times to reduce the random deviation, which is 220 simulations. The conclusion provides a comprehensive understanding of reliability and shape simplification.

2. Ballast particle and box model

For railway ballast, the irregular shape and Particle Size Distribution (PSD) are the geometry factors influencing the reliability of results. Among them, the irregular shape largely increases the complexity of a model and the calculation efforts. For example, as shown in Table 1, Type 11 contains 269 spheres, and each sphere should be supervised and updated during the calculation. This problem largely restricts the feasibility of DEM simulations.

Based on the influence of shape simplification on the reliability of results, 11 ballast particle models are generated, considering their complexity. The same templates to generate those shapes are imported into the software PFC3D[40]. As shown in Table 1-1, those ballast shapes are generated by controlling the arrangement of spheres with 2 parameters in the software: Distance and Ratio[41-43]. Different parameters contribute to different complexity (irregularity) of particles, and then influence the macroscopic and mesoscopic results.

Table 1-1. different ballast models



Where Type 11 and Type 1 to Type 5 are related to the simplification by decreasing the Distance (Group 1). Distance adjusts the amount of overlapping of the adjacent spheres, and it ranges from 0 to 180. Type 2 and Type 6 to type 10 are related to the increase in Ratio (Group 2). This parameter controls the size ratio of the biggest and smallest spheres filling in the template, ranging from 0 to 1. Parameter changes reduce particle fidelity (reliability) with different extents of simplification. In addition, Type 11 is the reference type; it has the most complex arrangement of spheres and can be regarded as a real ballast.

In addition, to correct the contact behaviour loss by shape simplification, the rolling resistance is added to Type 9 (Group 3) and Type 10 (Group 4). The rolling resistance is a frictional coefficient which can compensate for the interlock loss. In this series of simulations, the rolling resistance is applied to Type 9 and Type 10, with the value of 0.1, 0.3, 0.5 and 0.7. Because the rolling resistance is only a computational parameter without any physical meaning, Type 10 (ball) also uses the rolling resistance of 5, 10 and 100. Those conditions are expected to show the significance of the correction effect of the parameter.

The particles used in this research contain 22 types and 4 groups. Based on the box model with a sleeper, considering the difference in the Distance, the Ratio, and the rolling resistance. The assembly of particles are in the same Particle Size Distribution (as shown in Figure 1-2), and a porosity of 0.27. And the dimension of the models based on those particles are all the same.

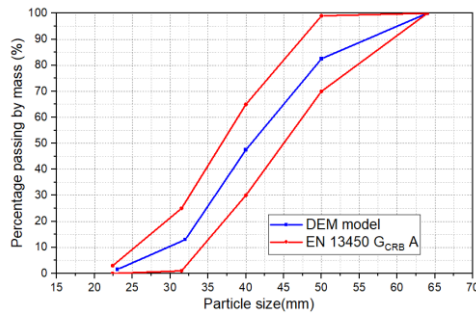


Figure 1-2. Particle Size Distribution

The model used in this research is a 300mm(L)*300mm(W)*200mm(H) box with particles in the box according to the PSD and a 100mm(L)*100mm(W)*75mm(H) sleeper is embedded in the ballast layer. The model is shown in Figure 1-3. A 5Hz cyclic loading is applied to the sleeper to show the behaviour of different shapes. The loading amplitude is 10 kN, the maximum value is 10.38 kN, and the minimum value is 0.38 kN, which relates to the sleeper's weight. The total simulated period is 1.05s, and the model stops at the peak of the loading. The contact model is linear contact model, contact parameters are listed in Table.2. Those parameters, excluded the rolling resistance, are the same for different shapes.

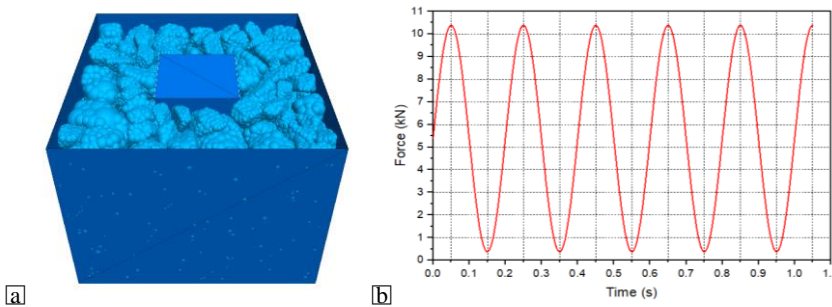


Figure 1-3. Box model with sleeper embedded, and the loading mode

Table 1-2. Contact parameters of DEM model

Parameter	Ballast particle	Sleeper/Box
Tangential stiffness (N/m)	1.0e7	6.0e8
Normal stiffness (N/m)	1.0e7	6.0e8
Friction coefficient (Linear contact model)	0.5	0.5
Friction coefficient (Rolling resistance)	0.1/0.3/0.5/0.7/5/10/100	-
Mass density (kg/m ³)	2630	-
Damping coefficient	0.7	0.7

By the loading method, the ballast settlement is obtained, presenting as the final displacement of the sleeper. The contact number and contact force are recorded at the stopping state, where the loading is at the peak value. The scale of the model is relatively small, so every condition is built and calculated ten times using the different random number generators. The presented results in this paper

are the average value. Finally, all those data are compared to analyse the influence of particles on the behaviour of an assembly.

3. Results and analysis

The results obtained in the DEM simulations contain three parts: firstly, the coordination number before and after loading indicates the shape difference. Secondly, the sleeper displacement is the macroscopic result which presents the influence of particle shape and correction parameters on the behaviour of non-particle elements. Thirdly, the average and maximum contact force are mesoscopic results, showing particles' behaviour influenced by shape simplification. These three parts comprehensively include all the results of numerical simulations based on DEM. Moreover, the time consumption of different shapes is recorded to highlight the performance of efficiency.

Coordination number

The coordination number is the average contact number of particles, and it is the total contact number divided by the total particle number. This indicator is directly connected with the particle shape, influencing the mesoscopic force behaviour. The coordination number is the average contact number of particles, and it is the total contact number divided by the total particle number. This indicator is directly connected with the particle shape, influencing the mesoscopic force behaviour. A bigger value means more contact points, thus, when the loading is applied, more contact is participating in bearing, and the force distribution is more uniform. In a numerical simulation, this phenomenon presents a lower average contact force, thus influencing the conclusion of how the ballast degraded.

As shown in Figure 1-4(a), these data are the balanced model(before loading). The irregularity of particles influences the changes in coordination number. Separately, for distance decrease and ratio increase, the changes are all as expected. However, the influence is not always significant, considering the shape changes by different parameters. For group 1, the particles are simplified, but the angularity is not decreased (even increased), which still provides the interlock.

On the contrary, the angularity of group 2 is decreased with the Ratio increase, thus presenting fewer contact points. The coordination number slightly changes for the same shape with different rolling resistance, but it is at a similar level. Especially the number decreased from 2.7 to 1.7, comparing the Type 10 (reference shape) with the Type 11(ball shape).

Figure 1-4(b) shows the coordination number at the finish status(after loading). It is increased by comparing the same shape before and after loading because the sleeper works as a compactor under cyclic loading. What should be noticed is that the Type 10 (ball shape) without rolling resistance, the coordination number is decreased. It is because the ball shape is more likely to rotate, rearrange, and squeeze, thus flow away. Explanations also can be proved in the following section, the sleeper displacement.

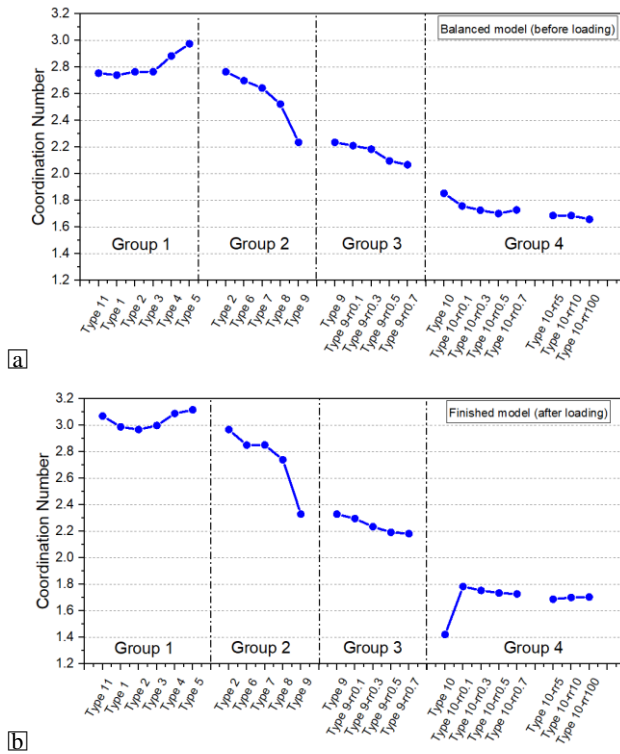


Figure 1-4. The influence of shape simplification on coordination number: (a) Before loading (b) After loading

PII-I

Sleeper displacement

The macroscopic results are normally used to present or validate the behaviour of a design (for example, the sleeper) which interacts with particles instead of researching the behaviour of particles. In this research, the sleeper displacement is the macroscopic result, the sleeper interacted with ballast, but different kinds of particles may lead to a similar result.

The sleeper displacement of different shapes after loading is shown in Figure 1-5(a). For the process of Distance decrease (Group 1), the sleeper displacement is slightly influenced but at a similar level. It indicated that the macroscopic results are not influenced by Distance. It is because the shape is simplified, but the interlock is not lost too much. It also can be seen in the coordination number analysis.

On the contrary, with the ratio increase(Group 2), the shape changes to rounder, and the sleeper displacement decreased. When the shape becomes a ball (Type 10), the sleeper displacement is largely increased and far beyond the range of others. It indicated that the Ratio increase is significant for the results.

When the rolling resistance of 0.1 is added, the value returns to the reasonable range. Results also show that when the applied rolling resistance is 0.3, the displacement is even closer to the reference than Type 7 (15 spheres). It proved that the rolling resistance could compensate for the interlock loss and contribute to the reliability of the macroscopic results. In addition, for Type 9 (2 balls made

particle), the influence of adding rolling resistance is not as significant as it is on Type 10 (ball). Because this kind of shape still provides resistance to rotation by itself.

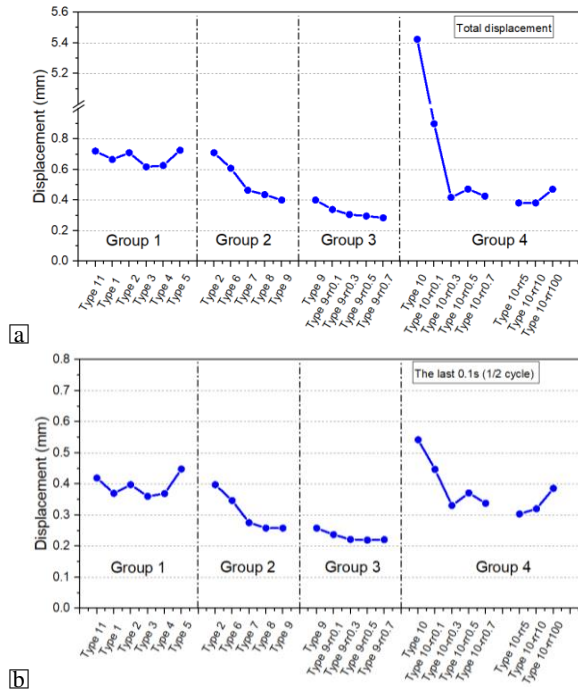


Figure 1-5 The influence of shape simplification on sleeper displacement: (a) In total, (b) In the last $\frac{1}{2}$ cycle

The loading is 1.05s, and if the initial 0.95 seconds is treated as a stabilization process, the last 0.1s (1/2 cycle) can be regarded as a simulation of compression under the applied loading from 0.38kN to 10.38kN. The sleeper displacement of this period is shown in Figure 1-5(b). This figure shows the difference between different shapes more obvious, the fluctuations of group 1 present the slight influence of Distance decreasing. The results of other groups present the accuracy loss caused by angular loss, and the correction by adding rolling resistance. It is also in accordance with the conclusions obtained with the whole cyclic loading. However, for the rolling resistance bigger than 0.3, the displacement of the sleeper fluctuates, and it proved that the extra high rolling resistance (the value of 5, 10, and 100) does not contribute to further influence. All the results present that the sleeper displacement is uniformly accumulated.

As described above, in macroscopic results, where the behaviour of particles is not the first consideration, the accuracy of results is predictable. Thus, the structure-focused simulations can choose ball shape particles and apply the rolling resistance to reduce the calculation effort. And the rolling resistance of 0.3 already shows the compensation on the interlock loss by shape simplification.

Contact force

Contact force on a particle is the mesoscopic result. It is the advantage of using DEM-based simulations. However, the macroscopic results of different particle shapes can be similar. The contact force shows the difference. This difference is crucial to the reliability of the results. The contact force is related to the coordination number. In different groups, the coordination number is increased with

the Distance decrease and Ratio decrease. In contrast, the contact force (Table 1-3,) is increased because less number of contact points participate in the loading bearing. Significant changing can be found here, compared with the sleeper displacement. For example, when the shape is simplified from the reference Type 11 to Type 5, the average contact force increases from 58.9N to 67.3N, and for Type 10 without rolling resistance, this value soars to 139.8N. In addition, when the rolling resistance is added to Type 10, the average contact force still ranges from 92.7N to 103.2N, which is around a 57% to 75% increase compared with the reference. Similar to the sleeper displacement, the rolling resistance does not correct the results of Type 9 (2 balls made particle). As shown in Figure 1-6(a).

The comparison between Type 4 and Type 5 in group 1 should be highlighted. However, the changes in the coordination number of those types are an increase trend, which means more contact points are participating in bearing, but the average contact force is also increased. This phenomenon disobeys the theory of large coordination number leads to smaller average contact force, because the particle shape of Type 4 and Type 5 is no longer an ‘natural coarse’ surface due to those protuberances or unevenness caused by small overlap.

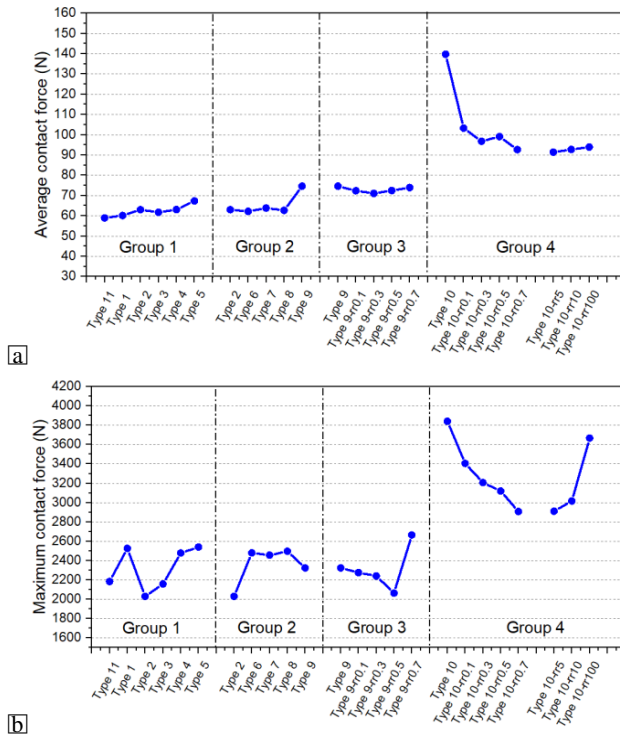


Figure 1-6. The influence of shape simplification on contact: (a) Average contact force, (b) Maximum contact force

The maximum contact force is shown in the following Figure 1-6(b). However, some fluctuations are observed, which makes a slight difference in shape simplification. But, the comparison between Type 10 (ball) and others is still significant. Because the maximum contact force is related to the force concentration.

As a further explanation, the number of contacts counted by force range is listed in the following Table 1-3, those numbers are also the average value of 10 random repeated simulations. It can be seen that most forces are smaller than 1kN. Results show that the shape simplification by Distance decrease leads to a relatively smaller number in the high force range due to the “unnatural coarser surface”. And, for most of the contacts (more than 99%) in the lower range(<500), the contact number insignificantly fluctuates. Those results explain why the macroscopic results are not significantly influenced by Distance. On the contrary, the simplification by Ratio increase leads to a decreasing trend of the contact number in the lower force range and a sharp decrease in the total contact number. Under the same loading condition, the contact number of a higher range is increased. When applying the rolling resistance on Type 10 to correct the force behaviour, the total contact number increased, and the number distribution in each range was more uniform than Type 10 without rolling resistance.

All the above results show that shape simplification can lead to a distortion in mesoscopic results, decreasing the accuracy from high to low. Whereas the macroscopic results are not sensitive to shape simplification and can be corrected. Shape simplification can be used depending on the demanded balance of time consumption and accuracy.

Table 1-3. Contact number of different shape (counted by force)

Force range (N)	Type 1	Type 2	Type 3	Type 4	Type 5	Type 6	Type 7	Type 8	Type 9	Type 10
>3000	0.2	0.4	0.1	0.3	0.2	0.1	0.3	0.2	0.1	1.7
2000-	1	0.8	0.4	0.7	0.4	1.1	0.6	1.3	0.7	3.2
3000-	7.7	5.9	6	4.9	4.3	3.8	6.4	6.5	6.7	15.2
2000-	26.8	23.3	23.3	22.7	21.8	19.9	24.1	25.2	22.4	35.7
500-	231	244.1	230.8	242	234.9	236.9	201.3	223.3	212.5	222.3
100-	1292.4	1332.6	1322.2	1287.8	1331.6	1363	1273.6	1303.4	1285.7	1057.8
500										600
<100										
Total	1540.6	1607.1	1582.8	1557.9	1593.6	1624.2	1506.6	1559.3	1528.8	1316.8

Force range (N)	Type 9 rr0.1	Type 9 rr0.3	Type 9 rr0.5	Type 9 rr0.7	Type 10 rr0.1	Type 10 rr0.3	Type 10 rr0.5	Type 10 rr0.7	Type 10 rr1.0	Type 10 rr1.5	Type 10 rr2.0
>3000	0.1	0.1	0	0.3	0.6	0.6	0.6	0.6	0.5	0.8	1.1
2000-	0.5	0.3	0.6	1	3.1	2.2	2.1	2.1	2.7	2.6	3.4
3000-	7.3	6.8	7.2	8.8	12.7	11.4	13.3	13.3	9.2	10.4	11.2
2000-	30.1	28.6	28.1	25.8	33.2	29.6	27.9	25.3	27.2	27.1	23.9
500-	200.8	191.3	194.3	183.4	181.2	173.3	162.1	146.7	160.4	153.5	147.2
100-	1060.9	1040.1	1020	1006.9	791.8	770.4	775.5	790.9	753.4	763.7	778.1
500											
<100											
Total	1299.7	1267.2	1250.2	1226.2	1022.6	987.5	981.5	978.9	953.4	958.1	964.9

Time consuming

For the same dimension, for example, the box model, the accuracy of a DEM simulation is contrary to the complexity of the used particle shapes. High-fidelity particles lead to high computational efforts. The time consumption is the restriction of calculation. Thus it is the direct motivation of model simplification. In this research, the time consumption of models with a different shapes is recorded. As shown in Figure 1-7, the time consumption of the model is directly related to the complexity and number of elements. The time used for the calculation of the reference Type 11 is around 5 hours. When the shape is simplified to Type 2, the time is reduced to less than 0.5 hours, and when the shape is simplified to a ball, the simulation of 1.05s uses around 3 minutes.

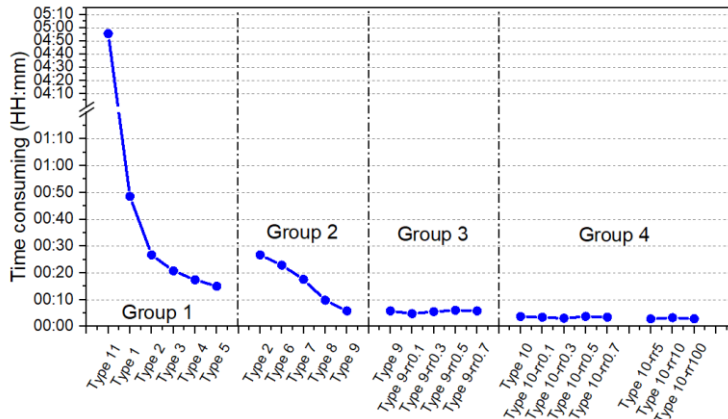


Figure 1-7. The influence of shape simplification on calculation effort

4. Conclusions

In railway ballast-related research, DEM simulation is commonly used because it can properly present the behaviour of granular material. However, due to the characteristics of the ballast layer and the algorithm of DEM, the efficiency of calculation restricts the scale and complexity of a model. Under this consideration, simplifications are used to increase the feasibility of this kind of numerical simulation. In this paper, shape simplification is mainly focused on and analysed. 11 different shapes are generated, and the rolling resistance (frictional coefficient) is applied to the simplest ball and 2-sphere shape. The macroscopic and mesoscopic results are both obtained, compared and analysed by a series of box loading tests, including the coordination number, contact force, and sleeper displacement. The main conclusions are:

1. The coordination number is directly influenced by the complexity of particle shape. Simplifying the shape reduces the number of elements and increases computational efficiency. However, simplified shapes generally result in a decrease in the coordination number (CN), which leads to fewer contacts contributing to load-bearing capabilities. During the loading process, the coordination number typically increases as the layer becomes more compacted. However, in the case of ball-shaped particles, the coordination number decreases because the balls are more prone to being squeezed away, resulting in an unnatural failure mode.

2. Sleeper displacement is one of the macroscopic results. It is least affected by particle shape. The simplification by Distance decrease slightly influences the sleeper displacement, whereas the Ratio increases significantly decrease the displacement. In addition, the sleeper displacement of the ball shape is extremely large due to its failure.
3. The contact force represents a mesoscopic outcome that is influenced by shape simplification. It is important to consider the effects of both decreasing distance and increasing ratio on the contact behaviour. Additionally, in cases where the shape is not naturally irregular, the contact forces may deviate from the expected trends observed with other simplifications.
4. Results proved that the rolling resistance could compensate for the interlock loss and contribute to the reliability of the macroscopic results. Especially for ball shape, the rolling resistance corrects the unnatural failure when the rolling resistance is bigger than 0.3. However, extra high rolling resistance cannot further increase the reliability.
5. In the simulated loading process in the research, compared with the reference shape, a decrease in Distance (from 160 to 140 or 130) can decrease the calculation time from 5 hours to less than 1 hour, whereas the influences on both macroscopic and mesoscopic results are insignificant. The ball shape only uses 5 minutes to finish the same simulation, but the mesoscopic results are distorted. It can only be used in the large-scale and macroscopic results-based model.

Acknowledgement

This is from work undertaken as part of the IN2ZONE project, which has received funding from the Shift2Rail Joint Undertaking (JU) under grant agreement 101014571 – IP/ITD/CCA – IP3.”

Reference

- [1] J. Mak, Y. Chen, M.A. Sadek, Determining parameters of a discrete element model for soil–tool interaction, *Soil and Tillage Research* 118 (2012) 117-122.
- [2] P.A.Cundall, O.D.L. Srrack, A discrete numerical model for granular assemblies, *geotechnique* 29(1) (1979) 47-65.
- [3] M.P. Fransen, M. Langelaar, D.L. Schott, Application of DEM-based metamodelling in bulk handling equipment design: Methodology and DEM case study, *Powder Technology* 393 (2021) 205-218.
- [4] Z. Wei, Y. Lifu, M. Gang, C. Xiaolin, Z. Lai, K. Xu, DEM analysis of the size effects on the behavior of crushable granular materials, *Granular Matter* 18(3) (2016).
- [5] G. Jing, X. Zhang, W. Jia, Lateral resistance of polyurethane-reinforced ballast with the application of new bonding schemes: Laboratory tests and discrete element simulations, *Construction and Building Materials* 221 (2019) 627-636.
- [6] F.A. Tavarez, M.E. Plesha, Discrete element method for modelling solid and particulate materials, *International Journal for Numerical Methods in Engineering* 70(4) (2007) 379-404.
- [7] J. Ai, J.-F. Chen, J.M. Rotter, J.Y. Ooi, Assessment of rolling resistance models in discrete element simulations, *Powder Technology* 206(3) (2011) 269-282.
- [8] P. Aela, L. Zong, M. Esmaeili, M. Siahkouhi, G. Jing, Angle of repose in the numerical modeling of ballast particles focusing on particle-dependent specifications: Parametric study, *Particuology* 65 (2022) 39-50.
- [9] Y. Guo, C. Zhao, V. Markine, G. Jing, W. Zhai, Calibration for discrete element modelling of railway ballast: A review, *Transportation Geotechnics* 23 (2020) 100341.
- [10] A. Orosz, J.P. Radics, K. Tamas, Calibration Of Railway Ballast DEM Model, *ECMS 2017 Proceedings* edited by Zita Zoltay Paprika, Péter Horák, Kata Váradi, Péter Tamás Zwierczyk, Ágnes Vidovics-Dancs, János Péter Rádics, 2017, pp. 523-528.
- [11] P. Aela, L. Zong, Z.-Y. Yin, M. Esmaeili, G. Jing, Calibration method for discrete element modeling of ballast particles, *Computational Particle Mechanics* 10(3) (2022) 481-493.
- [12] N. Ouhbi, C. Voivret, G. Perrin, J.-N. Roux, Railway Ballast: Grain Shape Characterization to Study its Influence on the Mechanical Behaviour, *Procedia Engineering* 143 (2016) 1120-1127.
- [13] J. Eliáš, Simulation of railway ballast using crushable polyhedral particles, *Powder Technology* 264 (2014) 458-465.
- [14] E. Tutumluer, Y. Qian, Y.M.A. Hashash, J. Ghaboussi, D.D. Davis, Discrete element modelling of ballasted track deformation behaviour, *International Journal of Rail Transportation* 1(1-2) (2013) 57-73.
- [15] M. Lu, G.R. McDowell, The importance of modelling ballast particle shape in the discrete element method, *Granular Matter* 9(1-2) (2006) 69-80.
- [16] Y. Guo, Y. Ji, Q. Zhou, V. Markine, G. Jing, Discrete Element Modelling of Rubber-Protected Ballast Performance Subjected to Direct Shear Test and Cyclic Loading, *Sustainability* 12(7) (2020) 2836.
- [17] N.T. Ngo, B. Indraratna, C. Rujikiatkamjorn, Simulation Ballasted Track Behavior: Numerical Treatment and Field Application, *International Journal of Geomechanics* 17(6) (2017) 04016130.
- [18] K. Giannis, A. Kwade, J.H. Finke, C. Schilde, The Effect of Particle Shape on the Compaction of Realistic Non-Spherical Particles-A Multi-Contact DEM Study, *Pharmaceutics* 15(3) (2023).
- [19] S. Lommen, M. Mohajeri, G. Lodewijks, D. Schott, DEM particle upscaling for large-scale bulk handling equipment and material interaction, *Powder Technology* 352 (2019) 273-282.
- [20] G. Jing, W. Jia, X. Wang, V. Markine, R. Nälsund, Y. Guo, Experimental and numerical study on lateral resistance of frictional sleeper with arrowhead groove, *Transportation Geotechnics* 30 (2021) 100638.
- [21] Y. Guo, W. Jia, V. Markine, G. Jing, Rheology study of ballast-sleeper interaction with particle image Velocimetry (PIV) and discrete element modelling (DEM), *Construction and Building Materials* 282 (2021) 122710.

- [22] W. Jia, V. Markine, M. Carvalho, D.P. Connolly, Y. Guo, Design of a concept wedge-shaped self-levelling railway sleeper, *Construction and Building Materials* 386 (2023).
- [23] P. Aela, P. Jitsangiam, X. Li, G. Jing, Influence of ballast bulk density and loading conditions on lateral resistance of concrete sleeper components, *Proceedings of the Institution of Mechanical Engineers, Part F: Journal of Rail and Rapid Transit* (2023).
- [24] X. Wang, S. Zhang, H. Pan, Z. Zheng, Y. Huang, R. Zhu, Effect of soil particle size on soil-subsoiler interactions using the discrete element method simulations, *Biosystems Engineering* 182 (2019) 138-150.
- [25] T.A. Kettler, J.W. Doran, T.L. Gilbert, Simplified Method for Soil Particle-Size Determination to Accompany Soil-Quality Analyses, *Soil Science Society of America Journal* 65(3) (2001) 849-852.
- [26] Z. Hossain, B. Indraratna, F. Darve, P.K. Thakur, DEM analysis of angular ballast breakage under cyclic loading, *Geomechanics and Geoengineering* 2(3) (2007) 175-181.
- [27] E. Mahmoud, A.T. Papagiannakis, D. Renteria, Discrete Element Analysis of Railway Ballast under Cycling Loading, *Procedia Engineering* 143 (2016) 1068-1076.
- [28] S. Lobo-Guerrero, L.E. Vallejo, Discrete Element Method Analysis of Railtrack Ballast Degradation during Cyclic Loading, *Granular Matter* 8(3-4) (2006) 195-204.
- [29] B. Indraratna, *Advanced Rail Geotechnology-Ballasted Track*, CRC Press 2011.
- [30] C. Esveld, *Modern railway track*, MRT-Productions, The Netherlands, 2001.
- [31] M. Koohmishi, M. Palassi, Degradation of railway ballast under compressive loads considering particles rearrangement, *International Journal of Pavement Engineering* (2018) 1-13.
- [32] H. Boler, Y. Qian, E. Tutumluer, Influence of Size and Shape Properties of Railroad Ballast on Aggregate Packing, *Transportation Research Record: Journal of the Transportation Research Board* 2448(1) (2014) 94-104.
- [33] T. Abadi, L. Le Pen, A. Zervos, W. Powrie, Measuring the Area and Number of Ballast Particle Contacts at Sleeper-Ballast and Ballast-Subgrade Interfaces, *International Journal of Railway Technology* 4(2) (2015) 45-72.
- [34] C. Chen, B. Indraratna, G. McDowell, C. Rujikiatkamjorn, Discrete element modelling of lateral displacement of a granular assembly under cyclic loading, *Computers and Geotechnics* 69 (2015) 474-484.
- [35] B. Suhr, S. Marschnig, K. Six, Comparison of two different types of railway ballast in compression and direct shear tests: experimental results and DEM model validation, *Granul Matter* 20(4) (2018) 70.
- [36] Y. Guo, V. Markine, X. Zhang, W. Qiang, G. Jing, Image analysis for morphology, rheology and degradation study of railway ballast: A review, *Transportation Geotechnics* 18 (2019) 173-211.
- [37] B. Suhr, K. Six, Simple particle shapes for DEM simulations of railway ballast: influence of shape descriptors on packing behaviour, *Granul Matter* 22(2) (2020) 43.
- [38] Y. Guo, C. Zhao, V. Markine, C. Shi, G. Jing, W. Zhai, Discrete element modelling of railway ballast performance considering particle shape and rolling resistance, *Railway Engineering Science* 28(4) (2020) 382-407.
- [39] M. Obermayr, C. Vrettos, P. Eberhard, T. Däuwel, A discrete element model and its experimental validation for the prediction of draft forces in cohesive soil, *Journal of Terramechanics* 53 (2014) 93-104.
- [40] I.C.G. Inc., PFC 5.0 document, (2018).
- [41] W. Jia, V. Markine, Y. Guo, G. Jing, Experimental and numerical investigations on the shear behaviour of recycled railway ballast, *Construction and Building Materials* 217 (2019) 310-320.
- [42] J.F. Ferrellec, G.R. McDowell, A simple method to create complex particle shapes for DEM, *Geomechanics and Geoengineering* 3(3) (2008) 211-216.
- [43] R. Taghavi, Automatic clump generation based on mid-surface, *Proceedings, 2nd International FLAC/DEM Symposium, Melbourne, , (2011) 791-797.*

Paper II

Efficiency analysis and optimisation of DEM for railway ballasted track simulations: multi-layer shape model of lateral resistance

Wenli Jia, Valeri Markine, Yunlong Guo

Published in *Transportation Geotechnics*.2023 (40):100977

Abstract

The railway ballast layer provides the function of bearing loading, resisting geometry degradation, and drainage. In those related research, the behaviour of ballast assembly can be obtained by laboratory (or in-situ) tests. Limited simulation methods can be used to analyse the behaviour of ballast particles at the mesoscopic level. The numerical simulations based on the Discrete Element Method (DEM) are employed, which treat every ballast particle as a calculation component. However, the efficiency of DEM simulation is very low due to the algorithm and a very large number of elements. This paper analysed the efficiency-related questions of the DEM modelling. The influence of particle shape and contact properties on the force behaviour is studied. Further, an optimised multi-layer ballasted track model is introduced based on the most influential ballast areas. In such areas, particles are generated with an irregular shape to ensure the reliability of results, and particles except that area are generated with a rolling resisted ball shape to decrease the number of elements. A series of lateral resistance simulations are conducted to show and validate the accuracy and efficiency of this method in the dimension of the single sleeper section. Results show that this optimised multi-layer model building method largely improves efficiency, and it can provide accurate data.

Keyword: Railway ballast, DEM, simulation efficiency, model optimisation, railway track

1. Introduction

Railway ballast, produced by crushed hard stones, is the building material of the substructure of railway tracks. The ballast layer is the compacted assembly of ballast particles, which performs the function of bearing and elasticity to rail, redistributing the force transmitted from the sleeper, providing resistance to the sleeper to keep the track geometry, and providing drainage ability and maintenance ability [1]. A ballasted track is shown in Figure 2-1. In order to fulfil those functions, ballast particles should have properties of enough strength, a coarse surface, and an angular shape. In addition, the assembly should be within a range of Particle Size Distribution (PSD)[2].

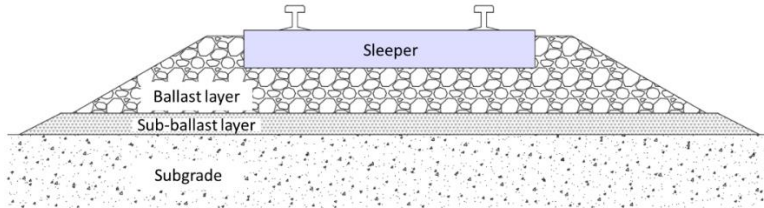


Figure 2-1. Ballasted track

The research methods for railway studies typically include tests (laboratory and in-situ) and numerical simulations (Discrete Element Method and Finite Element Method)[3-7]. Especially for railway ballast, research is commonly conducted with DEM simulations. Because in the DEM model, the ballast layer is built by particles, thus the contact behaviour between particles can be found. This mesoscopic numerical tool makes up for the limitation of tests and FEM.

In order to capture accurate results, the DEM model should present the irregular shape of the ballast, and a proper contact model should be applied to simulate the physical reality. For example, in reference[8], as shown in Figure 2-2, the scale of the model is a single sleeper section, the ballast particles are generated based on templates from real ballast 3D scanning, and the linear contact model is verified by in-situ tests. That model can be regarded as a high-fidelity model, where the spatial and transient information is simulated accurately.

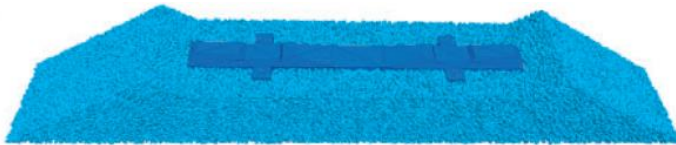


Figure 2-2. DEM model of a single sleeper(wing-shape) section[8]

However, due to the complexity of the particle shape of the high-fidelity model and the algorithm of DEM, the efficiency of DEM simulations has become a major problem. The DEM simulations of a large-scale model (or the long-term behaviour) show an unacceptable time cost (maybe years). Under this limitation, the DEM model for ballast research is normally built on a small scale, such as the direct shear test, triaxial compression test, ballast box test, etc.

The model simplification methods are studied on how to use a low-fidelity model to present the aiming results[9-11]. The low-fidelity model can increase efficiency by missing some physical performance. For example, up-scaling the particle size can decrease the particle number, thus decreasing the calculation cost. However, the low fidelity model may not present the physical reality, but methods can be built biased to the target by modelling approaches. It contains 2 main types:

First is the model fitting. This method uses a mathematical relation to calculate the relationship between results obtained from the simplified model and the accurate model (or experimental tests).

Thus, proper parameters are needed, and the results typically are key performance indicators. The description of this method is shown in the following equation(1).

$$F(x) \sim \tilde{F}(x, a) = \tilde{F}(f(x), a) \quad (1)$$

The second method is the reduce order modelling. This method is based on the simplified model (such as, in state space dimension, degrees of freedom), while it still includes the needed spatial and transient information. The description of this method is shown in the following equation(2).

$$F(x) \sim \tilde{F}(x, a) = \tilde{F}(f(x), a) + C(x, a) \quad (2)$$

Based on those simplification methods, particle size is the first choice to be focused on, which can solve the efficiency problem for powder and soil materials simulations. Reference[12] uses the up-scaling method to reduce the number of elements in a model of large-scale bulk handling equipment and the iron ore pellets model. When using the up-scaling method, the efficiency increased by 55 times (77m³ powders and grab tool). In reference[13], the soil particle uniformly ranges from 10mm to 20mm. The fine particles are discarded to increase efficiency and are regarded as not critical to aiming results. In addition, the cohesion behaviour between particles is simulated by adding a parallel bond parameter to the contact model. In reference[14], the influence of soil particle size on soil-subsoiler interactions is analysed, and the results indicated the most proper particle size and its efficiency.

Focusing on ballast-related research, the simplification method based on particle size is not a proper choice because the PSD is a key factor, and several characteristics of the ballast layer are size-related. In addition, the size ratio between ballast and sleeper (or other test devices) is relatively small compared with the size ratio between soil (or powder) and related tools. In Reference[15-18], the shear boxes are 5 to 10 times bigger than the largest ballast particle size. In comparison, to obtain an accurate result of sand (or soil), the shear box has to be at least 40-60 times bigger than the largest particle size[19].

Under the above considerations, the simplification method for ballast is normally in 2 types. The first method is using a 2D model instead of a 3D model. In reference[20], a 2D DEM model is used to analyse the breakage behaviour under cyclic loading. In reference[21], a 2D DEM model is used to simulate the direct shear tests and cyclic loading for settlement tests. This dimensional simplification can highly improve the efficiency, making the simulation of long-term behaviour possible, but the problem of accuracy of the 2D model is obvious due to 1-dimension loss.

The second method is reducing the complexity of the irregular shape, using a ball or a simple group of balls to represent the irregular real ballast shape, such as in reference[22], a 2-ball generated particle is used to present the ballast shape. Also, in the reference, a cross-section of 0.15m in width of the ballasted track is used to increase efficiency. In reference[23], a cluster of disks is used to present the ballast shape. The number of disks of a cluster ranges from 2 to 9 according to the particle size. Also, in the reference, the simulations are carried out in 2D to increase efficiency.

In addition, the model calibration methods are typically taken into consideration because the ballast properties are influenced by the simplified shape. Such as, the repose angle is used to qualify the behaviour in reference[24-26]. However, there is also evidence that the macroscopic results of an assembly can be obtained and verified, but the contact between the particle is inconsistent with mesoscopic results[27]. The shape simplification method improves efficiency by reducing the number of elements, but the shape loss will lead to unclear force behaviour (as illustrated in chapter 2).

Overall, the DEM modelling method limitation is due to the low efficiency, and previous simplification methods to improve the efficiency have drawbacks. Based on the above-mentioned

background, the aiming of this paper is to improve the efficiency of DEM calculations. Firstly, this paper analyses the influence of particle shape on force behaviour by using a ballast box model, and the particle shape is selected. In addition, the contact model and its parameters are introduced. Based on the particle shape, the linear contact model for the irregular shape and the linear contact model with rolling resistance for the ball shape are analysed based on the literature review. Finally, a multi-layer model of a single sleeper section is built, and the efficiency and reliability are validated.

2. Particle shape

Particle shape is the key factor related to the accuracy of the results because the irregular ballast particle shape provides the uneven force transmission and force re-distribution path. And the interlock caused by angular limits the displacement and rotation of ballast, thus providing strength and elasticity.

The basic DEM particle is a ball, and a cluster of balls can be generated as the clump element by controlling the arrangement of balls in a template. In the arrangement rules, the distance parameter controls the overlap, and the ratio parameter controls the radius, as illustrated in Figure 2-3[18]. By this method, a clump particle can be generated very close to a real ballast shape, with considerable balls, as shown in Figure 2-4.

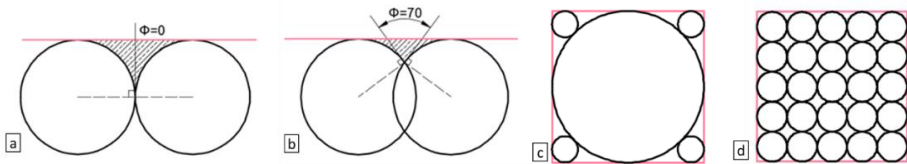


Figure 2-3. Definition of the distance and ratio: a) Distance=0, b) Distance=70, c) Ratio=0.2, d) Ratio=1 [18]

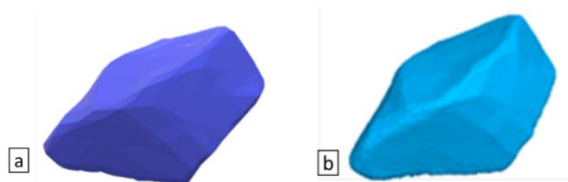


Figure 2-4. A real shape clump generated in PFC3D software, (a) Geometry from 3D scanning, (b) Clump with 13148 balls

The high-fidelity particle contributes to high accuracy. Firstly, the irregular shape contributes to force transmission. The comparison between a ball shape and an irregular shape illustrates it. As shown in Figure 2-5, once the relative position between the 2 components and the centre of mass is the same, the motion and force transmission will be relatively the same. Wherever the force is applied, this relative position has a high possibility of being the same in a ball but a very low possibility of being the same in an irregular shape.

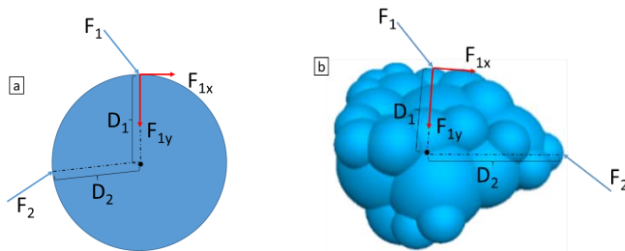


Figure 2-5. Applied force on the sphere and irregular shape: a) ball shape, b) clump shape

Secondly, the angular shape is related to the contact force distribution between particle-particle because a curved surface will lead to more contact points. As shown in Figure 2-6 (the black dots are the contact point), if the particle surface consists of several spherical surfaces, the contact points will change (also shown in Table 2-1: Total contact number) and lead to different behaviours of compressional and frictional force.

P11-II

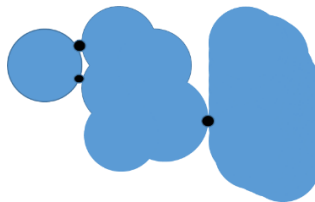


Figure 2-6. Different contact caused by spherical surface (black dot: contact point)

A comparison between different degrees of simplifications is used to illustrate the difference. In this series of simulations, the 3 models were built all the same, except for the particle shape. It shows the contact behaviour when a wedged shape sleeper inserts into the ballast layer. The contact parameters are listed in following Table 2-2 (Section 3). This box model contains 3 parts, the sleeper, ballast box, and ballast particles, as shown in following Figure 2-7, and the Particle Size Distribution (PSD) is shown in Figure 2-8 (all the models in this paper use the same PSD). After the model reaches an initial balanced state, a 4mm/s velocity is applied to the sleeper. Firstly, the sleeper is lifted 4mm, then lowered to compact the ballast, and finally, stop the sleeper when it reaches the initial location. This process simulates the sleeper-ballast contact behaviour under 4mm settlement. The ending state of the model was saved to show the influence of particle shape on contact behaviour.

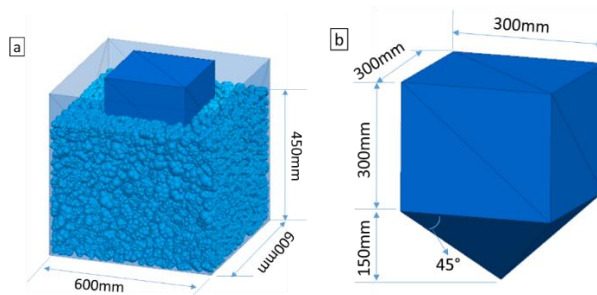


Figure 2-7. Ballast box model: a) sleeper, b) Ballast box

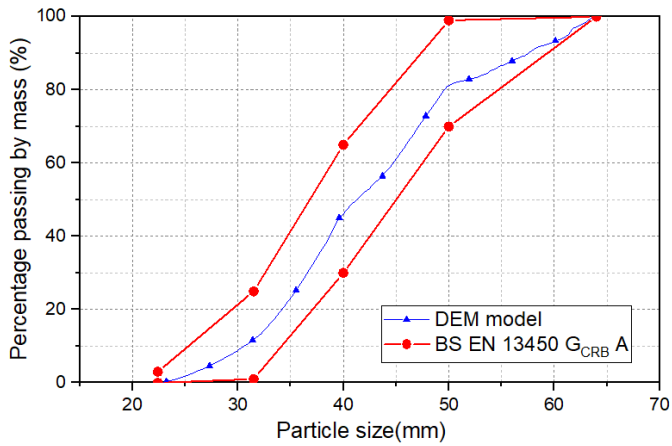


Figure 2-8. Particle size distribution (PSD)


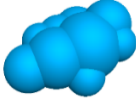
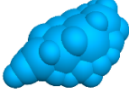
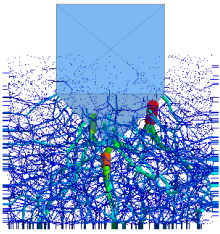
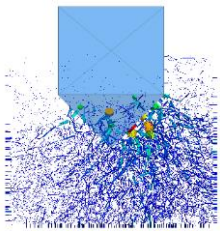
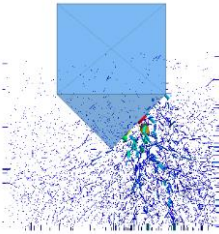
Under the same sleeper displacement, the results are concluded in Table 2-1. The Distance/Ratio and 3 representative particles are listed. By using those different simplifications of particle shapes, results show differences in several aspects, such as the force distribution, maximum contact force, and displacement.

As shown in Table 2-1, the number of contacts in the ball-built model is 5991, whereas the value of the clump-built model with spherical surfaces is 11573, and the value of that with non-spherical surfaces is 10536. The contact number of the ball-built model is 48% and 43% less than the clump-built model. Also, the clump with a spherical surface provides more contact points than that of a clump with non-spherical surfaces, but the force distribution changes from uniform to chain form. This unclear force distribution disobeys the physical behaviour of a ballast assembly. It should be avoided in ballast research.

The shape influences the force behaviour because of the contact number and force distribution difference. The maximum contact force between the particle-particle of the ball-built model is 1.3kN, compared with the value (13.0 kN and 21.9kN) of the clump-built model, which decreases between 90% and 96%. Similar results also can be observed in the maximum contact force between the particle-sleeper, the value of the ball-built model is 13.5kN, and the clump-built model is 101.6kN and 80.1kN. Those results show the influence of particle shape. It also contributes to the importance of using irregular ballast particle shapes.

However, complex particle shape leads to a higher number of elements in a DEM model, and the higher number leads to higher calculation costs. The efficiency and simplification of ballast particle shape are developed in the following chapter. It combines the high-fidelity part and low-fidelity part in a model, realised by using the irregular shape in the most influential area and the ball particle in other less influential areas.

Table 2-1. Influence of different particle shapes on contact behaviour

Shape description	Ball	Clump (spherical surfaces)	Clump (non-spherical surfaces)
Representative particle shape			
D/R value	NA	D120/R0.5	D130/R0.4
Contact force distribution			
Total contact number	5991	11573	10536
Maximum contact force particle-particle (kN)	1.3	13.0	21.9
Maximum contact force particle-sleeper (kN)	13.5	101.6	80.1

3. Contact properties

The complexity of particle shape influences the total number of elements in a model, thus influencing the calculation efficiency. The contact parameters are also vital to efficiency. Because the force and displacement behaviours should be calculated and updated based on a defined timestep, if the timestep is too long, the high increment of force and displacement leads to the model explosion.

Considering that the ballast layer is a non-cohesive granular assembly, the linear contact model can be used to simulate the contact behaviour between ballast particles (or ballast-sleeper). Those contact parameters contain the shear stiffness, the normal stiffness, the friction coefficient, and the reference gap. Contact parameters work together with the physical parameters of elements, which include density and particle size distribution. Under external conditions, for example, the applied force, the sample will show its performance. The details of the calculation are as follows.

In the linear contact model, the contact force is calculated based on: F^l is the linear force. As the following equation (3) and (4).

$$F^l = -F_n^l \hat{n}_c + F_s^l, \quad M_c \equiv 0 \quad (3)$$

$$F_s^l = -F_{ss}^l \hat{e}_c + F_{ss}^l \hat{e}_c \quad (4)$$

Where: F_n^l is the normal component, when $F_n^l > 0$ is tension

F_s^l is the shear component

The displacement of a particle is a universal value. Within a timestep Δt , the displacement is calculated with the relative increase value $\Delta\delta$, and the surface gap g_s , which is set to define whether a contact is valid. As the flowing equation (5) and (6):

$$\Delta\delta_n = \alpha\Delta\delta_n; \Delta\delta_s = \alpha\Delta\delta_s \quad (5)$$

$$\alpha = \begin{cases} \frac{g_s}{g_s - (g_s)_o}, & (g_s)_o > 0 \text{ and } g_s < 0 \\ 1, & \text{otherwise} \end{cases} \quad (6)$$

Where, $(g_s)_o$ is the surface gap at the beginning of one timestep.

The force-displacement law of the linear model consists of the following steps:

1. Update the linear normal force based on the normal-force update mode. As the flowing equation (7).

$$F_n^l = \begin{cases} \begin{cases} k_n g_s, & g_s < 0 \\ 0, & \text{otherwise} \end{cases}, & M_l = 0 \text{ (absolute update)} \\ \min((F_n^l)_o + k_n \Delta\delta_n, 0), & M_l = 1 \text{ (increase update)} \end{cases} \quad (7)$$

Where, k_n is the normal stiffness,

$(F_n^l)_o$ is the linear normal linear contact force at the beginning of the timestep.

2. Update the linear shear force. As the flowing equation (8)-(11).

$$F_s^* = (F_s^l)_o - k_s \Delta\delta_s \quad (8)$$

$$F_s^\mu = -\mu F_n^l \quad (9)$$

$$F_s^l = \begin{cases} F_s^* & , \quad \|F_s^*\| \leq F_s^\mu \\ F_s^\mu \frac{F_s^*}{\|F_s^*\|} & , \quad \text{otherwise} \end{cases} \quad (10)$$

$$s = \begin{cases} \text{true} & , \quad \|F_s^l\| \leq F_s^\mu \\ \text{false} & , \quad \text{otherwise} \end{cases} \quad (11)$$

Where, s is the state of slip determination,

μ is the friction coefficient,

k_s is the shear stiffness,

Based on that, to keep the model stable, the timestep in a calculation cycle will be influenced by contact parameters and kinematic behaviour, and the kinematic-related timestep is calculated as the following equation (12)-(14):

$$a_i = \frac{(F_i + g_i m_g + F a_i)}{m_i} \tag{12}$$

$$t = \frac{(-v_0 + \sqrt{v_0^2 + 2a_0x})}{a} \tag{13}$$

$$t_{kin} = \frac{(-v_{max} + \sqrt{v_{max}^2 + 2a_{max}\epsilon})}{a} \tag{14}$$

Then, the actual timestep used in any cycle is taken as a fraction of this estimated critical value, which is the stiffness constraint, as the following equation (15), in 1-dimension.

$$t_{crit} = \min \left(\sqrt{\frac{m}{k}} \right) (1 - dimensional) \tag{15}$$

With this method, the stiffness will be estimated by summing the contribution from all contacts using only the diagonal terms of the contact stiffness matrix. The final critical timestep is taken to be the minimum of all critical time steps computed for all degrees of freedom of all bodies.

P11-II

The stiffness used for ballast particles is set with a certain value. For example, in reference[28], the normal stiffness and shear stiffness are 2e6 and 1e6 for ballast-ballast contacts. In reference[29], the research defined the normal stiffness 4.2e7 as and shear stiffness are 5.5e7. On the other hand, reference[30] summarised the contact stiffness value that the commonly used stiffness ranges from 1e6 to 5e9. Within the range, the force behaviour is proved suitable for ballast simulation.

However, lower stiffness leads to a larger timestep thus less time consuming, so a proper value should be chosen to fit the ballast behaviour of reality. In a low-fidelity model, the irregular shape can be simplified to a ball, and the interlock between particles can be simulated by adding rolling resistance to the linear contact model. The rolling resistance-related parameter is the friction coefficient (or stiffness). With this setting, the rolling effect of a ball can be restricted[25, 31, 32]. In FPC3D software, the rolling resistance is set by rolling friction. When rolling resistance is added, the contact moment in is Equation (3) is updated to the Equation (16). And as shown in Figure 2-9.

$$\begin{aligned} F^l &= -F_n^l \widehat{n}_c + F_s^l, \quad M_c = M^r \\ M^r &= M^r - k_r \Delta\theta_b \end{aligned} \tag{16}$$

Where, M^r is the rolling resistance moment to restrict the rotation,

k_r is the rolling resistance,

$\Delta\theta_b$ is the relative bend-rotation increment of a contact

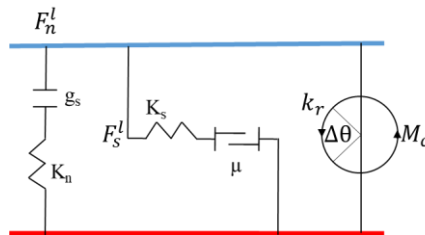


Figure 2-9. Linear contact with rolling resistance

In reference[32], the influence of stiffness and rolling friction is analysed by a series of direct shear simulations (ball-built model), and results are shown in the following Figure 2-10. In addition, a case of rolling resistance also can be seen in the next chapter, the comparison between 0.3 rolling friction coefficient and without it.

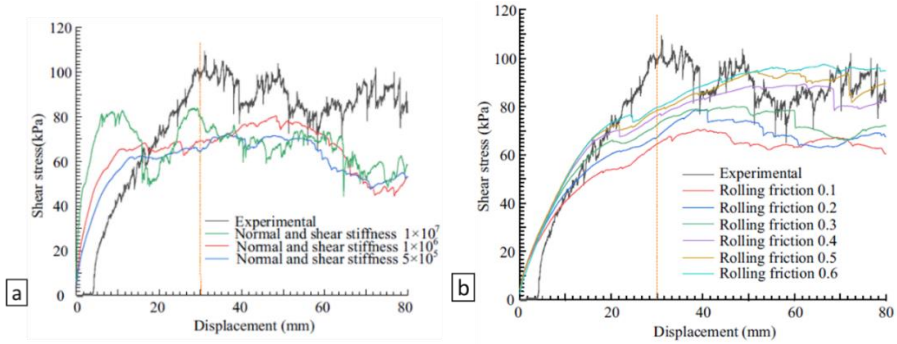


Figure 2-10. Shear stress influenced by: a) Stiffness, b) Rolling friction coefficient [32]

Based on those results, the contact parameters in this paper are listed in the following Table 2-2.

Table 2-2. Contact parameters

Parameters	Ballast (Clump)	Ballast (ball)	Sleeper
Tangential stiffness(N/m)	2e7	2e7	5e9
Normal stiffness(N/m)	2e7	2e7	5e9
Friction coefficient (Linear contact)	0.5	0.5	0.5
Friction coefficient (Rolling resistance)	-	0.3	-
Mass density(kg/m ³)	2800	2800	NA
Weight (kg)	-	-	380
Damping coefficient	0.7	0.7	-

4. Efficiency optimisation

With the above-mentioned knowledge, a multi-layer model can be used to improve DEM efficiency. As a case to show the efficiency, the single sleeper section of a ballasted track is built.

Firstly, the reference model, using the clump for all particles, is shown in Figure 2-11. In this section, the shoulder width is 500mm, the ballast height (under sleeper) is 350mm, the shoulder slope is 1:1.75, the top width is 600mm, and the sleeper is 2600mm*280mm*185mm(L*W*H). This was the commonly used model before optimised. The linear contact model is used, and the contact parameters are listed in Table 2-2. This model contains 647323 elements of particles, 86 elements as the sleeper and boundary wall (The boundary wall is shown with the transparency setting and is not displayed in the following models). Related research using this model by the author can be seen in reference[18, 33-35]. Thus, its reliability and accuracy have been validated.

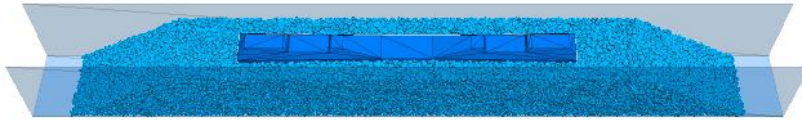


Figure 2-11. Clump-built model of a single sleeper section

Also, a model with ball particles is built, as the additional reference, to show the behaviour loss of shape simplification, as shown in Figure 2-12. For this model, with and without rolling resistance are calculated separately. All the contact parameters are shown in Table 2-2. This model contains 24394 elements of particles, 86 elements as the sleeper and boundary wall.

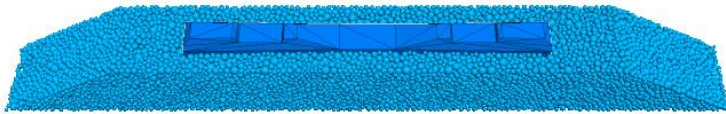


Figure 2-12. Ball-built model of a single sleeper section

Further, the model is simplified by the multi-layer method to reduce the number of elements while keeping relatively high-fidelity results. This method uses the ball shape as ballast in the bottom layer and the irregular shape (clump) in the area where sleeper contact with the ballast. In detail, the lower layer of the ball is 265mm in height, and the clump layer is 80mm under the sleeper bottom and 185mm in the crib. The 80mm equals 2 times bigger than the average ballast size. It makes sure the sleeper is well-contact with the clump particles.

This method can largely decrease the element number and present the high-fidelity contact between sleeper-ballast. However, the bottom layer is simplified, but rolling resistance is added to the ball-ball contact to simulate the interlock within the irregular particles. The clump-clump contacts model is the linear contact model. All the contact parameters are listed in Table 2-2. As shown in Figure 2-13, this model contains 14887 elements of balls and 229222 elements of the clump, which are 264109 elements of particles in total. The number of elements for the sleeper and boundary wall is 86, which is the same as the reference model. Compared with the model built with clump, this multi-layer model reduces the number of elements by 59%.



Figure 2-13. Multi-layer model with clumps and balls of a single sleeper section model

Further, the simplification can be optimised depending on the different test types, according to the loading condition (loading controlled test) or displacement condition (displacement controlled test). For example, in a settlement test, the loading condition is vertically applied to the sleeper, and the most influential ballast is located at the bottom of the sleeper. Thus, the bottom ballast particles should be the clump, and other particles (crib and shoulder ballast) can be simplified to the ball. This means the multi-layer model is optimised based on the force distribution. The method is shown in the following Figure 2-14.

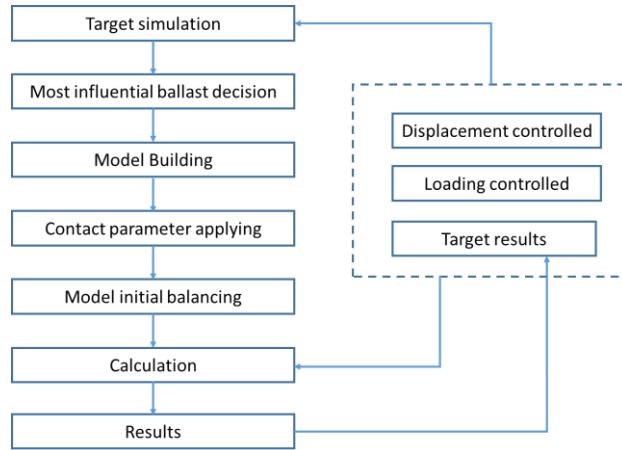


Figure 2-14. Process of multi-layer model simulation

In order to verify the efficiency and reliability of the optimisation method, the lateral resistance test is simulated with the reference model, the multi-layer model, and the optimised multi-layer. The loading resistance test is displacement controlled. A certain velocity is applied to the sleeper, the direction is lateral and horizontal, and the test is quasi-static status. The target results are the force distribution, lateral resistance, and source contribution (sleeper bottom, end, and side).

In the author's previous work, Particle Image Velocimetry (PIV) was used to analyse the displacement distribution[34]. By this method, the ballast displacement can be obtained through video analysis. As shown in the following Figure 2-15, a box of ballast in the dimension of a single sleeper section was used. One side of the box is made of glass. Thus the camera can capture the displacement of ballast particles under the sleeper. Another camera was placed above the ballast shoulder to record that part.

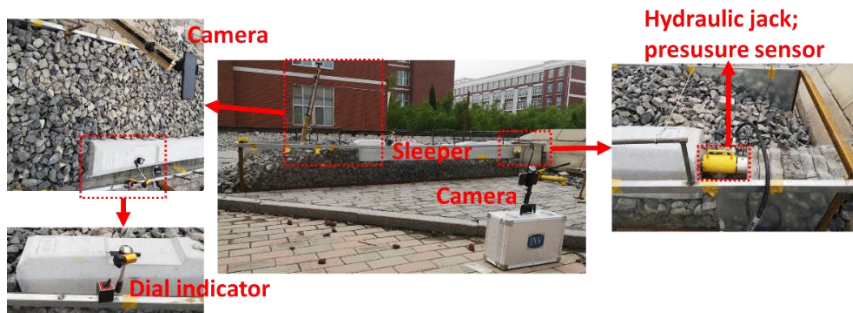


Figure 2-15. PIV setting on lateral resistance test[34]

The ballast displacement map is shown in Figure 2-16. This result provides the most influenced (displacement) ballast area, which can be used as a guide to building a DEM model. Normally the lateral resistance tests are controlled to stop at 4-5mm sleeper displacement to better show the ballast behaviour, reference [34] pushed the sleeper to 20mm. Considering the normal condition, ballast displacement under 7mm sleeper displacement is enough to be used as guidance in multi-layer modelling.

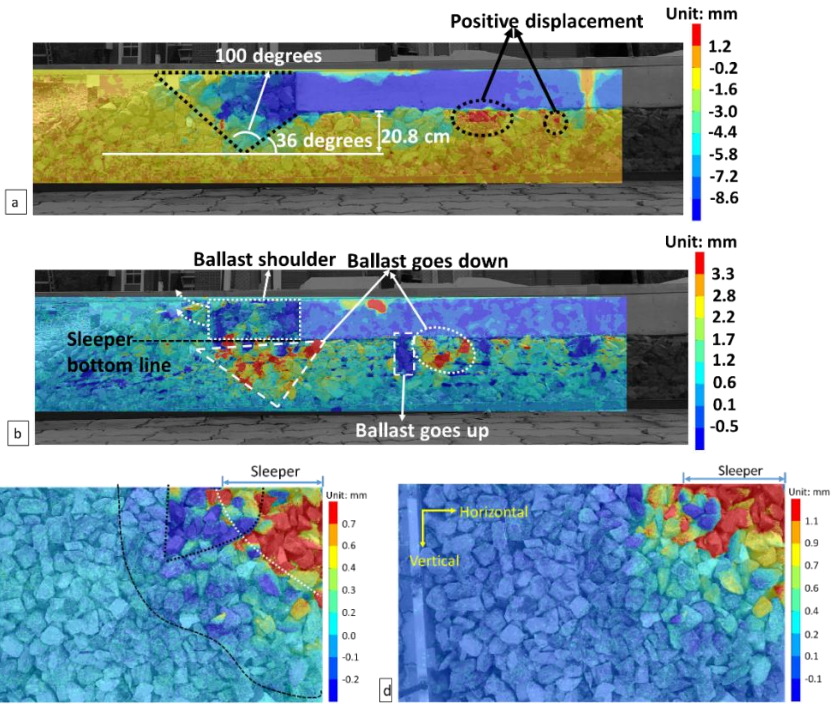


Figure 2-16. PIV data of the lateral resistance test (under 7mm sleeper displacement): a) Side-view of ballast horizontal displacement, b) Side-view of ballast vertical displacement, c) Top-view of the ballast horizontal displacement, d) Top-view of the ballast vertical displacement [34]

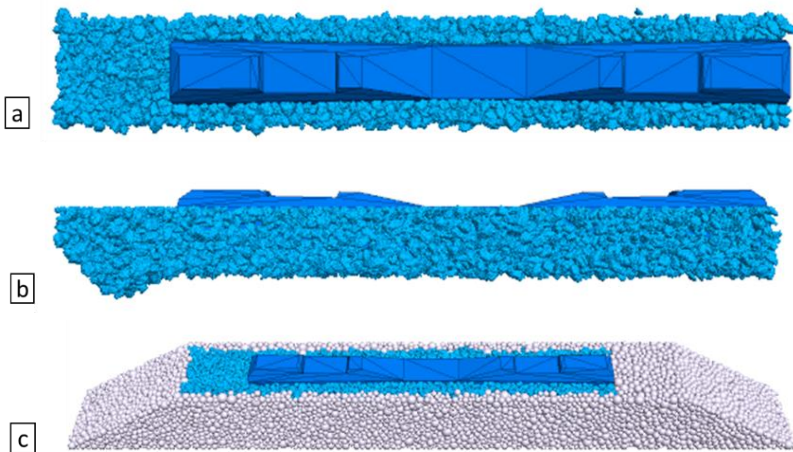


Figure 2-17. Optimised multi-layer model of a single sleeper section: a) Top-view of the clump-build layer, b) Side-view of the clump-build layer, c) Over-view of the multi-layer model

As shown in Figure 2-17, an optimised multi-layer DEM model was built, where the ballast in the most influential area is generated by the clump elements with linear contact model, and other particles are the ball elements with rolling resistance linear contact model. This model-building method makes sure that the number of elements is decreased to the largest extent. It contains 19358 elements of balls and 131388 elements of clumps, which are 150746 elements for particle generation. And the number of elements for the sleeper and the boundary wall is 86. Compared with the reference model (fully clump-built model, in Figure 2-10), the total number of elements decreases by 77%.

In order to validate the optimised model, a single sleeper pushing test is conducted on the 3 different models. A lateral velocity is applied to the sleeper, which is $4e-3$ mm/s. This low speed ensures the simulation is in a quasi-static state. The weight of the sleeper is 380kg in the test. In the simulation, the weight is presented by adding a vertical servo force on the sleeper. The simulation is stopped when the sleeper displacement reaches 5mm. During this process, the contact force-displacement data of the sleeper is recorded. In addition, the force distribution at the end state is saved to show the difference between each model, thus providing validation. The time consumption shows efficiency. All the simulations were conducted on a workstation with Dual Xeon E5 processor and 64G memory. Results are listed in following Table 2-3.

In Table 2-3, the clump-built model costs 43.38 hours, whereas the ball model only costs 2.5 and 3 hours. This result shows the heavy influence of element number on efficiency. With the optimisation, the efficiency is largely increased. The multi-layer model (half clump and half ball) costs 15.75 hours. For the multi-layer model with further optimisation, the time consumption is 10.41 hours, and the force behaviour is also the closest to the results of the clump-built model. The force-displacement curves of the sleeper are shown in the following Figure 2-18. The increasing trend and peak force between the reference model and the optimised multi-layer model are in a similar state.

Table 2-3. Key performance of lateral resistance simulations

Particle type	Time consuming	Peak lateral force (sleeper)	Maximum contact force (particle)
Clump (Reference model)	43h 23 min	12.03kN	2.18kN
Multi-layer Half clump/ half ball by height	15h 45 min	9.92kN	1.56kN
Multi-layer Optimised by most influential ballast area	10h 25min	11.20kN	2.93kN
Ball With rolling resistance	2h 32 min	16.02kN	4.65kN
Ball Without rolling resistance	3h 05 min	3.76kN	0.37kN

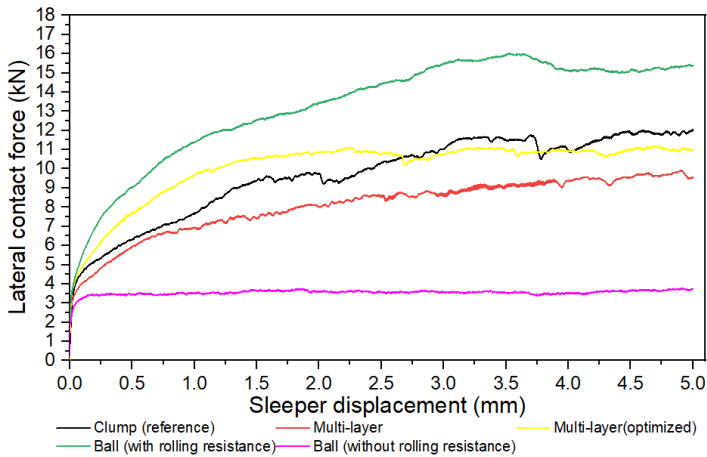


Figure 2-18. Sleeper displacement-lateral contact force curve

On the contrary, the results of the ball-built models (with and without rolling resistance) are all less reliable. The particle displacement at the end of the simulation is shown in Figure 5-19, where the ball model with rolling resistance has an extra disturbance on the crib side, which is against the results of the reference model. The force distribution (Figure 5-20) also proves the impossibility of acquiring high reliability using a ball-built model because it shows clear force chains in the crib area but unclear force chains in the shoulder area.

In addition, it can be observed that the added rolling resistance highly increases the peak lateral force from 3.76kN to 16.02kN because the rolling resistance restricts the particle, thus compensating the interlock of angular loss, as expected. The peak lateral force of the ball-built model with the rolling resistance is even higher than the clump-built model. But, it does not mean using a lower value of rolling resistance can reach better fitness. Because the mesoscopic results should also be taken into consideration.

Figure 5-19 and Figure 5-20 proved the accuracy of the results. The particle displacement is presented. The optimised multi-layer model is very high compared with the results of the reference model. In comparison, other models are not in accordance with the tests. That means the optimised multi-layer model has not only higher efficiency but also higher reliability.

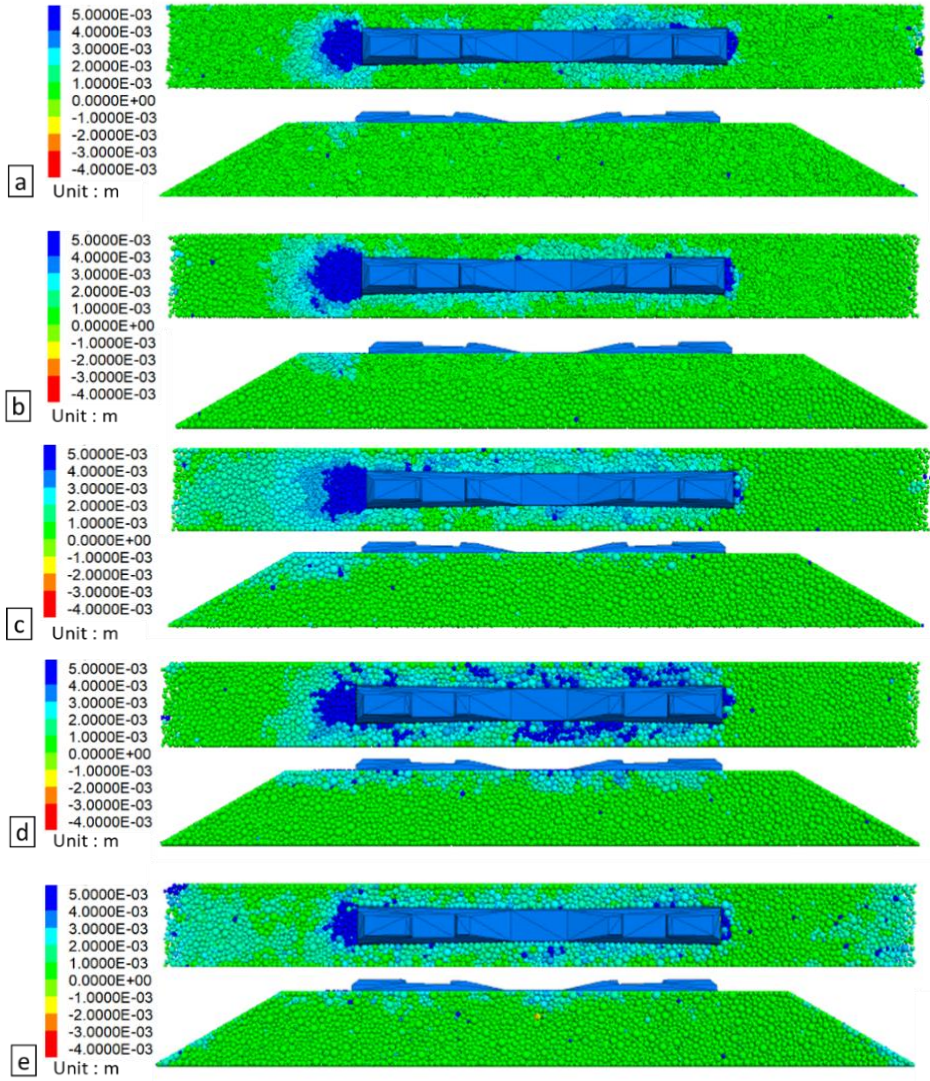


Figure 2-19. Ballast displacement after 5mm sleeper displacement: a) Reference model (all particles are clump), b) Multi-layer model (Half clump and half ball, by height), c) Optimised multi-layer model (based on most influential ballast area), d) Ball-built model (with rolling resistance), e) Ball-built model (without rolling resistance)

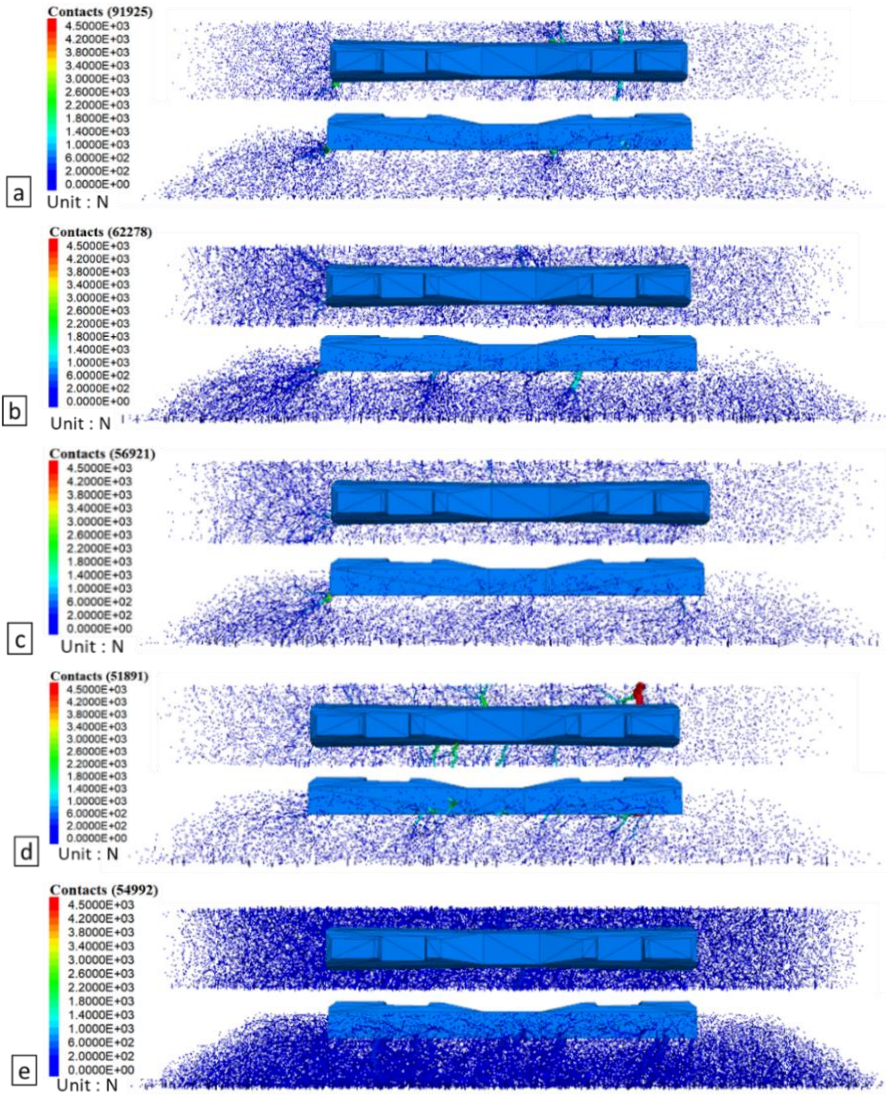


Figure 2-20. Contact force chain after 5mm sleeper displacement: a) Reference model (all particles are clump), b) Multi-layer model (Half clump and half ball, by height), c) Optimised multi-layer model (based on most influential ballast area), d) Ball-built model (with rolling resistance), e) Ball-built model (without rolling resistance)

5. Conclusion

For ballast research, the DEM simulations can provide mesoscopic results. However, the efficiency problem restricts the feasibility of this method. In order to improve the calculation efficiency of DEM, several methods can be used, but all those methods are not proper for ballast research. With this consideration, this paper explained the importance and influence of particle shape and contact properties of the DEM model for ballast and introduced an optimised multi-layer model-building method. This method, based on the aiming simulations, simplifies the irregular ballast shape to ball shape and uses irregular shape (clump) in the most influential area. As an illustration, to show the accuracy and efficiency of the optimised model, later resistance simulations are used. The results of different models are validated by comparing them with a reference model (clump-build), which is used in the author's previous work. The main conclusions are listed below:

1. Particle shape in a DEM model influences the force behaviour of the ballast layer. In a ball-build model, the simple particle shape leads to fewer contact numbers and lower contact force. For the clump-built model, the spherical surface of a clump leads to a higher contact number and clear force distribution.
2. Contact model is the law for force-displacement calculation. Among those parameters, stiffness influences calculation efficiency, and the rolling resistance (rolling friction) applied to a ball element can restrict the rolling behaviour, thus maintaining the loss of irregular shape.
3. However, the rolling resistance can compensate for the interlock loss of irregular shape, but the reliability of force distribution and particle displacement is low.
4. The idea of the optimised multi-model is to decrease the number of elements used in a model. It is realised by using irregular shapes in the most influential area and balls in other areas. The case shows this method can increase efficiency and keep accuracy.
5. The most influential area is different for different simulations. Therefore, selecting the proper area is the first step of model building. The selection should be based on the type of simulations and the target results. In this paper, the lateral resistance is simulated, and the most influential area is defined by particle displacement, which is obtained by previous tests using the PIV method.

Acknowledgement

This is from work undertaken as part of the IN2ZONE project, which has received funding from the Shift2Rail Joint Undertaking (JU) under grant agreement 101014571 – IP/ITD/CCA – IP3.

Reference

- [1] C. Esveld, *Modern railway track*, MRT-Productions, The Netherlands, 2001.
- [2] B. Indraratna, *Advanced Rail Geotechnology-Ballasted Track*, CRC Press 2011.
- [3] H. Wang, V. Markine, Modelling of the long-term behaviour of transition zones: Prediction of track settlement, *Engineering Structures* 156 (2018) 294-304.
- [4] H. Wang, V. Markine, X. Liu, Experimental analysis of railway track settlement in transition zones, *Proc Inst Mech Eng F J Rail Rapid Transit* 232(6) (2018) 1774-1789.
- [5] H. Huang, B. Brennecke, Track Stiffness Transition Zone Studied with Three-Dimensional Sandwich Track Model, *Transportation Research Record: Journal of the Transportation Research Board* 2374(1) (2013) 136-142.
- [6] B. Indraratna, D. Ionescu, H.D. Christie, Shear behaviour of railway ballast based on large Scale triaxial tests, *Journal of Geotechnical and Geoenvironmental Engineering* 124(5) (1998) 439-449.
- [7] M. Lu, G.R. McDowell, The importance of modelling ballast particle shape in the discrete element method, *Granular Matter* 9(1-2) (2006) 69-80.
- [8] G.Q. Jing, P. Aela, H. Fu, H. Yin, Numerical and experimental analysis of single tie push tests on different shapes of concrete sleepers in ballasted tracks, *Proceedings of the Institution of Mechanical Engineers, Part F: Journal of Rail and Rapid Transit* 233(7) (2018) 666-677.
- [9] V. Toropov, V. Markine, The use of simplified numerical models as mid-range approximations, 6th Symposium on Multidisciplinary Analysis and Optimization, 1996.
- [10] D.J. Lucia, P.S. Beran, W.A. Silva, Reduced-order modeling: new approaches for computational physics, *Progress in Aerospace Sciences* 40(1-2) (2004) 51-117.
- [11] R. Jin, X. Du, W. Chen, The use of metamodeling techniques for optimization under uncertainty, *Structural and Multidisciplinary Optimization* 25(2) (2003) 99-116.
- [12] S. Lommen, M. Mohajeri, G. Lodewijks, D. Schott, DEM particle upscaling for large-scale bulk handling equipment and material interaction, *Powder Technology* 352 (2019) 273-282.
- [13] J. Mak, Y. Chen, M.A. Sadek, Determining parameters of a discrete element model for soil-tool interaction, *Soil and Tillage Research* 118 (2012) 117-122.
- [14] X. Wang, S. Zhang, H. Pan, Z. Zheng, Y. Huang, R. Zhu, Effect of soil particle size on soil-subsoiler interactions using the discrete element method simulations, *Biosystems Engineering* 182 (2019) 138-150.
- [15] H. Gong, W. Song, B. Huang, X. Shu, B. Han, H. Wu, J. Zou, Direct shear properties of railway ballast mixed with tire derived aggregates: Experimental and numerical investigations, *Construction and Building Materials* 200 (2019) 465-473.
- [16] H. Huang, E. Tutumluer, W. Dombrow, Laboratory Characterization of Fouled Railroad Ballast Behavior, *Transportation Research Record: Journal of the Transportation Research Board* 2117(1) (2009) 93-101.
- [17] B. Indraratna, N.T. Ngo, C. Rujikiatkamjorn, J.S. Vinod, Behavior of Fresh and Fouled Railway Ballast Subjected to Direct Shear Testing: Discrete Element Simulation, *International Journal of Geomechanics* 14(1) (2014) 34-44.
- [18] W. Jia, V. Markine, Y. Guo, G. Jing, Experimental and numerical investigations on the shear behaviour of recycled railway ballast, *Construction and Building Materials* 217 (2019) 310-320.
- [19] J. Wang, M. Gutierrez, Discrete element simulations of direct shear specimen scale effects, *Géotechnique* 60(5) (2010) 395-409.
- [20] E. Mahmoud, A.T. Papagiannakis, D. Renteria, Discrete Element Analysis of Railway Ballast under Cycling Loading, *Procedia Engineering* 143 (2016) 1068-1076.
- [21] Y. Guo, Y. Ji, Q. Zhou, V. Markine, G. Jing, Discrete Element Modelling of Rubber-Protected Ballast Performance Subjected to Direct Shear Test and Cyclic Loading, *Sustainability* 12(7) (2020) 2836.
- [22] C. Chen, G.R. McDowell, An investigation of the dynamic behaviour of track transition zones using discrete element modelling, *Proceedings of the Institution of Mechanical Engineers, Part F: Journal of Rail and Rapid Transit* 230(1) (2014) 117-128.

- [23] Z. Hossain, B. Indraratna, F. Darve, P.K. Thakur, DEM analysis of angular ballast breakage under cyclic loading, *Geomechanics and Geoengineering* 2(3) (2007) 175-181.
- [24] C. Coetzee, Calibration of the discrete element method: Strategies for spherical and non-spherical particles, *Powder Technology* 364 (2020) 851-878.
- [25] P. Aela, L. Zong, M. Esmaili, M. Siahkouhi, G. Jing, Angle of repose in the numerical modeling of ballast particles focusing on particle-dependent specifications: Parametric study, *Particuology* 65 (2022) 39-50.
- [26] J. Chen, R. Gao, Y. Liu, Numerical Study of Particle Morphology Effect on the Angle of Repose for Coarse Assemblies Using DEM, *Advances in Materials Science and Engineering* 2019 (2019) 1-15.
- [27] M. Obermayr, C. Vrettos, P. Eberhard, T. Däuwel, A discrete element model and its experimental validation for the prediction of draft forces in cohesive soil, *Journal of Terramechanics* 53 (2014) 93-104.
- [28] X. Bian, W. Li, Y. Qian, E. Tutumluer, Micromechanical Particle Interactions in Railway Ballast through DEM Simulations of Direct Shear Tests, *International Journal of Geomechanics* 19(5) (2019) 04019031.
- [29] F. Khatibi, M. Esmaili, S. Mohammadzadeh, DEM analysis of railway track lateral resistance, *Soils and Foundations* 57(4) (2017) 587-602.
- [30] Y. Guo, C. Zhao, V. Markine, G. Jing, W. Zhai, Calibration for discrete element modelling of railway ballast: A review, *Transportation Geotechnics* 23 (2020) 100341.
- [31] J. Ai, J.-F. Chen, J.M. Rotter, J.Y. Ooi, Assessment of rolling resistance models in discrete element simulations, *Powder Technology* 206(3) (2011) 269-282.
- [32] Y. Guo, C. Zhao, V. Markine, C. Shi, G. Jing, W. Zhai, Discrete element modelling of railway ballast performance considering particle shape and rolling resistance, *Railway Engineering Science* 28(4) (2020) 382-407.
- [33] G. Jing, X. Zhang, W. Jia, Lateral resistance of polyurethane-reinforced ballast with the application of new bonding schemes: Laboratory tests and discrete element simulations, *Construction and Building Materials* 221 (2019) 627-636.
- [34] Y. Guo, W. Jia, V. Markine, G. Jing, Rheology study of ballast-sleeper interaction with particle image Velocimetry (PIV) and discrete element modelling (DEM), *Construction and Building Materials* 282 (2021) 122710.
- [35] G. Jing, W. Jia, X. Wang, V. Markine, R. Nålsund, Y. Guo, Experimental and numerical study on lateral resistance of frictional sleeper with arrowhead groove, *Transportation Geotechnics* 30 (2021) 100638.

Paper III

Design of a concept wedge-shaped self-levelling railway sleeper

Wenli Jia, Valeri Markine, Mario Carvalho, David P. Connolly, Yunlong Guo

Published in Construction and building materials

Abstract

Differential railway track settlement can result in ballast voids, leading to sleepers that hang from the rail and are no longer supported by the ballast. These hanging sleepers are damage for track component. As a solution, this paper proposes and investigates a new concept sleeper with a wedge-shaped geometry, intended to stimulate the migration of ballast into any voids, thus reducing the occurrence of hanging sleepers. A series of scaled laboratory tests and 2D and 3D discrete element simulations are used to investigate different wedge-shaped geometries. The investigations include the wedge type (single long wedge versus multiple mini-wedges) and the wedge angle (30, 45, 60 degrees). First, the scaled laboratory tests are used to study the performance of different wedge geometries. Next, 3D DEM simulations are performed to analyse the contact forces in the ballast due to different wedge designs. Finally, 2D DEM simulations are performed to study the settlement behaviour. The main conclusions are that a single long wedge is preferable compared to multiple smaller wedges. when the wedge sleeper angle is larger than the ballast's angle of repose, particles have the freedom to migrate into the settlement induced voids. Also, an increased wedge sleeper angle stimulates greater particle migration and thus improves the support correction. However the longer wedge also leads to a decrease in effective ballast height under sleeper which may make retrofitting on existing lines challenging.

Key word: Railway transition zone, Railway sleeper-tie, Differential settlement, Discrete element ballast modelling, Scaled ballast testing, Ballast voiding

1. Introduction

Railway tracks are supported by a variety of types of sub-structures, including subgrade, bridges, and tunnels. The connecting area between support structures with different stiffness's is named a transition zone[1, 2]. As an example, when trains travel over a transition zone from an embankment to a concrete abutment, the change in stiffness leads to differential settlement. This can result in hanging sleepers that are unsupported by the ballast layer[3]. Both differential settlement and hanging sleepers constitute geometry irregularities. An overview of those problems is shown in Figure 3-1.

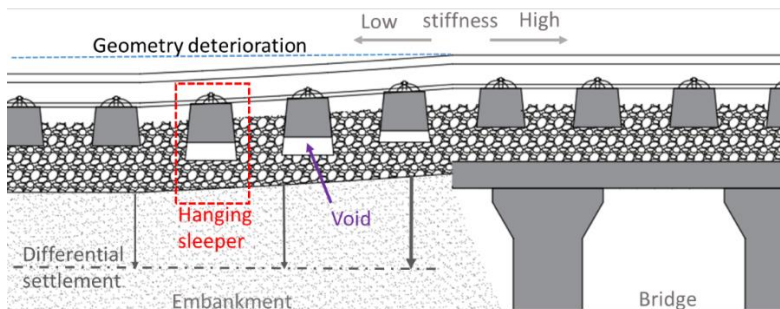


Figure 3-1. Differential settlement and hanging sleepers at a transition zone. Modified from [3]

When a train passes unsupported sleepers, their impact on the ballast surface when excited generates a dynamic force, thus further enlarging the differential settlement and voids [3-5]. This results in a progressive degradation loop. Track irregularities are an important contributor to the increase in dynamic loads [6-8], and compared with plain line, the degradation of ballast and other track components at transition zones is much faster. Thus higher maintenance costs are needed to ensure the safety and stability of the railway [9].

A variety of studies have proposed preventive solutions to decrease the differential settlement by lowering the dynamic force and the plastic deformation within the ballast layer on the embankment side. These solutions focus on smoothing the stiffness change in transition zones [10-14] because sudden stiffness changes result in high dynamic forces [15-18]. In addition, reinforcement on the ballast layer increases its strength [19-22], thus increasing its resistance to deformation.

However, the above preventive solutions still have some challenges [23, 24]. Also, after implementing these solutions, hanging sleepers can still develop and produce high dynamic forces. To eliminate these, maintenance actions are performed, such as tamping/stone blowing [25] and using adjustable fasteners [26]. However, these manual actions can be costly, short-lived and also some maintenance activities (e.g. tamping) can be challenging to perform at certain transition zone configurations.

In an attempt to prevent the development of hanging sleepers the Automatic Irregularity-Correcting Sleeper (AICS) was developed [27], capable of expanding in the vertical direction to fill the void and thus ensure contact between ballast and sleeper. The AICS consists of two automatic subsidence compensating (ASC) mechanisms. The ASC device consists of two nested boxes. When there is differential settlement in the track, the outer box sinks together with the ballast, with a granular material (e.g. stainless steel ball bearings) filling the gap between the inner and outer boxes. As a result, the granular material compensates for the unequal settlement. To minimise installation time, and negate the need to remove the existing sleepers, a alternative short-sleeper version (AICS-SS) was developed[28]. It could be more easily installed and could be placed between existing sleepers.

Another Self-Compensating Sleeper (SCS) concept using granular material is presented in [29]. The SCS has conical shaped cavities from the top surface to the bottom that house granular material with smaller particle size distribution compared to ballast. When the track is lifted, the granular material in the sleeper cavities falls into the cavities under the sleeper, thus helping to fill the voids and maintain sleeper-ballast contact.

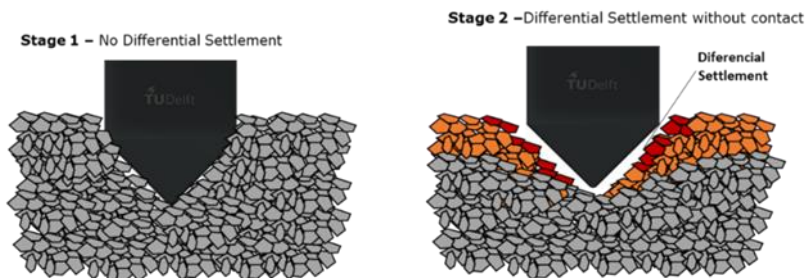
In contrast to using granular compensation mechanisms, an alternative was proposed using automated air-bag technology [30]. When the ballast settles, the air bag restricts movement in the opposite direction by air injection. This helps to minimise gaps between the sleeper and the ballast. Another alternative proposed using hydraulic oil under pressure to automatically compensating for the loss of sleeper-ballast contact during track differential settlement [31].

The above solutions are useful for preventing the growth of voids at transition zones, however are semi-active solutions and may have increased cost compared to a standard sleeper. Further, they may require resetting after they have met their vertical expansion limit. Passive solutions may help overcome these issues, for example by using a dual ballast gradation approach [32-35]. This involves first installing ballast with standard PSD up to the sleeper bottom level. This will ideally be well-compacted to provide a solid foundation for the sleeper. Then, the crib/shoulder ballast above, which is more for confinement rather than vertical support, is installed, but with a smaller PSD. Then, if voiding starts to develop, the smaller upper crib/shoulder particles automatically migrate into the voids to minimise their growth.

A challenge with using a dual-gradation approach is that it can be challenging to ensure compatibility with railway standards. Therefore, as an alternative, this paper proposes the use of a wedge-shaped sleeper. The concept is that the wedge allows larger particles to flow between it and any voids that may develop. Therefore it increases the contact between sleeper and ballast. To design a wedge sleeper, first the concept is explained in detail, and the working principle and challenges in design are presented. Next the methodology is described, including the scaled laboratory tests, 3D and 2D DEM simulations. Then, the analysis of the results, including the influence of wedge type (single-wedge and multi-wedge) and the wedge angle (30, 45 and 60-degree) on the support correction effect are presented.

2. Wedge sleeper concept

The rail is fixed to the sleeper via a clip meaning in the presence of differential ballast settlement a gap can appear between the sleeper and ballast. The working principle of the wedge sleeper is that the crib and shoulder ballast can, via gravitational forces and dynamic vibration during train passage, migrate into the gap between sleeper and ballast. The wedge shape helps to promote the migration of ballast, which works autonomously and is related to the angle of repose of the ballast. The correction behaviour is illustrated in Figure 3-2.



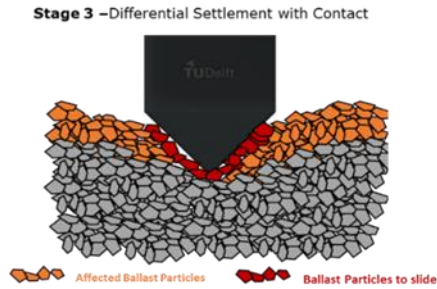


Figure 3-2. Void correction concept using wedge sleeper

Two designs for the wedged sleeper were tested. First, the single wedge was tested, which is the simplest design to promote ballast migration underneath the sleeper. The multiple wedge solution follows the same principle while also aiming for material saving and allowing particle flow in two directions. Therefore potentially both lateral and longitudinal ballast migration can contribute to correction.

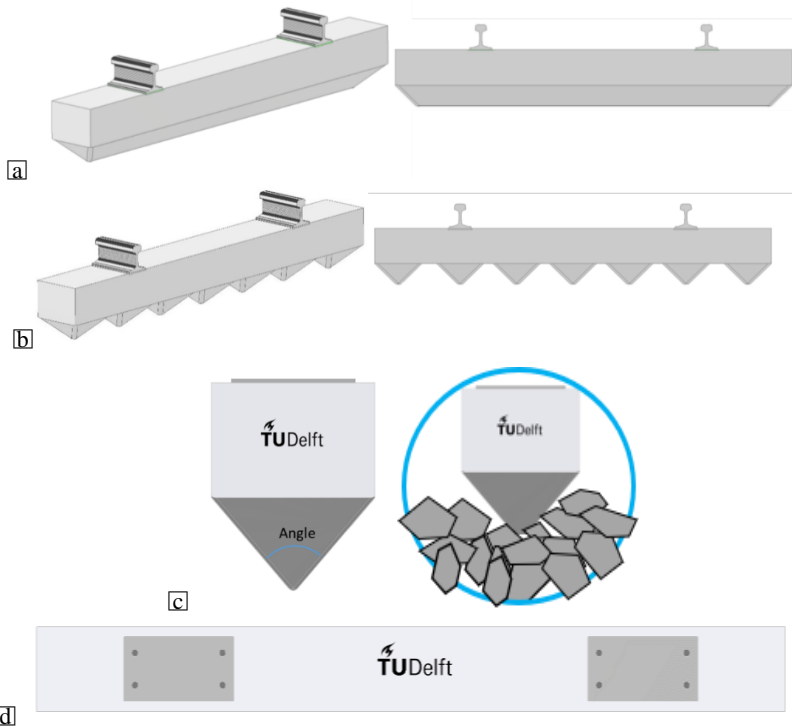


Figure 3-3. Wedge-sleeper designs. (a) Single wedge design, (b) Multi-wedge design, (c) Side-view of both designs, (d) Top-view of both designs

The design of full-scale sleepers is shown in Figure 3. The idea of improving sleeper performance by adding extra components has been used in several designs[36, 37]. In this paper, the prototypes are based on the existing mono-block sleeper (Lankhorst type 202), with a dimension of 2600 mm*250 mm*200 mm (L*W*H). It is High-Density Polyethylene Polymer (HDPE) with reinforcing bars. The

material is flexible to modification to meet the requirements, such as weight, strength, and dimension of reinforcement.

Some key design parameters of the wedge(s) are the angle and height. For example, when the angle is larger than the repose angle of the ballast, the displacement and rotation of the ballast can contribute to void correction. Thus, the wedge angle is crucial to the design. In general, a larger angle increases the possibility of ballast movement. However, this decreases the effective depth of ballast below the sleeper, thus weakening the function of the ballast, for example, lowering the elasticity and strength. In addition, the sharper the tip of the wedge, the higher the force concentration on both itself and the ballast. This can cause accelerated degradation/breakage of both the tip and ballast stones. Therefore these issues are investigated in this paper.

3. Methodology

3.1 Overview

This paper aims to use a combination of scaled laboratory testing and discrete element modelling (2D and 3D) to investigate:

1. Performance of different wedge types. Scaled laboratory tests are used to investigate both single and multi-wedge designs. The tests provide understanding of general wedged sleeper behaviour.
2. Performance of different wedge angles. 3D discrete element modelling is used, capable of simulating the contact between the sleeper and ballast. It is used to study the effect of wedge angle and the relationship between ballast migration and sleeper height.
3. The effect of support correction effects: validating the predicted correction under different settlement levels, and the influence of the correction behaviour on the force state of sleeper and ballast layer. To study the long-term behaviour under different settlement levels, 2D discrete element modelling is used.

The laboratory testing and numerical simulations are now described.

3.2 Laboratory testing

First, scaled laboratory testing was used to investigate wedge angles and types (single or multi-wedge), with a mono-block sleeper used as a reference. Wooden sleepers with the dimensions 300x45x45mm were used, comparable with the typical sleepers used in the Netherlands, with a scale factor of 1:7.5. The rails were U profiles (channel steel) of 10x20x10mm. Thus, to evaluate the settlement correction of the TU Delft Sleeper designs, their scale was set as approximately the same as one of the ballast particles. The relationship between the average ballast particle dimension (40mm) and the gravel particle (6mm) was 1:6.6.

A retaining box of 1900x700x250mm was filled with gravel to act as ballast. A steel beam, of 300mm of height, is used to replicate a bridge, thus creating a transition zone between the ballast and bridge. The sleepers under test are shown in Figure 3-4(a), and the scaled transition zone is shown in Figure 3-4(b) and (c). The scaled train vehicle passed over the transition zone 16 times for each designs, and the displacement of sleepers was recorded using a video gauge system with targets placed on each sleeper end. Comparing the particle size, sleeper size, and the introduced settlement, the scaled tests provide an easier condition to qualify the correction. Under this condition, if the sleeper cannot show a good performance, the sleeper is considered to be even worse in reality. Thus, the scaled tests were only used to primarily qualify the performance.

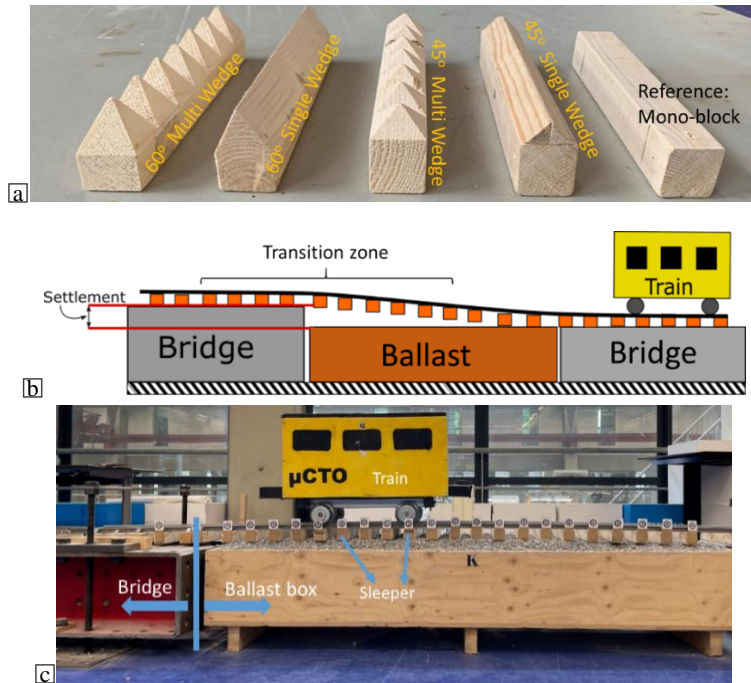


Figure 3-4. Scaled testing. (a) 5 different types of sleepers under test, (b) Schematic of the scaled laboratory transition zone, (c) Final laboratory model

3.3 Discrete element modelling

Discrete Element numerical simulation (DEM) was used to develop a detailed understanding of the contact behaviour between the sleeper and the ballast particles [38-40]. The cooperation between the 2D and 3D methods (co-simulations) is employed in this research.

Because of the huge calculation efforts, the 3D model is impossible to simulate a long-term time period, but the results are more accurate[41]. In comparison, the 2D models are time-saving but less accurate due to one dimension loss. The co-simulations are developed, which use the 2D model as the supplement for the efficiency loss of the 3D model, and it uses the results of the 3D model as a resource of calibration to improve the reliability of the 2D model. This combination largely improves the feasibility of the DEM modelling method.

Also, due to the efficiency problems, different loading processes are applied. The 3D simulations used a 1-cycle loading, which is close to the quasi-statics process, mainly to obtain the contact behaviour between sleeper and ballast. Whereas the 2D models used cyclic loading, by which the repeated train loading and restriction from rail and fasteners are simulated, and the sleeper displacement is the main focus.

3.3.1 3D model

The 3D model includes 3 parts: a box, ballast particles, and a sleeper, as shown in Figure 5. The ballast particles are clumped elements, made by assembling several balls together to present one ballast particle. The ballast box and sleeper are wall elements, which are assemblies of triangle facets [42].

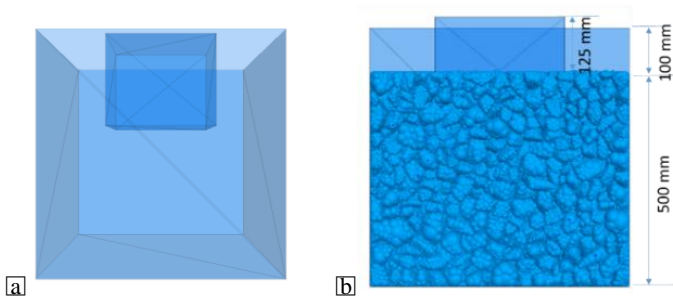
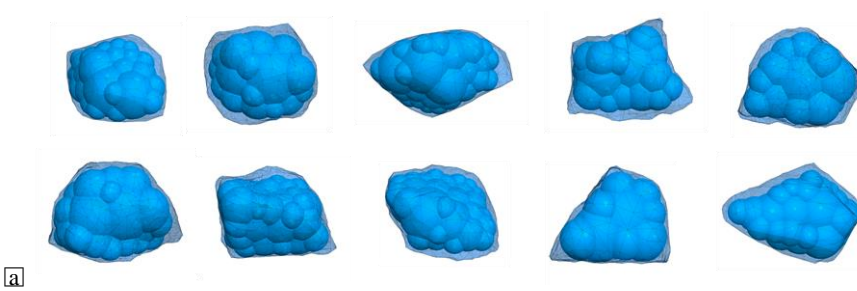


Figure 3-5. Sleeper & Ballast box model. (a) Box and sleeper, (b) Box filled with ballast

The 3D model is comprised of the following key parts:

1. The ballast box (formed from wall elements) is the container for the ballast particles, with dimensions: 600*600*600mm. The box is filled with ballast clumps to 500 mm height. Wall elements. The walls contains the force condition, but cannot transmit forces to another side and move under unbalance forces. It is generated typically as the boundary.

2. Ballast particles (formed from 3D clump elements) are generated from 10 different templates, as shown in Figure 3-6(a). The templates were derived from real ballast particles using 3D scanning (Figure 3-6(b)), which makes sure that the contact behaviour between ballast particles is reliable in geometry. The Particle Size Distribution (PSD) of the ballast particles in the ballast box is shown in Figure 3-6(c).



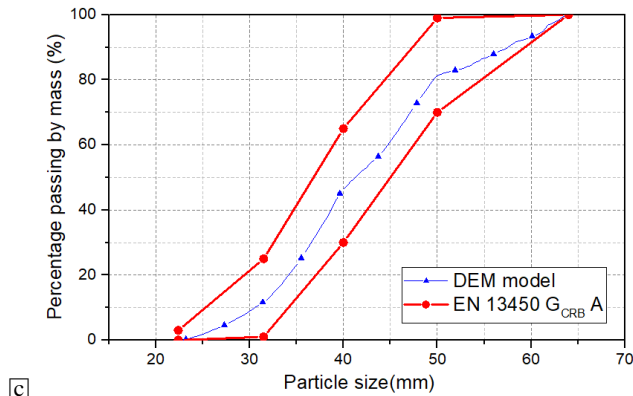


Figure 3-6. DEM ballast particle size distribution, (a) Ballast particle Templates, (b) 3D scanning of ballast shape, (c) Particle size distribution

3. Sleepers (formed from wall elements) were simulated according to the different wedge geometries under test. The mono-block reference sleeper has dimensions 300*300*250mm and also acted as the basis for the different wedge geometries (Figure 3-7). Considering ballast's angle of repose ballast [40], the wedge angles were chosen as 30 degrees, 45 degrees, and 60 degrees. The height of the sleepers is a function of the wedge angle, and are: 87mm, 150mm, and 260mm, respectively. Those sleepers are located at the same position by controlling the location of the sleeper top height, which is 125mm higher than the ballast top surface, as shown in Figure 3-5.

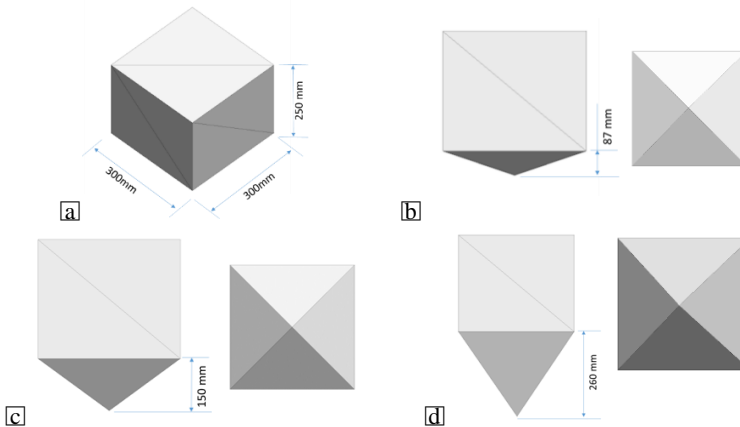


Figure 3-7. Wedge sleepers designs used in the DEM model, (a) Mono-block sleeper, (b) 30-degree wedged sleeper, (c) 45-degree wedged sleeper, (d) 60-degree wedged sleeper

4. The contact model is used to define the force-displacement behaviour for ballast-ballast contact and ballast-wall contact. The linear contact model is used with the parameters listed in Table 1. All parameters were verified in earlier studies [43-46]. Additional details regarding the contact models and parameters can be found in [42].

Table 3-1. Linear contact model Parameters for ballast box model

Parameters	Ballast (Clump)	Sleeper
Tangential stiffness(N/m)	$2e^8$	$5e^9$
Normal stiffness(N/m)	$2e^8$	$5e^9$
Friction coefficient	0.5	0.5
Mass density(kg/m ³)	2800	-
Damping coefficient	0.7	-

The support correction effect was validated using a loading simulation with a pre-set settlement condition. Considering the computational cost of 3D DEM simulation, a 1 cycle loading process is used. It is controlled by applying a positive or negative z-direction velocity (4 mm/s) to the sleeper. The loading process was divided into 3 stages as shown in Figure 3-8 (and Figure 3-3):

Stage 1: Lift the sleeper 4 mm, for the purpose of introducing initial ballast settlement.

Stage 2: Stopping the sleeper movement at a fixed position, followed by time window to allow the ballast to move (under gravity) and fill the ballast-sleeper void. The time window was controlled with 50k calculation cycles to ensure the ballast movement was sufficient. Note that the calculation cycle is a timestep for the software to determine and update information used to keep the kinetic balance of the model through all calculation processes. It is different from the loading cycle and presents no physical significance.

Stage 3: Lower the sleeper 4mm back to its initial location. This process is used to calculate the force behaviour after settlement.

PII-III

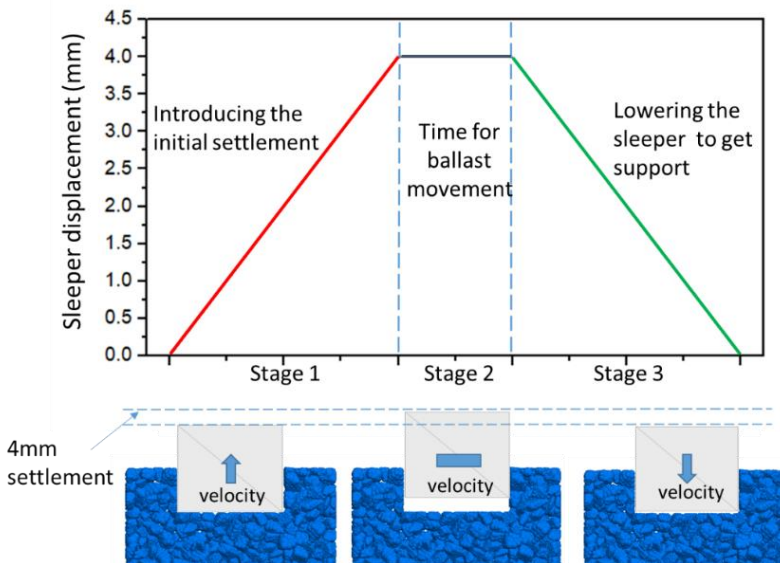


Figure 3-8. Loading process in 3D DEM simulations

3.3.2 2D model

It is challenging to use 3D FEM simulations to study long-term ballast settlement. Thus, as an alternative, a series of 2D DEM simulations were used. The 2D model contained particles simplified as ball shapes to maximise computational efficiency. 3D simulations were used to calibrate the 2D model and thus ensure accuracy. The 2D model is comprised the following key parts:

The ballast box is built using wall elements and had dimensions: 600*500mm. The ballast layer was 450mm in total, where 350mm is under the bottom of the mono-block sleeper (or the bottom of the cubic part of the wedged sleeper), and 100mm is filling in the crib.

The ballast particles are simulated using ball elements.

The wedged sleepers are built using wall elements, according to the cross-section of KLP sleeper type 202, which is a High-Density Polyethylene Polymer developed by Lankhorst and used as the prototype in the IN2ZONE project. The main part of wedged sleeper (also the mono-block sleeper) is 150 mm*250mm. The only wedge considered was the 45 degrees case, which has a height of 125mm.

The contact model is linear, capable of considering rolling resistance. The rolling resistance can simulate the interlock between particles, thus compensating for the loss of using ball particles.

The 2D model is shown in Figure 3-9, and the contact parameters are shown in Table 3-2.

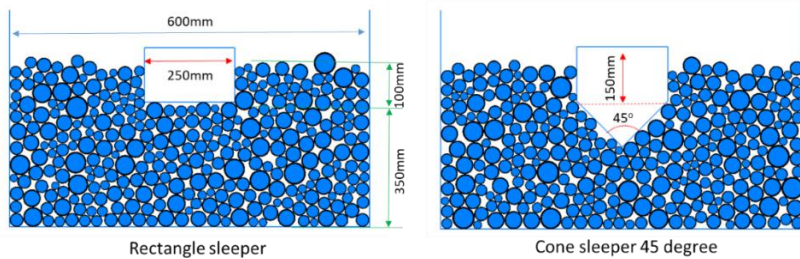


Figure 3-9. 2D ballast box model

Table 3-2. Contact parameters for 2D model

Parameters	Ballast (Ball)	Sleeper
Tangential stiffness(N/m)	$5e^8$	$1e^9$
Normal stiffness(N/m)	$2e^8$	$1e^9$
Friction coefficient	0.5	0.5
Rolling resistance coefficient	0.3	-
Mass density(kg/m^3)	2800	-
Damping coefficient	0.7	-

Due to the characteristics of the DEM wall elements, the sleepers could not obtain an acceleration for an unbalanced force [47]. Therefore a suitable loading method was important to simulate the long-term behaviour under repeated loading from the train and the positional restriction from the rail/fasteners. The loading approach was the displacement and force double-controlled method, which is described in the following 4 stages, and Figure 3-10:

Step1: Lift the sleeper 5mm to produce an initial settlement.

- Step2:** Set a downward velocity (4mm/s) on the sleeper. Stop the sleeper when the ballast-sleeper contact force reaches 40kN (corresponding to the contact force in [6]). This step is force controlled, aiming to simulate the process when a wheel passes and produces loading on the sleeper.
- Step 3:** Reverse the velocity direction (so now upward 4mm/s). Stop the sleeper when it reaches the location from step 1. In this step, the sleeper movement is displacement controlled, aiming to simulate the process when wheels have passed the sleeper. Then, reverse the velocity downwards and repeat step 2 and step 3. Step 2 and step 3 combine together, making up the whole process of the train passage.
- Step 4:** After several cycles, the correction effect of the sleeper leads to a steady state. The total loading was around 500 cycles, and the calculation cycles were around 600k.

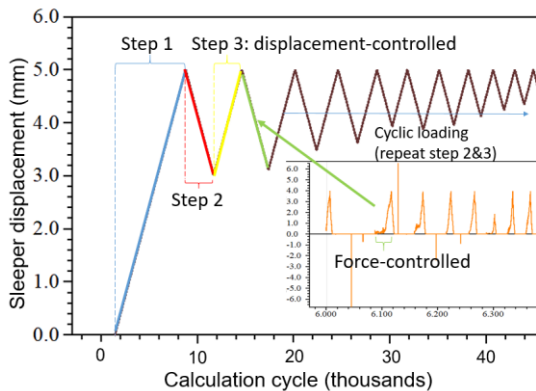


Figure 3-10 Loading process of the 2D model

4 Analysis

4.1 Wedge sleeper type

The scaled laboratory tests were used to compare the different designs against the reference sleeper. The results of the final displacement of the sleepers are shown in Figure 3-11. The sleeper displacement proves the function of the support correction. The smaller displacement of the wedged sleeper shows better correction under 10mm initial settlement. Due to the tests lifting the bridge 10mm as the initial settlement, and the ballast particle size is around 6mm, the mono-sleeper also showed a 5.8 mm correction. In comparison, all the wedged sleepers showed a better correction effect than the mono-block sleeper. The correction of the 45-degree sleeper is approximately 7.4mm, and the correction of 60-degree sleeper is approximately 8mm.

The single-wedge showed no significant difference in displacement compared with the multi-wedge sleeper. After 16 runs, voids between the sleeper and ballast layer were observed between the wedges of the multi-wedged sleeper, as shown in Figure 3-12. This phenomenon is mainly related to the complex contact surfaces of the multi-wedge sleeper. Only longitudinal ballast movement filled the void, but minimal lateral ballast movement (between the wedges, dark area in the red circle) contributed to the correction. Therefore the multi-wedged design was discarded and the remaining analyses focused on single-wedge solutions.

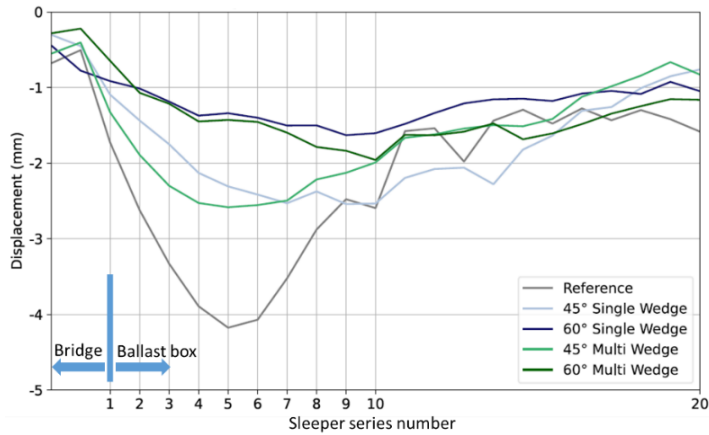


Figure 3-11 Final sleeper displacement under 10mm initial settlement

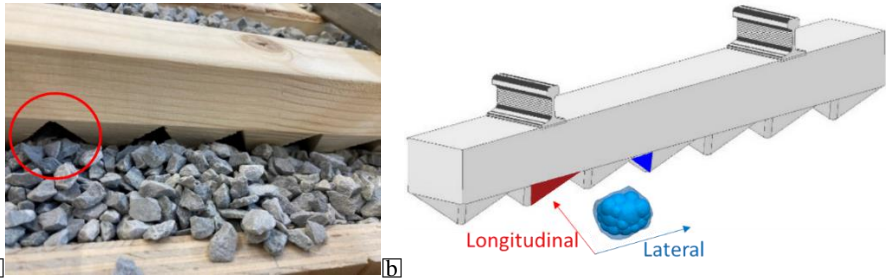


Figure 3-12. Voiding under multi-wedged sleeper after 16 runs, (a) Laboratory tests, (b) schematic diagram

4.2 Wedge sleeper angle

To analyse the influence of wedge angle on the support correction effect, the contact behaviour between the sleeper and the ballast particles was obtained using 3D DEM simulations.

During the loading process, the displacement of the sleeper and the contact force between the sleeper and ballast were recorded. Figure 3-13 shows the results corresponding to the 45-degree sleeper. Two points (Point a and Point b) and 1 range (Range c) were used to analyse the force performance of the wedge sleeper.

Point a: When the sleeper lifting process is finished and stops at the position represented for settlement. The biggest frictional force (z-direction) can be seen near this point. It presents the frictional interaction between the hanging sleeper and ballast.

Point b: The point where the contact force between the sleeper and particles begins to increase rapidly. Thus the displacement at this point can be regarded as ballast beginning to provide effective support. The global displacement at this point is an indicator. A higher value presents a better support correction.

Range c: The increase in contact force during the last 1 mm displacement in Stage 3. A higher value indicates a better support correction.

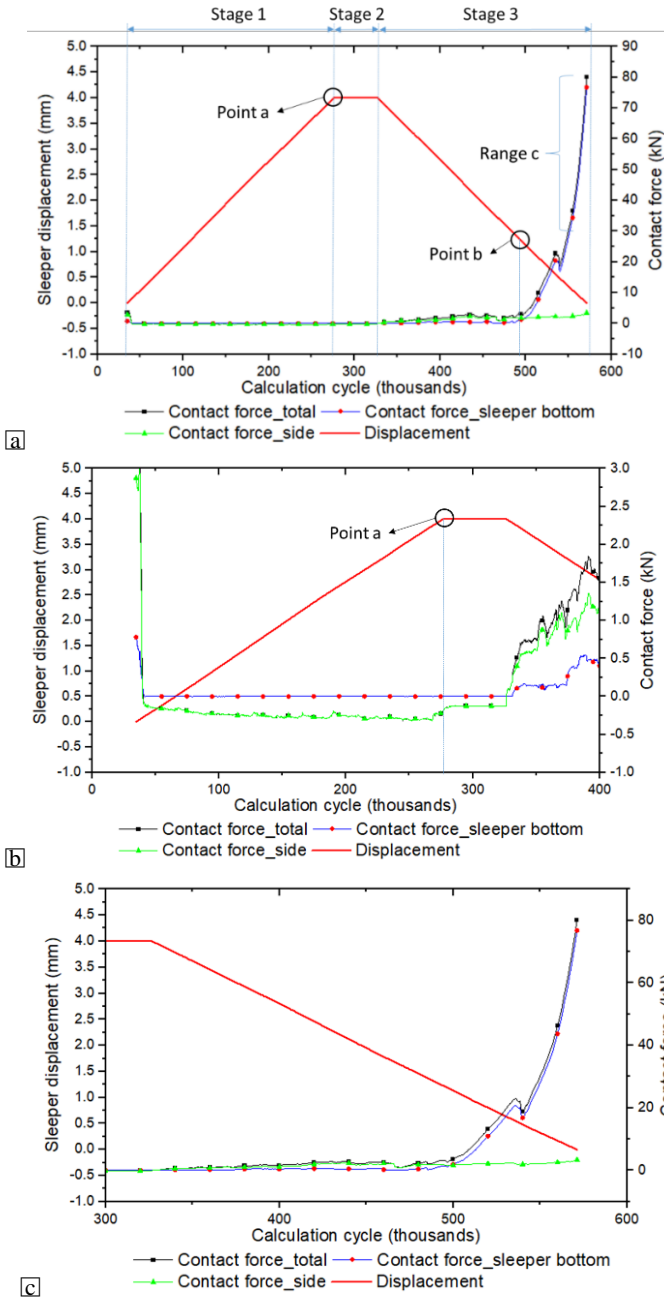


Figure 3-13. Sleeper displacement and contact force for the 45-degree wedged sleeper, (a) Sleeper displacement and contact force, (b) Stages 1 & 2 (zoomed), (c) Stage 3 (zoomed)

The contact forces of 30 and 60 degree wedge sleepers are shown in Figure 3-14, and detailed results are concluded in Table 3-3, which reflects the support correction effect due to the different angles. When the wedge angle increased from 30 degrees to 45 degrees, the sleeper displacement at point b increased from 0.86mm to 1.51mm. When the wedge angle was 60 degrees, the sleeper displacement was 2.36mm. These results demonstrate that a bigger wedge angle led to a better settlement correction.

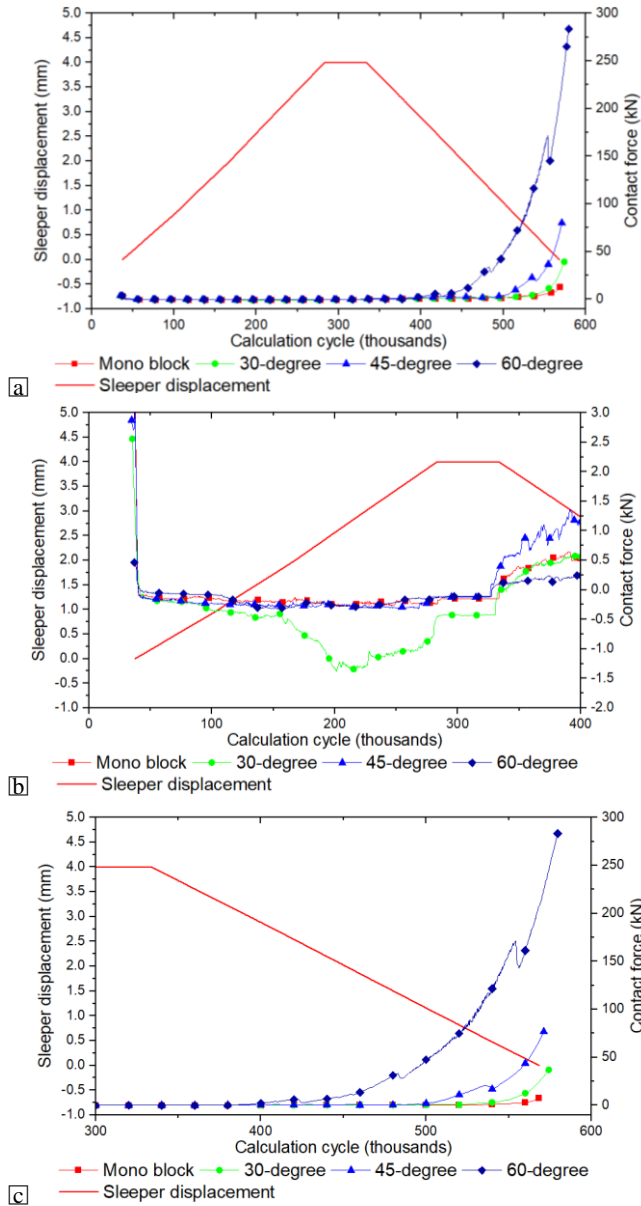


Figure 3-14. Sleeper displacement and contact force on different sleepers. (a) Total contact force, (b) Contact force on sleeper side, (c) Contact force on sleeper bottom

Table 3-3. Key results of wedged sleeper

Wedge angle (degree)	Biggest frictional force (Z-direction) (kN)	Displacement when sleeper begins to get support (mm) (point b)	Force increase in last 1 mm (kN) (range c)	Peak sleeper contact force (Z-direction) (kN)
30	-0.14	0.86	1.56	39.31
45	-0.32	1.51	74.95	80.12
60	-0.34	2.36	21.88	284.33
Mono-block	-0.29	0.98	11.71	13.49

The correction is related to the angle of repose for ballast, which is normally observed to range from 30 to 45 degrees [40, 48, 49]. When the slope of the ballast-sleeper interface is higher than that range, ballast particles have the freedom to migrate into the ballast-sleeper void. This statement also explains why an increased correction effect occurred with the angle increase. The correction increase from 30 to 45 degrees, or from 45 to 60 degrees, is much higher than that from 0 to 30 degrees. In addition, because the sleeper is displacement controlled, the peak contact force, maximum force and the force increase in the last 1mm are all increased along with the angle increase. This behaviour shows that a higher angle can lead to better support.

Note that the settlement came from the upward sleeper lifting in the simulations. In contrast direction, the settlement comes from the ballast deformation in reality. So, the higher peak contact forces on the wedge sleeper are caused by the higher compaction when compelling the sleepers back to a designed position. The extra high contact forces will not appear because the real settlement pattern will not produce extra compaction between sleeper and ballast.

However, the mono-block sleeper also can be regarded as a 90 degree wedge, which may produce the steepest slope for ballast particles to slide into the void. The results do not prove the hypothesis because under the same settlement, the mono-block sleeper provides a smaller void and the possible restriction on ballast, compared with wedged sleeper. The void under the sleeper is related to both settlement and the wedge angle, as shown in Figure 3-15. In addition, the side of the mono-block restricts ballast rotation and displacement.

PII-III

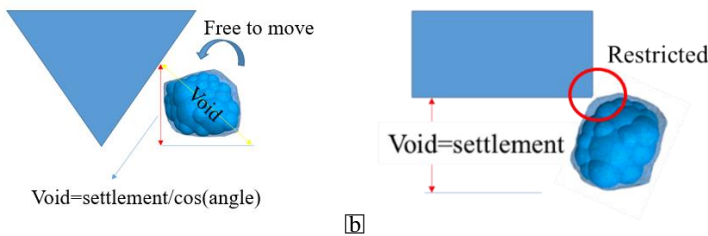


Figure 3-15. Ballast in the void after settlement, (a) Wedged sleeper, (b) Mono-block sleeper

The maximum contact forces are shown in Figure 3-16, which are 8.66kN, 21.85 kN, and 48.20kN, corresponding to 30, 45, and 60-degree wedged sleepers, and 3.92kN of the mono-block sleeper, respectively. The increase of maximum contact force shows an increasing trend. It was in accordance with the increasing wedge angle and proved that a higher wedge angle leads to better support. As for the ballast-sleeper contact force distribution, the maximum contact forces (red dot in Figure 3-16) are observed on the slope of the wedge. In contrast, the maximum contact forces of the mono-block sleeper are observed at the edge of the bottom.

A higher angle leads to improved support correction behaviour, force distribution, and maximum contact force. However, the effective ballast thickness for the 60-degree wedged sleeper is less than 100mm, which is not enough to provide resilience [50]. Thus, 45 degrees was selected as the solution to take forward for the long-term settlement analysis.

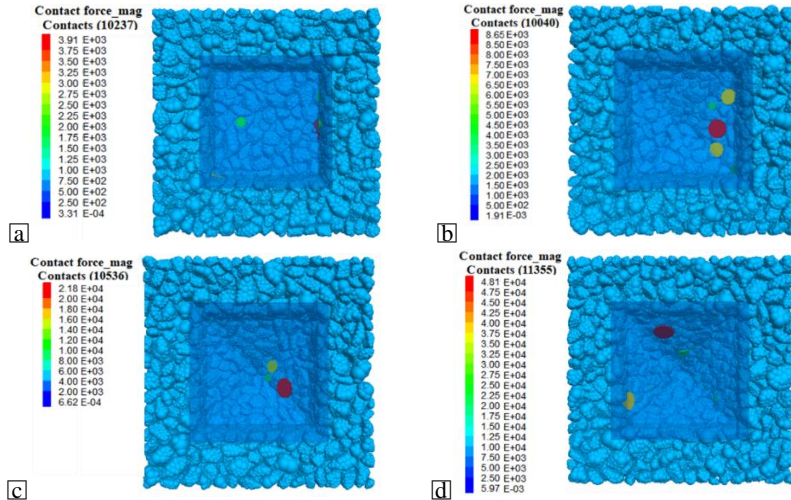


Figure 3-16. Contact force on sleeper (unit: N). (a) Mono-block sleeper (b) 30-degree wedged sleeper, (c) 45-degree wedged sleeper, (d) 60-degree wedged sleeper

4.3 Settlement behaviour

4.3.1 2D model calibration

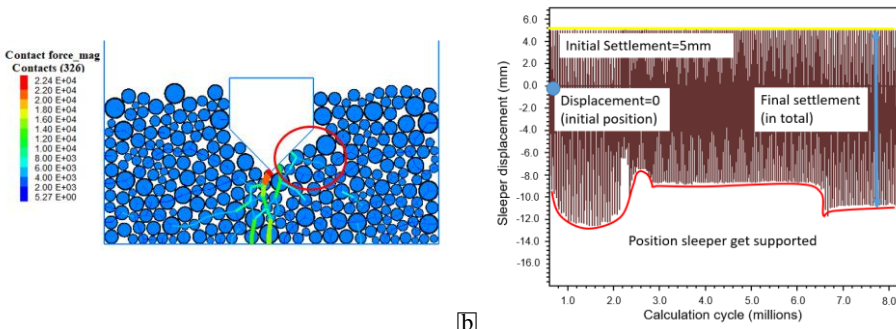
2D DEM simulations were used to study longer-term settlement behaviour instead of 3D simulations due to the efficiency problem. The 2D models are time-saving, making the long-term analysis to be possible, but accuracy is low. The calculation shows that even if the same parameters are used to build models, results still vary. Thus, each condition (different sleepers under different settlements) is calculated 20 times. Then the contact force results, especially the force distribution of the 3D model, are used to calibrate the 2D model.

The calibration is to distinguish and discard the failure model. For example, the contact force distribution and displacement results in Figure 3-17 show a representative model of failure calculation. The force and compaction status of ballast are against the results of 3D simulations.

Note that the curve shape in Figure 3-17b is similar to that shown in Figure 3-10, but it contains around 500 loading cycles (8.2million calculation cycles) in a limited axle length, thus leading to a dense and black layout. As an explanation, the curve contains 4 parts:

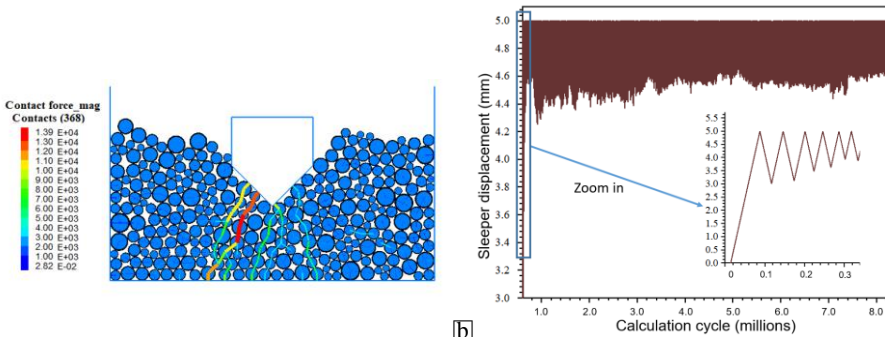
- 1) The zero point is the sleeper location before settlement;
- 2) The top yellow line is the location of the sleeper after the initial settlement. The location is fixed because of the restriction of the fastening system and rail;
- 3) The red bottom line is the location of the sleeper when the loading (of the wheel) is fully applied on the sleeper;
- 4) The distance between the yellow line and the red line is the settlement under cyclic loading.

In detail, the settlement of the failure model is 16mm in total, and no settlement correction through all the loading cycles. This behaviour is caused by the contact between the sleeper bottom and the ballast is un-compacted. In addition, the maximum contact force is 2.25kN, which is observed at the tip of wedged sleeper, but this peak force did not appear in the 3D model (Figure 3-16). All of the force and compaction status of ballast are against the results of 3D simulations. For this reason, this simulation is considered to be a failure then discarded.



a) b) *Figure 3-17. A case of wedged sleeper with bad correction, (a) Contact force distribution (unit: N), (b) Sleeper displacement (unit: m)*

A representative 2D model, whose results are in accordance with 3D results, are shown in Figure 3-18. In this case, the settlement correction happens at the very beginning of the cyclic loading, the final correction is more than 4mm, and the sleeper is stable through the cyclic loading process. The maximum contact force is 13.9kN. The contact force distribution is similar to that of the 3D ballast box model (Figure 3-16). Both the force distribution and maximum contact force are in accordance with the 3D simulations. This model is accepted for further analysis.



a) b) *Figure 3-18. A case of wedged sleeper with good correction, (a) Contact force distribution (unit: N), (b) Sleeper displacement (unit: m)*

For the mono-block sleeper, the model and results are also calibrated by the results of 3D models, although most of the 2D results are at a similar level. Among them, a representative result is shown in Figure 3-19. The correction effect is not observed. The maximum force appears near the edge of the sleeper bottom. The force distribution and maximum contact force are in accordance with the 3D simulations.

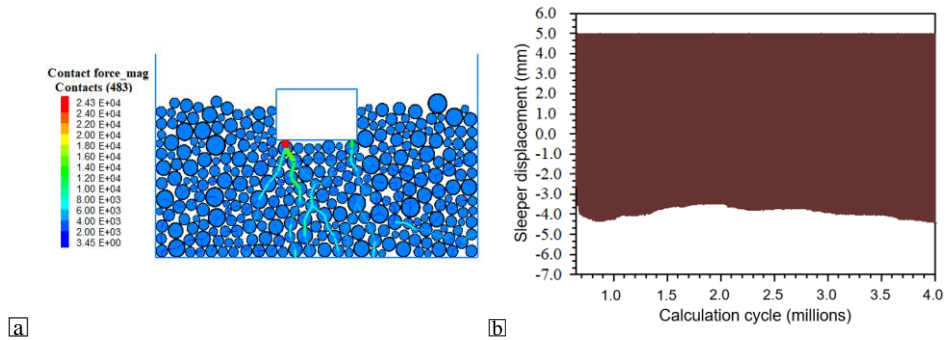


Figure 3-19. A case of mono-block sleeper, (a) Contact force distribution (unit: N), (b) Sleeper displacement (unit: m)

The DEM simulations provide both mesoscopic results and macroscopic results. In the 3D models, the particle shape and contact behaviour were verified in the author's previous research. By the calibration, the mesoscopic results of 2D models are qualified, then the failure model is discarded, and the left 2D models show similar results in mesoscopic. Because the macroscopic results are the external appearance of mesoscopic behaviour, those 2D models are also verified by the 2D/3D calibration.

4.3.2 Settlement behaviour

As mentioned above, the 2D models are calibrated according to the results of 3D models. The results of the accepted models are listed in Table 3-4. The 3 representative results are selected to show the deviation according to the force range. Those are the biggest value, the middle value, and the minimum value of the maximum contact force. Note that the negative value means no correction, but a further settlement beyond the initial setting is observed after the loading process.

Table 3-4. Results of the 2D model under 5mm initial settlement

Sleeper type	Correction (mm)	Final settlement (mm)	Maximum contact force (kN)
Mono-block sleeper	-4.3	9.3	24.31
	-3.8	8.8	37.96
	-4	8	17.57
Wedge sleeper	5	0	18.49
	4	1	23.40
	5	0	13.94

The settlement of mono-block sleeper after cyclic loading is 8mm to 9.3mm, whereas the settlement of wedged sleeper is only 0mm or 1mm. The maximum contact force for the mono-block sleeper range from 17.57kN to 37.96kN, whereas the maximum contact force of wedged sleeper range from 13.94kN to 23.40kN, the decrease ratio is around 20% to 38%. In addition, the force distribution area of a mono-block sleeper is much smaller than the wedged sleeper (as shown in Figure 3-18 and Figure 3-19). That is to say, the wedged sleeper not only provides a support correction effect but also decreases the maximum force.

Further, a calibrated 2D model is employed to analyse the correction effect under a higher settlement. The initial settlement is enlarged to 10mm, 15mm and 20mm, and the results are listed in Figure 3-

20 to Figure 3-22 and Table 3-5. Results show that the wedged sleeper can correct all the settlements under 5mm and 10mm conditions. When the settlement increases to 15mm and 20mm, the correction is still effective, and the force behaviour is similar to that of cases under 5mm settlements.

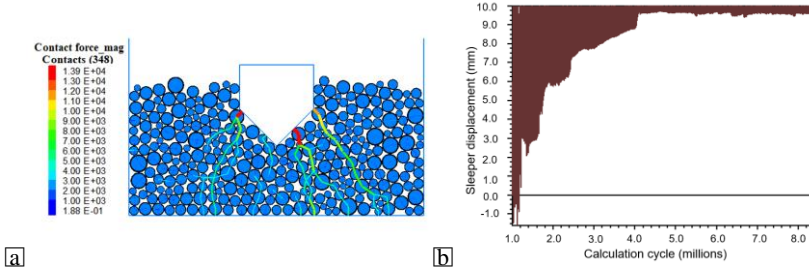


Figure 3-20. A case of wedged sleeper with good correction under 10mm settlement. (a) Contact force distribution (unit: N), (b) Sleeper displacement (unit: m)

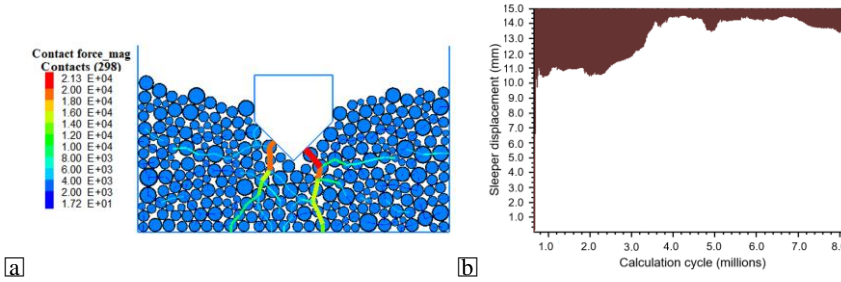


Figure 3-21. A case of wedged sleeper with good correction under 15mm settlement. (a) Contact force distribution (unit: N), (b) Sleeper displacement (unit: m)

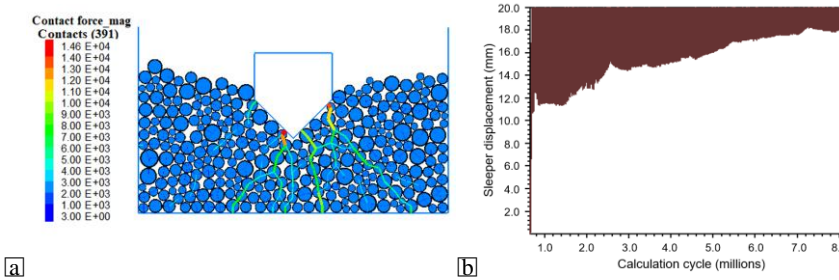


Figure 3-22. A case for wedged sleeper with good correction under 20mm settlement. (a) Contact force distribution (unit: N), (b) Sleeper displacement (unit: m)

Table 3-5. Correction for higher settlement

Settlement (mm)	Correction (mm)	Maximum contact force (kN)
10	10	14.0
15	14	21.31
20	18	14.60

5. Conclusions

Railway track transition zones are areas with rapidly changing track stiffness. It is common for hanging sleepers to develop on the softer side due to differential settlement. To address this problem, this paper proposed and investigated a new concept sleeper with a wedge-shaped geometry. First, scaled laboratory tests are used to study the performance of different wedge geometries, and it is found that a single long wedge is preferable compared to multiple smaller wedges. Next, 3D DEM simulations are performed to analyse the contact forces in the ballast due to different single wedge designs. Finally, 2D DEM simulations are performed to study the long-term settlement behaviour. The main conclusion were:

1. When the bottom angle of wedged sleeper is larger than the repose angle of ballast material, particles have the freedom to migrate into the settlement induced voids
2. An increased wedge sleeper angle stimulates greater particle migration and thus improved, the support correction. However the longer wedge also leads to a decrease in effective ballast height under sleeper.
3. The ability of wedge-shaped sleepers to reduce the presence of sleeper voids is promising, however further study is needed.
4. Compared with the mono-block sleeper, the wedged sleeper reduces the contact force between the sleeper and the ballast due to a wider contact area.

Following with the paper finished, the full-scale (45-degree) wedge sleeper was produced. The long-term behaviour was analysed based on a series of large-scale laboratory tests. Primary results were obtained, which are in accordance with the results of numerical simulations. Further works and optimisation of the sleeper is ongoing.

Acknowledgments

This is from work undertaken as part of the IN2ZONE project, which has received funding from the Shift2Rail Joint Undertaking (JU) under grant agreement 101014571 – IP/ITD/CCA – IP3.”

Reference

- [1] R. Sañudo, L. dell'Olio, J.A. Casado, I.A. Carrascal, S. Diego, Track transitions in railways: A review, *Construction and Building Materials* 112 (2016) 140-157.
- [2] J.-A. Zakeri, V. Ghorbani, Investigation on dynamic behavior of railway track in transition zone, *Journal of Mechanical Science and Technology* 25(2) (2011) 287-292.
- [3] A. Paixão, E. Fortunato, R. Caçada, Design and construction of backfills for railway track transition zones, *Proceedings of the Institution of Mechanical Engineers, Part F: Journal of Rail and Rapid Transit* 229(1) (2013) 58-70.
- [4] H. Wang, V. Markine, Modelling of the long-term behaviour of transition zones: Prediction of track settlement, *Engineering Structures* 156 (2018) 294-304.
- [5] H. Huang, B. Brennecke, Track Stiffness Transition Zone Studied with Three-Dimensional Sandwich Track Model, *Transportation Research Record: Journal of the Transportation Research Board* 2374(1) (2013) 136-142.
- [6] H. Wang, V. Markine, Dynamic behaviour of the track in transitions zones considering the differential settlement, *Journal of Sound and Vibration* 459 (2019) 114863.
- [7] C. Charoenwong, D.P. Connolly, P.K. Woodward, P. Galvín, P. Alves Costa, Analytical forecasting of long-term railway track settlement, *Computers and Geotechnics* 143 (2022) 104601.
- [8] C. Charoenwong, D.P. Connolly, K. Odolinski, P. Alves Costa, P. Galvín, A. Smith, The effect of rolling stock characteristics on differential railway track settlement: An engineering-economic model, *Transportation Geotechnics* 37 (2022) 100845.
- [9] D. Li, D. Otter, G. Carr, Railway Bridge Approaches under Heavy Axle Load Traffic: Problems, Causes, and Remedies, *Proceedings of the Institution of Mechanical Engineers, Part F: Journal of Rail and Rapid Transit* 224(5) (2010) 383-390.
- [10] M. Sol-Sánchez, F. Moreno-Navarro, M.C. Rubio-Gámez, Viability analysis of deconstructed tires as material for rail pads in high-speed railways, *Materials & Design* 64 (2014) 407-414.
- [11] T. Xin, Y. Ding, P. Wang, L. Gao, Application of rubber mats in transition zone between two different slab tracks in high-speed railway, *Construction and Building Materials* 243 (2020) 118219.
- [12] Y. Çati, S. Gökçeli, Ö. Anil, C.S. Korkmaz, Experimental and numerical investigation of usp for optimization of transition zone of railway, *Engineering Structures* 209 (2020) 109971.
- [13] M. Esmacili, M. Siahkouhi, Tire-derived aggregate layer performance in railway bridges as a novel impact absorber: Numerical and field study, *Structural Control and Health Monitoring* 26(10) (2019) e2444.
- [14] P. Chumyén, D.P. Connolly, P.K. Woodward, V. Markine, The effect of soil improvement and auxiliary rails at railway track transition zones, *Soil Dynamics and Earthquake Engineering* 155 (2022) 107200.
- [15] R. David, L. Dingqing, *Design of Track Transitions*, Washington, DC: The National Academies Press, 2006.
- [16] A. Namura, T. Suzuki, Evaluation of countermeasures against differential settlement at track transitions, *Quarterly Report of RTRI* 48(3) (2007) 176-182.
- [17] W. Li, X. Bian, Dynamic Performance of Pile-supported Bridge-embankment Transition Zones Under High-speed Train Moving Loads, *Procedia Engineering* 143 (2016) 1059-1067.
- [18] Y. Qian, E. Tutumluer, Y.M.A. Hashash, J. Ghaboussi, D.D. Davis, Ballast Settlement Ramp to Mitigate Differential Settlement in a Bridge Transition Zone, *Transportation Research Record: Journal of the Transportation Research Board* 2476(1) (2015) 45-52.
- [19] B. Indraratna, M.A. Shahin, W. Salim, Use of geosynthetics for stabilizing recycled ballast in railway track substructures, *Proceedings of NAGS2005/ GRI 19 Cooperative Conference* (2015) 1-15.
- [20] B. Indraratna, S. Nimbalkar, T. Neville, Performance assessment of reinforced ballasted rail track, *Proceedings of the ICE: Ground Improvement* 167(1) (2014) 24-34.

- [21] B. Indraratna, M.M. Biabani, S. Nimbalkar, Behavior of Geocell-Reinforced Subballast Subjected to Cyclic Loading in Plane-Strain Condition, *Journal of Geotechnical and Geoenvironmental Engineering* 141(1) (2015) 04014081.
- [22] G. Jing, L. Qie, V. Markine, W. Jia, Polyurethane reinforced ballasted track: Review, innovation and challenge, *Construction and Building Materials* 208 (2019) 734-748.
- [23] P. Schneider, R. Bolmsvik, J.C.O. Nielsen, In situ performance of a ballasted railway track with under sleeper pads, *Proceedings of the Institution of Mechanical Engineers, Part F: Journal of Rail and Rapid Transit* 225(3) (2011) 299-309.
- [24] S. Kaewunruen, A. Aikawa, A.M. Remennikov, Vibration Attenuation at Rail Joints through under Sleeper Pads, *Procedia Engineering* 189 (2017) 193-198.
- [25] M. Sol-Sánchez, F. Moreno-Navarro, M.C. Rubio-Gámez, Analysis of ballast tamping and stone-blowing processes on railway track behaviour: the influence of using USPs, *Géotechnique* 66(6) (2016) 481-489.
- [26] H. Wang, V. Markine, Corrective countermeasure for track transition zones in railways: Adjustable fastener, *Engineering Structures* 169 (2018) 1-14.
- [27] K. Muramoto, T. Nakamura, T. Sakurai, A study of the effect of track irregularity prevention methods for the transition zone between different track structures. *Quart Rep RTRI* 2012;53(4):211-5.
- [28] K. Muramoto, T. Nakamura, T. Sakurai, A Hanging Sleepers Preventing Method using Automatic Irregularity-Correcting Short Sleeper, 11th World Congress on Railway Research, (2016).
- [29] P. Insley, P. Sharpe, Self-compensating sleeper and method of maintaining a railroad track, 2020, Europe, Patent No. EP3608472A1.
- [30] S.H. Lee, J.W. Lee, C.Y. Choi, H.J. Jang, Automatic subsidence correcting apparatus for loose sleeper between different track structures, and constructing method thereof. Korea, Patent No. KR101374526B1;KR20130137465A.
- [31] S.H. Lee, J.W. Lee, Rail tie having embedded automatic differential settlement compensation apparatus using oil pressure for railroad tracks, 2014, Korea, Patent No. EP3112533A1;EP3112533A4;EP3112533B1;KR101625841B1;KR20150100338A;US10138604B2;US2017009405A1;WO2015129996A1.
- [32] C. Calla, Two layered ballast system for improved performance of railway track, Coventry University, (2003).
- [33] T. Abadi, L.L. Pen, A. Zervos, W. Powrie, Improving the performance of railway tracks through ballast interventions, *Proceedings of the Institution of Mechanical Engineers, Part F: Journal of Rail and Rapid Transit* 232(2) (2016) 337-355.
- [34] P. Claisse, M. Keedwell, C. Calla, Tests on a two-layered ballast system, *Proceedings of the Institution of Civil Engineers - Transport* (156) (2003) 93-101.
- [35] H. Li, G. McDowell, Discrete element modelling of two-layered ballast in a box test, *Granular Matter* 22(4) (2020).
- [36] G.Q. Jing, P. Aela, H. Fu, H. Yin, Numerical and experimental analysis of single tie push tests on different shapes of concrete sleepers in ballasted tracks, *Proceedings of the Institution of Mechanical Engineers, Part F: Journal of Rail and Rapid Transit* 233(7) (2018) 666-677.
- [37] Y. Guo, H. Fu, Y. Qian, V. Markine, G. Jing, Effect of sleeper bottom texture on lateral resistance with discrete element modelling, *Construction and Building Materials* 250 (2020).
- [38] X. Zhang, C. Zhao, W. Zhai, DEM Analysis of Ballast Breakage Under Train Loads and Its Effect on Mechanical Behaviour of Railway Track, *Proceedings of the 7th International Conference on Discrete Element Methods* (2017) 1323-1333.
- [39] C. Chen, B. Indraratna, G. McDowell, C. Rujikiatkamjorn, Discrete element modelling of lateral displacement of a granular assembly under cyclic loading, *Computers and Geotechnics* 69 (2015) 474-484.
- [40] P. Aela, L. Zong, M. Esmacili, M. Siahkouhi, G. Jing, Angle of repose in the numerical modeling of ballast particles focusing on particle-dependent specifications: Parametric study, *Particuology* 65 (2022) 39-50.

- [41] N.T. Ngo, B. Indraratna, C. Rujikiatkamjorn, Simulation Ballasted Track Behavior: Numerical Treatment and Field Application, *International Journal of Geomechanics* 17(6) (2017) 04016130.
- [42] Y. Guo, C. Zhao, V. Markine, G. Jing, W. Zhai, Calibration for discrete element modelling of railway ballast: A review, *Transportation Geotechnics* 23 (2020) 100341.
- [43] G. Jing, W. Jia, X. Wang, V. Markine, R. Nålsund, Y. Guo, Experimental and numerical study on lateral resistance of frictional sleeper with arrowhead groove, *Transportation Geotechnics* 30 (2021) 100638.
- [44] W. Jia, V. Markine, Y. Guo, G. Jing, Experimental and numerical investigations on the shear behaviour of recycled railway ballast, *Construction and Building Materials* 217 (2019) 310-320.
- [45] G. Jing, X. Zhang, W. Jia, Lateral resistance of polyurethane-reinforced ballast with the application of new bonding schemes: Laboratory tests and discrete element simulations, *Construction and Building Materials* 221 (2019) 627-636.
- [46] Y. Guo, W. Jia, V. Markine, G. Jing, Rheology study of ballast-sleeper interaction with particle image Velocimetry (PIV) and discrete element modelling (DEM), *Construction and Building Materials* 282 (2021) 122710.
- [47] I.C.G. Inc., PFC 5.0 document, (2018).
- [48] J. Chen, R. Gao, Y. Liu, Numerical Study of Particle Morphology Effect on the Angle of Repose for Coarse Assemblies Using DEM, *Advances in Materials Science and Engineering* 2019 (2019) 1-15.
- [49] M.A. Wnek, E. Tutumluer, M. Moaveni, E. Gehringer, Investigation of Aggregate Properties Influencing Railroad Ballast Performance, *Transportation Research Record: Journal of the Transportation Research Board* 2374(1) (2013) 180-189.
- [50] B. Indraratna, T. Ngo, *Ballast railroad design: smart-uow approach*, CRC Press 2018.

Paper IV

Experimental and numerical investigations on the shear behaviour of recycled railway ballast

Wenli Jia, Valeri Markine, Yunlong Guo, Guoqing Jing

Published in *Construction and building materials*. 2019(217):310-320

Abstract

Ballast degradation is frequently observed under cyclic loading and results in bearing capacity and drainage problems of the ballasted track. Periodical maintenances are needed to keep stability and safety, such as cleaning and replacement, which produce a huge amount of wasted ballast. Thus, reusing deteriorated ballast can become a considerable method for sustainable railway development and environmental protection. One application is adding the cleaned deteriorated ballast (i.e. recycled ballast) into fresh ballast. Furthermore, it is a common situation that applies a mixture of fresh and deteriorated ballast during railway operations. To study the mechanical behaviour of this mixture and find out the criterion weight proportion of the recycled ballast, a series of large direct shear tests were performed with different weight proportions (0%, 10%, 20%, 30%, 40%, and 50%) of recycled ballast mixed into fresh ballast under different normal stresses (50, 100 and 200 kPa). In addition, a numerical simulation based on the discrete element method (DEM) was used to illustrate the shear strength, contact forces, coordination numbers and displacements of ballast particles. Results show that the shear strength reduction of the mixture is insignificant when mixed with less than 30% recycled ballast. With the recycled ballast proportion increasing, the shear strength and coordination number reduce, and the displacements get larger. This research provides a foundation for the application of recycled ballast, and on the other hand, adding fresh ballast can be a solution to reinforce deteriorated ballast beds.

Keywords: Railway ballast; Recycled ballast; Direct shear tests; Discrete element method

1. Introduction

Railway ballast is generally specified as a crushed, angular hard rock with particle size distributed from 20mm to 65mm [1]. The performance of a ballast bed is influenced by several characteristics. Thus several procedures are performed to check them before track construction. For instance, the LAA loss is applied to qualify the abrasion resistance, and the particle size distribution (PSD) is obtained by sieving to fulfil the characteristics of drainage and elastics [2]. With these characteristics, the main functions of the ballast layer can provide a solid and elastic foundation for the sleepers and bear and transmit the stress from the rails to the subgrade, which is caused by passing trains and good drainage ability [3-4].

However, the function of the ballast bed will deteriorate along with the ballast degradation under the heavier axle and higher speed train load, including particle breakage, abrasion, translation and rotation. In this process, ballast particles turn to less angularity, and the surface texture is worn from coarse to smooth, where the particle size also diminishes, which affects the PSD and produces fine particles, which are the main fouling composition [5]. Finally, differential settlement, poor drainage and capacity reduction are occurred [6-7]. Especially with the heavier axle and higher speed loading nowadays emerging, those problems are severer [8].

It needs to be noted that with the development of the railway, maintenance is more and more frequent, a large amount of fresh ballast is exploited, and deteriorated ballast is produced as waste. In Europe, the maintenance cost varies from 30000 to 100000 Euros per kilometre per year [9], causing both excessive economic consumption and environmental problems. Besides, the construction continues growing with the expectation of completing the Trans-European Transport Network (TEN-T) core network by 2030 and the TEN-T comprehensive network by 2050 [10]. Thus, enhancing the performance and prolonging the lifespan of the ballasted track and sustainable development of the ballasted track is needed to be found out.

The deteriorated ballast behaviour has been studied with a variety of research using laboratory tests or numerical simulations. For instance, Ebrahimi et al. [11] conducted triaxial tests focusing on the behaviour of ballast mixed with fine particles from coal or angular breakage, and results show that under high confine pressure, the deformation of fouling ballast is similar to clean ballast. However, ballast in the track bed is under nearly no confined pressure. For this, Indraratna et al. [12] studied the deformation and degradation of recycled ballast under simulated field loading on both fresh and recycled ballast with cyclic triaxial tests, and results show that the settlement of recycled ballast is 2 times higher than fresh ballast. The drainage problem was analysed by Tennakoon et al. [13], and the results show the drainage changes from good to very poor when the ballast has deteriorated.

Because of the considerable effects of ballast degradation, some research was carried out to qualify the status of ballast. For example, Qian et al. [14] employed the image analysis method to qualify ballast deterioration corresponding with fouling index (FI) after Los Angeles Abrasion (LAA) tests, and Guo et al. [15] also analysed the ballast degradation based on 3-D image analysis method focusing on the influence of particle size and shape.

More importantly, several methods were proposed for deteriorated ballast bed performance improvement, including the geogrid, elastic materials (rail pad, ballast mat and crumb rubber), and polyurethane. The geogrid can increase the shear strength of the ballast layer by strengthening the interlock between ballast particles [16], and the study in [17] shows that geogrid can decrease permanent settlements under cyclic loading. Elastic materials can adjust the stiffness and decrease vibration and noise, further prolonging the service life of the ballasted track [18-20]. For example, the crumb rubber applied in ballast particles was studied in [21] and [22], finding that the 10% (by weight) and 3~5 mm crumb rubber plays a significant role in reducing ballast degradation. Polyurethane reinforcement can also improve the ballast bed performance by bonding granular ballast

together as a whole structure. Through this method, the capacity and stability can be largely improved, and it also can be used for stiffness adjustment in transition zones [23-25].

Although these methods have reinforcing effects, periodical maintenance is still needed to keep the high performance of the ballasted track, including tamping, geometry adjustment and ballast renewal [16]. Thus, fresh ballast consumption stays at a high level. Besides, some maintenance problems occur along with the reinforcement methods mentioned above. For example, after spraying polyurethane, ballast is bonded by high tensile strength. Tamping maintenance is hard to be employed because the tines of a tamping machine cannot insert into the ballast layer, and the problem occurs after geogrid installation, where the geogrid can cause higher settlement on recycled ballast [26-28]. With the shortage of those reinforcement methods, a new method for reinforcement and the way to treat deteriorated ballast have become hot topics.

In addition, these studies illustrated the behaviour of deteriorated ballast, proposed a standard to distinguish the deteriorated ballast or suggested methods for performance improvement. The ballast bed in operation commonly consists of deteriorated and fresh ballast because of ballast degradation or ballast renewal. The behaviour of the mixture is still not clear at present, and further works need to be carried out.

The ballast renewal operation is a method using fresh ballast to reinforce the deteriorated ballast bed. In reverse, adding cleaned and re-sieved deteriorated ballast (i.e. recycled ballast) into fresh ballast also can be a reuse method. However, in this aspect, the current research is limited, and the proportion of recycled ballast, which does not influence the whole required performance, is not clear. Thus, except for the performance of the mixture of deteriorated and fresh ballast, the criterion proportion is also needed to be found out.

Towards this research gap, the performance of deteriorated ballast mixed with fresh ballast is studied with experimental tests and numerical simulation. The direct shear test is utilised to measure the mixture shear strength, and DEM direct shear test model is applied to study the mesoscopic behaviour, including the contact forces, coordination numbers and displacements of ballast particles. This research assists in disposing of the waste ballast and proposing guidance for ballast bed maintenance.

2. Experimental tests

2.1 material specifications

The deteriorated ballast was mixed with fresh ballast in different ratios of 10%, 20%, 30%, and 50% by weight. Moreover, fresh ballast only (0%) and deteriorated ballast only (100%) are concluded as reference groups. The strength and deformation behaviour is tested by a series of large-scale direct shear tests.

The fresh ballast used in this research was obtained from crushed basalt, which is in accordance with the Code for Design of High-Speed Railway (TB/T2140-2008, China [29]). Table 4-1 shows the Particle Size Distribution (PSD), and Table 4-2 shows the main mechanical properties of ballast particles.

Table 4-1. PSD of ballast particles

Sieve Size (mm)	5-31.5	22.4	31.5	40	50	63
Ballast % Passing	71	0	7	33	71	100
TB/T2140-2008 % Passing	≥50	0	1-25	30-65	70-99	100

Table 4-2. Characteristics of ballast

Properties	Test value	Standard value
LAA (%)	17.8	≤18
Aggregate Crushing Test (%)	6.9	< 8
Particle density kg/m ³	2630	> 2550
Ratio of flat particle	5	≤18
Ratio of elongated particle	7	≤18

The deteriorated ballast was obtained from the LAA machine using fresh ballast. According to the standard LAA test procedure (by BS EN 1097-2:2010 [30] and ASTM C-131-01[31]), the abrasion process was conducted at a speed of 32r/min and for 500 rolling turns. After the tests, all of the deteriorated ballast was washed and dried, which is defined as recycled ballast. Five deteriorated ballast particles are shown in Figure 4-1. Afterwards, the recycled ballast particles were sieved and mixed according to the PSD, as shown in Table 4-1.



Figure 4-1 Recycle ballast after cleaning

In this paper, 7 different specimens were used, which is fresh ballast only, 10% recycled ballast and 90% fresh ballast; 20% recycled ballast and 80% fresh ballast; 30% recycled ballast and 70% fresh ballast; 50% recycled ballast and 50% fresh ballast; recycled ballast only. The specimens are shown in Figure 4-2.

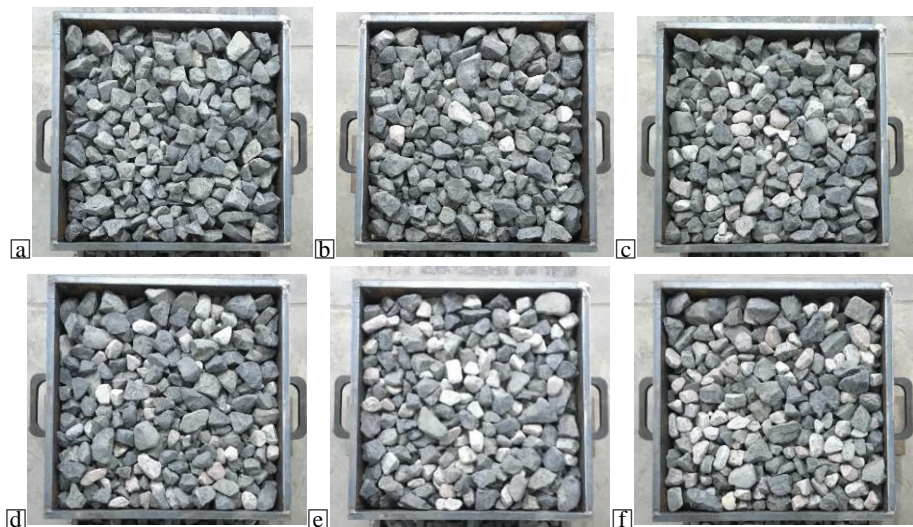




Figure 4-2 Specimens depending on the mixing ratio of recycled ballast: a) Fresh ballast only, b) 10% recycled ballast, c) 20% recycled ballast, d) 30% recycled ballast, e) 40% recycled ballast, f) 50% recycled ballast, g) Recycled ballast only

2.2 Direct shear test

The direct shear test is a basic mechanical test for granular materials. It can present several properties of the material, such as shear strength, cohesion and friction angle, which influence the interaction between particles. In this paper, the mechanical behaviour of degraded-fresh ballast is evaluated by the direct shear test, and the large-scale strain-controlled direct shear apparatus is shown in Figure 4-3. It consists of one lower and one upper shear box with different sizes. Where the inner size of the lower box is 600mm×700mm in plane and 250mm in height, while the upper box is 600mm×600mm in plane and 300mm in height with a cover plate in 595mm×595mm to transmit the normal stress. Behind the lower box and the foundation, several bearings are set to decrease friction, and 4 bearings are installed on the side in case of the box rotation when pushing.

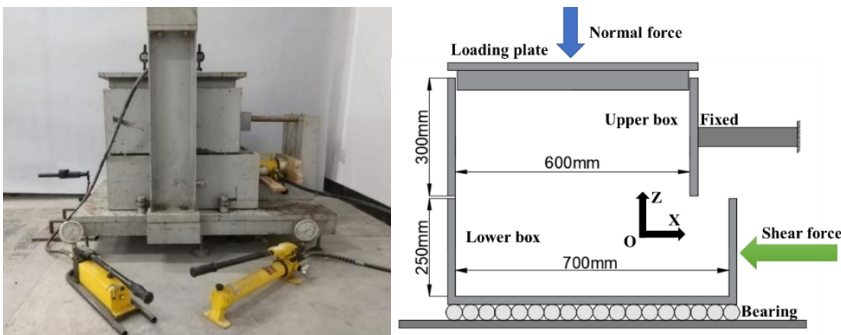


Figure 4-3. Large-scale direct shear apparatus

The recycled-fresh ballast mixture was filled in the shear box and compacted by layers using a vibrating compactor. Each layer is 100mm in height, and the total weight of 359kg was controlled to reach the same porosity (0.3) in every specimen. Certain normal stress (50kPa, 100kPa or 200kPa) was applied to the mixed sample using a hydraulic jack, and the weight of the loading plate is considered as a part of normal stress. Under consistent vertical pressure, the sample was sheared with a loading rate of 0.3mm/min by horizontally pushing the bottom shear box. The lateral displacement and vertical displacement were recorded by LVDT with accuracy at 0.001 mm, and a pressure sensor connected with data logger INV3018A was used to measure the lateral shearing forces during the test. The maximum horizontal displacement was set to 60 mm, which equals 10% strain in total. Every condition was tested 3 times, and the results were presented by the average value.

3. Test results

3.1 Shear strength

Figure 4-4 shows the shear stresses of different proportions of recycled ballast: 0%, 10%, 20%, 30%, 50%, and 100% under different normal stresses.

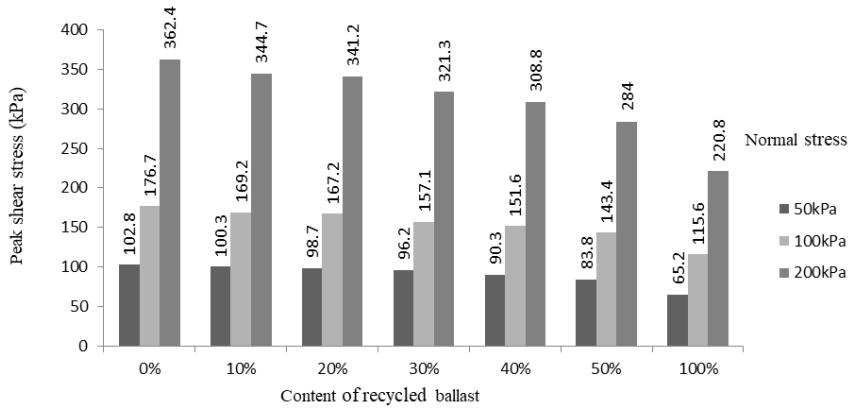


Figure 4-4. Shear strength under different normal stresses

In the case of normal stress of 50kPa, 100kPa and 200kPa, the shear strength of recycled ballast is only 65.2 kPa, 115.6 kPa and 220.8 kPa, respectively. Compared to the data of pure fresh ballast, the strength is significantly decreased by 34.6%, 36.5%, and 39.1%, respectively. As for the 10% recycled ballast mixture compared with pure fresh ballast, 2%, 4%, and 5% reduction can be observed. When the proportion of recycled ballast increases to 20%, the decreasing percentage is 4%, 5%, and 6%. Those reductions are all below or near 5%, which can be defined as insignificant influences. For 30% recycled ballast, the decreasing ratio is a little larger, with 6%, 11% and 11%, respectively. Thus, in the aspect of the shear stress, the mixtures which below 30% recycled ballast can be regarded as well-function. However, when the mixing proportion of recycled ballast is larger than 30%, the reduction ratio exceeds 20%, which strongly influences the shear strength of the ballast.

The main differences between fresh and recycled ballast are the angularity and surface texture, and those two parameters influence the cohesion and friction of ballast particles. Figure 4-5 shows the linear fitting of data, and referring to Eq.1, the cohesion and friction angle can be acquired [32], and the results are shown in Tab.3.

$$\tau_f = c + \sigma_n \tan \psi \quad \text{Eq.1}$$

where: c —cohesion; ψ —friction angle

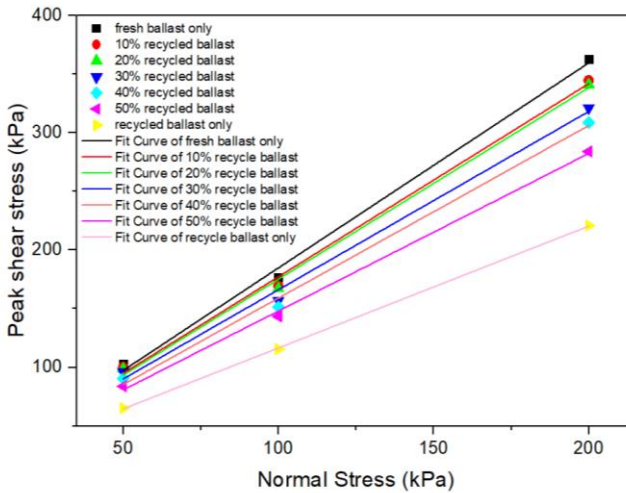


Figure 4-5. Linear fitting between normal stress and shear stress

Table 4-3. Cohesion and friction angel by linear fitting

Content of recycled ballast	Cohesion (kPa)	Friction angle (degree)	R ²
fresh ballast only (0%)	9.95	60.27	0.99426
10% recycled ballast	12.55	58.77	0.99361
20% recycled ballast	11.7	58.56	0.99374
30% recycled ballast	14.1	56.71	0.99053
40% recycled ballast	11.7	55.85	0.99327
50% recycled ballast	13.5	53.39	0.99690
recycled ballast only (100%)	12.6	46.13	0.99978

It can be seen that the friction angle of pure fresh ballast is 60.27°. When mixed with 10% and 20% recycled ballast, the friction angles are slightly lower but very close to that of pure fresh ballast. When the proportion of recycled ballast is over 30%, the friction angle reduces considerably, and the lowest value is observed from pure recycled ballast (46.13°). Compared to fresh ballast, recycled ballast has less angularity and smoother surface texture due to abrasion. Those changes influence the contacts between particles. Thus the interlock between ballast particles is weakened, and the rounder particles are easier to rotate.

3.2 Deformation characteristics

Figure 4-6 shows the average evolution of ballast shear dilatancy for 7 different proportions of recycled ballast. Under 100kPa, the shear dilatancy of fresh ballast is 5.0223 mm, and the value increases to 5.32~5.93 when mixing with 10%, 20%, and 30% recycled ballast, and 6.2208 mm with 40% recycled ballast. A similar trend can be seen under the normal stress of 50kPa and 100kPa. That is to say, with the mixing proportion of recycled ballast under 30%, the shear dilatancy increases within 1 mm. Thus the deformation characteristic is at the same level. However, when the proportion of recycled ballast is no less than 30%, it has significant influences on shear dilatancy. The data was increased by more than 20% and even by 70% for the pure recycled ballast, compared with fresh ballast. In addition, with the normal stress increasing, the displacements at the peak shear force decrease for the specimen with the same mixing proportion. Moreover, it appears that the higher

proportion of fresh ballast used, the lower shear dilatancy is observed. It demonstrates that the addition of fresh ballast can reduce ballast shear dilatancy.

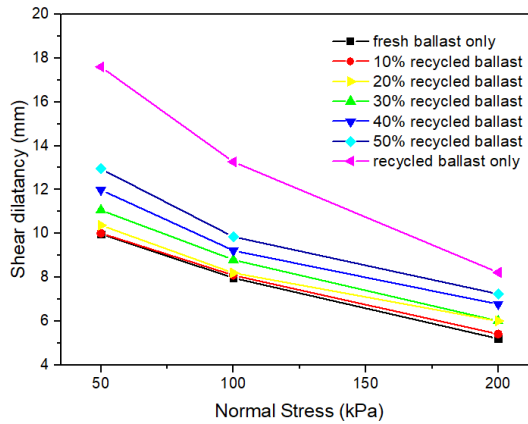


Figure 4-6. Shear dilatancy

4. DEM simulation

As a conventional test, the direct shear test is widely applied for characterising the mechanical properties of granular materials [33-36]. However, the experimental tests can only obtain the macroscopic behaviour of ballast, and the interlock of particles cannot be observed or recorded. The discrete element method (DEM) has been widely used to simulate granular materials. In this method, the discrete nature of ballast particles can be simulated accurately by providing an insight into the mechanical characteristics. Thus, the contact number, contact force distributions, etc., which are difficult to measure in the laboratory, can be obtained. In this paper, DEM simulations are carried out with PFC3D corresponding to the experimental test.

4.1 Ballast particles

Particle shape is one important factor influencing the ballast characteristics in the DEM stimulation [37-39]. To generate the irregular particles, Tutumluer et al. [40] employed the BLOCKS3D in deformation analysis, and Ngo et al. [41-42] used non-overlapping spheres to present ballast particles in dynamic analysis and overlapping spheres in direct shear simulations. All of them stressed the importance of ballast particle shape.

Therefore, this research used 3-D scanning based on laser equipment for shape obtaining. One ballast particle is placed on a white pedestal with black dots and then scanned by the laser lights. The white pedestal rotates slowly to help to get a whole particle vision. The point cloud data of the ballast surface were obtained in this stage. Then, according to the point data, a closed curve surface of scanned ballast was built. The precision of this curve surface is related to the accuracy of scanning devices. A very close morphology can be obtained and saved with a laser scanner as a shape file [43].

In this study, 50 fresh ballast and 50 recycled ballast particles were selected randomly, afterwards, scanned by the hand-held laser scanner (Handy Scan 700TM) with an accuracy of 0.030 mm. the scanning process is shown in Figure 4-7(a). Figure 4-7(b) and (c) show fresh and recycled ballast shapes. Further, those shape files are imported in PFC3D as a template to generate ballast particles.

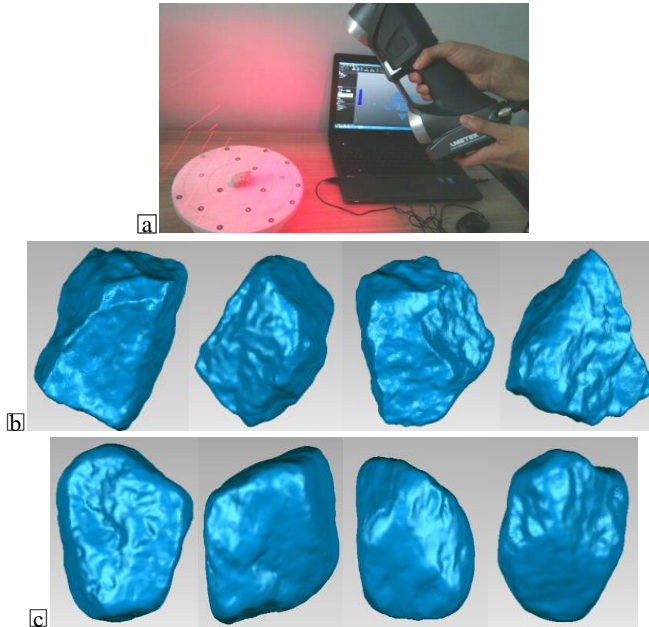


Figure 4-7. 3D scanning setup: a) The hand-held laser scanner, b) Fresh ballast, c) Recycled ballast

In the present method, a clump element in PFC can generate an irregular shape. After importing the template of a real shape of ballast, the volume of that is filled optimally with overlapping spheres of different sizes, and those spheres are bonded as a whole particle. When the number of spheres inside the clump is enough, it can accurately present the shape of ballast particles. However, such a clump could hardly be usable in a DEM simulation as it would require a huge amount of calculation time [39]. Therefore, different settings need to be included in the template to intentionally simplify the particle shape and limit the number of spheres for one clump, finally reducing the computational time.

In the process of clump generation in PFC3D, two main parameters are used, i.e. the Ratio and the Distance [44]. The Ratio corresponds to the radius of the smallest to largest spheres kept in a clump with a value of 0 to 1. Figure 4-8 illustrates the simplified definition of the Ratio in 2D, where the square is a template for clump generation, and the disks are basic elements. With the Ratio increase, the template is filled with more disks to reach a similar filling status in a corner, but the more disks are used, the more contacts are generated, thus causing a reduction in calculation efficiency.

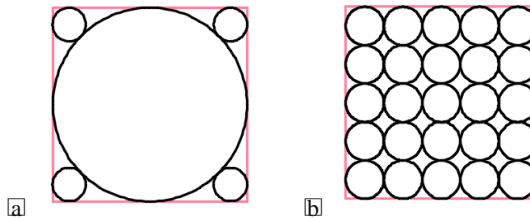


Figure 4-8. Simplified definition of the Ratio: a) Ratio=0.2, b) Ratio=1

The Distance corresponds to an angular measure of smoothness which can be used to present the angularity changes between deteriorated and fresh ballast. Its value varies from 0 to 180, corresponding to the angle of the tangent line in the point of intersection, which is simplified in 2D and illustrated in Figure 4-9.

As the definition, the Distance is a parameter which can control the filling status of the border. With the value decrease, the blank in the border (the shadow in Figure 4-9) is smaller. A small Distance value leads to a higher calculation cost by more disks filled in the template. It should be noted that those 2 parameters cannot be applied severally. For example, the Distance in Figure 4-8 is 0, and the Ratio in Figure 4-9(a) and (b) is 1. Besides, in a ballast template, the border is roughness with surface texture, and the corner is irregular with angularity.

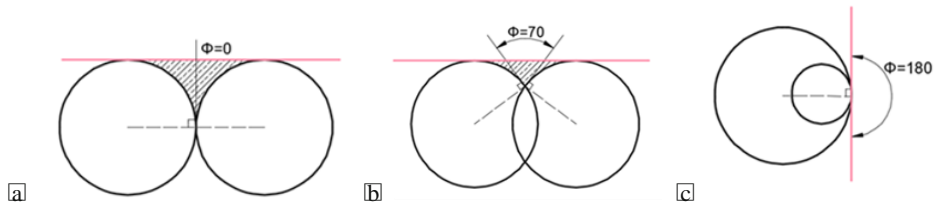
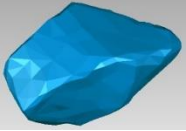


Figure 4-9. Simplified definition of the Distance: a) Distance=0, b) Distance=70, c) Distance=180

Furthermore, the combination of Distance and Ratio is analysed, aiming to generate reasonable ballast particles. As shown in Table 4-4, several ballast particles with different parameters are created using the same scanned ballast template. From those outputs, the Ratio less than 0.3 and a Distance bigger than 120 can be regarded as reasonable parameters to present ballast shape.

Table 4-4 The combination of Distance and Ratio

	Ratio 0.1	Ratio 0.3	Ratio 0.6
Distance 60			
Distance 90			
Distance 120			
Distance 150			

In addition, image analysis as an advanced method that can determine the degradation status of ballast [5] is employed in this part. To qualify the influence of the parameters, two clumps are generated with one template, where the clump in Figure 4-10 (a) is set with more angularity with Distance 120, Ratio 0.3 to present fresh ballast, and the clump in Figure 4-10 (b) is smoother with Distance 150, Ratio 0.3 to present recycled ballast. The border of those 2 ballast models is exported in 2D image as Figure 4-10 (c) and (d) for roundness calculation.

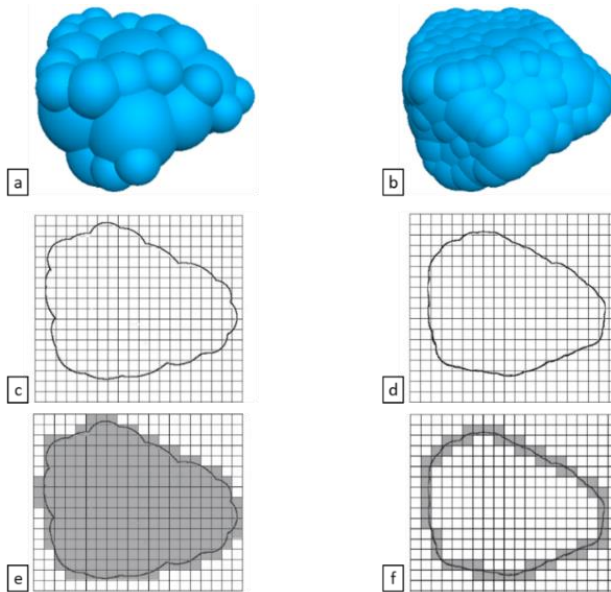


Figure 4-10. Ballast particle models in DEM simulations: (a) Fresh ballast, (b) Recycled ballast, (c) The border of fresh ballast, (d) The border of recycled ballast, (e) The sketch map of A , (f) The sketch map of p

By the method of Janoo et al [45], the roundness can be calculated with the following Eq. 2

$$R_n = \frac{4\pi A}{p^2} \quad \text{Eq. 2}$$

In Eq.2, R_n is the Roundness Index (RI), and the value for a perfect circle is 1, which means the most rounded shape. With the value closer to 1 the shape is rounder and less angular. A is the area of the particle projection corresponding to the number of pixels (0.2639mm/pixel) within the border, as shown in Figure 4-10(e). And, p is the perimeter of the particle corresponding to the number of pixels surrounding the ballast, as shown in Figure 4-10 (f). According to Eq.2, the RI of fresh ballast is 0.6737, and the value for recycled ballast is 0.7729. In this regard, the difference between those two kinds of ballast can be presented.

Another characteristic of deteriorated and fresh ballast is that different frictional coefficient is used to present the wear of the surface texture. The linear contact model is selected for ballast particles due to its cohesion-less physics [46], and the mechanical parameters of the ballast particles and the shear box in PFC3D are summarised in Table 4-5, which are referred from former studies [47-48] and verified corresponding to laboratory tests. The influence of ballast breakage and abrasion in the

direct shear test is negligible. Thus, breakage was not included in the simulation to enhance the efficiency of the calculation.

Table 4-5 Parameters of linear contact model in simulations

Parameters	Fresh Ballast	recycled ballast	Shear box
Distance	120	150	-
Ratio	0.3	0.3	-
Tangential stiffness(N/m)	$1e^8$	$1e^8$	$6e^8$
Normal stiffness(N/m)	$1e^8$	$1e^8$	$6e^8$
Friction coefficient	0.5	0.47	0.2
Mass density(kg/m ³)		2630	
Damping coefficient		0.7	

4.2 Direct shear test model

The modelled ballast particles are filled in the shear box model (wall element) with a porosity of 0.3 by the method of particle replacement and radius expansion (McDowell et al. [49]). In the first stage, balls were filled in the shear box with the required PSD and cycled to a relevant dense state using self-gravity. Then record the radius and the address of the sphere centre, and using a clump, replace those balls with the recorded information. After this procedure, the clump in the shear box has reached a dense state. However, the contact forces between clumps are not balanced, for this radius expanding method was used to adjust the size of the clump. Specifically, a random, very small expansion coefficient such as 0.9971 or 1.0043 was applied to the clump radius, thus modifying the contact status between particles, finally reaching the stabilised state. During this procedure, the radius is expanded slightly, and the PSD has a slight change, but it still stays at the setting curve with the unbalance force well-settled.

The direct shear was achieved by moving the lower boundary walls with a constant velocity of 6 mm/s until a total lateral displacement of 60 mm (10% strain). Meanwhile, constant normal stress was provided by the servo system. The DEM model is shown in Figure 4-11, where the different colours correspond to various particle sizes.

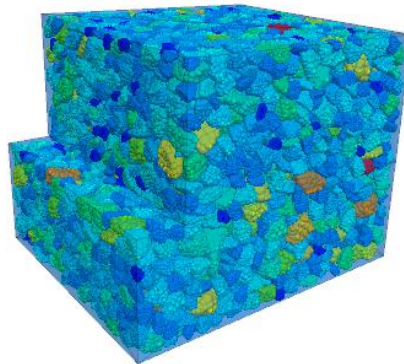


Figure 4-11 The DEM numerical model of ballast direct shear test

4.3 Verification

The strain-stress curve of simulations and laboratory test of pure fresh ballast, 50% recycled ballast and pure recycled ballast are shown in Figure 5-12, where the peak data and changing trend is highly matched. Therefore, the simulation method used in this paper can be regarded as valid and reliable.

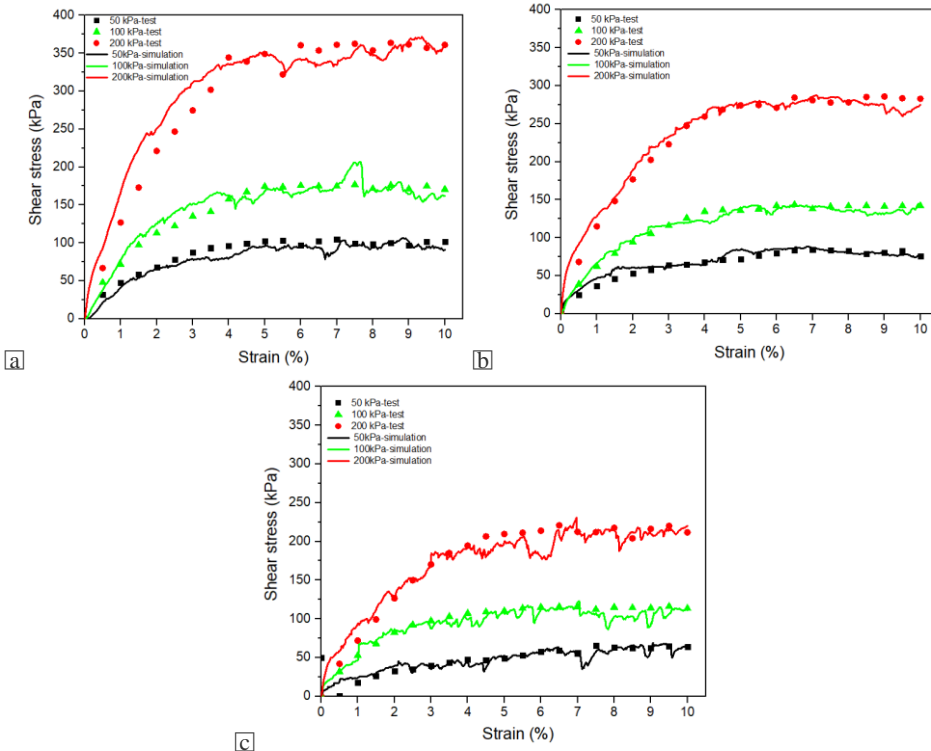


Figure 4-12. Comparison of the simulation and the laboratory test results: a) Fresh ballast only, b) 50% recycled ballast, c) Recycled ballast only

5. Results of numerical simulation

Figure 4-13 shows the average coordination number (CN) of ballasts with different proportions of recycled ballast subjected to different normal stresses (50, 100 and 200kPa). Results present that the CN increased with the normal stress, and it increased with the proportion of fresh ballast due to tighter interlock between fresh ballast. Compared with fresh ballast only, the CN of recycled ballast only has a 1.1-1.7 reduction, which also means that recycled ballast has lower capacity and stability. While, The CN for 10%-30% recycled ballast is similar to fresh ballast, especially under high normal stress. The maximum contact force is shown in Figure 5-14, fresh ballast only presents a higher contact force than mixed with recycled ballast during the shear procedure, and a smaller maximum displacement was observed, which is shown in Figure 4-15. The coarser surface texture of fresh ballast contributes more friction thus making particles harder to rotate and displace. Based on these results, it can be concluded that the contact characteristics of fresh ballast are an advantage over recycled ballast, and fresh ballast can bear higher stress and generate smaller deformation. With the presence of recycled,

those data are decreased, but with the percentage of 10%-30% recycled ballast, the reduction is insignificant.

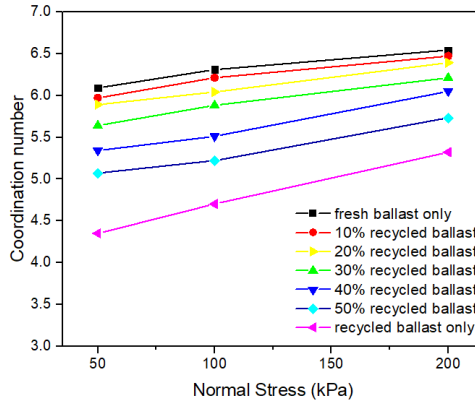


Figure 4-13 Average coordination number

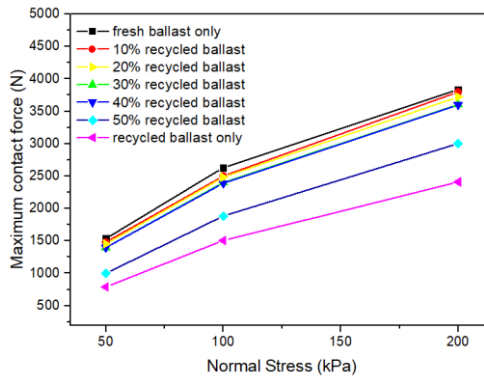


Figure 4-14 Maximum contact force

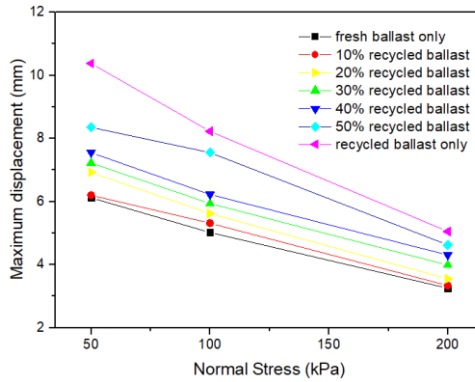


Figure 4-15 Maximum displacement

6. Conclusion

In this paper, the fresh-recycled ballast mixture was analysed by a series of experimental direct shear tests and numerical simulations based on the DEM, with the aim of investigating the mechanical characteristics of recycled ballast. The DEM simulations were in good agreement with laboratory results, and the conclusions were given as follows:

1. Due to the angularity loss and surface texture reduction, the interlock between recycled ballast is weaker than fresh ballast. With an increase in the mixing proportion of recycled ballast, the mixture shear strength and friction angle are decreased, and shear dilatancy is increased. Especially for the mixture of more than 50% recycled ballast, those changes are significant. However, when the proportion of recycled ballast is smaller than 30%, the reduction in shear stress is negligible.
2. In the numerical simulations, clump was used to present ballast particles based on the 3D scanning method, and different settings of the Ratio and Distance in ballast generation can distinguish the fresh ballast and recycled ballast, making the result more reliable. Both the coordination number and maximum contact force have a downward trend when the recycled ballast volume ratio increases, resulting in an increase in the maximum displacement of ballast particles.
3. Recycled ballast behaves with a lower level of capacity and stability than fresh ballast. However, it should be highly noted that adding recycled ballast with less than 30% does not influence the total performance. Thus, adding recycled ballast to fresh ballast could be a method for reusing the deteriorated ballast bed under the criterion ratio. Also, this result can be a guide for maintenance which uses fresh ballast to reinforce recycled ballast.

Acknowledgments

The paper was supported by the Natural Science Foundation of China (Grant No. 51578051) and China Scholarship Council.

References

- [1] Hudson A, Watson G, Le Pen L, et al. Remediation of Mud Pumping on a Ballast Railway Track. *Procedia Engineering*. 2016, 143: 1043-1050.
- [2] Selig E T, Waters J M. *Track geotechnology and substructure management*. Thomas Telford, 1994.
- [3] D Angelo G, Thom N, Presti D L. Bitumen stabilized ballast: A potential solution for railway track-bed. *Construction and Building Materials*. 2016, 124: 118-126.
- [4] Wang Z, Jing G, Yu Q, et al. Analysis of ballast direct shear tests by discrete element method under different normal stress. *Measurement*. 2015, 63: 17-24.
- [5] Yunlong Guo, Valeri Markine, Xuehui Zhang, Weile Qiang, Guoqing Jing. Image analysis for morphology, rheology and degradation study of railway ballast: A review. *Transportation Geotechnics*. 2019(18):173-211.
- [6] Indraratna B, Tennakoon N C, Nimbalkar S S, et al. Behaviour of clay-fouled ballast under drained triaxial testing. *Geotechnique: international journal of soil mechanics*. 2013, 5(63): 410-419.
- [7] Indraratna B, Nimbalkar S, Rujikiatkamjorn C. Enhancement of rail track performance through utilisation of geosynthetic inclusions. *Geotech. Eng. Jl. of the SEAGS & AGSSEA*. 2014, 45(1): 17-27.
- [8] Xuecheng Bian, Wei Li, Jing Hu, Hongming Liu, Xiang Duan, Yunmin Chen. Geodynamics of high-speed railway. *Transportation Geotechnics*. 2018(17):69-76.
- [9] N. Jimenez-Redondo, N. Bosso, L. Zeni, A. Minardo, F. Schubert, F. Heinicke, A. Simroth, Automated and cost effective maintenance for railway (acem-rail), *Transport Res. Arena 48 (2012) 1058–1067*.
- [10] UIC- International Union of railways 2015. *Rail Transport and Environment Facts and Figures*.
- [11] Ebrahimi A, Tinjum J M, Edil T B. Deformational behaviour of fouled railway ballast. *Canadian Geotechnical Journal*. 2014, 52(3): 344-355.
- [12] Indraratna B, Salim W. Deformation and degradation mechanics of recycled ballast stabilised with geosynthetics. *Soils and Foundations*. 2003, 43(4): 35-46.
- [13] Nayoma Tennakoon, Indraratna Buddhima, Cholachat Rujikiatkamjorn. The Role of Ballast-Fouling Characteristics on the Drainage Capacity of Rail Substructure. *Geotechnical Testing Journal*, 2012(35): 629-640
- [14] Qian Y , Boler H , Moaveni M , et al. Characterizing Ballast Degradation Through Los Angeles Abrasion Test and Image Analysis. *Transportation Research Record: Journal of the Transportation Research Board*, 2014, 2448(2448):142-151.
- [15] Yunlong Guo, Valeri Markine, Song J, et al. Ballast degradation: Effect of particle size and shape using Los Angeles Abrasion test and image analysis. *Construction & Building Materials*, 2018, 169:414-424.
- [16] M. Sol-Sánchez., G. D'Angelo. Review of the design and maintenance technologies used to decelerate the deterioration of ballast railway tracks. *Construction and Building Materials*, 2017, 157:402-415.
- [17] Atalar C, Das B M , Shin E C , et al. Settlement of geogrid-reinforced railroad bed due to cyclic load. *Proc.int.conf.on Soil Mech. & Geothch.engrg*, 2001(3):2045-2048.
- [18] Egana J I , Vinolas J , Seco M . Investigation of the influence of rail pad stiffness on rail corrugation on a transit system. *Wear*, 2006, 261(2):216-224.
- [19] Jayasuriya C, Indraratna B, Trung Ngoc Ngo. Experimental study to examine the role of under sleeper pads for improved performance of ballast under cyclic loading. *Transportation Geotechnics*. 2019 (19): 61-73.
- [20] Kaewunruen S , Remennikov A . An Experimental Evaluation of the Attenuation Effect of Rail Pad on Flexural Behaviour of Railway Concrete Sleeper under Severe Impact Loads. *Australasian Structural Engineering Conference: Engaging with Structural Engineering*. Meeting Planners, 2008.
- [21] Y. Guo, V. Markine, W. Qiang, H. Zhang, G. Jing, Effects of crumb rubber size and percentage on degradation reduction of railway ballast, *Construction and Building Materials* 212 (2019) 210-224.

- [22] M. Sol-Sánchez, N. H. Thom, F. Moreno-Navarro, et al. A study into the use of crumb rubber in railway ballast[J]. *Construction and Building Materials*, 2015, 75:19-24.
- [23] PK Woodward, Kennedy J, Medero GM, Banimahd M. Application of in situ polyurethane geocomposite beams to improve the passive shoulder resistance of railway track. *Proceedings of the Institution of Mechanical Engineers Part F Journal of Rail & Rapid Transit*. 2011;3(226): 294-304.
- [24] Kruglikov AA, Yavna VA, Ermolov YM, Kochur AG, Khakiev ZB. Strengthening of the railway ballast section shoulder with two-component polymeric binders. *Transportation Geotechnics*. 2017(11): 133-43.
- [25] Lakušić S, Ahac M, Haladin I. Track stability using ballast bonding method. The 10th Slovenian Road & Transportation Congress. Portoroz, Slovenia 2010.
- [26] Indraratna B, Shahin M A, Salim W. Use of geosynthetics for stabilizing recycled ballast in railway track substructures. *Proceedings of NAGS2005/GRI 19 Cooperative Conference*. 2005: 1-15.
- [27] Indraratna B, Nimbalkar S, Christie D. The performance of rail track incorporating the effects of ballast breakage, confining pressure and geosynthetic reinforcement. *Geotechnical engineering for transportation projects*. 2009: 617-626.
- [28] Indraratna B, Nimbalkar S, Christie D, et al. Field assessment of the performance of a ballast rail track with and without geosynthetics. *Journal of Geotechnical and Geoenvironmental Engineering*. 2010, 136(7): 907-917.
- [29] TB/T2140-2008. Railway ballast. China, Ministry of Railways, 2008.
- [30] British-Adopted European Standard. Tests for mechanical and physical properties of aggregates. Methods for the determination of resistance to fragmentation. BS EN 1097-2:2010
- [31] ASTM. Standard Test Method for Resistance to Degradation of Small-Size Coarse Aggregate by Abrasion and Impact in the Los Angeles Machine, ASTM Designation C-131-01. Philadelphia American Society for Testing Materials, 2006.
- [32] Huang H, Tutumluer E, Dombrow W. Laboratory Characterization of Fouled Railroad Ballast Behaviour. *Transportation Research Record Journal of the Transportation Research Board*, 2009, 2117(2117):93-101.
- [33] Simoni A, Housley G T. The direct shear strength and dilatancy of sand-gravel mixtures. *Geotechnical & Geological Engineering*. 2006, 24(3): 523.
- [34] Suhr B, Six K. On the effect of stress dependent interparticle friction in direct shear tests. *Powder Technology*. 2016, 294: 211-220.
- [35] Infante D J U, Martinez G M A, Arrua P A, et al. Shear Strength Behaviour of Different Geosynthetic Reinforced Soil Structure from Direct Shear Test. *International Journal of Geosynthetics and Ground Engineering*. 2016, 2(2): 1-16.
- [36] Ngo N T, Indraratna B, Rujikiatkamjorn C. Study on the interface behaviour of a geosynthetics-reinforced fouled ballast using the discrete element method. 2016, 730-738.
- [37] Lu M, McDowell G R. The importance of modelling ballast particle shape in the discrete element method. *Granular matter*. 2007, 9(1-2): 69.
- [38] Shin H, Santamarina J C. Role of particle angularity on the mechanical behaviour of granular mixtures. *Journal of Geotechnical and Geoenvironmental Engineering*. 2012, 139(2): 353-355.
- [39] Ferrellec J, McDowell G R. A method to model realistic particle shape and inertia in DEM. *Granular Matter*. 2010, 12(5): 459-467.
- [40] Tutumluer, E., Qian, Y., Hashash, Y.M.A., Ghaboussi, J. and Davis, D.D. Discrete element modelling of ballasted track deformation behaviour. *International Journal of Rail Transportation*, 2013,1(1-2), pp: 57-73.
- [41] Ngo, N.T., B. Indraratna, and C. Rujikiatkamjorn, Simulation Ballasted Track Behavior: Numerical Treatment and Field Application. *ASCE-International Journal of Geomechanics*, 2017,17(6): p. 04016130.
- [42] Ngo, N.T., Indraratna, B. and Rujikiatkamjorn, C. DEM simulation of the behaviour of geogrid stabilised ballast fouled with coal." *Computers and Geotechnics*, 2014,55: 224-231.

- [43] Zhang X , Zhao C , Zhai W . DEM Analysis of Ballast Breakage Under Train Loads and Its Effect on Mechanical Behaviour of Railway Track. International Conference on Discrete Element Methods. Springer Singapore, 2016.
- [44] PFC3D User's Manual (Version 5.0). Minnesota Itasca Consulting Group Inc, 2015.
- [45] V. Janoo. Quantification of shape, angularity, and surface texture of base course materials. Hanover (NH): Cold Regions Research and Engineering Lab; 1998.
- [46] J. Liu, P. Wang, J. Liu. Macro-and micro-mechanical characteristics of crushed rock aggregate subjected to direct shearing. Transportation Geotechnics. 2015, 2: 10-19.
- [47] Lim W L, Mcdowell G R. Discrete element modelling of railway ballast. Granular Matter. 2005, 7(1): 19-29.
- [48] Ferrellec J, Mcdowell G. Modelling realistic shape and particle inertia in DEM. Geotechnique. 2010, 60(3): 227-232.
- [49] McDowell, G.R., Harireche, O., Konietzky, H., Brown, S.F. and Thom, N.H. Discrete element modelling of geogrid-reinforced aggregates. Proceedings of the ICE - Geotechnical Engineering 2006,159(1): 35-48.

Paper V

Analysis of furnace slag in railway sub-ballast based on experimental tests and DEM simulations

Wenli Jia, V.L Markine, Guoqing Jing

Published in Construction and building materials. 2021 288(1):123114

Abstract

Under the high requirement of ballast materials and the frequent maintenance of high-speed and heavy-haul railways, the maintenance cost and material consumption become an important problem. Several methods are used to increase the stability and service life of railway structures. Also, using recycled materials in ballast bed construction can be a way for sustainable railway development. Thus, the idea of using furnace slag as the sub-ballast was put forward in this research. To qualify the performance of furnace slag, a series of tests were carried out, including the single particle crushing test, direct shear test, and box stiffness test, and the crushed stone, which is the traditional sub-ballast material, was used as a comparison. In addition, the test and numerical simulation on box stiffness were carried out. Results show that furnace slag has less possibility of breakage and abrasion. Its shear resistance is 16.46% to 19.48% higher and 20.44% to 26.04% decrease in shear dilatancy. However, the stiffness of single particles shows not much difference. The box stiffness test and simulation indicated that furnace slag has a higher capacity and better elasticity. Based on that, this research provides the feasibility of using furnace slag as the sub-ballast, and it contributes to an environment-friendly way of railway construction.

Keyword: Furnace slag; Sub-ballast; Stiffness tests; Direct shear test; DEM

1. Introduction

The ballasted track bed consists of two granular layers, the ballast layer and the sub-ballast layer, and it is normally constructed of crushed stone. The function of the ballast bed is to provide a bearing for rails, resistance to sleepers, keep the geometry of the track, and be responsible for draining water away from the track and elastics of the tracks. With the development of the railway, the axle load and the speed of trains increase largely, putting a higher requirement for the function of ballasted track bed [1]. To keep the safety and stability of railway, more and more frequent maintenance is needed, such as tamping and ballast renewal. As a consequence, the consumption of materials and labour during those maintenance processes causes great economic costs and environmental problems. Prolonging the life span of ballasted tracks by reinforcement method and sustainable railway systems using recycled materials are needed to be studied.

In one aspect, several methods are used to reinforce the ballast layer. For example, the use of geogrid increase the resistance between ballast and decrease the settlement [2], and it can be used not only in the ballast layer but also in the sub-ballast [3, 4]. Geocell has a similar function to geogrid in reinforcement [5]. Elastic mat or pad (ballast mat, rail pad, and under sleeper pad) can increase the elasticity, decrease the vibration, and enlarge the area of force distribution, thus decreasing the process of ballast degradation [6-8]. Polyurethane can bond ballast in the contact point, thus increasing the capacity and keeping the drainage ability at the same time [9, 10]. Those reinforcement methods all show their effect and have been proved in practice.

In another aspect, using recycled materials is also a good way for sustainable development. For example, the rubber from tires can be a resource for rubber mat or pad manufacture [11], and directly adding crushed rubber into the ballast layer also can decrease the ballast degradation [12-14]. Research on degraded ballast shows that it can be reused by mixing it with fresh ballast [15]. Another material is slag, which is a byproduct of iron production (around 12% to 16% of slag by weight is generated [16]). Based on this huge amount and the similar properties with crushed stone, slag has been used in construction, also drawing the attention of railway area.

Slag can be divided into furnace slag and steel slag, according to the different processes in iron steel making. Furnace slag is a byproduct in the first stage when using iron ore to produce pig iron, and steel slag is a byproduct when using iron to produce steel. Among them, steel slag can replace granular materials in normal concrete manufacture [17-19], asphalt concrete [20] and pavement [21]. With similar properties to stone and even better prosperities in interlock performance, higher density (3100-3500kg/m³), and high resistance to abrasion [22, 23], steel slag also can be used in the ballast layer. Delgado et al. [16] studied the mechanical performance of inert steel slag ballast by comparing it with granite ballast (both of them are scaled with 1:2.5 size). Results show that slag has higher shear strength and lower deformation in long-term behaviour. Esmaeili et al. [22] did the comparing tests on lateral resistance between steel slag and limestone ballast. Results show a 27% increase can be observed by using steel slag. Morata et al. [24] employed steel slag as a track bed layer, and results show it has an improvement in track stiffness, track stability, bearing capacity (strength), and durability. Although that research shows the good performance of steel slag in the railway system, a vital problem of electrical conductivity exists, because of the chemical composition of steel slag [25]. This property will cause communication problems for railway safety.

Another kind is furnace slag with a particle size of 10-30mm. It has a smaller density than steel slag, which is around 2000kg/m³, and its strength is also lower than steel slag. With those properties, furnace slag is considered not a proper material for the ballast layer. But in another way, it can be a resource for sub-ballast.

Sub-ballast is a granular layer that provides bearing to the ballast layer, and as a filter to prevent ballast direct contact with soil foundation or soil fill in ballast layer under cyclic loading [26, 27].

The requirement of physical properties for sub-ballast is a lot lower than ballast, i.e. the Los Angeles Abrasion index (LAA), compression strength, the Particle size distribution is in a range from 0.075mm to 45mm, and it has no electrical conductivity requirement. Indraratna et al. [28] studied several parameters (the permeability, stress-strain behaviour, strain energy absorption, particle breakage, swell pressure, and axial displacement under cyclic loading) of the mixture of furnace slag, coal wash, and rubber crumbs working as sub-ballast. The results of Indraratna et al. [28] show that by controlling the ratio of different materials, the mixture can reach higher performance than the traditional sub-ballast.

Based on the research mentioned above, it is possible to use furnace slag as the sub-ballast. Thus, aiming to find out the behaviour of furnace slag for sub-ballast, this study conducted a series of tests and simulations, and a comparison between crushed stones was analysed. Direct shear tests were employed to show the shear performance, Single Particle Crushing Tests (SPCT) and LAA tests were employed to show the strength and the resistance to abrasion, the image analysis based on 3D scanning was used to show the shape property, and simulations based on DEM was used to show the shear behaviour in mesoscopic.

2. Material specification

The furnace slag used in this research is shown in Figure 5-1(a). Its density is 2250kg/m^3 . With the function of the filter, the particle size of the sub-ballast needs to stay in a range of Particle Size Distribution (PSD), which is shown in Figure 5-2. So, the slag was sieved and remixed, and the PSD curve is also shown in Figure 5-2. In comparison, the traditional sub-ballast is granite material, i.e. the crushed stone, and it is showed in Figure 5-1(b), with the density of 2800kg/m^3 , and it is saved and mixed by the same PSD with furnace slag.

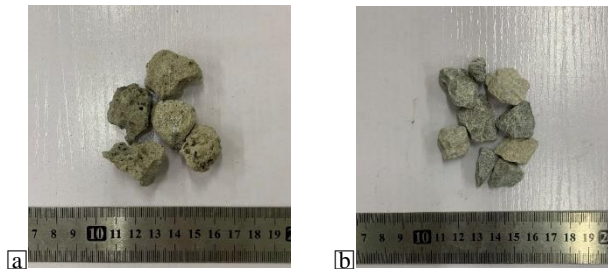


Figure 5-1. Material for tests: (a) Furnace slag, (b) Crushed stone

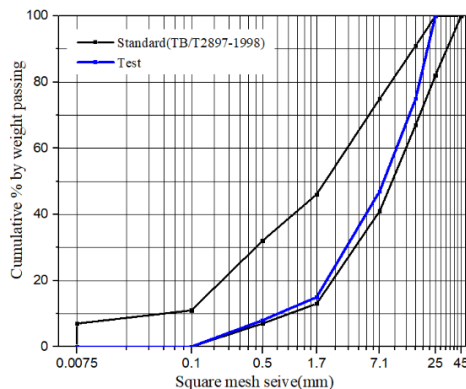


Figure 5-2. Particle size distribution for sub-ballast

2.1 Single particle crushing strength

During the daily operation of the railway, particle breakage is a key process contributing to degradation; thus, SPCT was employed to find out the crushing property of a single particle, and the test device is shown in Figure 5-3. During this test, the sample was crushed by stress controlling method, i.e. after located the slag, the loading plate was moving with a certain force to time speed (0.1kN/s) until the particle breakage happened. The stress-displacement curve was supervised by the auto-controlling system. During the crushing process, the breakage is initiated with the fracture by tensile failure, and it can be described in Eq.1 [29]. Due to the influence of particle size, 3 different size (5mm, 10mm and 20mm) was selected, and each size included 5 particles.

$$\sigma = F/d^2 \quad \text{Eq.1}$$

Where, d is the diameter of particle which is also related to the distance of loading plate and the platform, F is the compressive force, and σ is the tensile stress

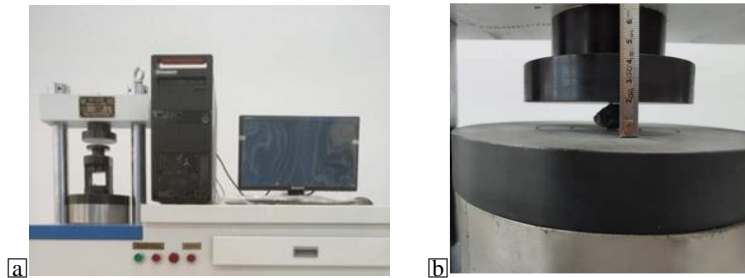


Figure 5-3. Single particle crushing test: (a) Test device, (b) Crushing plate

The peak compressive force, sorted by different particle sizes, is shown in Figure 5-4(a), and the tensile strength, calculated refer to Eq.1, is shown in Figure 5-4(b). Because the crushing test is not only related to particle size but also the loading point, loading direction, and particle geometry. The peak compressive force and the tensile strength are shown with a range where 5 particles for each size are included. Especially for furnace slag, the inner void is in an inhomogeneous distribution. Thus the test results show a relatively wide range. In Figure 5-4, it is obvious that the strength of furnace slag is higher than the traditional sub-ballast. The value increases by 39%, 20%, and 26% for 5mm, 10mm, and 20mm, respectively. For both furnace slag and crushed stone, when the particle size increase, the peak compressive force is increased, but the tensile strength is decreased, thus proving that the bigger particle is more likely to break.

The crushing process can be explained by the displacement and force curves. In Figure 5-5, the curve of 6 particles was drawn as a representative, whose peak compressive force is approximate to the mean value. According to the curve, the crushing process began when the compressive force appeared. The first stage is the initial contact of the loading plate and particle. It shows a slow increase of the compressive force, and some fluctuations were observed because of the angularity breakage. Those fluctuations are more obvious in the test for furnace slag due to the inner void. Then the second stage shows a linear relationship between the deformation and the force. After the compressive force reaches a peak value, the curve shows a linear decrease, indicating the final failure.

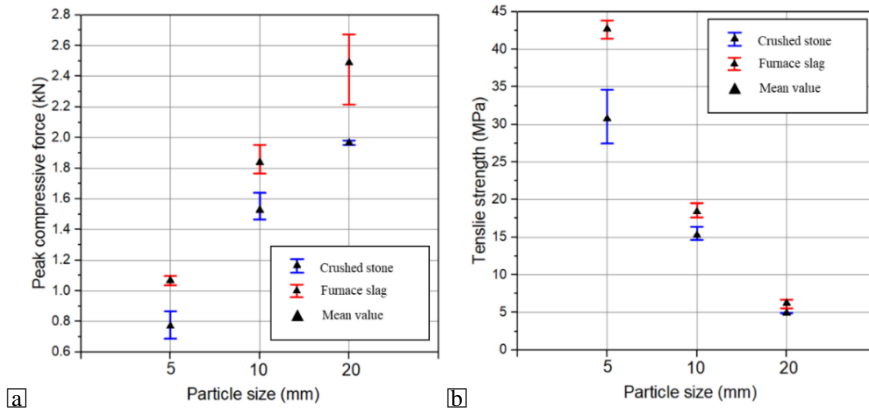


Figure 5-4 Data of SPCT (a) Compressive force, (b) Tensile strength

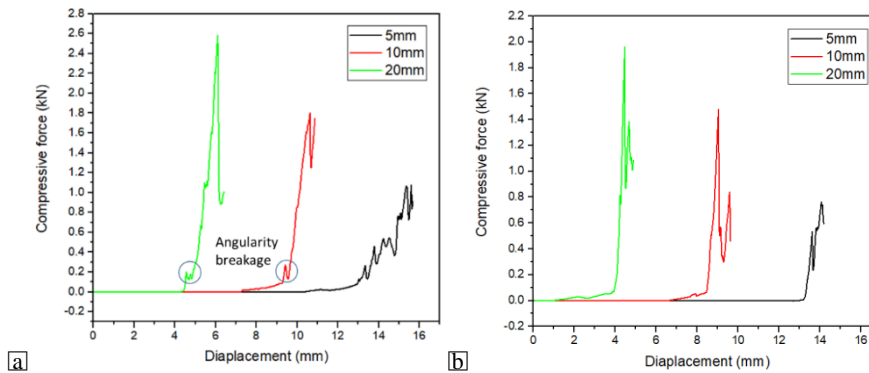


Figure 5-5 Displacement-compressive force curve: (a) Furnace slag, (b) Crushed stone

Except for 5mm particles, for which the existence of fluctuation affects the analysis, the second stage of the crushing can be regarded as an elastic shortening process, and it presents the stiffness of the material. By calculating the slope, the stiffness of 10mm furnace slag is 1.78e6N/m to 3.75e6N/m, 20mm furnace slag is 2.14e6N/m to 2.52e6N/m, and the value for 10 crushed stone is 2.11e6N/m to 3.93e6N/m, 20mm crushed stone is 1.42e6N/m to 2.25N/m, as shown in Table 5-1. However, the results are in a relatively big range, it can be seen that furnace slag has a higher stiffness than crushed stone.

Table 5-1. Particle stiffness according to SPCT (*e6N/m)

Material	Size	Particle 1	Particle 2	Particle 3	Particle 4	Particle 5	Average
Furnace slag	10mm	3.48	2.56	3.18	3.75	1.78	2.95
	20mm	2.00	2.52	2.11	2.14	2.42	2.23
Crushed stone	10mm	3.24	2.29	2.11	3.93	2.77	2.87
	20mm	2.19	1.42	2.25	1.55	2.01	1.88

2.2 Resistance to abrasion

In addition, the abrasion resistance is shown by LAA tests, as shown in Figure 5-6. For sub-ballast, the test sample should be departed into 2 parts: 10-16mm particle 2500g, and 16-20mm particle 2500g. 8 iron balls, with a total weight of $3330 \pm 20\text{g}$, are mixed in the chamber. The test is conducted with the chamber rotating 500 rounds ($31 \sim 33\text{r/min}$) [30]. During this process, the particle is facing impaction and abrasion, and after the tests, the aggregate should be re-sieved and cleaned, weighted, and calculated by Eq.2.

$$LAA = \frac{G_1 - G_2}{G_1} \times 100\% \quad \text{Eq.2}$$



Figure 5-6 Los Angeles Abrasion: (a) Test apparatus, (b) Sample with iron ball inside the chamber

The Los Angeles abrasion index (LAA, %) is defined by Eq.2, where G_1 is the total weight of the particle before abrasion (g), and G_2 is the weight of particle size bigger than 1.7mm after abrasion (g). The test value for furnace slag is 26.04%, and for crushed stone is 31.28%. However, in the SPCT, furnace slag showed angularity breakage in the initial stage, which may increase the LAA, and the abrasion resistance is higher than the traditional sub-ballast. Overall, the SPCT and LAA show that furnace slag has better performance both on the resistance to breakage and abrasion.

3. Experimental tests

3.1 Direct shear test

The direct shear test apparatus is shown in Figure 5-7. Size scale in a direct shear test is an important factor, which will influence the accuracy of the result, Jewell et al. [31] suggested that the length of the shear box compared with the D_{50} should be larger than 50, Wang et al. [32] suggest that the size of the shear box should be at least 60 times larger than particle size for sand, and the standard ASTM D 3080-90 [33] suggested that the values should be larger than 10. In this research, the apparatus consists of a lower box and an upper box, with both sizes of $300\text{mm} \times 300\text{mm} \times 100\text{mm}$. The D_{50} of the sample with the PSD (as Figure 5-2) is around 7.1mm, and the biggest particle size is around 25mm. The sample is loaded and compacted in the shear box, and a plate covering the sample is used to transmit the normal pressure. A bearing set is put on the plate to keep the loading and diminish the friction between the upper box and the servo loading jack. Then the servo system begins to work, which controls the normal stress of 50kPa 100kPa and 200kPa, corresponding to different test conditions. During the shear process, the upper box moves with a speed of 0.2mm/min until the shear strain reaches 10% (30mm shear displacement). The shear stress, strain, and dilatancy are automatically recorded by the computer.

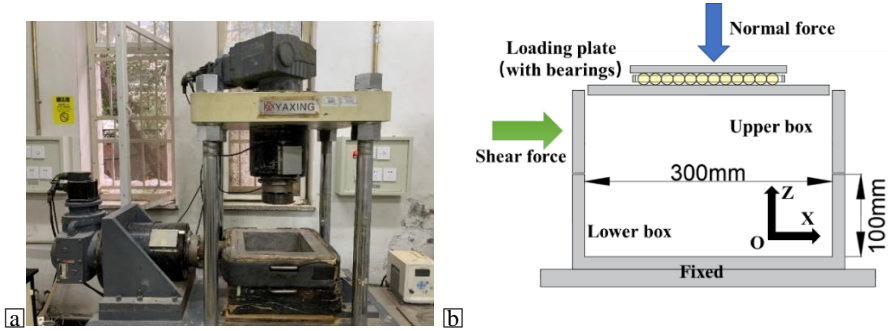


Figure 5-7 Direct shear test apparatus(a) Test apparatus, (b) Schematic diagram

Test results are shown in Figure 5-8. It should be noticed that, for furnace slag under 200kpa normal pressure, there is a drop-down that occurred around 22mm displacement due to some slide in the box. And an increase with fluctuation can be seen in the end state. However, those trends are different from others. The result is still valid because the peak force is observable. The peak shear stress of furnace slag is 83.27kPa, 140.25kPa, 245.28kPa, and for crushed stone, the peak shear stress is 71.50kPa, 117.95kPa, 205.29kPa, both of them are according to normal stress 50kPa, 100kPa, 200kPa, respectively. It can be seen that furnace slag all shows an increase compared with the traditional sub-ballast under 3 different normal stress. The increase reaches 16.46%, 18.91%, and 19.48%.

In addition, the normal stress and peak shear stress of different condition is shown in Figure 5-9(a). The linear fitting is related to 2 constants, the cohesion and the tangent of the friction angle. The use of furnace slag increases the frictional angle from 41.65 to 47.09, compared with crushed stone. The cohesion of furnace slag presents a bigger value than crushed stone, which is 30.75kPa and 27.83kPa, respectively. Since the same PSD is used for those 2 materials, the increase in friction angle and cohesion is mainly related to the particle shape and surface texture. In Figure 5-9(b), the final shear dilatancy of furnace slag is 5.99mm, 4.28mm, and 3.28mm, corresponding to the normal stress 50kPa, 100kPa, and 200kPa, and the value for crushed stone is 8.01mm, 5.80mm, and 4.12mm, respectively. The 20.44% to 26.04% decrease in dilatancy also indicates that furnace slag has better shear performance than crushed stone.

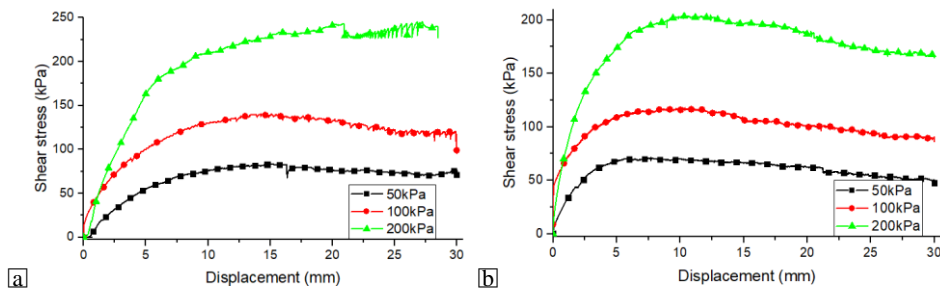


Figure 5-8 Displacement-shear stress curve: (a) Furnace slag, (b) Crushed stone

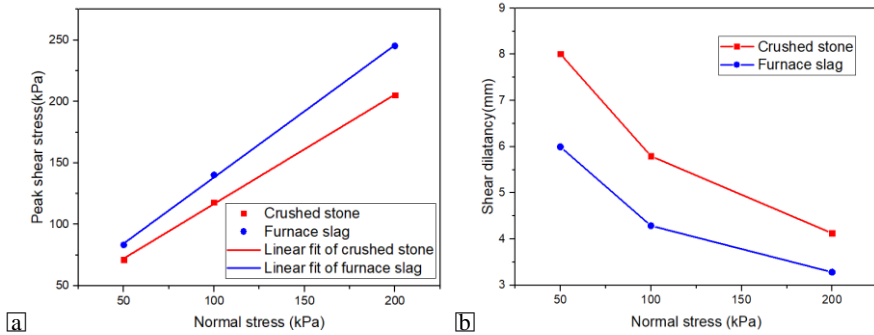


Figure 5-9 Peak shear stress and shear dilatancy: (a) Linear fitting, (b) Shear dilatancy

3.2 Stiffness tests

The stiffness tests were carried by the same device with direct shear tests (Figure 5-7), only changing the loading part with a 150mm diameter disk. The loading process for this part was realised by controlling the loading disk downward at a certain speed (0.2mm/min) which can be regarded as a quasi-static loading process, and the stop condition is when the displacement reaches 4mm. During the test, displacement and force are recorded for stiffness calculation.

Test results are shown in Figure 5-10. For furnace slag, the peak compressive force is 14.41kN (815.57kPa), and the displacement at peak force is 3.15 mm. For crushed stone, the peak compressive force is 11.89kN (673.02MPa), and the displacement at peak force is 2.06 mm. Under this test condition, the stiffness of furnace slag is 4.57e6N/m, and the value for crushed stone is 5.77e6N/m. Thus, both the capacity and elasticity of furnace slag are better than crushed stone. In addition, the numerical simulation for this test was used to analyse the contact and force distribution in the following.

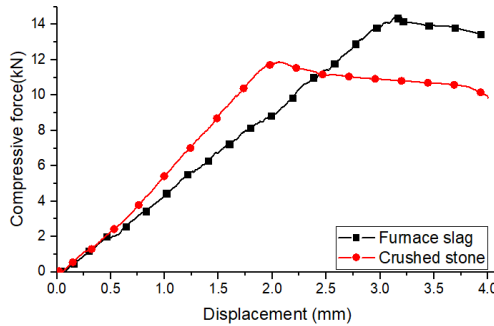


Figure 5-10 Test results for box stiffness

4. Numerical simulations

DEM is a method used to analyse the mesoscopic characteristic of aggregate materials. The coordination number, stress distribution, contact force, and displacement can be shown by this method. In this study, the simulation of the box stiffness test was carried out, and the simulation was conducted with the software PFC3D. In accordance with the laboratory test, the model builds a 300mm*300mm*200mm box and a 150mm diameter loading plate. These two components are both "wall" elements. This element can bear force but cannot transfer force, so the loading process was

conducted by applying a Z-velocity, and the macroscopic result was recorded by supervising the displacement and counterforce of the plate. Due to the particle size and porosity, the model contains more than 500,000 particles. Considering the model scale, particle size and time-consuming problem, the model uses a “ball” element to present the aggregate material. The model is shown in Figure 5-11. In addition, to differentiate furnace slag and crushed stone, the “kn” (shear stiffness) and “ks” (tangential stiffness) in a linear contact model were set referring to the average value of the results of SPCT. According to the direct shear test, the frictional coefficient of furnace slag is higher than crushed stone. Thus a higher frictional coefficient is set for the furnace slag model. Together with the reference from previous researches[34-36], the final parameter is shown in Table 5-2, and the validation is provided by the deformation and force curve in Figure 5-12, where the curve of the simulation fits the test results.

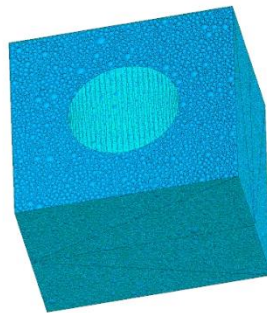


Figure 5-11 Model after initial balance

Table 5-2. Parameters of linear contact model in simulations

Parameters	Furnace slag	Crushed stone	Box
Tangential stiffness(N/m)	2.7e6	2.2e6	1e8
Normal stiffness(N/m)	2.6e6	2.3e6	1e8
Friction coefficient	0.5	0.4	0.2
Mass density (kg/m ³)	2250	2800	-
Damping coefficient	0.7	0.7	-

In Figure 5-12, the peak force of furnace slag is 14.03kN (14.41kN in laboratory test), and the displacement at peak force is 3.11 mm (3.15mm in laboratory test). For crushed stone, the peak compressive force is 11.44kN (11.89kN in laboratory test), and the displacement at peak force is 2.16mm (2.06mm in laboratory test).

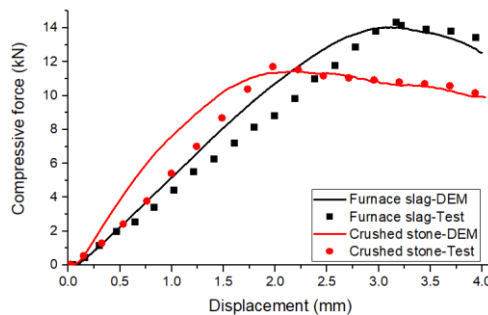


Figure 5-12 Validation for DEM model

Figure 5-13 shows the force chain at the peak state and finish state of the simulation, where the line presents the contact, and the colour presents the value of the force. In Figure 5-13 (a) and (c), the peak state shows a denser force chain than the finish state in Figure 5-13 (b) and (d). Especially in the top corner, along with the loading process after peak state, ballast in this area gradually loses its function. It is because under the unconfined top layer (except the loading plate), the interlock between the ballast is broken. When comparing the two materials, it's obvious that furnace slag shows a denser force chain and wider distribution, as the dash-line provides the explanation for the macroscopic result. In detail, at the peak state, the maximum contact force is 0.57kN and 0.46kN. At the finish state, the value is 0.75kN and 0.67kN for furnace slag and crushed stone, respectively. From peak state to finish state, the maximum contact force is increased. This behaviour is related to the force chain changes. During this process, force in some contacts exceeds the maximum capacity, thus leading to failure. With those contact no longer contributing and the loading continuing, the force in left effective contacts increase. Because the increase only happened in some contacts between the particle and the loading plate, as shown in Figure 5-13(b) and (d), it cannot offset the overall decrease trend of compressive force.

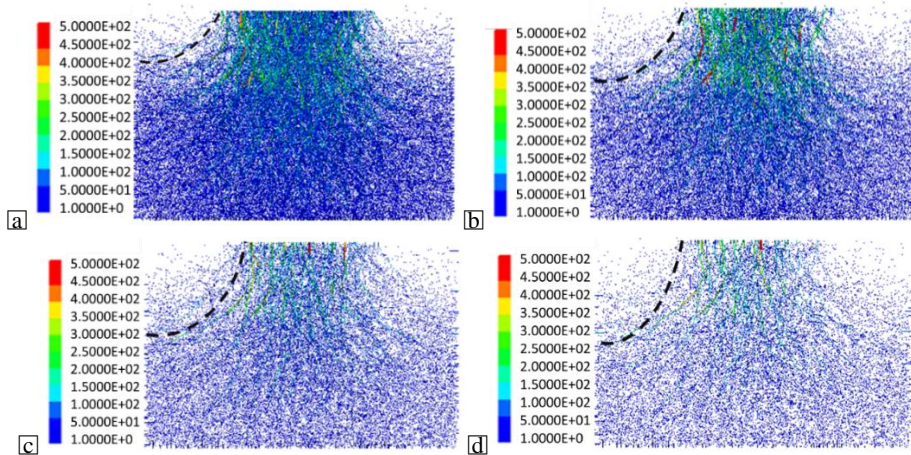


Figure 5-13 Force chain (unit: N): (a) Furnace slag at peak state, (b) Furnace slag at finish state, (c) Crushed stone at peak state, (d) Crushed stone at finish state

5. Conclusion

This research introduces the use of furnace slag as the sub-ballast in railway construction. Furnace slag is a byproduct of using iron ore to produce pig iron. Because of its characteristic, the reuse of furnace slag is not as wide as steel slag. However, compared with the requirement of the railway sub-ballast, furnace slag can be a good material and also works for environmental-friendly development. Several experimental tests were employed, including the Single Particle Crushing Test (SPCT), the Los Angeles abrasion Test (LAA), the direct shear test, the box stiffness tests, and the crushed stone (i.e. the traditional material for sub-ballast) was tested as the comparison. In addition, a DEM simulation in accordance with the box stiffness test was carried out. The main conclusions are listed below:

1. In SPCT, furnace slag shows a 20% to 39% increase in peak compressive force than the crushed stone. The result indicated that furnace slag is better in the resistance of particle breakage.

2. However, furnace slag shows more angularity breakage, the LAA value is still lower than crushed stone. It indicated a better resistance to abrasion, where the value for furnace slag is 26.04%, and for crushed stone is 31.28%.
3. In direct shear tests, furnace slag shows 16.46%, 18.91%, and 19.48% increase than crushed stone, corresponding to normal stress 50kPa, 100kPa, and 200kPa, respectively. Also, the performance of furnace slag is better in frictional angle, cohesion, and shear dilatancy.
4. In the box stiffness, the peak compressive force of furnace slag is 14.41kN (815.57kPa). For crushed stone, it is 11.89kN (673.02MPa). Under this test condition, the stiffness of furnace slag is 4.57e6N/m, and the value for crushed stone is 5.77e6N/m.
5. In the DEM model for box stiffness was built, furnace slag shows better performance than crushed stone in contact and force distribution.

Reference

- [1] C. Esveld, *Modern railway track*, MRT-Productions, The Netherlands, 2001.
- [2] B. Indraratna, S. Nimbalkar, T. Neville, Performance assessment of reinforced ballasted rail track, *Proceedings of the ICE: Ground Improvement* 167(1) (2014) 24-34.
- [3] X. Chen, Y. Jia, J. Zhang, Geogrid-reinforcement and the critical state of graded aggregates used in heavy-haul railway transition subgrade, *Transportation Geotechnics* 11 (2017) 27-40.
- [4] M.M. Biabani, B. Indraratna, S. Nimbalkar, Assessment of Interface Shear Behaviour of Sub-ballast with Geosynthetics by Large-scale Direct Shear Test, *Procedia Engineering* 143 (2016) 1007-1015.
- [5] B. Indraratna, M.M. Biabani, S. Nimbalkar, Behavior of Geocell-Reinforced Subballast Subjected to Cyclic Loading in Plane-Strain Condition, *Journal of Geotechnical and Geoenvironmental Engineering* 141(1) (2015) 04014081.
- [6] L. Le Pen, G. Watson, A. Hudson, W. Powrie, Behaviour of under sleeper pads at switches and crossings - Field measurements, *Proc Inst Mech Eng F J Rail Rapid Transit* 232(4) (2018) 1049-1063.
- [7] S. Kaewunruen, A.M. Remennikov, Sensitivity analysis of free vibration characteristics of an in situ railway concrete sleeper to variations of rail pad parameters, *Journal of Sound and Vibration* 298(1-2) (2006) 453-461.
- [8] M. Sol-Sánchez, F. Moreno-Navarro, M.C. Rubio-Gámez, The use of elastic elements in railway tracks: A state of the art review, *Construction and Building Materials* 75 (2015) 293-305.
- [9] G. Jing, L. Qie, V. Markine, W. Jia, Polyurethane reinforced ballasted track: Review, innovation and challenge, *Construction and Building Materials* 208 (2019) 734-748.
- [10] P.K. Woodward, J. Kennedy, O. Laghrouche, D.P. Connolly, G. Medero, Study of railway track stiffness modification by polyurethane reinforcement of the ballast, *Transportation Geotechnics* 1(4) (2014) 214-224.
- [11] M. Sol-Sánchez, F. Moreno-Navarro, M.C. Rubio-Gámez, An Analysis of the Performance of Deconstructed Tires for Use as Pads in Railroad Tracks, *Journal of Civil Engineering and Management* 22(6) (2016) 739-746.
- [12] Y. Guo, V. Markine, W. Qiang, H. Zhang, G. Jing, Effects of crumb rubber size and percentage on degradation reduction of railway ballast, *Construction and Building Materials* 212 (2019) 210-224.
- [13] M. Sol-Sánchez, F. Moreno-Navarro, G. Martínez-Montes, M.C. Rubio-Gámez, An alternative sustainable railway maintenance technique based on the use of rubber particles, *Journal of Cleaner Production* 142 (2017) 3850-3858.
- [14] B. Indraratna, Q. Sun, A. Heitor, J. Grant, Performance of Rubber Tire-Confined Capping Layer under Cyclic Loading for Railroad Conditions, *Journal of Materials in Civil Engineering* 30(3) (2018).
- [15] W. Jia, V. Markine, Y. Guo, G. Jing, Experimental and numerical investigations on the shear behaviour of recycled railway ballast, *Construction and Building Materials* 217 (2019) 310-320.
- [16] B.G. Delgado, A. Viana da Fonseca, E. Fortunato, P. Maia, Mechanical behavior of inert steel slag ballast for heavy haul rail track: Laboratory evaluation, *Transportation Geotechnics* 20 (2019).
- [17] M. Oge, D. Ozkan, M.B. Celik, M. Sabri Gok, A. Cahit Karaoglanli, An Overview of Utilization of Blast Furnace and Steelmaking Slag in Various Applications, *Materials Today: Proceedings* 11 (2019) 516-525.
- [18] J. Huang, C. Zou, D. Sun, B. Yang, J. Yan, Effect of recycled fine aggregates on alkali-activated slag concrete properties, *Structures* 30 (2021) 89-99.
- [19] M.A.R. B K A, C. Ngamkhanong, Y. Wu, S. Kaewunruen, Recycled Aggregates Concrete Compressive Strength Prediction Using Artificial Neural Networks (ANNs), *Infrastructures* 6(2) (2021).
- [20] Q. Li, H. Ding, A. Rahman, D. He, Evaluation of Basic Oxygen Furnace (BOF) material into slag-based asphalt concrete to be used in railway substructure, *Construction and Building Materials* 115 (2016) 593-601.
- [21] J.J. Emery, *Slag Utilization in Pavement construction, Extending Aggregate Resources*, ASTM STP 774, American Society for Testing and Materials (1982) 95-118.

- [22] M. Esmaili, R. Nouri, K. Yousefian, Experimental comparison of the lateral resistance of tracks with steel slag ballast and limestone ballast materials, *Proceedings of the Institution of Mechanical Engineers, Part F: Journal of Rail and Rapid Transit* 231(2) (2016) 175-184.
- [23] L.V. Fisher, A.R. Barron, The recycling and reuse of steelmaking slags — A review, *Resources, Conservation and Recycling* 146 (2019) 244-255.
- [24] M. Morata, C. Saborido, V. Fontserè, Slag aggregates for railway track bed layers: monitoring and maintenance, *Computers in Railways XV: Railway Engineering Design and Operation*, 2016, pp. 283-294.
- [25] C. Shi, Steel Slag—Its Production, Processing, Characteristics, and Cementitious Properties, *JOURNAL OF MATERIALS IN CIVIL ENGINEERING* 16(3) (2004) 230-236.
- [26] L. Dominic; , B. Indraratna, Assessment of Subballast Filtration under Cyclic Loading, *Journal of Geotechnical and Geoenvironmental Engineering* 136(11) (2009) 1519-1528.
- [27] A.S.J. Suiker;, E.T. Selig;, R. Frenkel, Static and Cyclic Triaxial Testing of Ballast and Subballast, *JOURNAL OF GEOTECHNICAL AND GEOENVIRONMENTAL ENGINEERING* 131(771-782) (2005).
- [28] B. Indraratna, Y. Qi, A. Heitor, Evaluating the Properties of Mixtures of Steel Furnace Slag, Coal Wash, and Rubber Crumbs Used as Subballast, *Journal of Materials in Civil Engineering* 30(1) (2018).
- [29] J.C.Jaeger, Failure of rocks under tensile conditions, *International Journal of Rock Mechanics and Mining Sciences & Geomechanics Abstracts* 4 (1967) 219-227.
- [30] Standard, TB/T2328.1-18 Test method for railway ballast, Ministry of Railway, China,1992.
- [31] R.A. Jewell; , C.P. Worth, Direct shear tests on reinforced sand, *Geotechnique* 37(1) (1987) 53-68.
- [32] J. Wang, M. Gutierrez, Discrete element simulations of direct shear specimen scale effects, *Géotechnique* 60(5) (2010) 395-409.
- [33] D.-. ASTM, Standard test method for direct shear tests of soils under consolidated drained conditions, ASTM, West Conshohocken, 1990.
- [34] F. Khatibi, M. Esmaili, S. Mohammadzadeh, DEM analysis of railway track lateral resistance, *Soils and Foundations* 57(4) (2017) 587-602.
- [35] E. Tutumluer, Y. Qian, Y.M.A. Hashash, J. Ghaboussi, D.D. Davis, Discrete element modelling of ballasted track deformation behaviour, *International Journal of Rail Transportation* 1(1-2) (2013) 57-73.
- [36] X. Bian, W. Li, Y. Qian, E. Tutumluer, Micromechanical Particle Interactions in Railway Ballast through DEM Simulations of Direct Shear Tests, *International Journal of Geomechanics* 19(5) (2019) 04019031.

Paper VI

Dynamic behaviour of ballast under hanging sleepers in railways track transition zones using FEM-DEM method

Wenli Jia, Haoyu Wang, Guoqing Jing, Valeri Markine

Under review

Abstract

Transition zones in railways are the locations with considerable changes in the vertical support due to the sudden stiffness change and differential settlement, which requires higher maintenance costs. Hanging sleepers are one of the most common defects in transition zones, which can cause a significant increase in sleeper velocity and ballast stress, leading to poor elasticity and drainage of tracks and spreading the issue to adjacent sleepers. To accurately study the dynamic behaviour of ballast particles under hanging sleepers in transition zones, a FEM-DEM method is developed, which consists of a FEM model simulating the train-track interaction in a transition zone and a DEM model simulating sleeper-ballast particle interaction of a hanging sleeper. The movement of the hanging sleepers under train passing is simulated in the FEM model and used as the input for the DEM method to calculate the detailed behaviour of ballast particles. The dynamic behaviour of ballast under multiple hanging sleepers in transition zones under good, moderate, and degraded conditions are studied using the FEM-DEM method. The main finding is that most contact forces between ballast particles under the hanging sleeper are small in all cases, which are between 0.1 kN and 0.5 kN. As the sleeper force increases, the contacts in the range of 0.5 kN and 2 kN become more and scattered distributed. It indicates that during the track degradation process, a high sleeper force tends to cause a wide range of small damage to the ballast rather than a small range of larger damage.

Keywords: Track transition zone, Dynamic behaviour of ballast particles, Hanging sleeper, FEM-DEM method.

1. Introduction

Transition zones in railway tracks are the locations with considerable changes in the vertical support, which are typically located near engineering structures, e.g., embankment-bridge transition zones in Figure 6-1(a) and (b). In transition zones, the supporting stiffness of the track changes dramatically, leading to a rapid change in the elevation of wheels and causing an increase in dynamic wheel loads [1-3]. Besides, different settlement behaviour of the track on the embankment and track on the bridge also causes track degradation in transition zones [4-6]. In addition, the geotechnical, construction and maintenance issues, e.g., poor quality of used materials, poor drainage conditions, and inadequate consolidation of the embankment, can also contribute track degradation in transition zones [7].

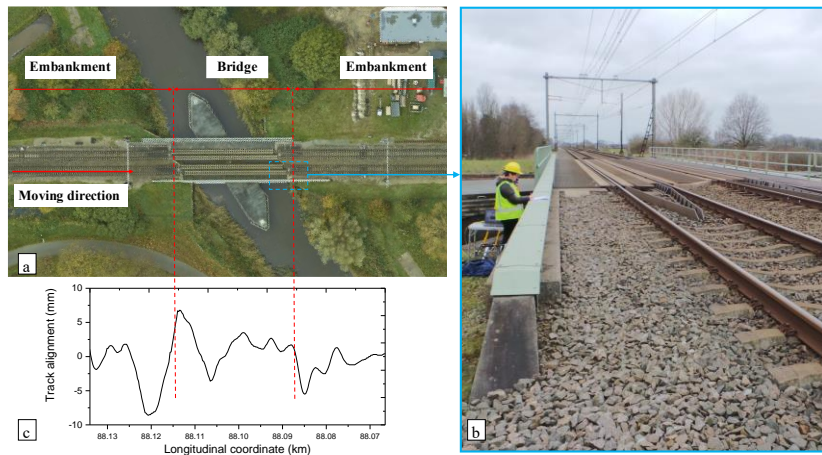


Figure 6-1. Typical railway transition zone: (a) Top view, (b) Side view, (c) Track longitudinal level.

As a result, track degradation in transition zones has been observed much more often than in free tracks, which includes the deterioration of the track geometry (see Figure 6-c), damage to the track components (e.g., rail surface defects, broken fasteners, hanging sleepers)[7-12] and passenger's comfort[13]. As a result, the maintenance cost spent on transition zones is much higher[14], which can be up to eight times[15].

Among all issues, hanging sleepers have been most often reported in transition zones, e.g., in [4, 6, 16], which are the sleepers not well supported by the ballast but hanging on the rails. When trains pass hanging sleepers, the velocity (kinetic energy) of the sleepers is increased significantly and consequently increases the ballast stress underneath. Also, because the movement of the sleepers is less constrained, the stress in the ballast under hanging sleepers may not be evenly distributed, causing stress concentration [4, 17]. As a result, ballast particles are often crushed or further compacted under hanging sleepers. Because ballast provides elasticity and drainage of tracks [18], the compacted ballast may cause a further increase in wheel loads, causing a vicious circle [19], and spread the issue to adjacent sleepers. Therefore, the dynamic behaviour of hanging sleepers in transition zones should be studied.

In the existing studies of transition zones, the Finite Element Method (FEM) is used, which can accurately analyse the interaction between trains, rails, sleepers, and ballast, e.g., [4, 15, 19-24]. However, ballast can only be a whole component, which is modelled by beam or solid elements. As a result, the movement of ballast particles and stress in ballast cannot be accurately studied.

On the contrary, the ballast particles can be modelled as balls or a cluster of spheres using the Discrete Element Method (DEM)[25-27]. Using the DEM, the movement of every ballast particle and the contact forces between ballast particles can be studied[28-30]. Thus, the dynamic behaviour of ballast particles under hanging sleepers can be accurately studied. However, due to the huge number of elements considered in a model, DEM models are always time-consuming.

To overcome the shortage, a FEM-DEM method is proposed in this paper. The interaction between the train and track in the transition zone with hanging sleepers is simulated in the FEM model. After calculation, the contact force between the hanging sleepers and ballast bed under train passing (referred to as sleeper force) can be achieved, which is used as the input for the sleeper-ballast model using the DEM method. In this way, the movement of ballast particles and forces between ballast particles under hanging sleepers in the transition zone can be accurately simulated.

The paper is organised as follows. The FEM-DEM method is introduced in Section 2. The simulation results are analysed in Section 3. The conclusions are provided in Section 4.

2.Method description

The proposed method composes a FEM model to analyse the interaction between train and track transition zone and a DEM model to analyse the interaction between sleeper and ballast, as shown in Figure 6-2. The maximum loads of sleepers under the train passing at various locations are calculated using the FEM model and used as input for the DEM model to calculate the detailed stress status of the ballast bed.

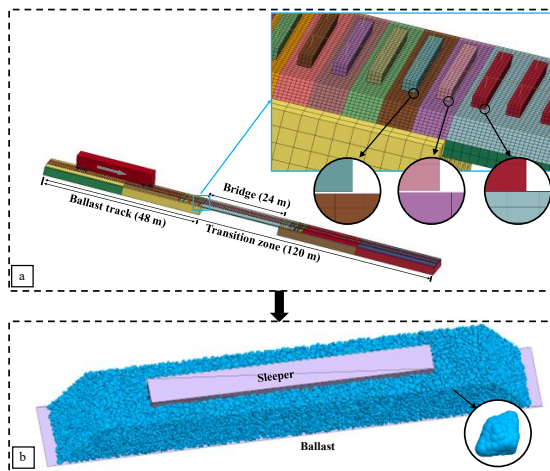


Figure 6-2. FEM-DEM method: (a) FEM model, (b) DEM model

2.1 FEM model

The FEM model is developed according to typical transition zones, which consist of two ballasted tracks on embankments and a slab track on a bridge (similar to the transition zone Figure 6-1). The model has a total length of 120m, with two ballasted tracks of 48 m and a bridge of 24 m. The model is briefly introduced here and a detailed description of the model can be found in [4] and [6].

The components of ballasted tracks are rails, fasteners, sleepers, ballast and subgrade. The rails are modelled by Hughes-Liu beam elements with 2*2 Gauss quadrature integration[31]. The cross-sectional and mass properties of the UIC54 rails are used. Fasteners are modelled by spring-damper

elements with nonlinear properties in the vertical direction. In compression, the stiffness of rail pads is used, while in tension, a much higher stiffness is used to simulate the clamping effect. The sleepers, ballast, and bridge are modelled by three-dimensional elastic bodies which are composed of the selective reduced integrated hexahedral solid elements [31], with element sizes of 75mm.

The sleepers on the embankment are connected to ballast using contact elements, while the sleepers on the bridge are directly fastened to the concrete slab. The contact element between sleepers and ballast is surface-to-surface contact [31]. It employs the penalty method, which places normal interface springs between all penetrating nodes and the contact surface. During the calculation, the penetrations between the bottom surface of sleepers and the top surface of ballast are searched for every time step. When it is found, a force proportional to the penetration depth is applied to resist and ultimately eliminate the penetration.

To model the differential settlement in the transition zone, a downwards displacement is applied to the ballast and subgrade layers in the ballasted tracks on both sides of the bridge, while the vertical geometry of the bridge remains unchanged. Due to the clamping of fasteners and bending of rails, the sleepers near the bridge are hung in the model as shown in Figure 6-2. In the paper, three conditions of transition zones are considered, including good, moderate, and degraded, which are modelled by the differential settlements of 0mm, 4mm, and 8mm, respectively, according to the measurements in [6, 16].

Table 6-1. Parameters of FEM model

Parameter	Value
Length of carbody (m)	23.0
Distance between bogie centres (m)	20.0
Distance between wheels (m)	2.5
Primary suspension stiffness (N/m)	4.2e5
Primary suspension damping (N×s/m)	1.8e4
Secondary suspension stiffness (N/m)	4.7e5
Secondary suspension damping (N×s/m)	3.5e4
Secondary suspension bending stiffness (Nm/rad)	1.0e4
Sleeper elastic modulus (Pa)	3.6e10
Sleeper Poisson ratio	0.2
Ballast elastic modulus (Pa)	1.2e8
Ballast Poisson ratio	0.2
Subgrade elastic modulus (Pa)	1.8e8
Subgrade Poisson ratio	0.2
Bridge elastic modulus (Pa)	3.5e10
Bridge Poisson ratio	0.2
Fastening system horizontal stiffness (N/m)	1.5e6
Fastening system horizontal damping (N×s/m)	5.0e4
Fastening system longitudinal stiffness (N/m)	1.5e6
Fastening system longitudinal damping (N×s/m)	5.0e4
Fastening system vertical (compression) stiffness (N/m)	1.2e8
Fastening system vertical (compression) damping (N×s/m)	5.0e4
Fastening system vertical (tension) stiffness (N/m)	1.2e11
Fastening system vertical (tension) damping (N×s/m)	5.0e4

The vehicle is modelled as a multibody system consisting of one carbody, two bogies and four wheelsets. The dimension of a Dutch passenger train is used. The primary and secondary suspensions are modelled by spring-damper elements. The axle load is 19 t, and the running speed is 144km/h,

which is in the range of the typical operational velocity in the Dutch railway system. The contact between the wheel and rail is modelled by a Hertzian spring. Other parameters of the model are shown in Table 6-1. The model is validated against field measurement, which can be found in [4].

2.1 DEM model

The DEM model is developed in accordance with the FEM model, wherein a sleeper of 2400 mm (length) \times 240 mm (width) \times 200 mm (height) and the corresponding dimension of the ballast bed are modelled, as following Figure 6-3 (a). The slope of the ballast is 1:1.5. The width of the ballast shoulder is 480 mm. The height of the ballast bed is 400 mm, wherein 300 mm is under the sleeper. The width of the ballast bed is 600 mm. The ballast particles are modelled by clump elements, the geometry of which is got from 3D scanning of real ballast particles and filled by spheres, as shown in Figure 6-3 (b). The sleeper is modelled as the wall element, as well as the boundary.

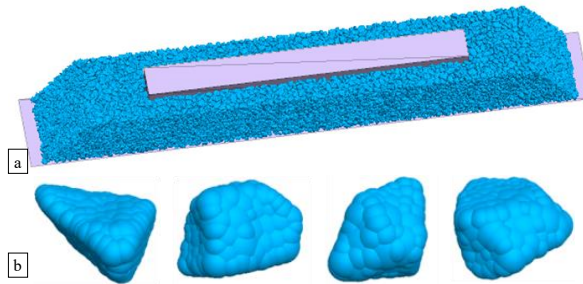


Figure 6-3. DEM model for sleeper and ballast: (a) Overview, (b) Representative ballast particles.

When developing DEM models, it is common to first generate particles in a loose state using a ‘rainy method’ and then compact them to the required porosity. In this study, the ballast particles are generated using an optimized method, which is 10 to 20 times faster. The method is introduced as follows.

Firstly, the shape files of ballast particles are imported, including the template for ballast particles, sleeper, and ballast box (ballast bed). After that, the sleeper and ballast box are generated according to those templates.

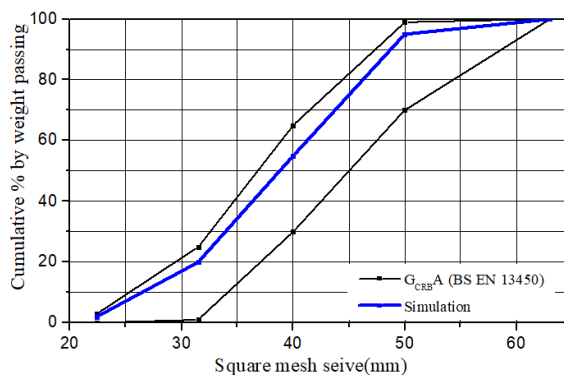


Figure 6-4. Particle Size Distribution of ballast particles used in DEM model

Secondly, spheres are filled into the ballast box, wherein the Particle Size Distribution (PSD) shown in Figure 6-4 is used, which is a category in EN 13450 and commonly used in the Netherlands. In addition, a porosity of 0.27 is used. It should be noted that the timestep for each calculation cycle in DEM models is normally defined by contact parameters (stiffness) and kinematic behaviour. Differently, a scaled timestep is used in this model to increase the calculation efficiency. Additional settings for convergence are discussed in the following steps.

In the third step, the contact parameters for spheres and ballast box are applied as well as the gravity. At the beginning of the calculation, spheres keep moving under gravity until the average ratio of the total unbalanced force to the total contact force reaches $1.0e-3$. After that, the position and radius of spheres are collected, which are replaced by clumps with the same volume. Besides, the same contact parameters are applied to the clumps, which are shown in Table 6-2. It should be noted that the contact is linear.

Table 6-2. Contact parameters of DEM model

Parameter	Ballast particle	Sleeper
Tangential stiffness (N/m)	1.0e8	6.0e8
Normal stiffness (N/m)	1.0e8	6.0e8
Friction coefficient	0.5	0.2
Mass density (kg/m ³)	2630.0	-
Damping coefficient	0.7	0.7

Because the volume is the controlled variable of clump replacement, the porosity remains at the same level as the initial setting. However, overlaps between clumps exist after replacement, due to the difference in the geometry of spheres and clumps. To eliminate the overlaps and consequent high contact forces, the radius of clumps is expanded. In this way, the convergence of the calculation can be achieved. It should be noted that the factor for expansion is very small, which is expressed as Equation 1. Thus, the effect on particle size is neglectable.

$$\beta = -1\lambda V_b \Delta\sigma k_{sum}^n \quad (1)$$

Where β is the expansion factor; λ is the dimension of the model, which is 3 in this case; V_b is the volume of the whole ballast box model (ballast bed); $\Delta\sigma$ is the stress difference; k_{sum}^n is a coefficient.

$\Delta\sigma$ is defined as Equation 2.

$$\Delta\sigma = \sigma_{in} - \sigma_m \quad (2)$$

Where σ_{in} is the input target stress and σ_m is the average stress of the model.

k_{sum}^n is defined as Equation 3.

$$k_{sum}^n = \sum_i (k_i^n (R_i^a + R_i^b) R_i) \quad (3)$$

Where R_i^a and R_i^b are the radius of the pebble (included in a clump and directly contacts other elements) at the contact end, which is 0 if the end is the wall element; R_i is the distance tangential component of the vector from the contact point to the centroid of the element; k_i^n is the stiffness of i^{th} contact.

In the last step, the timestep is changed back from the scaled one to the one that is defined by contact parameters and kinematic behaviour. After that, the model is stable for further calculation.

The modelling technique including a contact model between ballast particles has been used for the simulation of the direct shear test of ballast in [32] and good accordance between the simulation and laboratory tests has been achieved. Besides, the modelling technique has also been used in [25, 33].

3. Sleeper force in transition zone

The contact forces between sleepers and ballast during the train passing can be calculated by the FEM model. For convenience, the sleepers are numbered starting from the one closest to the bridge. The sleepers in the embankment-ballast transition (left of the bridge) have a negative sign, while those in the ballast-embankment transition (right of the bridge) are positive. When the train passes, sleepers are pushed downwards to the ballast, leading to an increase in contact forces between sleepers and ballast. Figure 6-5 shows an example of the time history of the contact force under the 4th sleeper on the left side of the bridge (refer to as Sleeper-4). The four peaks of sleeper force in Figure 6-5 (e) correspond to the four wheelsets of the train in Figure 6-5 (a)-(d).

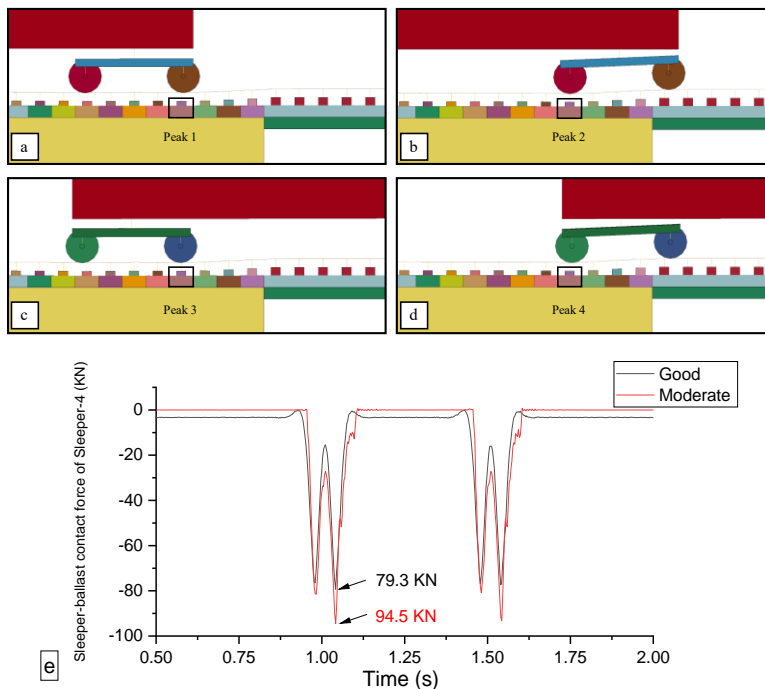


Figure 6-5. Bogie movements corresponding to four peaks of sleeper force at Sleeper-4: (a) Peak 1; (b) Peak 2; (c) Peak 3; (d) Peak 4; (e) Sleeper forces

It can be seen from Figure 6-5(e) that the sleeper force in the moderate case is nearly 0 kN before and after the peaks, which is due to that the sleeper is hung and not connected to the ballast. On the contrary, the sleeper force in the good case is around 3kN before and after the train passing, which is caused by the weight of the rails and sleeper. It can be also seen from Figure 6-5(e) that the maximum sleeper force in the moderate case is larger than that in the good case, which is 94.5kN and 79.3 kN respectively in the 2nd peak. This is due to the increase of wheel-rail forces caused by the sudden change in stiffness and differential settlement in the transition zone. More discussion of the train-track interaction in transition zones can be found in [4].

The maximum contact forces between sleeper and ballast in the good (0 mm differential settlement), moderate (4 mm differential settlement), and degraded (8 mm differential settlement) cases are collected as shown in Figure 6.

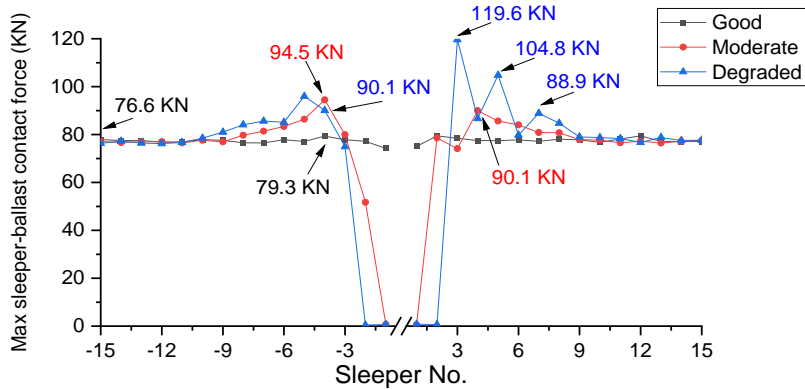


Figure 6-6. Maximum sleeper forces in good, moderate, and degraded cases

As seen in Figure 6-6, sleeper forces grow as the transition zone degrades. The maximum sleeper contact forces in the good case are slightly higher in the transition zone, for instance, 79.3kN at Sleeper-4, which is only 3kN higher than that far from the bridge (around 76.6kN). On the contrary, the sleeper forces in the moderate case are largely increased. The increased range is from the 3rd sleeper to the 9th sleeper on both sides, wherein the contact forces at Sleeper-4 and Sleeper+4 are the largest (94.5kN and 90.1kN, respectively). In the degraded case, the sleeper forces grow even more, which reaches 119.6kN in the bridge-embankment transition. Besides, the increased range is larger than that in the moderate case and with high fluctuation (see the three peaks in the bridge-embankment transition).

The sleepers with large sleeper forces in the transition zone are marked in Figure 6-6 and collected in Table 6-3, which is used as input for the DEM model to further analyse ballast behaviour.

Table 6-3. Typical sleeper forces in transition zones under various conditions

Case No.	Sleeper force (kN)	Increase to free track	Collected from
1	76.6	-	Free track
2	79.3	4%	Sleeper-4 in good
3	88.9	16%	Sleeper+7 in degraded
4	90.1	18%	Sleeper-4 in degraded; Sleeper+4 in moderate
5	94.5	23%	Sleeper-4 in moderate
6	104.8	37%	Sleeper+5 in degraded
7	119.6	56%	Sleeper+3 in degraded

4. Contact behaviour between ballast particles

In the DEM calculation, the sleeper is moved downward at 1mm/s to the ballast until the sleeper force reaches the expected values in Table 6-3. After that, the contact force between ballast particles is collected. In this way, the behaviour of ballast beds under hanging sleepers can be studied in detail.

The simulation results of the sleeper in the free track (Case 1) and the case of the sleeper with the largest contact force (Case 7) are compared, as shown in Figure 6-7, wherein both the side view and bottom view of the ballast layers are presented. The contact forces at the particle level (particle-particle and particle-sleeper) are colour coded according to their values. Note an upper limit of 2kN and a lower limit of 0.3kN are selected for better presentation. The contact forces larger than the upper limit are all shown in red, while the ones below the lower limit (0.3kN) are discarded.

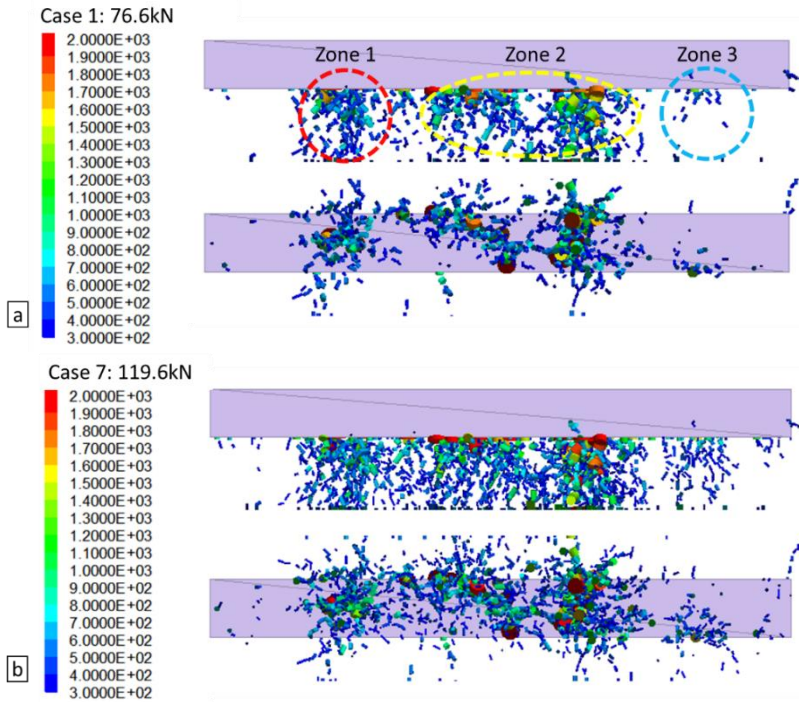


Figure 6-7. Contact force between ballast particles (a) Case 1: 76.6 kN; (b) Case 7: 119.6 kN

As shown in Figure 6-7, a cylinder represents a contact force and the ends of a cylinder are from the centres of ballast particles. Note that the contact forces at boundaries are between ballast particles and the wall element. It can be seen that both the amount and values of contact forces are much higher in Case 7 than in Case 1.

To see the difference better, the contact forces in Zone 1 (see Figure 6-7 (a)) are zoomed in as shown in Figure 6-8(a), wherein contact forces are also represented as spheres. Note that the location of the sphere indicates the contact area and the colour and size of the sphere indicate the value. In addition, different lower and upper limits are used for better presentation. Similarly, the contact forces in Zone 2 and 3 are shown in Figure 6-8(b) and (c), respectively.

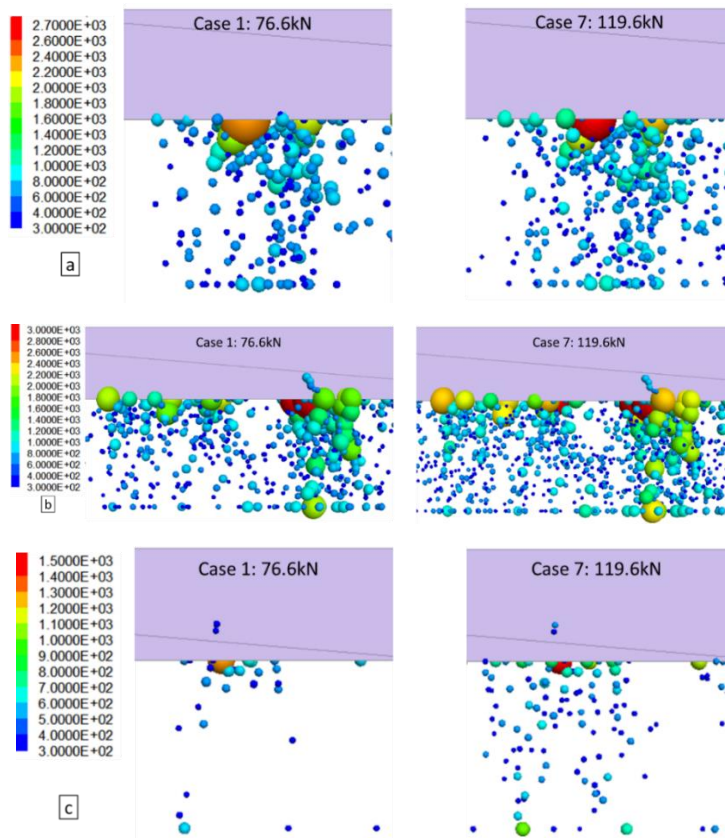
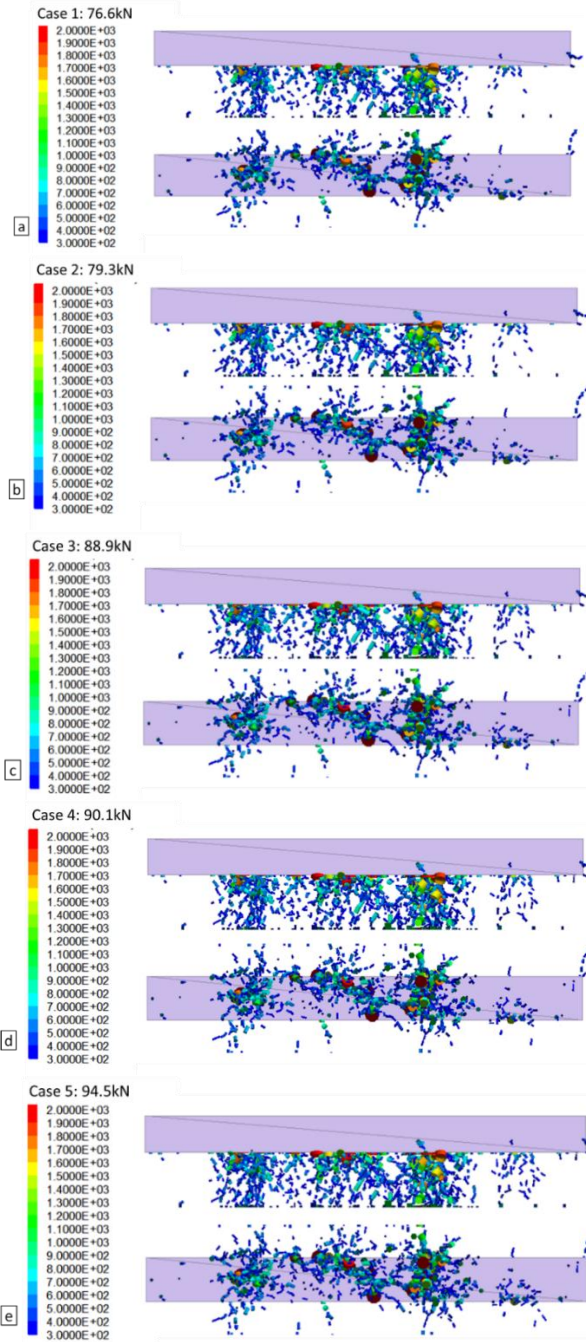


Figure 6-8. Contact force of the zoom-in areas: (a) Zone 1, (b) Zone 2, (c) Zone 3

As can be seen from Figure 6-8, the largest contact forces at particle level appear at the top layer of the ballast in all zones in both Case 1 and Case 7. This is reasonable since the ballast particles on the top layer are directly under the impact of the sleeper. The contact forces become gradually smaller as the ballast particles are deeper.

Comparing Case 1 with Case 7, it can be seen that when the sleeper force grows from 76.6kN to 119.6kN, increased by 56%, the average contact force between the sleeper and ballast particles grows from 0.218kN to 0.300kN, increased by 38%, while the maximum of that grows from 3.326kN to 4.307kN, increased by 29%. The percentage of increase in sleeper force is larger than that of the average (or maximum) of the contact forces between the sleeper and ballast particles. It is because the ballast transmits and re-distributes the load from the sleeper. This shows that the sleeper-ballast contact can be more accurately simulated using the DEM model and also proves the advantage of the FEM-DEM method.

The contact forces in the ballast of other cases (Case 2 to Case 6) are shown in Figure 6-9. Note that the results of Case 1 and Case 7 are also added to show the evolution of the contact forces. The statistical analysis of the contact forces in all cases is shown in Table 6-4.



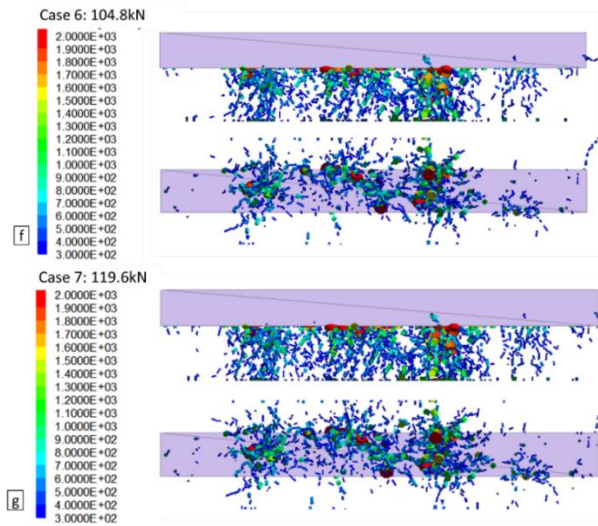


Figure 6-9. Contact forces between ballast particles: (a) Case 1: 76.6kN, (b) Case 2: 79.3kN, (c) Case 3: 88.9kN, (d) Case 4: 90.1kN, (e) Case 5: 94.5kN, (f) Case 6: 104.8kN, (g) Case 7: 119.6kN

Table 6-4. Contact number counting by force range.

Case No.	Sleeper force(kN)	Range of contact forces (kN)					Sum
		0.1-0.5	0.5-1	1-2	2-3	>3	
1	76.6	4080	240	47	3	1	4371
2	79.3	4254	256	47	4	1	4562
3	88.9	4733	300	59	6	2	5100
4	90.1	4830	303	61	9	2	5205
5	94.5	5042	327	65	9	2	5445
6	104.8	5550	385	73	11	2	6021
7	119.6	6153	468	92	14	3	6730

As seen in Figure 6-9 and Table 6-4, most contact forces are small in all cases, which are between 0.1kN and 0.5kN. Also, as the sleeper force increases, the contacts in the range of 0.5kN and 2kN become more and scattered distributed, the growth in the number of which is much larger than that higher than 2kN. It indicates that during the track degradation process, a high sleeper force tends to cause a wide range of small damage to the ballast rather than a small range of larger damage to the ballast.

To further study the relationship between sleeper force and ballast behaviour, the sleeper forces ranging from 70kN to 120kN with an interval of 2.5kN are calculated using the DEM model. The average and maximum contact forces between the ballast particle and sleeper, are collected and shown in Figure 6-10(a), where the x-axis also represents the total contact forces on sleeper. And, the total and maximum contact force between the ballast particle and bottom wall (sub-ballast) are collected and shown Figure 6-10(b). Note that the average forces on the bottom of all cases are smaller than 0.1kN, so they are not under consideration.

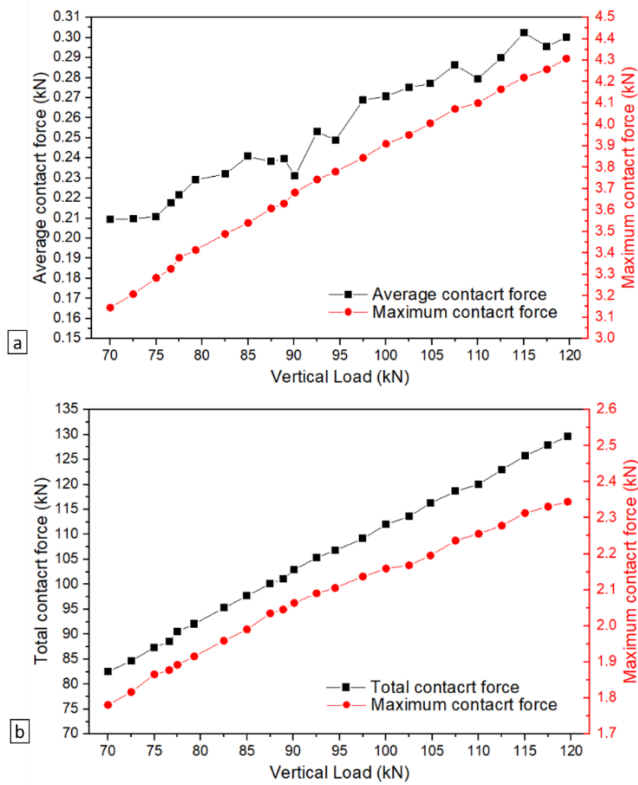


Figure 6-10. Relationship between sleeper contact force and ballast behaviour: (a) Contact forces between ballast particle and sleeper, (b) Contact forces between ballast particle and bottom.

As seen in Figure 6-10(a), both the average and maximum of contact forces between the sleeper and ballast particles are increased linearly as the sleeper force grows. Note that there are local drops in the curve of the average contact force at the 90.1 kN, 94.5 kN, 110 kN and 117.5 kN, which can be explained by the sudden change in ballast displacement caused by interlock failure (or ballast breakage in reality).

Compared to contact forces between the ballast particle and sleeper (Figure 6-10(a)), the pattern of contact forces between the ballast particle and bottom is much smoother, without fluctuation, as shown in Figure 6-10(b). Besides, the maximum is much smaller. This is because the contact forces are re-distributed in the ballast layer.

5. Conclusion

Transition zones in railways are the locations with considerable changes in the vertical support, due to the sudden stiffness change and differential settlement. As a result, track degradation in transition zones has been observed much more often than in free tracks, including the deterioration of the track geometry, damage to the track components, and passenger comfort, which leads to higher maintenance costs for railway companies. Hanging sleepers (the sleepers not well supported by the ballast but hanging on the rails) are one of the most common defects in transition zones, which can cause a significant increase in sleeper velocity and ballast stress. They can eventually lead to poor

elasticity and drainage of tracks and spread the issue to adjacent sleepers. To accurately study the dynamic behaviour of ballast particles under hanging sleepers in transition zones, a FEM-DEM method is developed, which consists of a FEM model simulating the train-track interaction in a transition zone and a DEM model simulating sleeper-ballast particle interaction of a hanging sleeper. The movement of the hanging sleepers under train passing is simulated in the FEM model and used as the input for the DEM method to calculate the detailed behaviour of ballast particles. Using the method, the dynamic behaviour of ballast under multiple hanging in transition zones under good, moderate, and degraded conditions. The following conclusions can be drawn, which can be used to guide maintenance in railway transition zones.

1. Impact forces of hanging sleepers grow as the transition zone degrades, the increased range of which is from the 3rd sleeper to the 9th sleeper on both sides of the bridge. The maximum sleeper ballast contact force is only slightly increased in the transition zones under the good condition. On the contrary, the sleeper forces are largely increased in the moderate and degraded cases, which are up to 94.5 kN (by 23%) and 119.6 kN (by 56%), respectively.
2. The percentage of increase in sleeper force is larger than that of the average of the contact forces between the sleeper and ballast particles, which are 56% and 38%. It is because the ballast transmits and re-distributes the load from the sleeper. This shows that the sleeper-ballast contact can be more accurately simulated using the DEM model and also proves the advantage of the FEM-DEM method.
3. When the hanging sleeper contacts the ballast, the largest contact forces between ballast particles appear at the top layer of the ballast in all zones in both Case 1 (76.6 kN) and Case 7 (119.6 kN). The contact forces become gradually smaller as the ballast particles are deeper in both cases.
4. The statistical analysis of the contact forces under various sleeper forces shows that most contact forces are small in all cases, which are between 0.1 kN and 0.5 kN. Also, as the sleeper force increases, the contacts in the range of 0.5 kN and 2 kN become more and scattered distributed. It indicates that during the track degradation process, a high sleeper force tends to cause a wide range of small damage to the ballast rather than a small range of larger damage to the ballast.
5. Both the average and maximum of contact forces between the sleeper and ballast particles under the hanging sleeper are increased linearly as the sleeper force grows. Similarly, the contact forces between the ballast particle and bottom under the hanging sleeper grow linearly but much smoother. This is because the contact forces are re-distributed in the ballast layer.

Reference

- [1] A. Lundqvist, R. Larsson, T. Dahlberg, Influence of railway track stiffness variations on wheel/rail contact force, in: Workshop Track for High-Speed Railways Porto, Portugal, 2006.
- [2] A.D. Kerr, B.E. Moroney, Track transition problems and remedies, *Bulletin*, 742 (1993), pp. 267-298.
- [3] Z.G. Li, T.X. Wu, Vehicle/track impact due to passing the transition between a floating slab and ballasted track. *Noise and Vibration Mitigation for Rail Transportation Systems*, Springer, 2008: 94–100.
- [4] H. Wang, V. Markine, Dynamic behaviour of the track in transitions zones considering the differential settlement, *Journal of Sound and Vibration* 459 (2019) 114863.
- [5] E.T. Selig, J.M. Waters, *Track geotechnology and substructure management*, Thomas Telford, 1994.
- [6] H. Wang, V. Markine, Corrective countermeasure for track transition zones in railways: Adjustable fastener, *Engineering Structures* 169 (2018) 1-14.
- [7] D. Li, D. Otter, G. Carr, Railway Bridge Approaches under Heavy Axle Load Traffic: Problems, Causes, and Remedies, *Proceedings of the Institution of Mechanical Engineers, Part F: Journal of Rail and Rapid Transit* 224(5) (2010) 383-390.
- [8] T.D. Stark, S.T. Wilk, Root cause of differential movement at bridge transition zones, *Proceedings of the Institution of Mechanical Engineers, Part F: Journal of Rail and Rapid Transit* 230(4) (2015) 1257-1269.
- [9] C. Alves Ribeiro, A. Paixão, E. Fortunato, R. Calçada, Under sleeper pads in transition zones at railway underpasses: numerical modelling and experimental validation, *Structure and Infrastructure Engineering* 11(11) (2014) 1432-1449.
- [10] B. Coelho, P. Hölscher, J. Priest, W. Powrie, F. Barends, An Assessment of Transition Zone Performance, *Proceedings of the Institution of Mechanical Engineers, Part F: Journal of Rail and Rapid Transit* 225(2) (2011) 129-139.
- [11] B.Z. Coelho, J. Priest, P. Hölscher, Dynamic behaviour of transition zones in soft soils during regular train traffic, *Proceedings of the Institution of Mechanical Engineers, Part F: Journal of Rail and Rapid Transit* 232(3) (2017) 645-662.
- [12] D. Li, M. ASCE, D. Davis, M. ASCE, Transition of Railroad Bridge Approaches, *Journal of Geotechnical and Geoenvironmental Engineering* 131(11) (2005) 1392-1398.
- [13] M. Banimahd, P.K. Woodward, J. Kennedy, G.M. Medero, Behaviour of train-track interaction in stiffness transitions, *Proceedings of the Institution of Civil Engineers - Transport* 165(3) (2012) 205-214.
- [14] N.J. Elizabeth, *The Bump at the End of the Railway Bridge*. Doctoral dissertation, Texas A&M University, (2009).
- [15] J.N. Varandas, P. Hölscher, M.A.G. Silva, Dynamic behaviour of railway tracks on transitions zones, *Computers & Structures* 89(13-14) (2011) 1468-1479.
- [16] H. Wang, V. Markine, X. Liu, Experimental analysis of railway track settlement in transition zones, *Proc Inst Mech Eng F J Rail Rapid Transit* 232(6) (2018) 1774-1789.
- [17] A. Lundqvist, T. Dahlberg, Load impact on railway track due to unsupported sleepers, *Proceedings of the Institution of Mechanical Engineers, Part F: Journal of Rail and Rapid Transit* 219(2) (2005) 67-77.
- [18] C. Esveld, *Modern railway track*, MRT-Productions, The Netherlands, 2001.
- [19] Y. Shan, B. Albers, S.A. Savidis, Influence of different transition zones on the dynamic response of track-subgrade systems, *Computers and Geotechnics* 48 (2013) 21-28.
- [20] X. Lei, L. Mao, Dynamic response analyses of vehicle and track coupled system on track transition of conventional high speed railway, *Journal of Sound and Vibration* 271(3-5) (2004) 1133-1146.
- [21] M. Shahraki, C. Warnakulasooriya, K.J. Witt, Numerical study of transition zone between ballasted and ballastless railway track, *Transportation Geotechnics* 3 (2015) 58-67.

- [22] J. Shi, M.P.N. Burrow, A.H. Chan, Y.J. Wang, Measurements and simulation of the dynamic responses of a bridge–embankment transition zone below a heavy haul railway line, *Proceedings of the Institution of Mechanical Engineers, Part F: Journal of Rail and Rapid Transit* 227(3) (2012) 254-268.
- [23] A. Namura, T. Suzuki, Evaluatin of countermeasures against differential settlement at track transitions, *Quarterly Report of RTRI* 48(3) (2007) 176-182.
- [24] A. Paixão, E. Fortunato, R. Calçada, Transition zones to railway bridges: Track measurements and numerical modelling, *Engineering Structures* 80 (2014) 435-443.
- [25] Y. Guo, W. Jia, V. Markine, G. Jing, Rheology study of ballast-sleeper interaction with particle image Velocimetry (PIV) and discrete element modelling (DEM), *Construction and Building Materials* 282 (2021) 122710.
- [26] X. Bian, W. Li, Y. Qian, E. Tutumluer, Micromechanical Particle Interactions in Railway Ballast through DEM Simulations of Direct Shear Tests, *International Journal of Geomechanics* 19(5) (2019) 04019031.
- [27] E. Tutumluer, Y. Qian, Y.M.A. Hashash, J. Ghaboussi, D.D. Davis, Discrete element modelling of ballasted track deformation behaviour, *International Journal of Rail Transportation* 1(1-2) (2013) 57-73.
- [28] X. Zhang, C. Zhao, W. Zhai, DEM Analysis of Ballast Breakage Under Train Loads and Its Effect on Mechanical Behaviour of Railway Track, *Proceedings of the 7th International Conference on Discrete Element Methods* (2017) 1323-1333.
- [29] G. Jing, W. Jia, X. Wang, V. Markine, R. Nälsund, Y. Guo, Experimental and numerical study on lateral resistance of frictional sleeper with arrowhead groove, *Transportation Geotechnics* 30 (2021) 100638.
- [30] M. Lu, G.R. McDowell, The importance of modelling ballast particle shape in the discrete element method, *Granular Matter* 9(1-2) (2006) 69-80.
- [31] J.O. Hallquist, *LS-DYNA theoretical manual*, Livermore Software Technology Corporation, Livermore, CA, 1998.
- [32] W. Jia, V. Markine, Y. Guo, G. Jing, Experimental and numerical investigations on the shear behaviour of recycled railway ballast, *Construction and Building Materials* 217 (2019) 310-320.
- [33] Y. Guo, H. Fu, Y. Qian, V. Markine, G. Jing, Effect of sleeper bottom texture on lateral resistance with discrete element modelling, *Construction and Building Materials* 250 (2020).

Acknowledgement

After spending around 5 years here, I have finally completed my PhD project. Writing the acknowledgments marks the end of this journey, yet memories begin to resurface from the very beginning. Many years later, as I faced the screen, I was to remember that distant evening when I wrote the first email to apply for this opportunity. At that time, I didn't know what the future held, as I was determined to pursue a PhD, but the decision about where to go was uncertain. Fortunately, I received a lot of support from you.

I would like to express my gratitude to my promotor and supervisor, Dr. Valeri Markine. Your instruction in academic skills, along with your patience, guidance, and trust, have significantly enhanced my abilities. Your relaxed demeanor has also influenced my approach to managing both my work and personal life, helping me maintain control over them.

I extend my heartfelt gratitude to my promotor, Prof. Rolf Dollevoet. Your contributions have been invaluable at every crucial stage of my PhD study—during interviews, Go/No-Go meetings, yearly meetings, and in daily affairs. Your visionary perspective has consistently inspired and motivated me to enhance the quality of my research work.

I would like to express my great thanks to Prof. Guoqing Jing. My research on ballast initially began under your supervision, you encouraged me to see the world, to see behind walls, to feel, and to achieve. Your support is invaluable to me and has been a great help during the most challenging days. Your passion and enthusiasm seem infinite, and maybe that's why you led me to the field of Discrete Element Methods instead of choosing Finite Element Methods.

Thanks to Haoyu Wang, Yunlong Guo, Guixian Liu, Hongmei Huang, Chuang Wang, Dong Ding, Weile Qiang, Hao Fu, Jinxiu Chang, Jianing Song, Peyman Aela, Yameng Ji, Ran Zhang, Yunchang Du, Xinyu Wang, Wenbo Du, Qiang Zhou, Lu Zong, Gang Huang, Jiale Xie, Xiaodong Han. We know each other since we were in Beijing, that's been my almost 9 years ago. Hongxiang Ding, Shizhuo Zhong, Boyin Fu, Zhao Wang, Rongyou Feng, Ying Liu, Zhuo Chen, Yimo Chen, Zhiqiang Lei, Metal forever.

Thanks to the friends I've met here, I still vividly recall the Chinese New Year dinner in 2019, which marked the first time I didn't celebrate this most important festival with my family. However, I didn't feel lonely because of your presence. Throughout these years, we've shared many joyful moments. To Xiangming Liu, Pan Zhang, Zhiwei Qian, Bin Zhu, Shaoguang Li, Hongrui Wang, Zhen Yang, Xiangyun Deng, Chen Shen, Yang Jin, Julian He, Li Wang, Xinxin Yu, and Mario Carvalho - our time together has been memorable. Special appreciation to Yuanchen Zeng and Fang Ren, with whom I shared an office; the atmosphere was always delightful. Many days began and ended with a greeting to you, saying hello, here I am, bye-bye, and see you tomorrow. Wishing you all good morning, good afternoon, good evening, and good night.

Finally, thanks to my family, great to have a life in the family.

Wenli jia

04-06-1992 Born in Chengde, China

Education

2011- 2015 BSc, Road and Railway Engineering
Shijiazhaung Tiedao University, China

2015-2018 MSc, Road and Railway Engineering
Beijing Jiaotong University, China

2018-2023 PhD, Railway Engineering
Delft University of Technology, The Netherlands

List of Publications

Thesis-related papers

1. **Wenli Jia**, Valeri Markine. Parameter and efficiency analysis on particle shape of railway ballast in DEM simulations. Proceedings of the Institution of Mechanical Engineers, Part F: Journal of Rail and Rapid Transit. 2023. Under review
2. **Wenli Jia**, Valeri Markine, Yunlong Guo. Efficiency analysis and optimisation of DEM for railway ballasted track simulations--the multi-layer model. Transportation Geotechnics.2023 (40):100977.
3. **Wenli Jia**, Valeri Markine, Mario Carvalho, David P. Connolly. Yunlong Guo. Design of a concept wedge-shaped self-levelling sleeper. Construction and building materials.2023. 2023 (386):131524.
4. **Wenli Jia**, Valeri Markine, Yunlong Guo, Guoqing Jing. Experimental and numerical investigations on the shear behaviour of recycled railway ballast. Construction and building materials. 2019(217):310-320.
5. **Wenli Jia**, Valeri Markine, Yunlong Guo, Guoqing Jing. Analysis of furnace slag in railway sub-ballast based on experimental tests and DEM simulations. Construction and building materials. 2021 288(1):123114.
6. **Wenli Jia**, Haoyu Wang, Valeri Markine. Dynamic behaviour of ballast under hanging sleepers in railways track transition zones using FEM-DEM method. Under review

Other publications

7. Guoqing Jing, Luchao Qie, **Wenli Jia***. Polyurethane reinforcement in ballasted track: review, innovation and challenge. Construction and building materials. 2019(208):734-748.
8. Guoqing Jing, Xu Zhang, **Wenli Jia**. Lateral resistance of high-speed railway ballast locally reinforced with polyurethane based on new bonding schemes: laboratory tests and discrete element simulations. Construction and building materials. 2019(221):627-636.
9. Guoqing Jing, **Wenli Jia**, Xinyu Wang, Valeri Markine, Roar Nålsund, Yunlong Guo. Experimental and numerical study on lateral resistance of frictional sleeper with arrowhead groove. Transportation Geotechnics. 2021.30(2):100638.
10. Yunlong Guo, **Wenli Jia**, Valeri Markine, Guoqing Jing. Rheology study of ballast-sleeper interaction with particle image Velocimetry (PIV) and discrete element modelling (DEM). Construction and Building Materials. 2021. 282(2):122710.
11. **Wenli Jia**, Valeri Markine, Yunlong Guo. Optimising performance of discrete element method (DEM) modelling of railway track. The 4th International Conference on Computational Structures Technology,2022 Montpellier.
12. Guoqing Jing, Aela Peyman, Qiang Zhou, **Wenli Jia**. Steel Slag Aggregate Characteristics Evaluation as Railway Ballast. Advances in Transportation Geotechnics IV. Lecture Notes in Civil Engineering, (2022) 165. Springer.

